Mechanical tensile testing and metallurgical investigation of the residual properties of stainless steel reinforcing bar after exposure to elevated temperatures

By

Fazal-ur Rehman

A thesis submitted for the degree of Doctor of Philosophy

College of Engineering, Design and Physical Science

Brunel University London

2022

Abstract

This thesis examines the behaviour of stainless steel reinforcing bar following exposure to elevated temperature. Stainless steel reinforcement in concrete is an increasingly popular structural solution for a variety of applications where corrosion resistance, excellent mechanical properties and long life-cycles with little maintenance are required. Prior to this work, there was no information available in the published literature on the post-fire properties of stainless steel reinforcing bar, although this data is vital for an engineer wishing to study the structural integrity of a reinforced concrete component or system following a fire.

Accordingly, this thesis presents a detailed analysis and discussion on both the tensile and metallurgical behaviour of stainless steel reinforcement, following exposure to various levels of elevated temperature of up to 900°C and also three different cooling methods, rapid-cooling in water, natural-cooling in air and slow-cooling in a furnace. The study includes austenitic stainless steel reinforcement in grades 1.4301, 1.4401 and 1.4436 as well as both hot-rolled and cold-worked duplex stainless steel bars in grade 1.4362, with a comparative carbon steel B500B grade also assessed.

Within the post-fire temperature segment of this thesis, an increase in strength of up to 15% is noted in the stainless steel following cooling after elevated temperature exposure, with consistent responses between the different cooling methods. The austenitic grade reinforcement in particular presented a very stable microstructure across the various testing regimes, whilst the duplex reinforcements manifested a more unstable microstructure in the post-fire temperature testing. In the final part of this thesis, elevated temperature tests are conducted under isothermal conditions on austenitic grade 1.4301 and duplex grade 1.4362, to study how their mechanical behaviour evolves with increasing levels of temperature exposure.

The study covers the most common stainless steel reinforcing bar grades available on the market and focuses on recreating practical and realistic fire scenarios where possible. The tests conducted show how the current design standards, currently based on carbon steel, are inadequate for efficient design of stainless steel RC structures and could benefit from independent guidance. To conclude, this thesis presents independent recommendations and guidance for engineers to assist in calculating the structural integrity of a component or system following a fire.

List of Publications

The work presented in this thesis has to led to a list of publications and conference presentations, as follows:

Journals

- **Rehman F**.; Cashell, K.A.; Anguilano, L. Experimental Study of the Post-Fire Mechanical and Material Properties of Cold-Worked Austenitic Stainless Steel Reinforcing Bar. *Materials* **2022**

- **Rehman F**.; Cashell, K.A.; Anguilano, L. Duplex. Post-fire structural properties of hot-rolled and cold-rolled duplex stainless steel reinforcing bar. *Fire Technology* **2022**

Conferences

- Rehman, F.; Mehwish, J.; Rabee, S.; Cashell, K.A. Fire Behaviour of Stainless Steel Reinforcement and Stainless Steel Concrete Beams. *Structures In Fire **2022**. Hong Kong*
- **Rehman F**.; Cashell, K.A.; Mehwish, J.; Anguilano L. Behaviour of stainless steel reinforcement in fire conditions. *CONFAB International Conference* **2019**. London.

Acknowledgment

In the name of Allah, the gracious, the merciful.

To begin, I would like to thank my primary supervisor, Dr Katherine Cashell, for giving me incomparable support and feedback throughout my PhD. I would also like to thank my secondary supervisor, Dr Lorna Anguilano, for her exceptional support and guidance throughout my PhD.

Best supervisory team ever, 10/10 would recommend.

In addition, I would like to thank the Civil and Environmental Engineering technical staff that supported me throughout my experimentations. I am also very thankful for the support I received from the Experimental Techniques Centre (ETC), thank you for helping me with a topic that I was completely new too, and the absolute enjoyment of working with Dr Nico Nelson and Dr Uchechukwu Onwukwe.

Throughout my time I at Brunel I have had the pleasure of working not only with the Civil and Environmental Department, but the whole college. I would like to give an extended thanks to all the staff members I may have troubled during my PhD.

Finally, I would like to thank my entire family for providing endless support towards my PhD. Their support is what has made any of this possible.

Contents

List of Figures

List of Tables

List of Notations

f_u	*Ultimate tensile strength*
$f_{0.2p}$	*0.2% Proof strength*
ε_f	*Total Strain at Failure*
ε_u	*Percentage total Elongation at Maximum Force*
Θ	*Temperature*
E	*Modulus of Elasticity*
k_E	*Reduction factor for the modulus of elasticity at elevated temperature*
E_Θ	*Slope of the linear elastic range at elevated temperature*
$k_{p0.2}$	*Reduction factor for 0.2% proof stress*
k_u	*Reduction factor for tensile stress*
λ_a	*Thermal conductivity*
C_a	*Heat capacity*
t	*Time*
L_t	*Total Length*
L_0	*Gauge Length*
L_c	*Parallel Length*
$f_{0.2p,\theta}$	*0.2% proof strength at elevated temperature*
$f_{u,\theta}$	*ultimate strength at elevated temperature*
$\varepsilon_{f,\theta}$	*total strain at failure, at elevated temperature*
$f_{0.2p,\theta,calc}$	*Calculated 0.2% proof strength at elevated temperature*
$f_{u,\theta,calc}$	*Calculated ultimate strength at elevated temperature*
$\varepsilon_{f,\theta,calc}$	*Calculated total strain at failure at failure, at elevated temperature*
ε_{fk}	*Reduction factor for total strain*
β	*Reliability index*
φ	*Resistance factor*

Chapter 1 Introduction

1.1 General

Stainless steel rebars are a well-accepted solution for concrete structures which are exposed to harsh environments, such as in marine or industrial settings, owing to their excellent corrosion resistance. In addition to these environments, there is also increasing focus on using stainless steel rebars as an alternative to traditional carbon steel bars in other scenarios owing to their excellent mechanical performance, long life cycle, and reduced requirements for expensive inspection and maintenance works.

This thesis is concerned with the behaviour of stainless steel reinforcing bar during and following a fire scenario and examines the tensile properties, and where possible the metallurgical properties, which affect its performance and structural integrity.

1.2 Need for Research

The use of stainless steels in structural applications has increased in recent years, as more design information has become available, and greater cost-effectiveness has been achieved. Much of the attention from the research community, however, has focused on bare stainless steel structural sections, such as I-sections and tubular members, with less focus given to stainless steel reinforcement for concrete. Nevertheless, stainless steel reinforcement is an increasingly popular solution for structures susceptible to corrosion and can result in lower maintenance costs and higher life spans (>125 years) in comparison with traditional carbon steel-reinforced concrete. However, unlike carbon

steel rebar, the understanding of how stainless steel reinforcement performs both during and following a fire scenario is very much unknown, owing to an absence of performance data in the available literature.

The post-fire behaviour of building structures and infrastructure is important for several reasons. First, having an immediate, realistic understanding of the residual strength and stiffness remaining in the structure following exposure to fire allows emergency response teams, fire fighters and investigators to make informed decisions about rescue and salvage operations, as well as the risk of collapse. In addition, this enables informed decisions to be made regarding the rehabilitation and repurposing of the structure. Failure to understand the post-fire response and capacity of structural materials and elements may result in unnecessary demolitions and loss of structures, which is neither environmentally nor economically sustainable.

Although the performance of stainless steel rebar in marine environments is reasonably well understood and has been the subject of some research (Cardoso et al., 2018; Bertolini and Gastaldi, 2011; William et al., 2009), existing information and previous studies on the fire performance of stainless steel rebars are limited. There is no design guidance is available for the post-fire mechanical performance of stainless steel rebar, with studies into performance of stainless steel rebar by Felicetti et al., (2009) and Zeng et al., (2012) limiting to austenitic stainless steel grades and focusing on the material response. For the elevated temperature response, a single study on both the isothermal and anisothermal response is available by Gardner et al., (2016).

1.3 Aims and Objectives

The primary aim of this thesis is the to investigate the residual tensile properties of stainless steel reinforcing bar following a fire scenario. This is so that engineers can make an informed decision about rehabilitation and structural integrity following a fire. A secondary aim is to present an understanding of the fire performance on stainless steel rebar, both during and following a fire scenario.

In order to understand the post-fire tensile behaviour of stainless steel reinforcement, it is important to understand the metallurgy and specifically the effects of the relevant phases of the microstructure (i.e., the austenite, ferrite, and martensite phases) on the behaviour. Therefore, this thesis aims to explore both the tensile and metallurgical properties of stainless steel reinforcement following exposure to elevated temperature, as well as their inter-relationship.

1.4 Thesis Outline

This thesis is divided into eight chapters in total, and so there are seven further chapters, summarised as follows:

Chapter 2 focuses on the background information and the existing literature needed to produce an effective study. This is done through a thorough explanation of the material properties, influencing elements, manufacturing methods and tensile properties. A broader understanding of how rebars work within reinforced concrete (RC) structures is briefly covered, with the chapter concluding on a breakdown of prior publications within the scope of this thesis. Chapter 3 describes the experimental methodology, covering a breakdown of the selected rebar grades, the heating and cooling cycle, tensile testing, metallurgical investigation and the elevated temperature testing arrangement.

Chapters 4, 5 and 6 present the results from the post-fire testing scenario, detailing the findings in the tensile testing through stress-strain graphs and metallurgical investigation through X-Ray diffractograms and microscopic imagery. Chapter 4 presents the austenitic stainless steel data, comparing against carbon steel grade B500B, whilst Chapter 5 presents the results for duplex stainless steel rebar. The findings for the complete post-fire testing module are discussed in Chapter 6, outlining the key findings and influences and then finishing on the proposed reduction factors.

Chapter 7 presents the findings for the elevated temperature testing, which covers one austenitic and duplex grade, discussing the results obtained against works done by Gardner et al., (2016). Chapter 8 concludes with the overall findings from this thesis, identifying the most notable observations. This is followed by the implications on design this work presents, and recommendations for further study.

Chapter 2 Literature Review

2.1 Introduction

This chapter presents a review of the available literature on stainless steel reinforcing bar as a structural material in reinforced concrete, and emphasis is placed on providing an insight into the material characteristics with a direct influence on the tensile response during or following exposure to elevated temperatures. Whilst stainless steel as a structural material has been the focus of active research in the past two decades, limited literature is available specifically on stainless steel rebar, especially in fire conditions therefore throughout this chapter there is some reference to alternative structural applications as a suitable comparative for the absence in literature.

Stainless steels are alloys with iron as the parent element that contain at least 10.5% chromium and 0.07% carbon content. The addition of chromium greatly increases the corrosion resistance, making stainless steel ideal for reinforcement in harsh environments, such as marine or industrial settings. The use of stainless steels in structural applications has increased in recent years as more design information has become available and greater cost-effectiveness has been achieved due to more efficient manufacturing. However, much of the attention from the research community has focused on bare stainless steel structural sections, such as I-sections and tubular members, with less focus given to stainless steel reinforcement for concrete. Nevertheless, stainless steel reinforcement is an increasingly popular solution for structures susceptible to corrosion and can result in lower maintenance costs and higher life spans (>125 years) in comparison to traditional carbon steel reinforced concrete.

The first recognised application of stainless steel as reinforcement was the Progresso Pier, Mexico, in 1941, where today's equivalent of grade 1.4301 stainless steel reinforcing bar was used. The pier is

still in use today (Nickel Institute, 2013). Between the years 1941-1970, there were very few if any notable stainless steel reinforcing bar applications. In the early 1970s, corrosion of reinforcement in RC structures became an active issue, and the Building Research Establishment (BRE) conducted a study that spanned over 20 years, concluding with the excellent performance of stainless steel (Gedge, 2003). Slowly since, stainless steel reinforcement has become more popular, leading to the modern-day, where it is considered the best possible reinforcement for structural applications prone to corrosion.

A recent example of its application includes the use of 15,000 tonnes of stainless steel to reinforce the Montreal Champlain Bridge, completed in 2019 and shown in Fig. 2-1 (Arup, 2020). This bridge spans 3.4 km over the St Lawrence River in Canada, and is often exposed to strong winds, heavy rainfall, seasonal snowfall and the regular use of de-icing salts. The design life of this structure is expected to be 125 years with minimal maintenance (Government of Canada, 2021). Another application is the Chinese River Delta Crossing, an ongoing project spanning 50 km through a series of bridges and tunnels which will connect Hong Kong, Macau and mainland China. To reduce the maintenance of this megastructure, 15,000 tonnes of stainless steel rebar is employed in the outer parts that are most susceptible to high chloride levels, thus ensuring a long life span (worldstainless.org, 2016).

Figure 2-1: New Montreal Champlin bridge (left) compared to the old Champlin bridge (right) (Arup, 2020).

2.2 Material Properties

This thesis is concerned with the influence of metallurgical properties on the tensile behaviour of stainless steel reinforcement, following exposure to elevated temperature. Therefore, the following sub-sections outline some of the key characteristics of stainless steel as well as the metallurgical properties of relevance to the current work. Comparatively some characteristics of carbon steel reinforcement are also presented.

2.2.1 Stainless Steel Families

Stainless steel alloys are generally categorised into five families based on their composition and crystallographic structure; these are the austenitic, ferritic, duplex, martensitic, and precipitation hardening grades. Austenitic and duplex stainless steels are most commonly employed in structural applications, although the ferritic grades are sometimes used in appropriate applications. The martensitic and precipitation hardening grades are rarely if ever used in construction applications and are more commonly employed in mechanical and aerospace engineering as well as for medical tools and cutting utensils. Although this study focuses on austenitic and duplex stainless steel reinforcing bars, a brief understanding of all grades is needed to understand the research presented herein.

Austenitic stainless steels are the most common type of stainless steel, accounting for 70% of all stainless steel production (Pramanik and Kumar, 2015). They offer an excellent combination of corrosion resistance, ductility, strength and toughness. Austenitic stainless steels behave very well at high temperatures and are readily weldable. The ferritic grades are cheaper than the austenitics due to a very low nickel content (Beddos and Parr, 1999). However, they also offer less corrosion resistance, ductility and strength than the austenitic alloys. Ferritic alloys perform well at high temperatures but are more challenging to weld than austenitics.

Duplex stainless steels are also known as austenitic-ferritic stainless steels, as they contain both an austenite and ferrite phase in their crystallographic structure. They offer higher corrosion resistance and strength than austenitic stainless steels whilst maintaining the ductility of ferritic stainless steels. Duplex stainless steel alloys have good weldability, which is advantageous for reinforcing bar which needs to be pre-assembled into reinforcement cages, such as for piles, diaphragm walls, columns and beams. Notably, the austenite phase is more stable within the duplex alloy than the ferrite phase when exposed to elevated temperatures. Martensitic stainless steels are extremely hard alloys but have poor ductility. They are prone to cracking when welding and perform similar to conventional carbon steels at high temperatures (International Stainless Steel Forum, 2020). The precipitation hardened stainless steels are similar to martensitic alloys in purpose, offering extreme hardness but somewhat

better ductility. Precipitation hardened alloys respond poorly to high temperatures but offer good weldability. Although only the austenitic and duplex alloys are used for rebar production of these five stainless steel families, there is a large number of variations in stainless steel rebar available for different applications whereas carbon steel presents a limited three variations based on ductility class.

2.2.2 Metallurgy of Stainless Steel

Stainless steel is an alloy of pure iron (Fe) as the parent element, where a minimum of 10.5% chromium and a maximum of 1.2% carbon content by mass are also present to form stainless steel (International Stainless Steel Forum, 2012). Therefore, the metallurgical properties of pure iron somewhat translate to stainless steel. Pure iron is allotropic by nature, meaning that as the temperature rises, the phase of the alloy changes. Originally the α-ferrite phase is present with a body centred cubic (BCC) grain structure, above 914°C the γ-austenite phase with a face centred cubic (FCC) grain structure emerges and is retained until 1391°C, where the pure iron will revert back to a body centred cubic (BCC) grain structure known as δ-ferrite which is stable until the melting point at 1536°C (Chadwick, G.A., 1972). Essentially the difference between these phases is how densely the atoms are packed. For iron, the FCC (or α-ferrite) phases are denser with an atomic packing factor (APF) of 0.74 whereas the BCC (γ-austenite) phase is slightly less dense with an APF of 0.68. Alloys with a higher APF have more workability, making the γ-austenite phase desirable in structural applications. Of the different stainless steel families, the austenitic alloys have FCC crystals, the ferritic alloys have BCC crystals, and the duplex alloys have a combination of FCC-BCC crystals. The grains of the martensitic and perception hardened families can vary greatly from alloy to alloy but are generally BCC. As the γ-austenite phase in pure iron is only achieved at an elevated temperature with the addition of various austenite-promoting elements such as nickel, this γ-austenite phase can be stabilised at ambient temperatures.

It is noteworthy to recognise some of the constituent elements in the stainless steel alloys used within this experiment, which are influential to the structural performance:

- Chromium (Cr): a highly resistive element to corrosion through its passive self-healing capability, and the most prominent addition in any stainless steel alloy. The addition of chromium helps strengthen and soften the alloy, whilst promoting a ferritic phase.
- Nickel (Ni): the primary austenite promoter in stainless steel and is an active corrosion resisting element. The addition of nickel promotes ductile behaviour whilst hardening the alloy.

- Molybdenum (Mo): an active corrosion resisting element with fire resisting properties at elevated temperatures of up to 500°C. As with chromium, molybdenum is a strong ferrite promotor.
- Manganese (Mn): an active deoxidiser crucial to the manufacturing of stainless steel through its ability to provide stability from cracking and tearing during the cooling process. At base temperatures, manganese is an austenite promoting element, whereas manganese will promote a ferrite phase at elevated temperatures.

2.2.3 Manufacturing of Reinforcing Bar

Another influential factor in the characteristics of the alloy is the method of production. For both carbon steel and stainless steel rebar, this can be broken down into either hot-rolling or cold-rolling. Hot-rolling the rebar is the practice of transforming the steel billet to finished rebar in one continuous chain of actions under controlled elevated temperature conditions, then allowing for subsequent cooling. Hot-rolling involves a continuous cycle of deforming the microstructure into a flat, pancake-like structure followed by a breakdown and recrystallisation into smaller grains. The smaller grains act as the primary strengthening mechanism. The Hall-Petch relationship explains this, which indicates that the smaller the grain size, the higher the material strength, up to the limitation of the material's theoretic max strength (Hansen, 2004).

Production through cold-rolling is working the steel billet into coils of steel wire at elevated temperature, then cooling them for more accessible transportation and storage. Following this, to form a useable product, the coil is continuously drawn through rollers in a cold state to mechanically induce strength into the steel alloy through the deformation of the grain providing new strengthening mechanisms. When grade 1.4301 stainless steels are cold-worked, the γ-austenite grains can undergo a stress-induced transformation into ε-martensite and then α´-martensite, or they may experience a strain-induced transformation resulting in twinning and then the formation of α´-martensite. For both scenarios, there is a formation of α´-martensite, as the chemical composition does not change, and the alloy remains austenitic. The act of cold-rolling leads to reducing the diameter of the finished rebar (Rodrigues et al., 2019). Fig. 2-2 shows a comparative grain response of both methods of production.

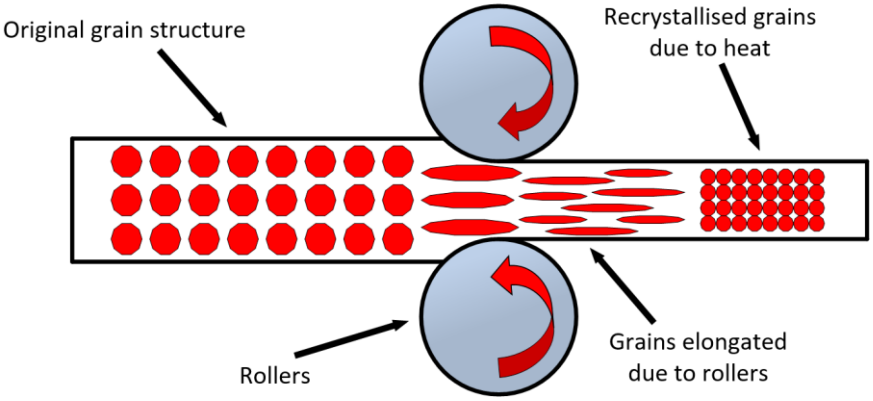

(a) Hot-rolling

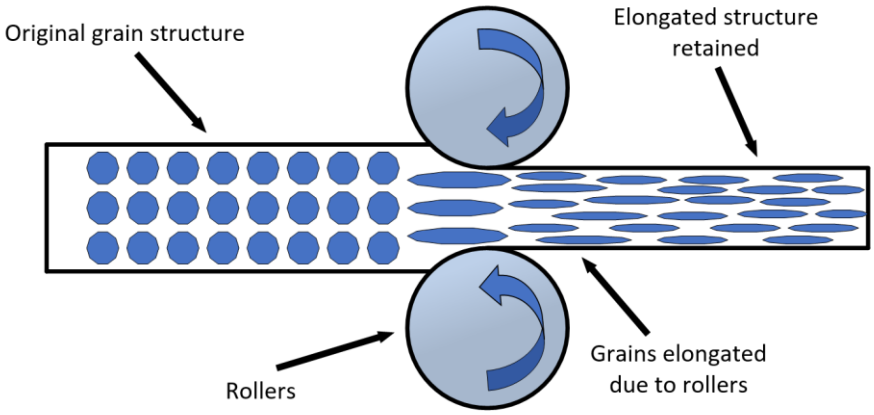

(b) Cold-rolling

Figure 2-2: Hot-rolling (a) showing the grain deformation followed by recrystallisation and cold-rolling (b) showing the grain deformed into the strengthening mechanisms.

Both production methods have their own attributes and drawbacks that are important to consider during specification. Cold-rolling allows for better transportation and provides manufacturers and suppliers with the ability to bulk stock rebars for on-demand availability, resulting in a reduced cost of the final product but a limitation in the variation of rebar available. The ribbing on cold-rolled rebars is more uniform and allows for better bond strength than hot-rolled bars. However, as cold-rolled rebars have to be coiled and rolled, they have a diameter limitation of between 16 and 20 mm. Hot-rolling rebars have easier workability during manufacturing and are generally possible to produce with no diameter limitation. However, hot-rolled rebar manufacturing is usually reserved for special requirements or larger diameter rebars due to the higher cost. Austenitic rebar is made exclusively through cold-rolling as austenite grains are very ductile, requiring mechanically induced strength.

There is currently no information available in the literature on the response of hot-rolled or cold-rolled stainless steel rebar following a fire and subsequent cooling. Also related to cold-rolling, a study by

Sun et al., (2014) found that cold-rolling in selected austenite alloys led to the formation of microcracking.

2.3 Mechanical Properties

2.3.1 Stress-Strain Relationship in Stainless Steel Alloys

There are no specific requirements for the manufacturing processes of stainless steel rebars, but BS 6744-10 (2016) provides requirements for the chemical composition and the testing methods for stainless steel bars used for concrete reinforcement. In accordance with this standard, the stainless steel rebar's minimum required mechanical property values are based on the carbon steel B500B specifications as given in Part 7 of BS 4449 (2016). The specifications for this grade of carbon steel reinforcement are presented in table 2-1, where $f_{0.2p}$ is the proof strength, f_u is the ultimate total strength, ε_u is the elongation at maximum force, and ε_f is the total strain at failure. BS 6744-11 (2016) also states that the stainless steel rebar is required to have a minimum total strain at failure ε_f of at least 14%. For clarity, Fig. 2-3 presents an ideal stress-strain response for stainless steel reinforcement, demonstrating the key characteristics against a carbon steel stress-strain response.

Table 2-1: Tensile Specifications for Rebar Manufacturing as Per BS 4449-7 (2016) for carbon steel rebar and BS 6744-11 (2016) stainless steel rebar.

	Proof Strength $f_{0.2p}$		Stress ratio $f_u/f_{0.2p}$		Percentage total Elongation at maximum force ε_u	
	Min	Max	Min	Max	Min	Max
Carbon steel B500B	480	650	1.08	-	5	-
Stainless steel (all grades)	480	-	1.08	-	5	-

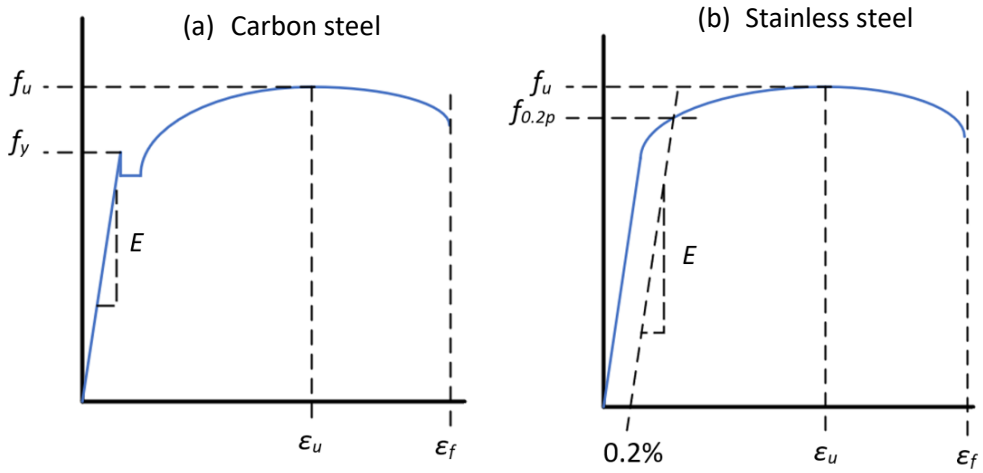

Figure 2-3: Ideal stress-strain curve response of (a) carbon steel and (b) stainless steel.

During the cold-rolling process, the steel coil is often manufactured for varying applications. Therefor different strength classes must be assigned during the cold-rolling stage exclusive of the rebar properties presented in BS 6744-11 (2016). A set of mechanical property conditions are set out by BS EN 10088-3 (2014) for general cold-rolled austenitic stainless steel bars of grade 1.4301 and 1.4401. The specifications are presented in table 2-2, where $f_{0.2p}$ is the proof strength, f_u is the ultimate total strength and ε_f is the total strain at failure. Each grade is assigned into two tensile strength classes dependent on the degree of cold-rolling.

Table 2-2: Tensile strength class categories for stainless steel as per BS EN 10088-3 (2014)

Grade	Tensile strength class	Proof Strength $f_{0.2p}$		Tensile Strength $f_{0.2p}$		Percentage total Elongation at maximum force ε_u	
		Min	Max	Min	Max	Min	Max
1.4301	+C700[b]	350	-	700	850	20	-
	+C800[a]	500	-	800	1000	12	-
1.4401	+C700[b]	350	-	700	850	20	-
	+C800[a]	500	-	800	1000	12	-

2.3.2 Modulus of Elasticity of Stainless Steel Alloys

The modulus of elasticity (E) measures a material's limit of elastic deformation when under stress. For rebar design specification, the modulus of elasticity is 190 GPa for austenitic stainless steels and 200 GPa for duplex and carbon steels (BS 6744, 2016). Currently, there is no standardised method for the determination of the modulus of elasticity of a metal such as ISO 6892-1 for tensile testing and therefor it is a difficult property to measure accurately. Due to the low levels of strain in the elastic

range. The most common approach is to conduct a tensile test, although this requires quite high specification equipment in order to get an accurate *E* reading. The primary objective of tensile testing is to deliver an accurate stress-strain graph. Lord and Morrell (2010) demonstrated the need for a specialist test setup for an accurate data set for the elastic modulus, highlighting the lack of feasibility in a practical scenario which may include several hundred specimens. This difficulty of gaining an accurate measurement of the elastic modulus was also discussed by Chen et al., (2016), where various methods of recording the modulus were examined, showing inconsistency across the data collected, especially under plastic straining. Both of these papers highlight the inaccuracies of measuring *E* for metals, with Lord and Morrell (2010) commenting that stainless steel has the most significant levels of inaccuracy of the materials examined. This inaccuracy is supported by works of Beddoes and Parr (1999), commenting that the elastic modulus for stainless steel bares a significant tie to the parent element, iron, and therefore at room temperature, the modulus of elasticity does not fall below 190 GPa or very rarely rise above 200 GPa.

Regardless of the level of work done to stainless steel rebar during production, at ambient temperature, the modulus of elasticity should remain the same. Even following any form of heat-treatment. However, at an elevated temperature state, the modulus of elasticity is subject to change and, as such, EN 1993-1-2 (2005) proposes a reduction factor ($k_E = E_\Theta/E$) which can be used on stainless steels, presented in Fig 2-4, where k_E is the reduction factor at elevated temperature, E_Θ is the slope of the linear elastic range at elevated temperature and *E* is the modulus of elasticity at ambient temperature. However, work done by Ala-Outinen (1996), Gardner et al., (2010) and Gardner et al., (2016), showed that these proposed reduction factor become quite inaccurate above temperatures of 600°C.

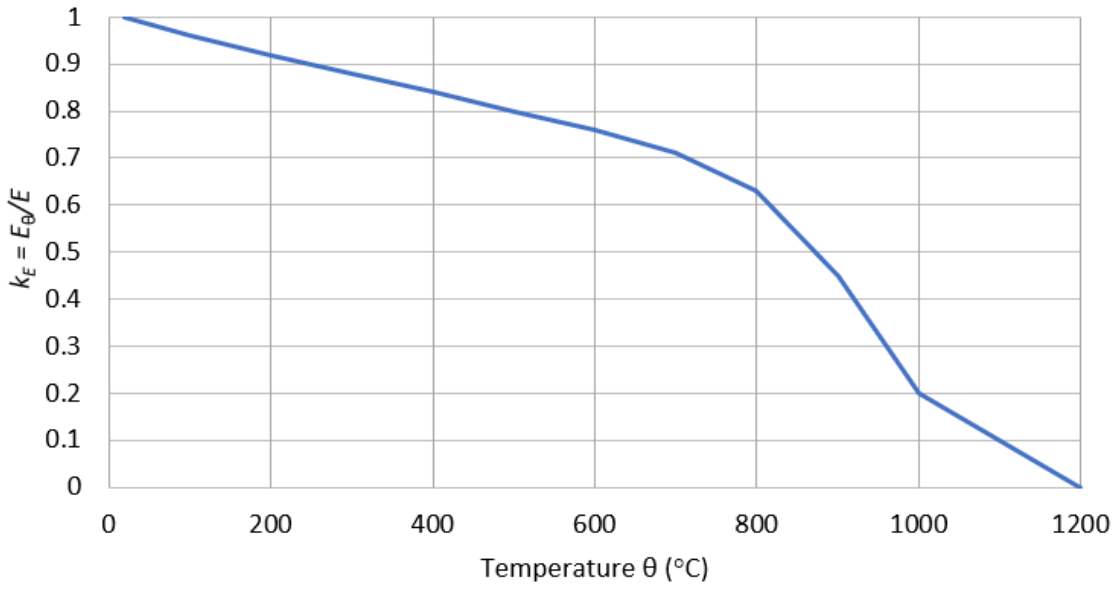

Figure 2-4: Reduction factor for the modulus of elasticity as presented in EN 1993-1-2 (2005).

2.3.3 Physical and Thermal Properties of Stainless Steel Alloys

The physical properties for each stainless steel family can vary greatly, as shown in table 2-3. Rebar-specific properties are not available and therefore, for this section, data is taken from bare stainless steel sections (The Steel Construction Institute, 2017) and compared against carbon steel. Moreover, although austenite is not ferromagnetic, in cold-rolling when the γ-austenite grains are transformed into α´-martensite, the α´-martensite grains become ferromagnetic.

Table 2-3: Comparative physical properties of stainless steel grades against carbon steel

Property	Austenitic	Ferritic	Martensitic	Duplex	Carbon Steel
Density (g/cm^3)	7.9-8.2	7.6-7.8	7.6-7.7	7.8	7.8
Thermal expansion (x10^{-6}/°C)	17-19	12-13	12-13	13	11.7
Thermal conductivity (W/m°C) 20°C	12-15	20-23	22-24	20	45
Heat capacity (J/kg°C) 20°C	440	460	460	400	490
Ferromagnetic	No	Yes	Yes	Yes	Yes

2.3.3.1 Thermal Expansion

Thermal expansion is the change in shape, area or volume of a material following exposure to a change in temperature. It can be characterised and measured through the coefficient of thermal expansion, which is a material property that describes how the size of a material changes with this change in temperature. When subjected to a change in temperature through heating, like all metallic materials,

stainless steel is also prone to expansion. In accordance with EN 1993-1-2 (2005), the thermal expansion factor for austenitic stainless steels is as given in equation 2-1:

$$\frac{\Delta \mathrm{l}}{\mathrm{l}} = \left(16 + 4.79 * 10^{-3}\Theta_{\mathrm{a}} - 1.243 * 10^{-6}{\Theta_{\mathrm{a}}}^{2}\right) * (\Theta_{\mathrm{a}} - 20)\ 10^{-6} \quad (2\text{-}1)$$

The corresponding formulation for duplex alloys is given in equation 2-2 (The Steel Construction Institute, 2017):

$$\frac{\Delta \mathrm{l}}{\mathrm{l}} = \left(13 + 4.79 * 10^{-3}\Theta_{\mathrm{a}} - 1.243 * 10^{-6}{\Theta_{\mathrm{a}}}^{2}\right) * (\Theta_{\mathrm{a}} - 20)\ 10^{-6} \quad (2\text{-}2)$$

where l is the length at 20°C, $\Delta \mathrm{l}$ is the temperature-induced expansion, and Θ is the steel temperature in °C. In comparison, carbon steel follows a non-liner path described in a three stage formula, equations 2-3, 2-4 and 2-5 as presented in EN 1993-1-2 (2005):

$$\frac{\Delta l}{l} = 2.416 * 10^{-4} + 1.2 * 10^{-5}\theta_a + 0.4 * 10^{-8} * {\theta_a}^{2} \quad \text{For } 20°C \leq \theta a < 750°C \quad (2\text{-}3)$$

$$\frac{\Delta l}{l} = 11 * 10^{-3} \quad \text{For } 750°C \leq \theta a < 860°C \quad (2\text{-}4)$$

$$\frac{\Delta l}{l} = -6.2 * 10^{-3} + 2 * 10^{-5}\theta_a \quad \text{For } 860°C \leq \theta a < 1200°C \quad (2\text{-}5)$$

Fig. 2-5 shows the different thermal elongation that occurs for austenitic stainless steel, duplex stainless steel and carbon steel alloys.

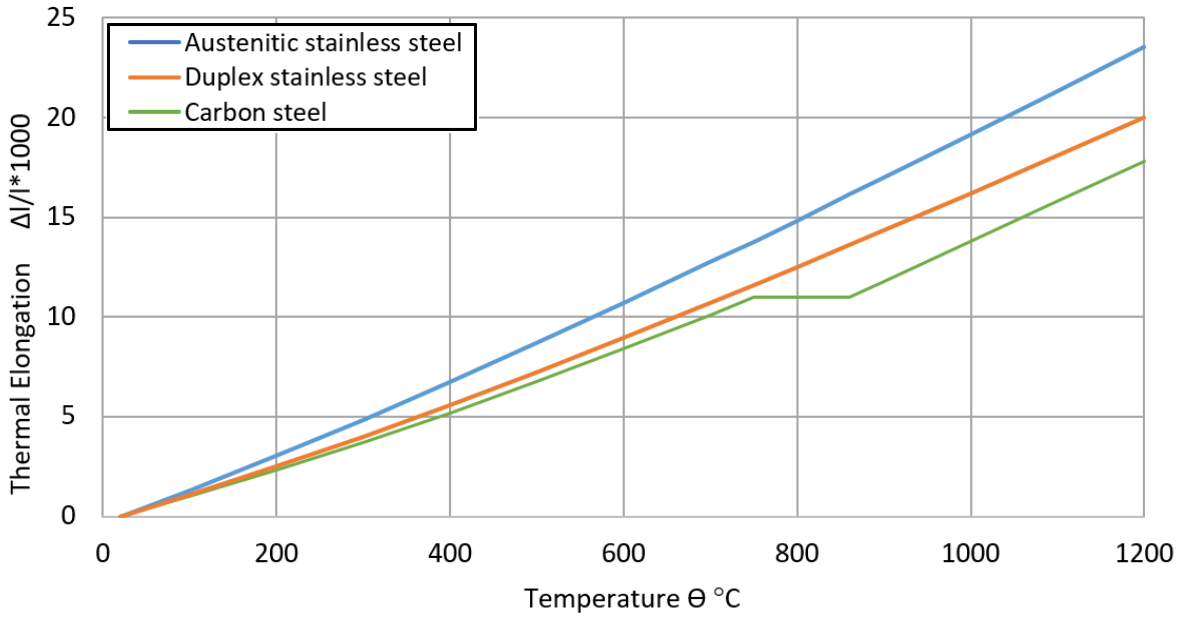

Figure 2-5: Thermal elongation against temperature, comparative between austenitic stainless steel, duplex stainless steel and carbon steel alloys.

2.3.3.2 Thermal Conductivity

Thermal conductivity is defined as the measure of a materials ability to conduct heat. In stainless steel, as the temperature of the alloy rises, it becomes more thermally efficient, resulting in a higher thermal conductivity at higher temperatures. Overall stainless steel alloys contain low thermal conductivity due to the nickel content, making them ideal for applications prone to fire exposure. This has led to austenitic superalloys such as Inconel being developed (SMC, 1998). EN1993-1-2 (2005) proposes formulas to calculate the thermal conductivity of stainless steel (equation 2-6) and a two-stage equation for carbon steel (equation 2-7 and 2-8). Where λ_a is the thermal conductivity and Θ is steel temperature in °C. Fig. 2-6 presents the comparative thermal conductivity of carbon steel and stainless steel.

$$\lambda_a = 14.6 + 1.27 * 10^{-2}\Theta \ \text{W/mK} \quad (2\text{-}6)$$

$$\lambda_a = 54 - 3.33 * 10^{-2}\Theta_a \ \text{W/mK} \quad \text{For } 20°C \leq \Theta_a < 800°C \quad (2\text{-}7)$$

$$\lambda_a = 27.3 \ \text{W/mK} \quad \text{For } 800°C \leq \Theta_a < 1200°C \quad (2\text{-}9)$$

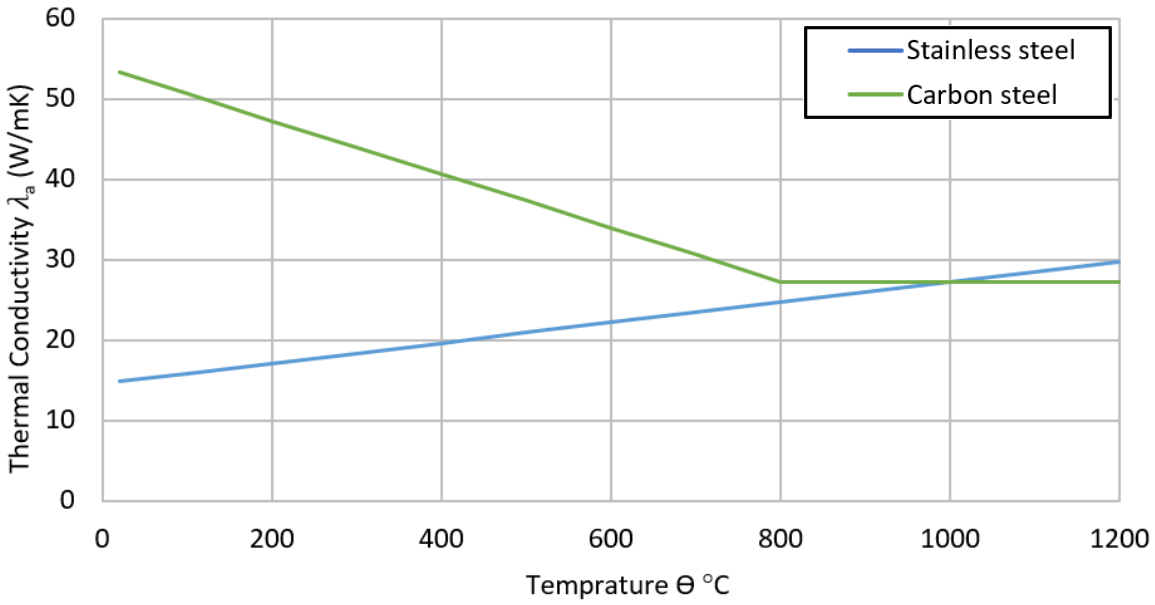

Figure 2-6: Thermal conductivity against temperature, comparative between stainless steel and carbon steel as per EN 1993-1-2 (2005)

2.3.3.3 Heat Capacity

In its simplest form, the specific heat capacity is the required energy needed to raise the temperature per unit mass. The overall heat capacity is similar for both austenitic and duplex stainless steel. Expressions for the determination of the heat capacity C_a for austenitic stainless steel is given in equations 2-4, in accordance with EN 1993-1-2 (2005). Comparatively the heat capacity for carbon steel follows an extremely non-linear pattern described in a four-stage formula (equations 2-11, 2-12, 2-13 and 2-14):

$$C_a = 450 + 0.280 * \Theta - 2.91 * 10^{-4}\Theta^2 + 1.34 * 10^{-7}\Theta^3 \quad \text{J/kgK} \qquad (2\text{-}10)$$

$$C_a = 425 + 7.73 * 10^{-1}\Theta_a - 1.69 * 10^{-3}{\Theta_a}^2 + 2.22 * 10^{-6}{\Theta_a}^3 \quad \text{J/kgK}$$

For 20°C ≤ Θ_a < 600°C (2-11)

$$C_a = 666 + \frac{13002}{738 - \Theta_a} \quad \text{J/kgK}$$

For 20°C ≤ Θ_a < 600°C (2-12)

$$C_a = 545 + \frac{17820}{\Theta_a - 731} \quad \text{J/kgK}$$

For 735°C ≤ Θ_a < 900°C (2-13)

$$C_a = 650 \quad \text{J/kgK} \qquad \text{For } 900°C \leq \Theta_a < 1200°C \tag{2-14}$$

where C_a is the specific heat capacity measured in J/kgK, and Θ is the alloy temperature in °C. Fig 2-7 presents the specific heat at any given temperature for stainless steel and carbon steel.

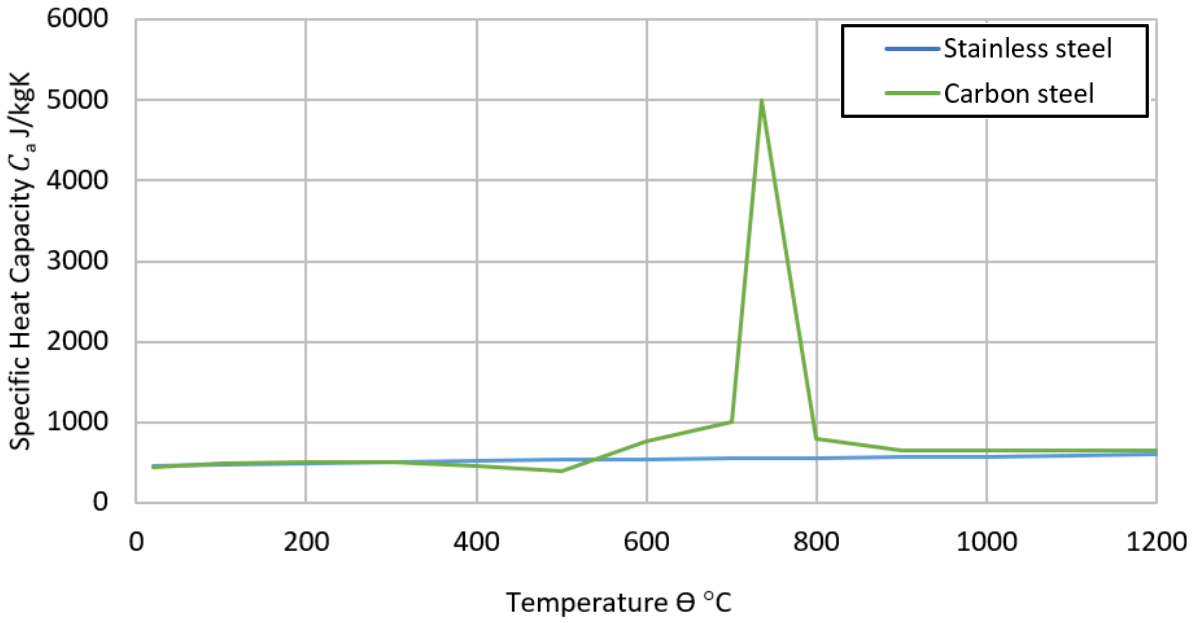

Figure 2-7: Specific heat capacity against temperature for stainless steel and carbon steel as per EN 1993-1-2 (2005).

2.4 Fires Scenarios in RC Structures

2.4.1 Fire in RC Structures

Although the testing of RC elements falls outside the scope of this thesis, this section highlights the relevant properties of RC structures during and following a fire scenario and subsequent cooling, aiming to understand the parameters of a real-life fire scenario and successfully translate this into the practical testing presented in Chapter 3. The residual response of reinforced concrete following a fire and subsequent cooling is reasonably well documented, with a sizeable database of studies being available such as works by Molkens et al., (2017), Chen et al., (2009), Yuli et al., (1996). However, currently the catalogue of research focuses on carbon steel as the primary reinforcement, resulting in very little research on stainless steel RC elements. Some data has been published on stainless steel sections in and following fire scenarios, this is discussed later in section 2.5.2.

One of the more common applications for stainless steel reinforced concrete is in bridges. Garlock et al., (2012) found that the most critical fire scenario for bridges is 'Tanker truck fires', also known as hydrocarbon fires, during which the temperatures rise very quickly in comparison to standard fires. Equations 2-5 and 2-6 are taken from EN 1991-1-2 (2002) and present the fire model for standard and hydrocarbon fires, respectively.

$$\theta = 20 + 345log_{10}(8t + 1) \quad (2\text{-}5)$$

$$\theta = 1080\,(\,1 - 0.325e^{-0.167t} - 0.675e^{-2.5t}\,) + 20 \quad (2\text{-}6)$$

where θ represents the temperature in °C and t is time in minutes. Fig 2-8 presents the time-temperature curve for both fire types, for comparison. It is observed that for the hydrocarbon fire, the temperature rises very quickly versus the standard fire curve, reaching a maximum temperature of 1100°C in 20 minutes versus a maximum temperature of 970°C for the standard fire curve after 60 minutes.

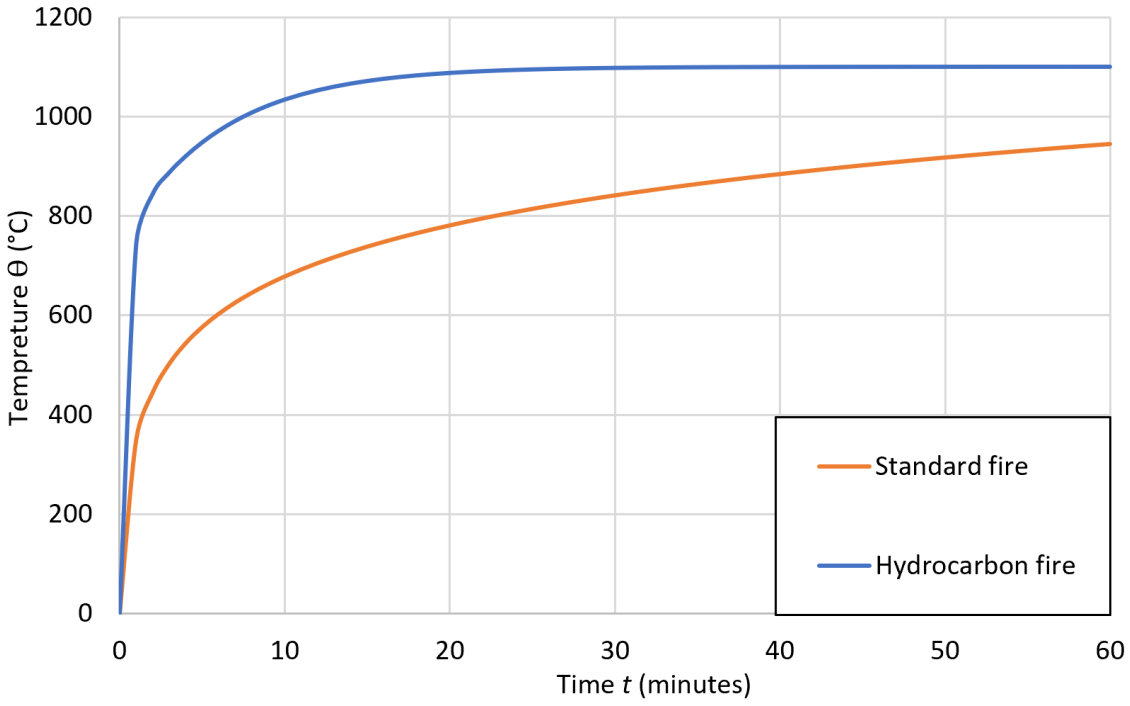

Figure 2-8: Model fire curve of standard fires versus hydrocarbon fires as per EN 1991-1-2 (2001).

When under fire conditions, the behaviour of the rebar embedded within concrete relies on the low thermal conductivity of concrete as a temporary heat shield, exposing the steel to lower temperatures than that actual fire (Raouffard and Nishiyama, 2016).

Practical experimentation for the residual properties of carbon steel reinforced elements conducted by Raouffard and Nishiyama (2016) present the expected thermal heating and cooling cycle if the critical temperature of the reinforcing steel is of interest during a fire. The study carried out experimentation on a 1/3 model reinforced concrete frame reinforced with carbon steel. Fig. 2-9, taken from Raouffard and Nishiyama (2016), presents the relation between the time, temperature, and reinforcement positions. The results found the central reinforcement to be least influenced by the elevated temperature, due to being well insulated, but also retained a lot more heat during the cooling cycle. Whilst in the outer members all four positions (beam mid-span, beam end, column top and joint) the reinforcement positioned in the corners saw the greatest rise in temperature, with the beam mid-span and column top rising to 500°C.

In addition, Raouffard and Nishiyama (2016) also conduct a comparative numerical analysis, which presented how the embedded temperature of the reinforcement is not accurately captured through simulation.

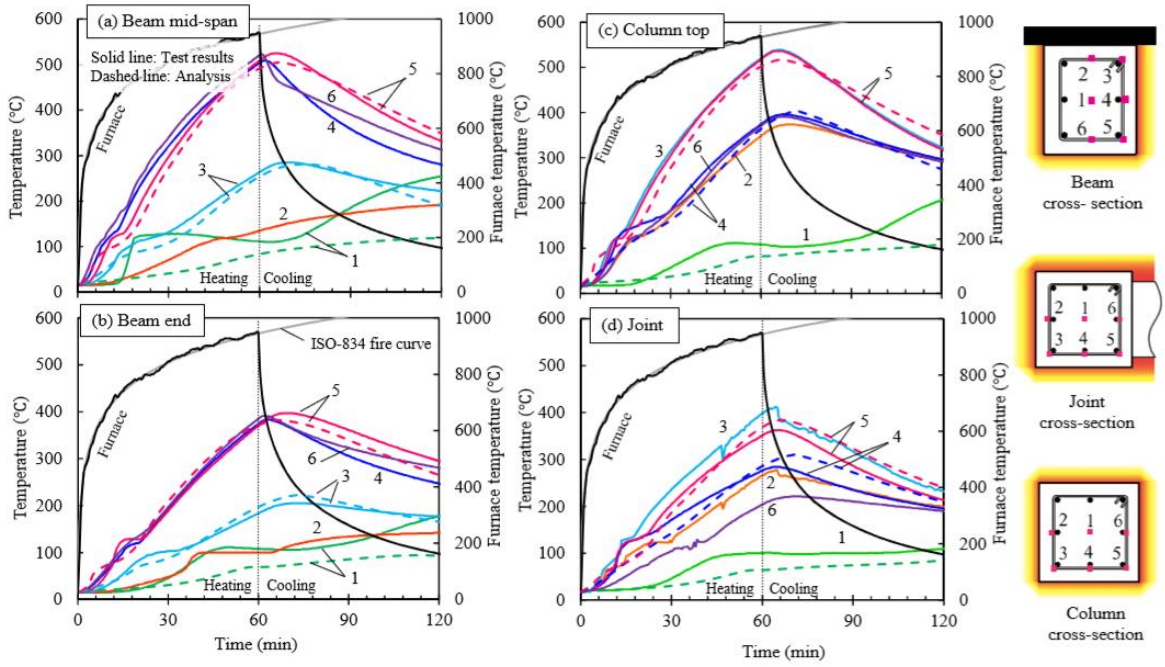

Figure 2-9: Summary of the actual temperature of reinforcing bar imbedded in concrete against the furnace (or radiant) temperature (Raoufford and Nishiyama, 2016).

Under the testing conditions of Raouffard and Nishiyama (2016), up until 600°C some cracking was observed, but no spalling. However, with prolonged exposure to fire, the concrete cover can be compromised due to either major external cracking or spalling. Spalling is the discharge of concrete from the surface layer due to concrete dehydration. Whilst external cracking is caused by thermal expansion of the reinforcement, cracking the concrete body with the assistance of concrete

dehydration. The bond between reinforcement and concrete is compromised in both scenarios, and the rebar is left exposed to the direct heating element. Dependent on the type of spalling, the outcome can be defined into one of four groups, during a fire this may be aggregate spalling which primarily does surface damage and is not of great concern. Corner spalling, which may see large pieces of concrete fail at the corner, further explaining why the study by Raouffard and Nishiyama (2016) found the corner pieces to show the highest rise in temperature. Explosive spalling, which can cause large pieces of concrete to fly off the concrete face and causing major structural damage. Post-cooling spalling, which can see the rapid drop of temperature expose the reinforcement. In Fig 2-10, Venanzi et al., (2008) shows how the rapid drop of temperature in concrete, following cooling by a fireman's hose, can through spalling, quickly leave concrete exposed and causing the rebar to fail.

Figure 2-10: Damage to a load bearing reinforced concrete column following a fire, leaving the steel exposed (Venanzi, et al., 2008)

When observing the damage done to concrete during a fire without external influences, such as a fireman's hose, the concrete performs well up to 700°C. Chang et al., (2006) presents the surface cracking of concrete when exposed to temperatures of 300°C, 500°C and 700°C then cooling through natural means inside a furnace. The surface of the 300°C presented minor cracking, whilst 500°C presented intermediate cracking and the 700°C presented major interlinked cracking. This can be seen in Fig. 2-11.

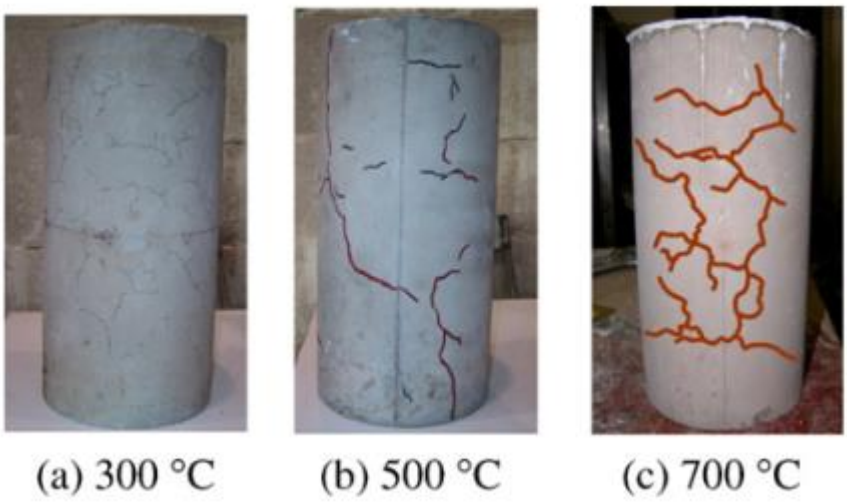

Figure 2-111: Cracking in concrete following heat treatment at (a) 300°C, (b) 500°C and (c) 700°C. Chang et al. (2006).

2.4.2 Fire Design of RC Structures

When considering the fire design of RC structures, Eurocode 2 (EN 1992-1-2) presents the most common spread rules for RC fire design. EN 1992-1-2 highlights the means of fire exposure on select members, under a variety of loading conditions, providing detailed guidance for RC elements. Guidance is provided solely for carbon steel reinforcement, with no guidance for stainless steel reinforcement. The guidance provided for the carbon steel is limited to elevated temperature exposure, with no guidance on post-fire reinforcement behaviour is given. Within the broader scope, Eurocode 3 (EN 1993-1-2) provides values for stainless steel structural members under elevated temperature conditions but does not include more recent grades such as 1.4362.

Other stainless steel rebar specific guides are scarce and of those available, such as the 'Guidance on the use of stainless steel reinforcement' by the Concrete Society (1998) and the 'Guide for the use of stainless steel reinforcement in concrete structures' by the Norwegian Building Research Institute (2006), provide no actual information on the fire design using stainless steel rebar. With the Concrete Society highlighting the behaviour of stainless steel rebar in fire as one of the most vacant research fields.

In more recent years, guidance for the elevated temperature behaviour stainless steel rebar has been published by Gardner et al., (2016), this is discussed independently later within this thesis.

2.5 Behaviour of Reinforcements and Structural Components

2.5.1 Stainless steel reinforcing bar

Current literature and previous studies into the post-fire performance and elevated temperature response of stainless steel rebars are limited. The complete works for the post-fire response are detailed in table 2-3. Felicetti et al., (2009) studied the mechanical response of rebars made from grade 1.4307 austenitic stainless steel, exploring cold-rolled and hot-rolled rebars. All of the specimens examined had a ribbed profile and were annealed. Zeng et al., (2012) presented some analysis on the post-fire response of grade 1.4401 rebars, although little details of the rebar specifications were provided (it is not known if the specimens were hot-rolled or cold worked, for example). In both of these experimental programs, the rebar specimens were heated to a target temperature of between 200 and 900°C, held at that temperature for a pre-determined period of soaking time, and then cooled to room temperature before a tensile test was conducted to obtain the post-fire tensile properties. Zeng et al., (2012) also included an analysis of the corrosion resistance of the rebars. Notably, both works cover austenitic rebars, and currently, there is no study into the duplex rebar response. Neither studies are conducted with the primary focus on presenting the residual tensile performance of stainless steel rebar, resulting in no recommendations for reduction factors. No design guidance is currently available for an engineer wishing to study the residual values of a stainless steel reinforced concrete structure following a fire and subsequent cooling.

Table 2-2: Previous research into the behaviour of stainless steel reinforcing bar.

		Heating			**Cooling**	
Source	Grade	Rate (°C/min)	Soaking time	Target temperature (°C)	Rate (°C/min)	Cooling method
Felicetti et al., (2009)	1.4307 (Cold-rolled and hot-rolled)	3	60mins	20, 200, 400, 550, 700, 850	3	Control cooling in Furnace
Zeng et al., (2012)	1.4401	n/a	60mins, 5hrs, 10hrs, 24hrs, 48hrs, 1 week	600, 700, 800, 900	n/a	Annealed

A study on the elevated temperature mechanical performance of stainless steel rebar was conducted by Gardner et al., (2016). Within this study, both isothermal and anisothermal testing was conducted on a total of 4 stainless steel grades (namely, grades 1.4307, 1.4311, 1.4162 and 1.4362). The

temperature range examined was from 20-1100°C, increasing in increments of 100°C. The study collected data for cold-rolled ribbed and plain bars in 12 mm and 16 mm diameter, recommends reduction factors based on the results and compares against the recommended reduction factors presented in EN 1992-1-2 (2004) based on cold-rolled carbon steel reinforcement. A two-stage Ramberg-Osgood expression adjusted for the elevated temperature response of stainless steel was also presented. The proposed reduction factors are presented in table 2-4.

Table 2-3: Reduction factors for stainless steel grades 1.4301 and 1.4362 as proposed by Gardner et al., (2016).

	Grade 1.4301			Grade 1.4362		
Temperature (°C)	$f_{0.2p}$	f_u	ε_u	$f_{0.2p}$	f_u	ε_u
20	1	1	1	1	1	1
100	0.8	0.86	0.56	0.83	0.94	1
200	0.67	0.77	0.42	0.75	0.87	1
300	0.62	0.74	0.42	0.69	0.79	1
400	0.58	0.74	0.42	0.58	0.7	1
500	0.53	0.68	0.42	0.43	0.59	1
600	0.48	0.59	0.33	0.27	0.47	1
700	0.39	0.43	0.25	0.14	0.33	0.8
800	0.28	0.26	0.15	0.07	0.2	0.6

2.5.2 Post-fire Stainless steel coupons

Although the focus of this thesis is stainless steel reinforcing bar in and following fire conditions, due to the scarcity of information directly associated with post-fire structural design, additional information is provided on stainless steel structural components and general materials.

Malaska et al., (2019) carried out an in-situ experiment on a 2.5m long grade 1.4301 austenitic stainless steel cellular beam to study the combined effects of mechanical and thermal loading. Following this, coupons where cut out by Molkens et al., (2020) from the cellular beam to conduct post-fire testing, these results where compared to a set of virgin coupons heated in a furnace and either quenched or naturally cooled. The study can be used to identify the comparison between a full scale fire test and singular coupons. The results showed that in comparison between the two studies, the shape of the dog bone coupon bared no influence on the final mechanical values. Whilst within the sets tested, there was an increase of yield strength of around 10-20%, against the virgin sample, at an exposure of level of 500°C and subsequent cooling.

Works of Gao et al., (2018) studied the behaviour of austenitic grades 1.4301 and 1.4401 stainless steel coupons following exposure to fire with either quenching or air-cooling. As the material did not

have any sort of strengthening mechanism, table 2-5 presents the minimum reduction coefficients having very little change in the yield and tensile strength.

Table 2-5: Reduction factors for austenitic grades 1.4301 and 1.4401 stainless steel coupons presented by Gao et al., (2018)

	Grade 1.4301		Grade 1.4401	
Temperature (°C)	$f_{0.2p}$	f_u	$f_{0.2p}$	f_u
20	1	1	1	1
200	0.96	0.99	0.99	0.99
300	0.96	0.99	0.99	0.99
400	0.96	0.99	0.98	1.00
500	0.96	0.99	0.98	1.01
600	0.93	0.99	0.97	1.01
700	0.81	1.01	0.96	1.01
800	0.88	1.010	0.92	0.99
900	0.83	1.00	0.89	0.99
1000	0.81	0.99	0.83	0.97
1100	0.70	0.96	0.79	0.94

On the literature of duplex stainless steel structural materials and coupons, work done by Tao et al., (2018) and Huang & Young (2018) are of interest. Tao et al., (2018) examined the residual post-fire response of two types of duplex coupons (1.4362 and 1.4462) to determine their full-range stress–strain curves following exposure to elevated temperature and subsequent air-cooling. Whilst Huang & Young (2018) examined a set of lean duplex grade 1.4162 coupons, in this examination the coupons where subject to localised heating in the fracture zone followed by subsequent slow-cooling. The grade 1.4362 and 1.4462 coupons both presented a rise in strength until 500°C followed by a slow decline, notably there is no sharp decline even following treatment to 1000°C. Within the works of Huang and Young (2018), the grade 1.4362 coupons show a consistent loss of both yield and tensile strength at every increment of temperature increase. The data taken from this literature will be later compared against the results collected.

2.6 Concluding Remarks

This chapter highlights the relevant existing information, with the objective of setting a contextual summary to an individual not familiar with the material properties presented later on. In summary, stainless steel is advantageous in selective scenarios compared to carbon steel in reinforced concrete, resulting in a gradual, steady rise in stainless steel use. To supplement this demand, engineers would

benefit from additional design documentation to address the post-fire response of the stainless steel reinforcing bar. Current information must be derived from either carbon steel reinforcements or structural stainless steel guidance, despite stainless steel in reinforcing bar form retaining unique properties.

The complete literature on stainless steel reinforcing bar exposed to elevated temperatures and subsequently cooled is covered, comparative information available on stainless steel structural members and coupons are also presented. Through this, the primary research gap is identified as stainless steel reinforcing bar currently lacking information on what the response would be following exposure to elevated temperatures. The information available in coupon form does not translate across due to the stainless steel grades used in rebar, due to the fundamental manufacturing method used in rebar, highlighted in section 2.2.3, causing a great variance in the final product. The performance of RC components within a fire scenario is also reviewed, highlighting the failure mechanisms and possible outcomes that would see the reinforcement exposed. These are of particular concern for stainless steel rebar, as stainless steel rebar is currently often used in extreme environments, making the failure of a concrete cover more likely.

For a practical study of the residual values after a fire scenario, the reinforcing bar should be studied with the objective of presenting adequate design guidance and further justifying this through a secondary material assessment. For the elevated temperature response, a single study has been conducted to understand the effects of stainless steel during a fire scenario. With little other information available, a practical study for confirmation of the results presented will be undertaken.

Chapter 3 Methodology

3.1 Introduction

This chapter aims to present detailed information on the practical testing programme used in this thesis, covering the materials selected as well as the methods used in the testing. The data collected throughout the practical testing programme can be broken down into three distinct categories. First is the residual tensile performance following a fire scenario and subsequent cooling. Second is the metallurgical investigation carried out to understand the tensile results further. The third is the elevated temperature tests, which assess the performance of the rebar when exposed to live fire conditions. The residual tensile testing and elevated temperature evaluation were carried out in the Civil Engineering laboratories at Brunel University, whilst the material investigation was conducted in the Experimental Techniques Centre (ETC), also at Brunel.

3.2 Pre-Testing Procedure

3.2.1 Material Selection – Rebar Choice and Specifications

A key aim of this work was to study material that is commonly used by engineers in practice and likely to be available from a supplier. Accordingly, the reinforcement was selected based on the available stock at local suppliers in the UK and Europe. Three different types of austenitic stainless steel reinforcement, two variations of the same grade of duplex stainless steel and one carbon steel rebar were included in the test programme, and the composition of each is given in table 3-1. The data in the table was provided by the suppliers whilst the limits are given in BS EN 10088-1 (2014). The

austenitic and carbon steel rebars are all cold-rolled, whilst for the duplex, one of each cold-rolled and hot-rolled batch is used.

The materials examined include:

i. Grade 1.4301 (in accordance with BS EN 10088 but also known as grade 304) with a diameter d of 8 mm: the cheapest and most commonly available chromium-nickel austenitic stainless steel reinforcement, which offers moderate corrosion resistance as well as good strength, stiffness and durability and excellent ductility.

ii. Grade 1.4401 (also known as grade 316) with a diameter d of 12 mm: a chromium-nickel-molybdenum stainless steel with very good corrosion resistance (similar level to the duplex grades) owing to the high molybdenum content, which also makes it more expensive than grade 1.4301 in terms of initial costs. Therefore, it is commonly employed in harsh environments such as marine or industrial settings. In terms of mechanical properties, it offers characteristics that are comparable to carbon steel in terms of strength, ductility, and stiffness.

iii. Grade 1.4436 (also known as grade 316L) with a diameter d of 8 mm: this is a very low carbon stainless steel, designated by the "L", which is otherwise similar to grade 1.4401 as described above. Grade 1.4436 has improved resistance to intergranular corrosion in the heat-affected zone (HAZ) of welds.

iv. Grade 1.4362 (also known as grade 2304) with a diameter d of 8 mm and 12 mm: this is a duplex stainless steel and a popular choice for reinforced concrete owing to its excellent combination of outstanding mechanical behaviour and corrosion resistance as well as cost-effectiveness. This has resulted in grade 1.4362 often being the only readily stocked duplex grade rebar.

v. Grade B500B carbon steel with a diameter d of 8mm: this is a common carbon steel rebar, offering moderate tensile properties but poor corrosion resistance. Carbon steel rebar is cheap to manufacture due to the lack of precious elements used in the alloy and is more readily available than stainless steel, making it ideal to use in structures that are at low risk from corrosion.

Table 3-1: Composition and method of production of tested steels.

Grade **Method of Production**	1.4301 *Cold-rolled*	1.4401 *Cold-rolled*	1.4436 *Cold-rolled*	1.4362 *Cold-rolled*	1.4362 *Hot-rolled*	B500B *Cold-rolled*
	Element (%wt)					
%C - Carbon	0.032	0.023	0.028	0.016	0.020	0.200
%Mn - Manganese	1.720	1.438	1.360	1.595	1.30	0.570
%Si - Silicon	0.460	0.366	0.360	0.509	0.680	-
%S - Sulphur	0.004	0.027	0.007	0.001	0.001	0.030
%P - Phosphorus	0.039	-	0.031	-	0.027	0.028
%Ni - Nickle	8.100	10.54	10.540	4.050	4.280	0.160
%Cr - Chromium	18.400	16.685	16.670	22.755	23.44	0.170
%Mo - Molybdenum	0.240	2.049	2.530	0.198	0.320	0.037
%N - Nitrogen	0.183	0.046	0.061	0.115	0.090	0.010
%Cu - Copper	-	0.317	-	0.308	0.460	0.490
%Ti- Titanium	-	0.005	-	0.022	-	-
%V - Vanadium	-	-	-	-	-	0.002

3.2.2 Specimen Categorization

Within this thesis, a reference system is adopted to label each specimen as follows: the first parameter denotes the material grade (either 1.4301, 1.4401 or 1.4436 for austenitic stainless steels and B500B for carbon steel, for duplex grades either H for hot-rolled and C for cold-rolled is added to the material grade of 1.4362), next is the target elevated temperature whilst the final parameter describes the cooling method used where Q is for quenched in water, A is for air-cooling, and S is for slow-cooling.

3.3 Heating and Cooling Cycles

The heating and cooling cycles were planned out with consideration to imitating a real-life fire scenario. The specimens were heated to a target temperature ranging from 100-900°C for the austenitic and carbon samples and 500-900°C for the duplex samples, at intervals of 100°C, in a Carbolite CWF 1100 furnace equipped with a Eurotherm 3216 control module at a rate of 10°C/min. The temperature measured was of the environment temperature within the chamber. Work done by Twilt (1998) found that when heating steel, a heating rate of between 5-50°C/min may be considered realistic, with 10°C considered to be a reasonable rate for a regular fire (Twilt, 1988). Although this work was focused on structural steel sections, it gives an indication of how temperature spreads through steel during a fire. Following this, the target temperature was maintained for 1 hour. The soaking time of 1 hour allowed for the stainless steel rebar to have adequate time for a mature microstructural transformation. This is especially important for rebar exposed to temperatures above

the critical recrystallisation temperature point of 727°C to gain an accurate understanding of the most unpredictable scenarios.

The highest temperature examined was 900°C and this was considered to be the upper bound for the temperature that rebar is likely to reach in a real fire. Moreover, if the bars were exposed to higher temperatures, they would deform to such an extent that they would not retain structural integrity. In this scenario, it is likely that large deflections will occur along with excessive cracking of the concrete, and therefore the rebars can reach very high temperatures. Fig. 3-1 shows the surface state of the grade 1.4301 rebars following exposure to various levels of elevated temperature and subsequent cooling by quenching the bars in water. It is clear that there were increasing levels of surface discolouration following exposure to higher temperatures.

The temperature exposure along the rebar was uniformly distributed, in a practical scenario if the cover is not exposed a slight uniform distribution would be seen due to the concrete acting as an oven enclosing the rebar. Whereas if the concrete proceeds to show major cracking or spalling, a more localised temperature spike would be seen on the rebar. Locally distributed heat exposure is more probable in a practical scenario, however within this study due to the stainless steel rebar showing an increase in both the yield and ultimate strength and the overall total length of the specimen being limited to 300mm, a uniform method of heat distribution was used to avoid failure outside of the heated zone. For the elevated temperature testing, presented in 3.3.3, a local heat distribution is used.

Figure 3-1: Grade 1.4301 following exposure to elevated temperature and subsequent cooling.

Following the heating phase of the programme, the specimens were cooled by one of three methods in order to determine the influence that cooling rate has on the post-fire behaviour. The cooling methods were selected to replicate the range of realistic scenarios and included (i) quenching in water, the most rapid method of cooling, to simulate a scenario in which firefighters hose down the specimen forcing a sudden drop in temperature, (ii) natural air-cooling, which is an intermediate cooling method in terms of rate and simulates a scenario where the rebar is left exposed following a fire and allowed to cool at a natural pace and (iii) slow-cooling, a slow, controlled cooling method inside the furnace at a rate of 1°C/min, which is to replicate a scenario in which the concrete layer does not expose the rebar, allowing for slower cooling over time. This resulted in three repetitions being carried out for every grade of rebar tested per temperature point. Fig. 3-2 presents an indictive diagram of the three cooling methods used within this thesis.

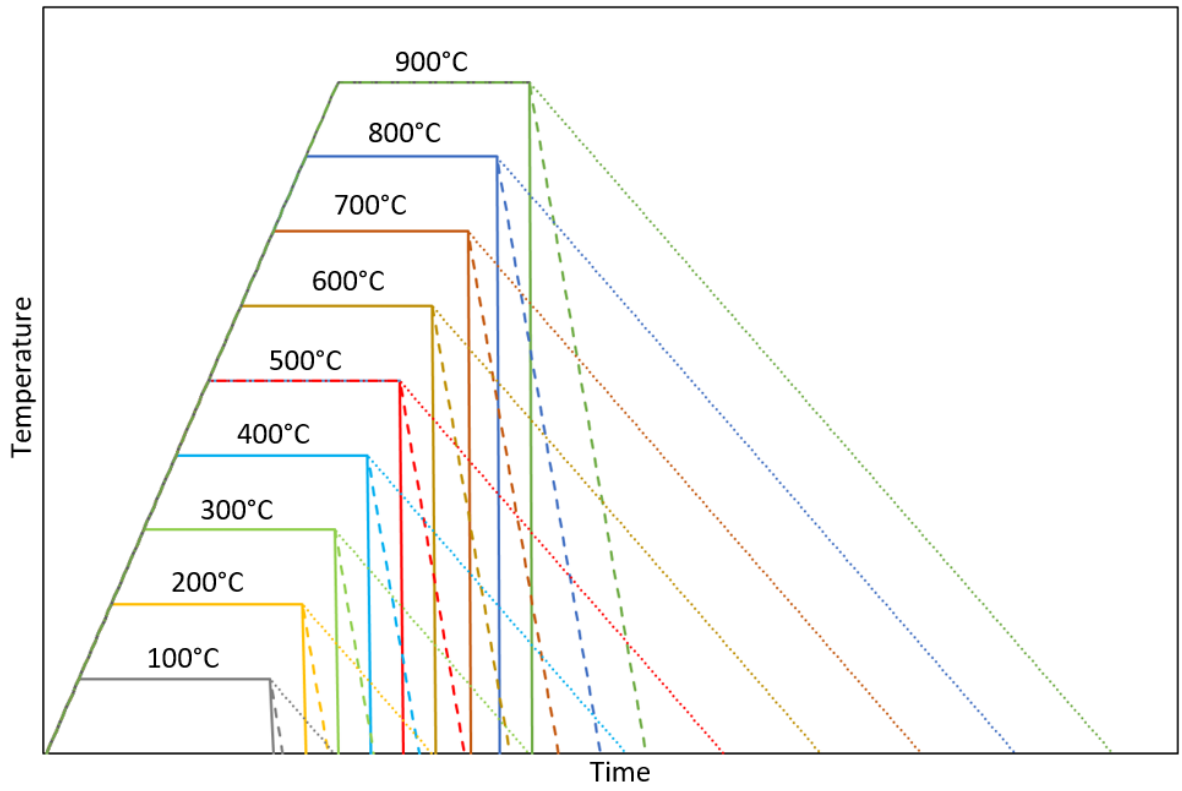

Figure 3-2: Temperature time relation of the three cooling methods used, with the solid lines presenting rapid-cooling through quenching in water, the dashed lines as natural air-cooling and the dotted lines as slow-cooling.

3.4 Testing Procedure

3.4.1 Residual Tensile Testing Setup and Standards

For the residual tensile testing, a total of 180 different specimens were examined for all stainless steel grades and the additional carbon steel grade. The specimens were pre-cut by the manufacturer to a length of 300 mm, as shown in Fig. 3-3. The diameter range shown is where the measurement was taken to calculate the cross-sectional area for the tensile coupon testing. This was measured from the actual bar, excluding the ribbing. The tensile tests were conducted in accordance with the guidance given in BS EN ISO 6892-1 (2016), and the samples had a total length (L_t) of 300 mm, a gauge length (L_0) of 50 mm and a parallel length (L_c) between the gripping jaws of 200 mm. A 10 kN preload was first applied to each specimen at a rate of 0.05 mm/min, as suggested by Huang and Young (2014). Then, an initial strain rate of 0.00007 s-1 was applied until a strain value of 1% was reached, followed by increasing the strain rate to 0.00025 s-1 over 5 minutes. This strain rate was maintained until fracture of the rebar occurred.

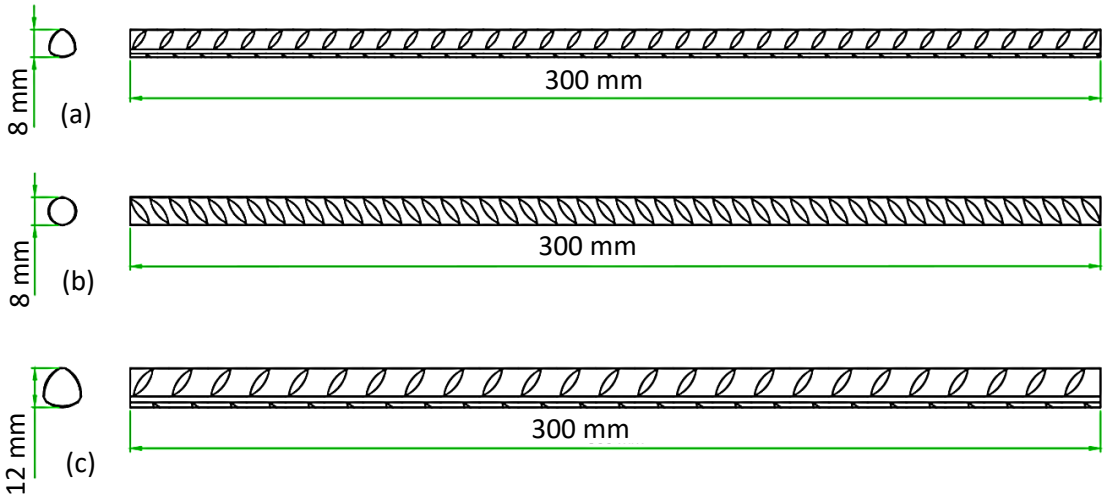

Figure 3-3: The ribbed rebar used in testing, with (a) for grades 1.4301 and 1.4436, (b) for 1.4362H and B500B and (c) for 1.4401 and 1.4362C.

The testing was conducted using an Instron 5584 electromechanical testing frame with a maximum load capacity of 150 kN. The strain measurements were recorded using an Instron EX2620-601 extensometer, as shown in Fig. 3-4, which recorded up to around 10% total strain. Higher strains were measured by the testing machine, and these values were corroborated using the extensometer data. In addition, in order to obtain a direct and reliable measurement after cooling of the ultimate tensile strain, the rebars were marked clearly at 10 mm intervals before testing, and then the final strain post-testing was determined by carefully placing the bars back together and measuring the total length between adjacent markings in the location of the break.

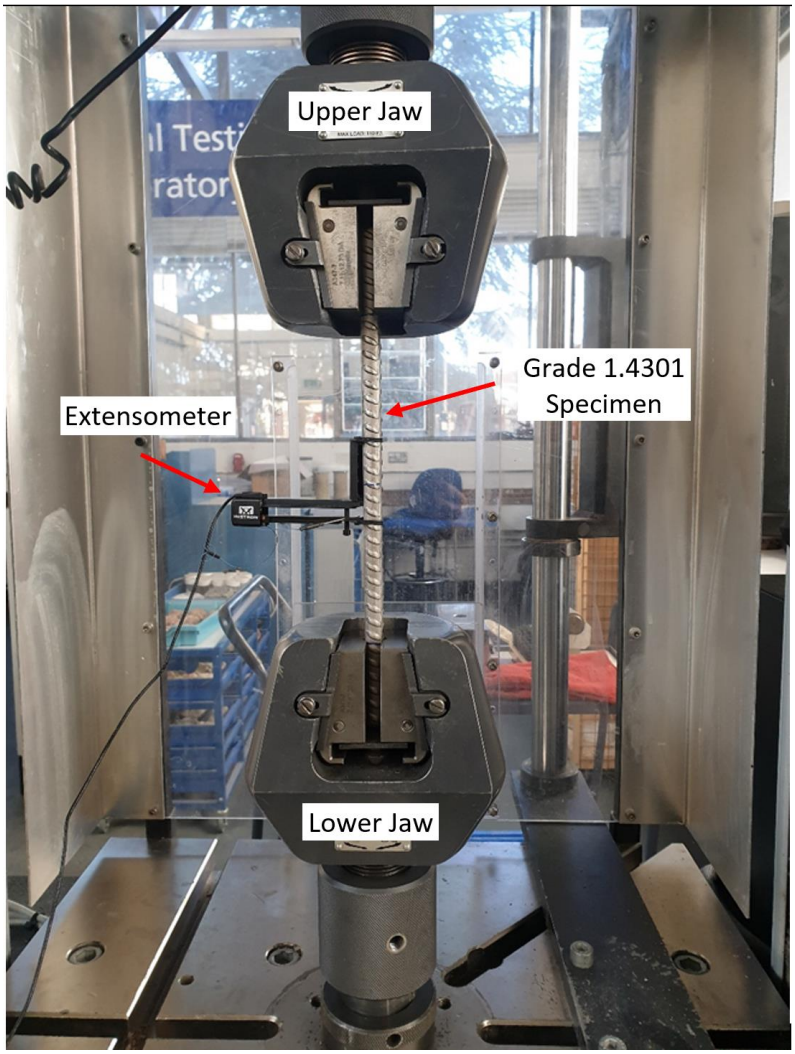

Figure 3-4: Setup for tensile testing on Instron 5584 frame with EX2620-601 extensometer.

3.4.2 Residual Material Preparation for Material Investigation

A total of 167 tests were conducted for the material investigation, 150 for a phase analysis using an X-Ray Diffractor (XRD), followed by 17 using a Scanning Electron Microscope (SEM), only the stainless steel grades were investigated. For the material investigation, care was taken to nullify unnecessary heat transfer by using waterjet cutting to prepare 15mm specimens; these were then either hand-polished or mounted in cold resin to polish before testing. The investigation was undertaken on the cross-sectional face of the rebar offcuts taken from the same manufacturing batch as the corresponding rebar in used for tensile testing. As stated before, a key aim of this study is to understand the relationship between the tensile performance of stainless steel rebars and their evolving metallurgical characteristics following exposure to various levels of elevated temperature and subsequent cooling. Accordingly, in this part of the investigation, the samples were initially inspected at each level of elevated temperature exposure and subsequent cooling method through a

phase identification analysis. Then, the samples with the most notable changes underwent further examination through a grain inspection.

The X-ray diffraction (XRD) was used as the primary method for the phase identification analysis, and this was carried out using a Bruker D8 Advance diffractometer, equipped with a copper source and Lynxeye position-sensitive detector. The data is presented in diffractograms, where the presence of the phase (intensity) is measured against the angle of discovery (2theta); these diffractograms were processed in the DIFFRAC.EVA phase identification software. The objective was to identify and monitor any phase changes that may occur during the heating and cooling cycle. For the grain inspection, a Zeiss Crossbeam was used; this utilised the use of a Transmission Electron Microscope (TEM) to provide highly magnified clear images. The images were then analysed using the Fiji Image software to obtain a visual inspection of the size, shape and dispersion of the grains.

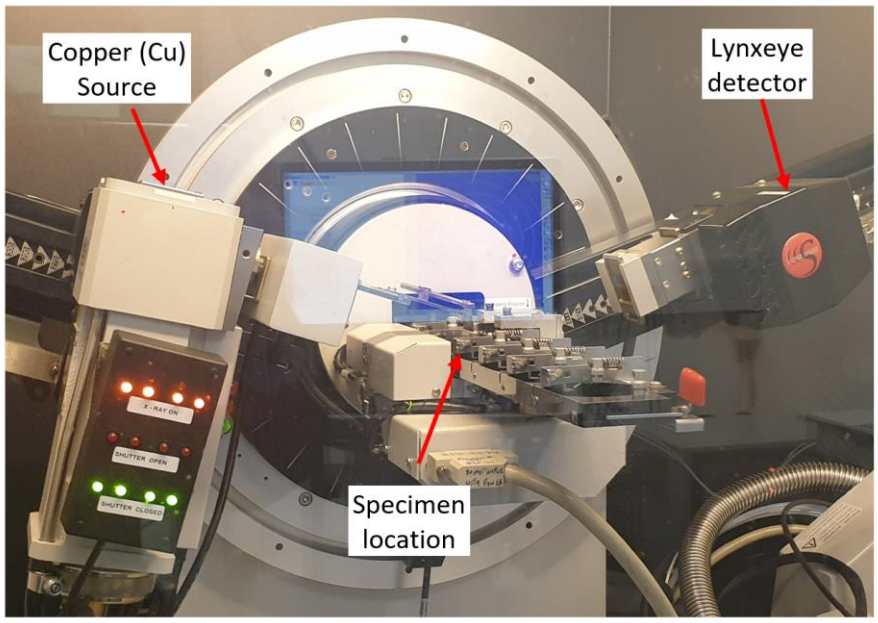

Figure 3-5: Bruker D8 Diffractor setup for phase analysis.

3.4.3 Elevated Temperature Testing

In the elevated temperature testing programme, a total of 18 specimens were tested. The grades selected for this experimental programme were austenitic grade 1.4301 and duplex grade 1.4362 reinforcing bar. Both bars were manufactured through cold-rolling to a diameter d of 12 mm. The aim of the testing was to understand further the isothermal performance of the stainless steel reinforcing bar. The testing setup compromised the Instron 5584 150kN electromagnetic testing frame with an Instron SF-16 2230 furnace and a three-zone Eurotherm 2416 temperature control unit for the

elevated temperature testing. For the strain measurement, an extended EX2620-601 extensometer was used. The actual extensometer is positioned underneath the furnace to prevent damage, whilst the strain measurement is translated through Inconel grade extensions mounted in the critical heating zone. The complete setup is shown in Fig. 3-6. The isothermal testing was conducted with guidance from BS EN ISO 6892-2 (2018). Each sample had a total length (L_t) of 750 mm, a gauge length (L_0) of 50 mm and parallel length (L_c) between the jaws of 650 mm, and the heating zone was localised to the central 300 mm, whilst the actual temperature was only achieved in the central 50 mm zone used for stain measurement.

The elevated temperature range chosen for the programme was 100°C to 800°C, rising in increments of 100°C. For the heating regime, the samples were exposed to a rise in temperature at a rate of 10°C/min until the target temperature was reached. Following this, all samples were soaked in the target temperature for 1 hour before loading. For the loading, a 10 kN preload was applied to all samples after the heating regime to remove slack, and then samples were subjected to a continuous displacement of 0.5 mm/min until absolute failure.

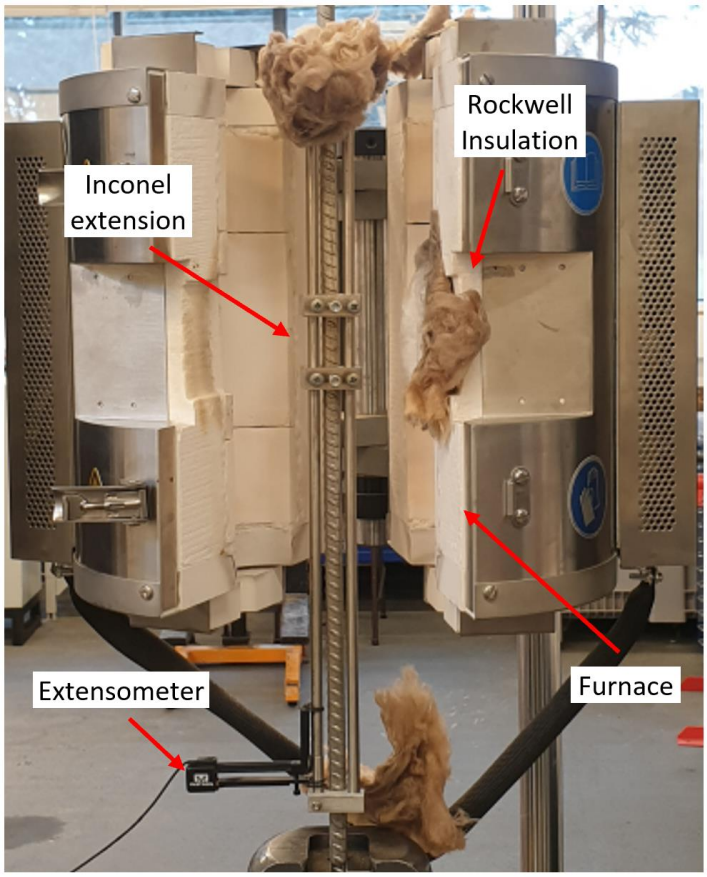

Figure 3-6: Complete test setup for elevated the temperature testing.

3.5 Concluding Remarks

This chapter summarises the practical examination methodology and procedures used within this thesis. In summary, the samples selected for testing are sourced from UK and EU suppliers and present an accurate representation of commercially available samples. A total of three different austenitic stainless steel grades, one duplex stainless steel grade with the two manufacturing variations and a commonly-employed “regular” carbon steel grade are included in the study.

For the testing procedure in the post-fire scenario, each grade undergoes the same variety of heating and cooling cycles, and then tensile testing. The metallurgical investigation is broken down into two parts, a broad XRD examination to identify any phase changes and then a detailed microstructural investigation through microscopic imaging. For the elevated temperature testing, tensile testing is carried out under isothermal conditions using a custom Inconel extension.

Chapter 4 Residual Response of Austenitic Stainless Steel Reinforcing Bar

This chapter presents and discusses the results obtained from testing the austenitic grades 1.4301, 1.4401 and 1.4436. As discussed previously, the tests included both tensile testing in the form of tensile coupon tests as well as a detailed metallurgical examination. For the tensile testing, all three grades where tested and presented varied results, whilst for the phase analysis all three displayed a similar response, resulting in only 1.4301 being further analysed and presented for the complete material analysis. Nevertheless, before the austenitic data can be presented, it is important to set a comparative benchmark to compare the austenitic data against and, as such, the tensile data for carbon steel grade B500B reinforcement is first presented.

4.1 Tensile Response of Carbon Steel B500B

The full stress-strain responses for the B500B carbon steel reinforcing bars, with a dimeter d of 8 mm, following exposure to various levels of elevated temperature followed by different cooling methods are shown in Fig. 4-1 for (a) the quenched samples, (b) the air-cooled samples and (c) the slow-cooled rebar samples. In addition, the data from the tests is given in table 4-1. It is noteworthy that these bars were cold-rolled during the production process, images of the rebar samples following testing are presented under appendix A in Fig A.4-1. Within the 300mm sample piece, the fracture zone was continuously centred into the central 50mm area measured by the extensometer. The first observation from the results is that, as expected, the overall shape of the stress-strain curves is quite different to those for the stainless steel bars, which are presented later in this thesis. In most cases, the carbon steel samples developed a clear yield point, followed by a yield plateau and then a small

degree of strain hardening with less overall ductility than the stainless steel samples. On the other hand, the stainless steel specimens had a more rounded, continuous constitutive response.

Table 4-1: Post-fire properties of Carbon Steel Grade B500B rebar. Labelled as the temperature of exposure followed by either -Q for quenched, -A for air-cooled and -S for slow-cooled.

	B500B					
Specimen	E (GPa)	$f_{0.2p}$ (N/mm^2)	f_u (N/mm^2)	ε_u (%)	ε_f (%)	n
Virgin	212.0	530.9	628.1	11.7	16.2	1.0
100°C-Q	201.2	533.2	621.8	10.5	12.5	1.0
200°C-Q	198.8	520.3	613.5	11.4	13.1	1.0
300°C-Q	197.1	513.2	615.3	10.7	15.0	1.0
400°C-Q	199.5	548.3	642.3	11.8	16.1	1.0
500°C-Q	194.6	559.4	657.9	13.1	17.7	1.0
600°C-Q	220.0	565.8	648.6	13.7	18.5	1.0
700°C-Q	209.5	479.5	583.9	13.9	18.6	1.1
800°C-Q	186.8	731.9	1130.3	1.9	2.6	0.9
900°C-Q	191.6	756.2	1070.1	2.7	3.4	0.9
100°C-A	198.5	527.2	620.1	12.2	16.5	1.0
200°C-A	218.6	531.3	611.4	12.0	13.8	1.0
300°C-A	199.2	532.4	628.7	14.1	19.1	1.0
400°C-A	217.4	533.1	625.3	11.2	15.5	1.0
500°C-A	203.3	533.0	624.9	12.7	17.4	1.0
600°C-A	197.0	526.4	611.6	14.7	19.4	1.0
700°C-A	202.5	438.2	526.3	13.1	17.8	1.1
800°C-A	201.0	392.2	528.6	24.5	30.9	1.1
900°C-A	215.5	336.7	505.7	23.0	28.2	1.2
100°C-S	209.1	536.0	628.1	13.0	17.5	1.0
200°C-S	201.7	532.2	618.5	11.5	13.4	1.0
300°C-S	204.7	535.4	628.6	11.5	15.8	1.0
400°C-S	199.5	522.8	618.1	10.8	13.3	1.0
500°C-S	205.2	523.9	618.2	11.6	16.0	1.0
600°C-S	197.0	524.7	600.6	15.5	20.4	1.0
700°C-S	192.9	423.6	510.9	14.9	19.6	1.2
800°C-S	198.6	327.7	468.4	27.6	33.6	1.2
900°C-S	197.2	280.7	449.5	25.5	31.8	1.3

With reference to the data in table 4-1, there are a number of interesting observations on the behaviour. Firstly, for the quenched samples, following exposure to relatively low elevated temperatures (up to 300°C), $f_{0.2p}$ and f_u reduced by 0-3% after cooling, respectively. On the other hand, for the samples that were cooled more slowly using the other methods, these corresponding values were almost identical to the virgin values, with no significant difference between the residual and virgin values observed. For all cooling methods, there was no notable difference in the residual strain

values following exposure to up to 300°C compared with the original values. Following exposure to higher temperatures, from 400°C-600°C, the residual values $f_{0.2p}$ and f_u increased by up to 7% and 5%, respectively, after quenching in water. The air-cooled and slow-cooled samples at 400°C and 500°C continued to retain $f_{0.2p}$ and f_u values almost identical to the virgin specimen, at 600°C, the $f_{0.2p}$ and f_u showed a loss of 1% and 3-4%, respectively. The residual strain values also showed an increase compared with the corresponding virgin values – these increases were between 17-32% for ε_u and 14-26% for ε_f. It is noted that the increase in residual strains was inversely related to the speed of cooling and therefore the greatest increase in residual ε_u and ε_f values occurred for the specimens that were cooled most slowly.

For the bars that were heated to higher temperatures, there was more significant changes to the residual properties. Following exposure to 700°C, the residual $f_{0.2p}$ and f_u values reduced by 9-20% and 7-19%, respectively. The corresponding residual strain values ε_u and ε_f increased by 12-27% and 10-21%, respectively, compared with the virgin values. Following exposure to higher temperatures of 800°C and above, there were clear changes in the residual behaviour, and these were more dependent on the cooling method compared with the other samples examined. With reference to Fig. 4-1(a), the bars that were cooled quickly by quenching in water had a significant change in stress-strain response following exposure to temperatures of 800-900°C. There was a significant increase in residual strength of 38-42% for $f_{0.2p}$ and 70-80% for f_u, against the virgin sample, and this was accompanied by a more sudden and less ductile failure. The is because the bars were effectively annealed; there was a change in phase and then the annealing occurred through quenching in water. The total strain at failure ε_f presented a loss of 84% for 800°C and 79% for 900°C against the virgin sample. This is caused by the carbon steel rebar being heated above the phase transformation temperature of 737°C and then being rapidly cooled, inducing the transformation of martensite, resulting in a stronger but more brittle rebar (Bhadeshia and Honeycombe, 2017).

The air-cooled and slow cooled samples exposed to temperatures of 800°C above presented a decline in strength and increase in strain. The residual $f_{0.2p}$ and f_u values reduced 26-47% and 16-28% respectively, when compared to the virgin sample. The residual strain values presented the greatest rise at 96-135% for ε_u and 74-107% for ε_f against the virgin sample.

Fig. 4-2 presents the results for the carbon steel rebars that were heated to 500°C, 700°C and 900°C and then cooled in the three different regimes, to directly assess the influence of cooling rate on the residual properties. As stated before, there was clearly a quite notable difference in the response for B500B-800-Q and B500B-900-Q, owing to the successful transformation to the martensite phase. For the other samples, in all cases, the quenched samples which were cooled the quickest in this test

series had the greatest residual strength regardless of the temperature that they were exposed to. This was followed by the air-cooled samples, whilst the slow-cooled samples had the lowest residual strengths. The residual strain increase for the slow-cooled samples was constantly greater than the air-cooled samples.

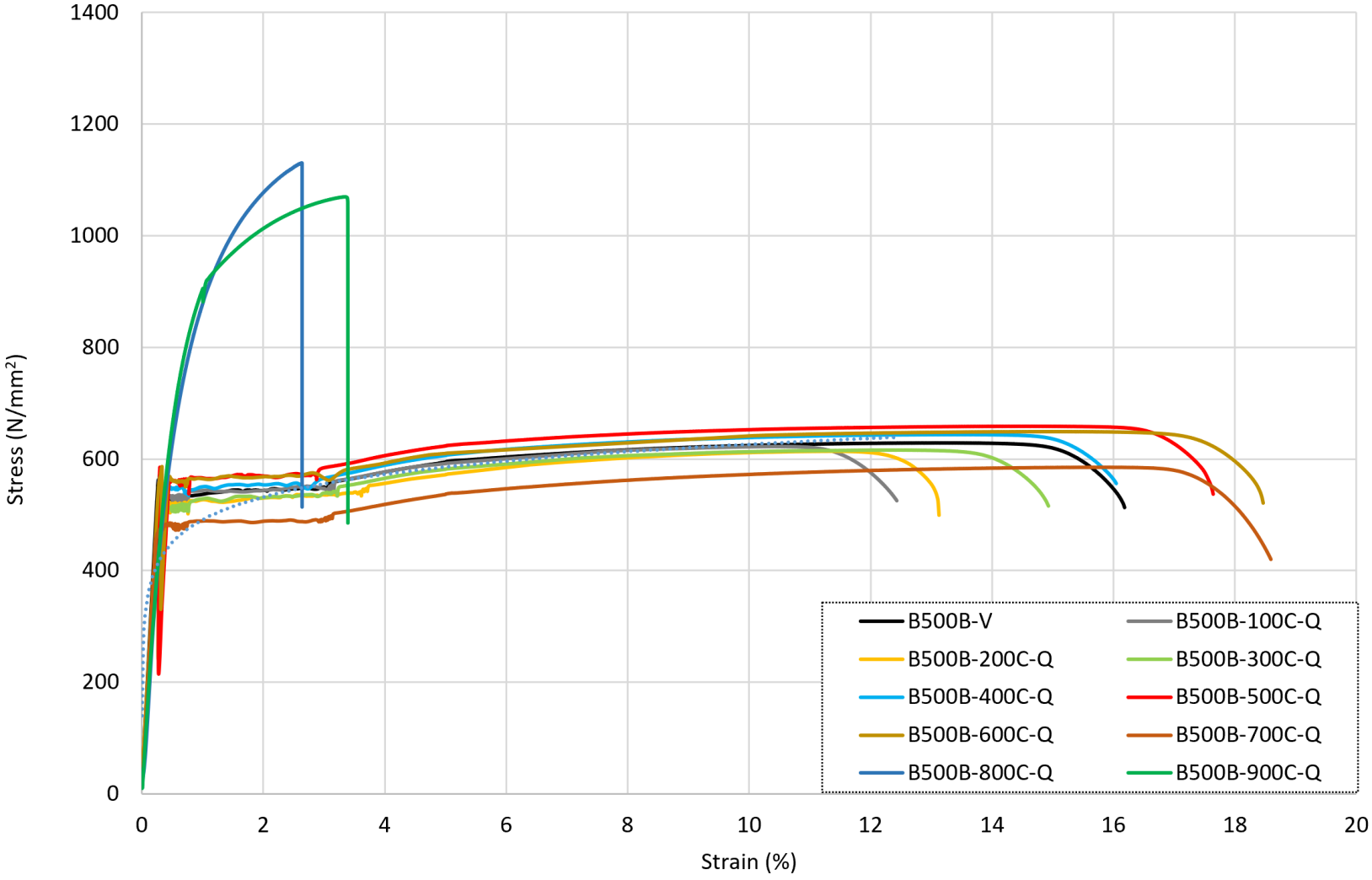
1400
1200
1000
800
600
400
200
0
Stress (N/mm²)
0
2
4
6
8
10
12
14
16
18
20
Strain (%)
B500B-V
B500B-100C-Q
B500B-200C-Q
B500B-300C-Q
B500B-400C-Q
B500B-500C-Q
B500B-600C-Q
B500B-700C-Q
B500B-800C-Q
B500B-900C-Q

(a)

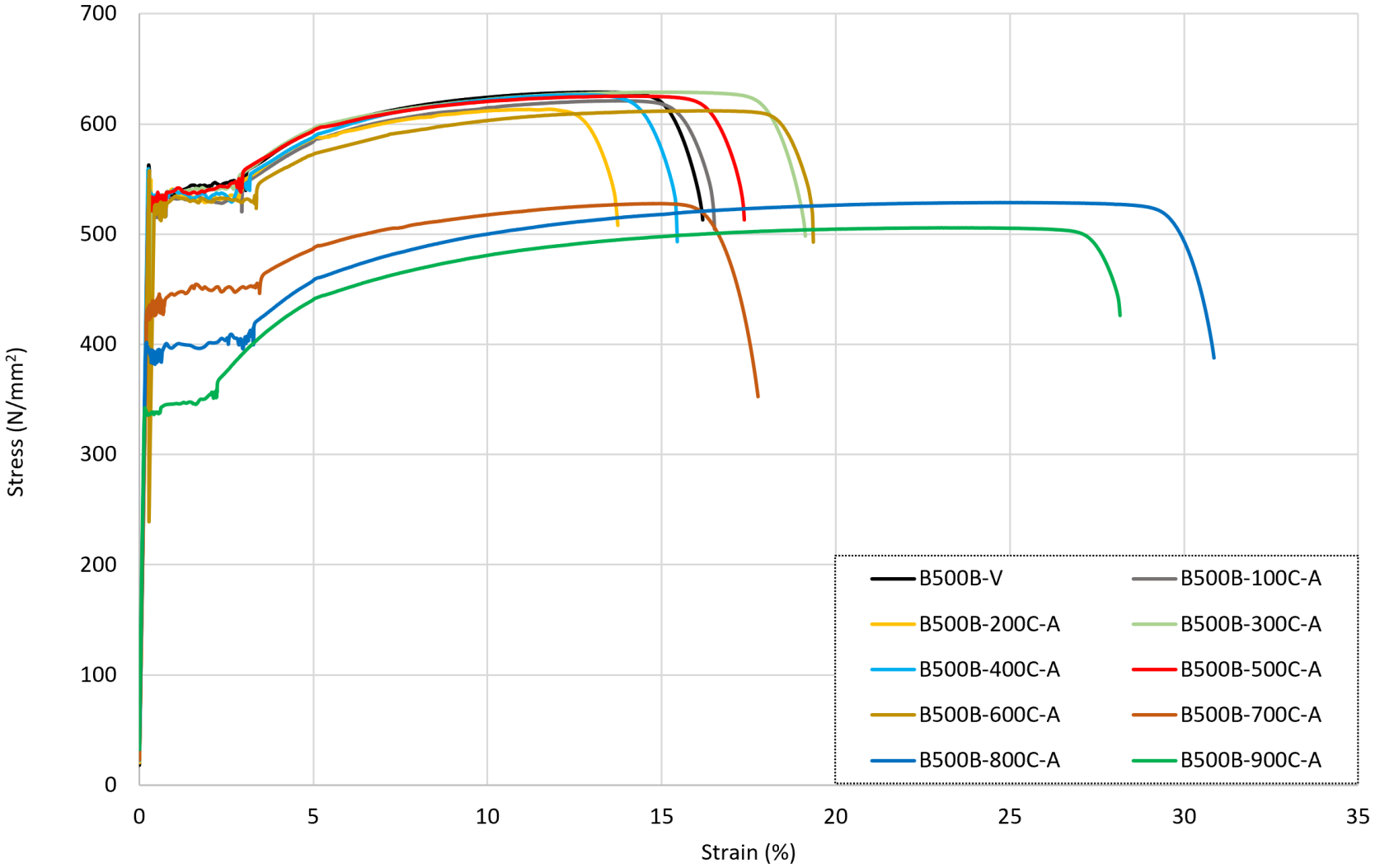
700
600
500
400
300
200
100
0
Stress (N/mm²)
0
5
10
15
20
25
30
35
Strain (%)
B500B-V
B500B-100C-A
B500B-200C-A
B500B-300C-A
B500B-400C-A
B500B-500C-A
B500B-600C-A
B500B-700C-A
B500B-800C-A
B500B-900C-A

(b)

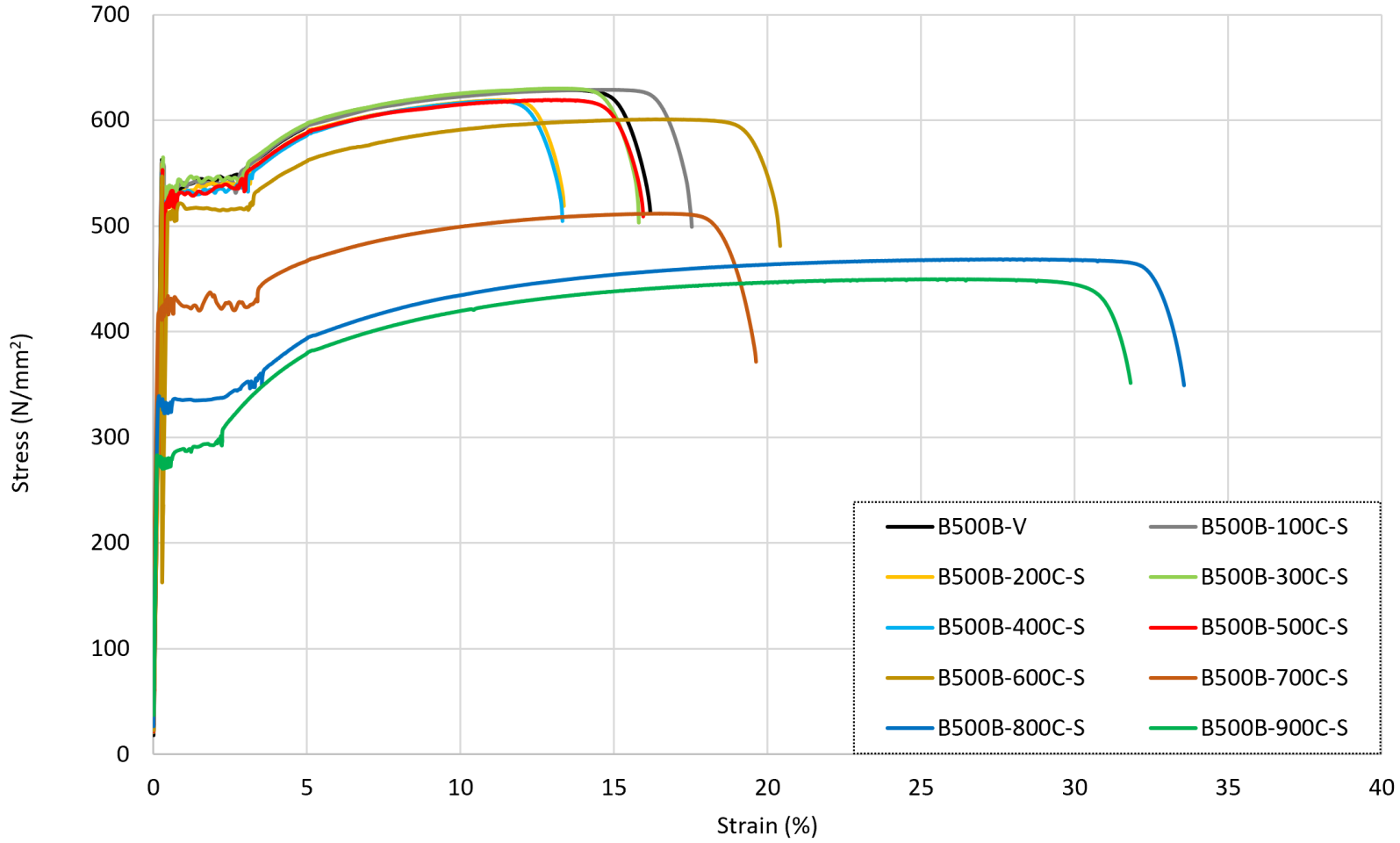

(c)

Figure 4-1: Stress-strain responses for B500B carbon steel rebars following exposure to elevated temperature and then (a) quenched in water, (b) cooled naturally in air and (c) slow-cooled in the furnace.

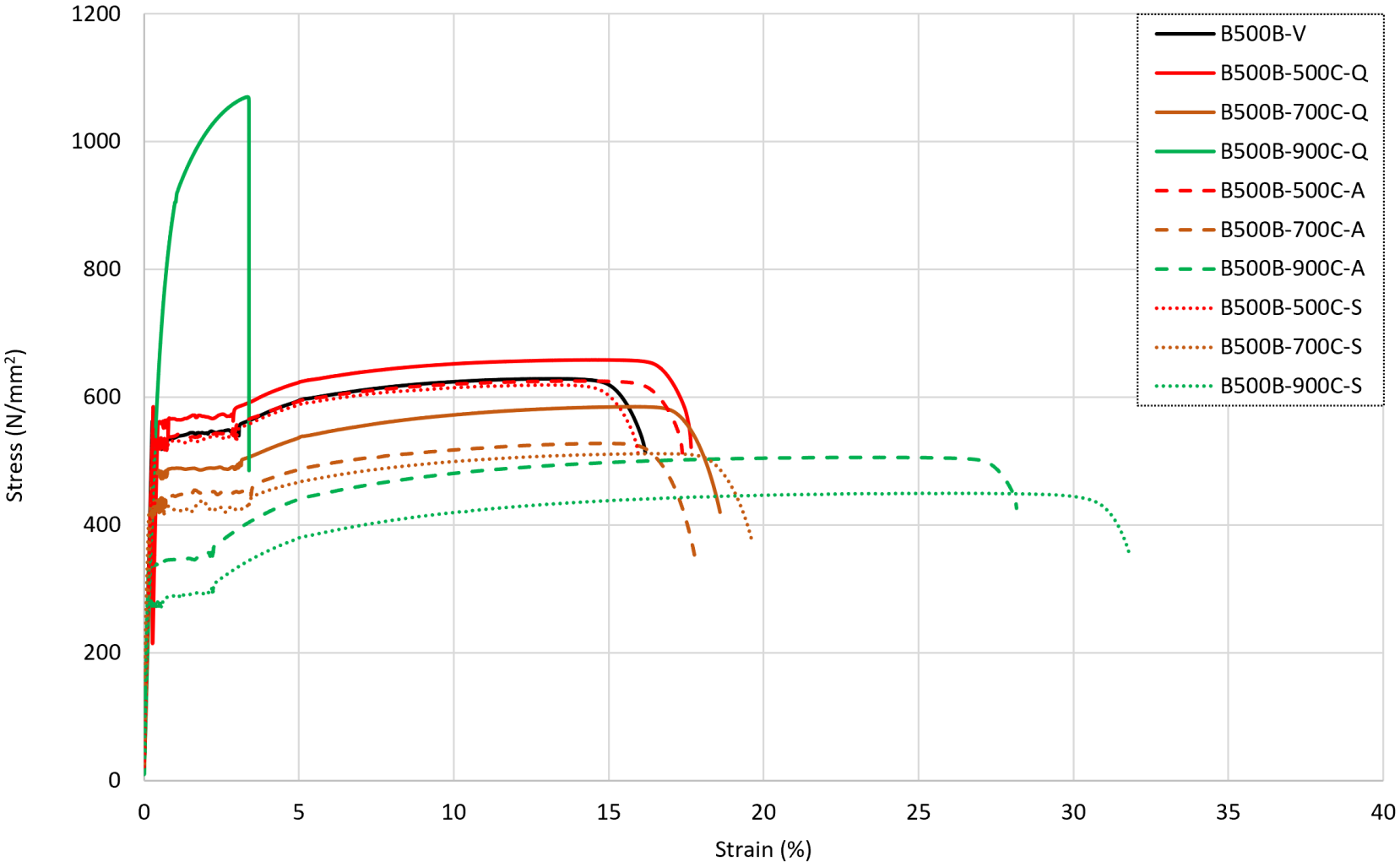

Figure 4-2: Stress-strain responses for grade B500B carbon steel rebars following exposure to 500°C, 700°C and 900°C followed by cooling.

4.2 Tensile Response of Steel Grade 1.4301

The full stress-strain responses for grade 1.4301 samples, with a diameter d of 8 mm, following exposure to various levels of elevated temperature and then cooling are presented in Fig. 4-3 for (a) samples that were cooled by quenching in water, (b) rebars that were air-cooled, and (c) the slow-cooled bars. In addition, the data from the tests is given in table 4-2. It is clear that following low-to-moderate levels of heat exposure, up to around 500°C, the strength was completely retained, and even marginally increased in some cases compared with the virgin unheated samples. In addition, the ductility remained relatively unchanged. When inspecting the post-test rebar, the fracture surface remained consistent to the central region, as with the carbon steel rebar. This can be seen Fig A.4-2 in Appendix A.

Table 4-2: Post-fire properties of Austenitic Grade 1.4301 rebar. Labelled as the temperature of exposure followed by either -Q for quenched, -A for air-cooled and -S for slow-cooled.

Grade	1.4301					
	E (GPa)	$f_{0.2p}$ (N/mm^2)	f_u (N/mm^2)	ε_f (%)	ε_u (%)	n
Virgin	192.3	727.3	910.7	9.7	23.5	0.9
100°C-Q	183.5	758.0	915.5	9.6	24.8	0.9
200°C-Q	189.0	784.8	934.9	9.6	19.9	0.9
300°C-Q	185.3	799.6	920.5	9.7	19.9	0.9
400°C-Q	183.4	813.7	934.1	9.6	19.1	0.9
500°C-Q	191.5	834.4	953.8	9.7	19.3	0.9
600°C-Q	195.1	792.3	943.5	16.2	22.6	0.9
700°C-Q	194.1	720.0	900.6	22.0	28.7	0.9
800°C-Q	181.9	461.9	773.1	38.0	44.1	1.1
900°C-Q	181.9	320.1	716.0	56.7	63.5	1.3
100°C-A	190.2	744.9	922.8	9.7	21.8	0.9
200°C-A	186.8	750.2	911.8	9.6	22.1	0.9
300°C-A	191.1	808.9	938.9	9.7	18.7	0.9
400°C-A	192.8	839.4	949.3	9.6	20.0	0.9
500°C-A	196.7	821.0	945.6	9.7	21.5	0.9
600°C-A	198.3	806.3	935.6	15.2	22.0	0.9
700°C-A	192.8	751.6	907.7	20.6	27.2	0.9
800°C-A	192.1	544.8	800.8	29.7	35.9	1.0
900°C-A	197.7	338.5	704.4	54.4	60.5	1.2
100°C-S	182.1	730.1	905.1	9.6	21.5	0.9
200°C-S	187.7	779.6	918.1	9.6	18.8	0.9
300°C-S	184.4	808.9	929.5	9.6	20.2	0.9
400°C-S	186.5	812.9	934.7	9.7	21.3	0.9
500°C-S	194.9	831.6	957.7	9.6	19.2	0.9
600°C-S	192.2	794.0	929.5	15.5	20.9	0.9
700°C-S	196.9	755.8	915.4	18.4	23.1	1.0
800°C-S	195.3	489.0	783.2	33.0	39.3	1.1
900°C-S	195.0	336.1	704.6	52.6	59.7	1.2

With reference to the data presented in table 4-2, it is shown that there was a 2-7% increase in the $f_{0.2p}$ value for every 100°C increment from the virgin (ambient) sample until the specimens that were exposed to 500°C; the total increase in $f_{0.2p}$ over this temperature exposure range was 15% and this value remained consistent regardless of the cooling regime. The increase was slightly lower for the f_u value although a similar trend is observed; this property increased by around 5% following exposure of to 500°C compared with the corresponding virgin sample. On the other hand, for the strain response, the ε_u value was relatively unchanged, remaining within 1% of the virgin sample value, whilst the total strain at failure ε_f generally showed a reduction in value for the samples that were heated up to 500°C before cooling of between 5%-20%; it is noteworthy that one sample that was quenched after being heated to 100°C had a 6% increase in ε_f but all other samples had a reduction in the ultimate strain.

After higher levels of elevated temperature exposure of between 600°C and 700°C, both $f_{0.2p}$ and f_u values almost fully returned to the corresponding virgin values. For the 600°C sample, the ε_u values increased by 56-67% whilst the ε_f values rose in comparison to the low-to-moderate specimens but still underperformed against the virgin sample. Following exposure to 700°C, this trend continued with an increase in ε_u by a further 41-60% and ε_f by 38-69%. This different strain behaviour resulted in a more rounded stress-strain response as shown in Fig. 4-3. This was most likely because the effects of cold-rolling on the material were lost after exposure to higher temperatures and were not regained following cooling. After exposure to higher temperatures of 800°C and 900°C, there was a notable loss in strength for the samples with $f_{0.2p}$ reducing by 25-36% for the 800°C samples compared with the room temperature behaviour and 53-56% for the 900°C specimens. There was a similar trend for f_u although the losses were less significant; a 12-15% reduction for the bars heated to 800°C and a 21-23% reduction for the 900°C specimens. On the other hand, the strain values were much higher than the equivalent virgin sample values, as ε_u increased by between 206-241% following exposure to 800°C compared with the virgin values and 441-483% for the 900°C samples. The total elongation, ε_f again showed a similar trend although to a lesser extent compared with ε_u, with a 54-89% increase for the 800°C bars and 156-172% for the 900°C samples, compared with the virgin samples. The modulus of elasticity E showed very little change following exposure to elevated temperature and subsequent cooling, with the lowest and highest values recorded across all tests being 181.9 and 197.7 GPa, respectively. These values are within 10% of the guideline value set out in BS 6744 of 190 GPa for austenitic stainless steels.

In order to conduct a closer inspection of the influence of cooling method on the post-fire behaviour, Fig. 4-4 presents grade 1.4301 rebars that were heated to either 500°C, 700°C or 900°C and then cooled by quenching in water, air-cooling and slow-cooling in the furnace; the data for the unheated virgin specimen is also included. In this image, the solid lines are for the quenched samples, the dashed lines for the air-cooled rebars and the dotted lines are for the slow-cooled specimens. It is evident that for these samples, the cooling method did not have a strong influence on the post-fire behaviour. For the bars exposed to higher levels of elevated temperature, the quenched specimens demonstrated greater ductility compared with the samples cooled more slowly, but the strength remained similar. For all levels of temperature exposure, the slow-cooled specimens had the lowest level of ductility following heating and cooling compared with the samples that were cooled either by quenching in water or naturally in air.

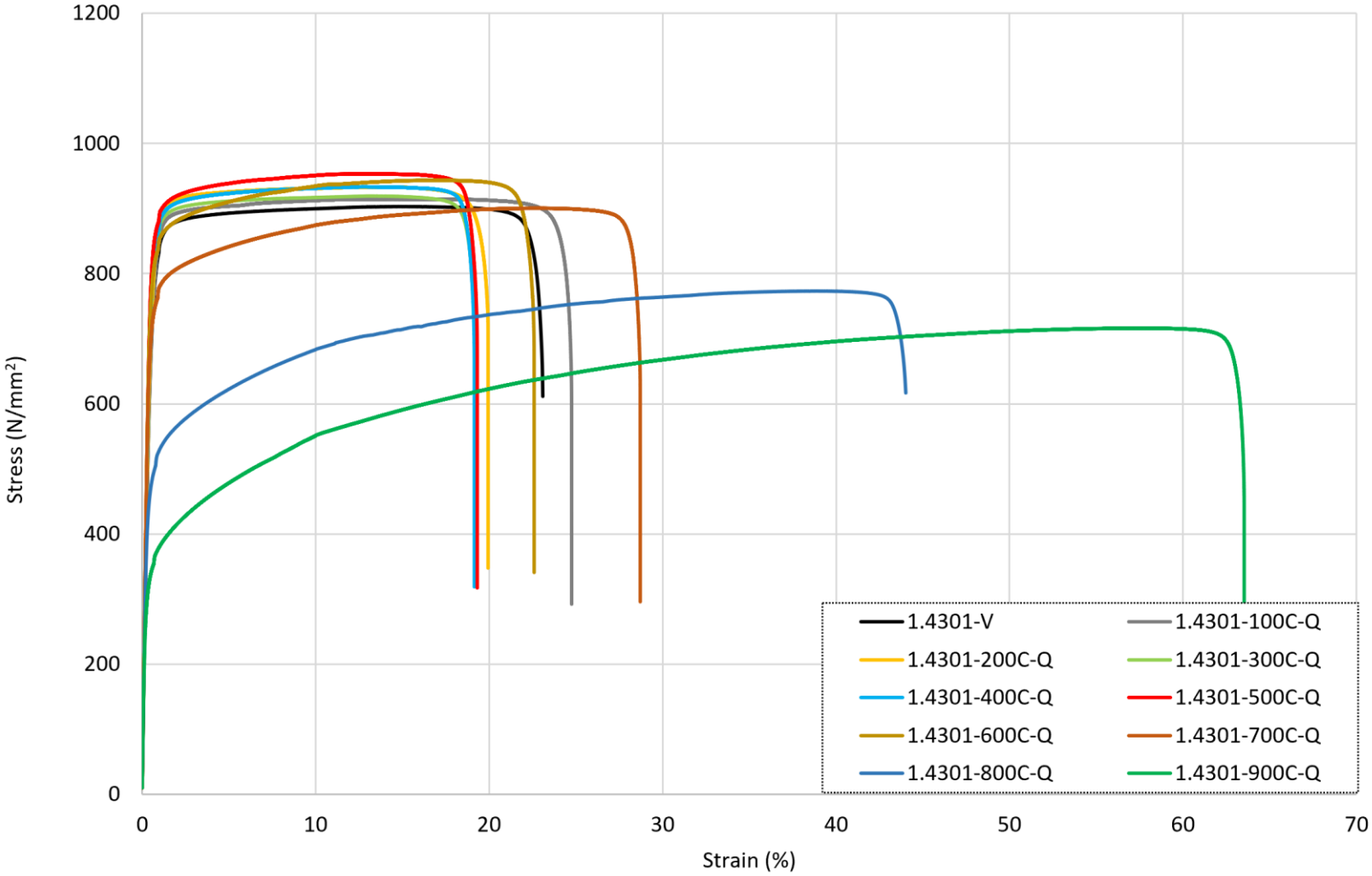
1200
1000
800
600
400
200
0
Stress (N/mm²)
0
10
20
30
40
50
60
70
Strain (%)
1.4301-V
1.4301-100C-Q
1.4301-200C-Q
1.4301-300C-Q
1.4301-400C-Q
1.4301-500C-Q
1.4301-600C-Q
1.4301-700C-Q
1.4301-800C-Q
1.4301-900C-Q

(a)

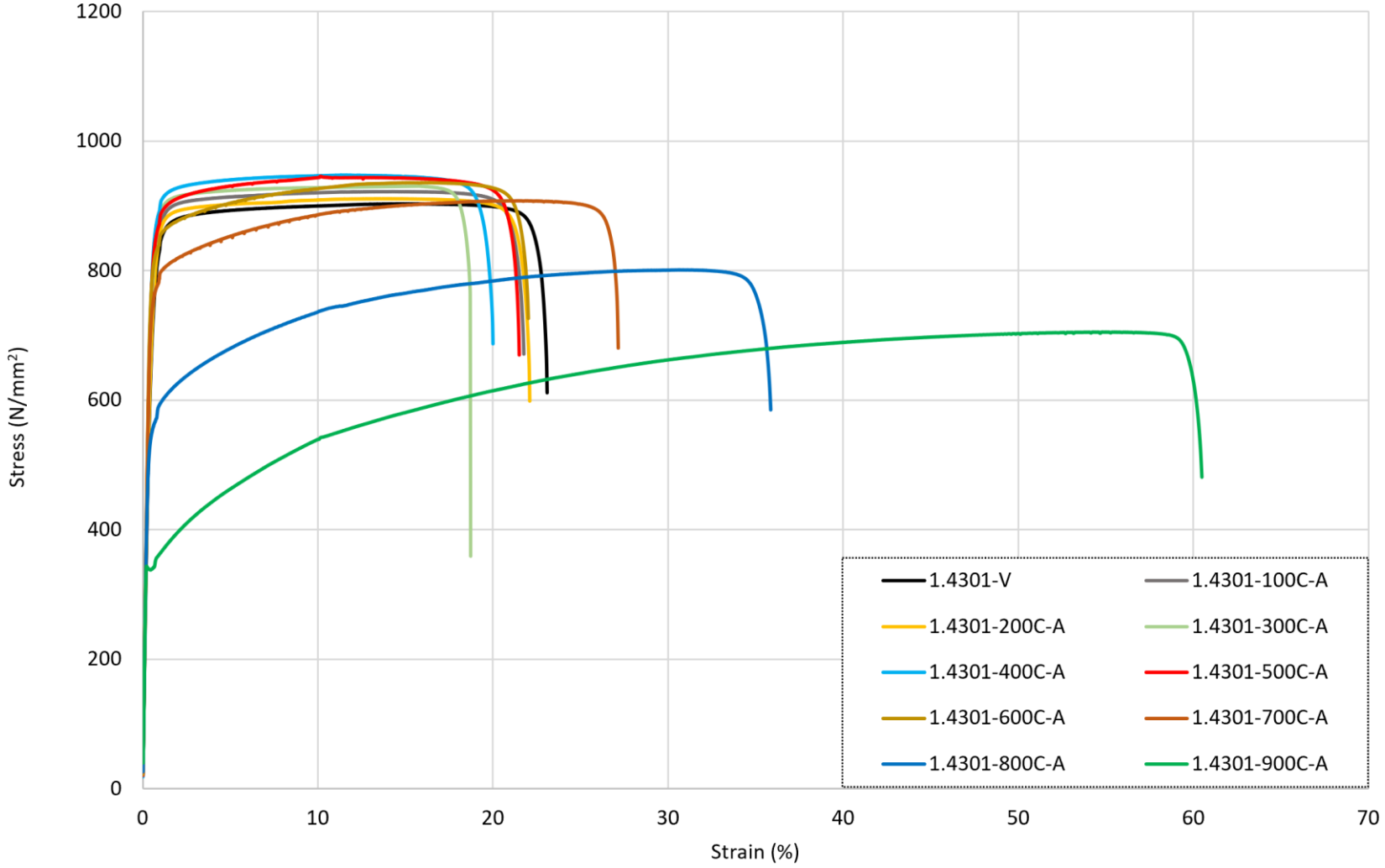
1200
1000
800
600
400
200
0
Stress (N/mm²)
0
10
20
30
40
50
60
70
Strain (%)
1.4301-V
1.4301-100C-A
1.4301-200C-A
1.4301-300C-A
1.4301-400C-A
1.4301-500C-A
1.4301-600C-A
1.4301-700C-A
1.4301-800C-A
1.4301-900C-A

(b)

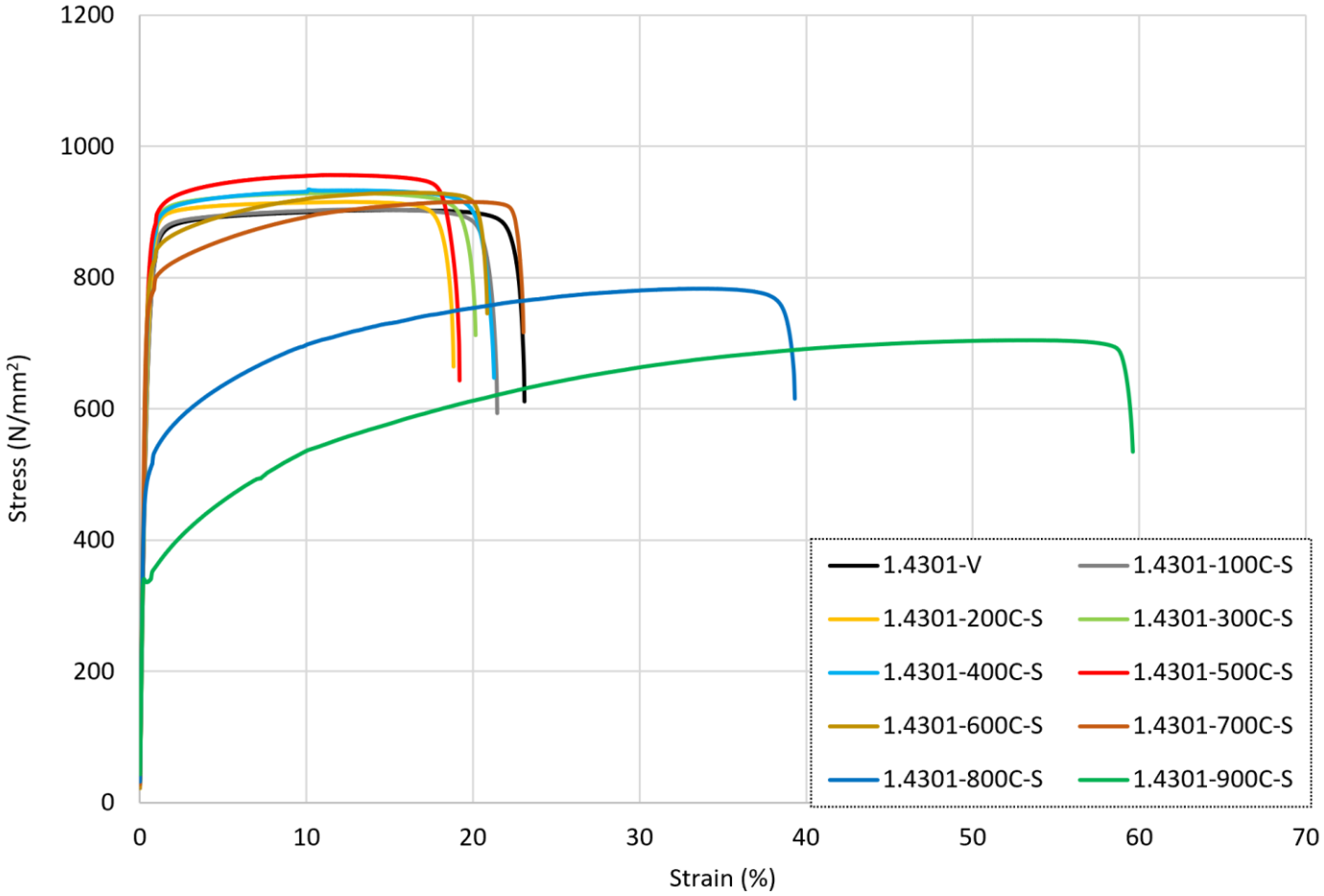

(c)

Figure 4-3: Stress-strain responses for grade 1.4301 stainless steel rebars following exposure to elevated temperature and then (a) quenched in water, (b) cooled naturally in air and (c) slow-cooled in the furnace.

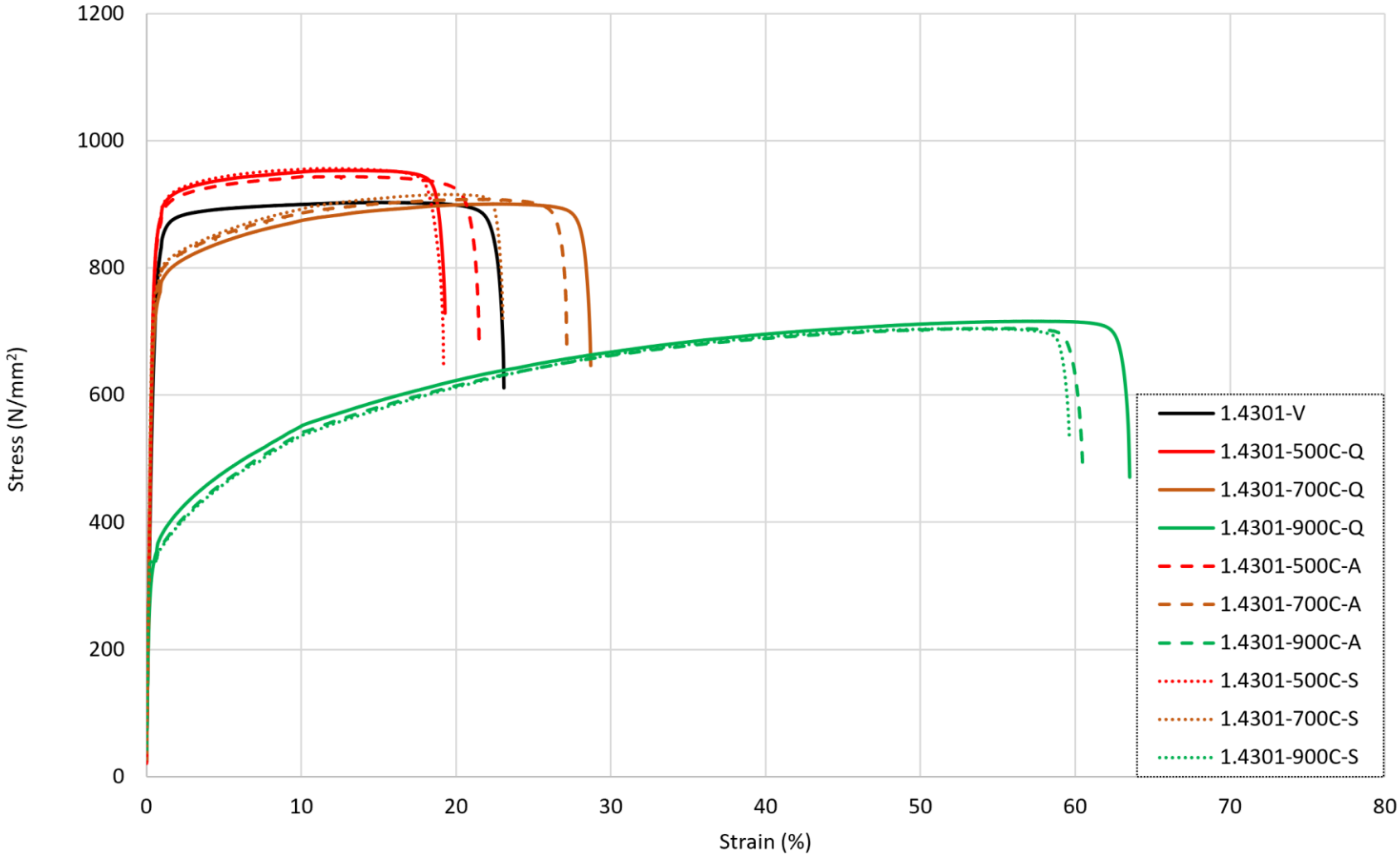

Figure 4-4: Stress-strain responses for grade 1.4301 stainless steel rebars following exposure to 500°C, 700°C and 900°C and various cooling.

4.3 Tensile Response of Stainless Steel Grade 1.4401

Fig. 4-5 presents the full stress-strain response for the grade 1.4401 samples, with a diameter d of 12 mm, which were heated to different levels of elevated temperature and then cooled either by (a) quenching in water, (b) air-cooling and (c) slow-cooling in the furnace. In addition, the data from the tests is given in table 4-3. It is observed that for samples that were heated up to around 500°C, there is very little change in the strength or ductility following cooling by any method. In this range, for samples that were heated up to 500°C, the data presented in table 4-3 shows that $f_{0.2p}$ and f_u increased by between 1-6% and 1-3%, respectively, compared with the virgin samples. For the strain response in this same temperature exposure range, both ε_u and ε_f increased by between 1%-10% compared with the virgin sample values. Observation of the fracture surface showed consistency of failure into the central region, this can be seen in Fig A.4-3, under Appendix A.

Table 4-3: Post-fire properties of Stainless Steel Grade 1.4401 rebar. Labelled as the temperature of exposure followed by either -Q for quenched, -A for air-cooled and -S for slow-cooled.

Grade	1.4401					
	E (GPa)	$f_{0.2p}$ (N/mm^2)	f_u (N/mm^2)	ε_f (%)	ε_u (%)	n
Virgin	191.6	604.0	723.6	14.3	20.0	1.0
100°C-Q	198.2	579.8	711.6	15.2	21.5	1.0
200°C-Q	195.5	580.4	717.2	14.2	19.4	0.9
300°C-Q	184.5	610.7	721.9	13.6	20.5	1.0
400°C-Q	183.8	637.3	743.0	13.7	20.2	1.0
500°C-Q	189.7	624.4	746.5	13.1	17.8	0.9
600°C-Q	187.4	569.5	715.9	17.9	22.7	0.9
700°C-Q	194.4	498.6	685.8	25.5	31.5	1.0
800°C-Q	187.2	424.7	649.7	32.1	38.9	1.1
900°C-Q	185.5	308.5	577.7	47.5	53.7	1.3
100°C-A	187.6	583.3	702.0	14.4	20.4	0.9
200°C-A	183.6	586.1	711.2	13.9	19.0	1.0
300°C-A	187.6	619.0	723.9	13.6	20.5	1.0
400°C-A	180.6	619.5	724.7	13.6	21.6	1.0
500°C-A	184.7	606.9	722.4	13.6	18.3	0.9
600°C-A	188.3	581.8	721.5	17.0	22.5	0.9
700°C-A	185.1	527.7	687.7	22.0	28.0	1.0
800°C-A	181.3	464.2	663.2	30.2	35.9	1.1
900°C-A	185.4	309.1	586.2	45.5	51.2	1.3
100°C-S	182.9	641.1	707.0	14.5	20.6	0.9
200°C-S	187.1	613.9	718.0	12.8	18.4	1.0
300°C-S	188.2	610.8	720.5	13.0	18.3	1.0
400°C-S	184.3	632.0	728.5	13.6	21.6	0.9
500°C-S	188.7	630.0	741.7	13.3	20.2	1.0
600°C-S	180.0	594.3	730.1	17.9	23.3	0.9
700°C-S	196.4	542.1	705.2	24.0	29.6	1.0
800°C-S	191.7	466.8	663.2	29.3	34.9	1.0
900°C-S	184.3	297.4	589.2	46.6	53.4	1.3

Generally, the samples retained (or lost and regained) their strength and ductility once they returned to room temperature following elevated temperature exposure. For specimens that were heated to 600°C or higher, there was a clearer change in the overall behaviour, with a more rounded response observed, and a slight loss in strength accompanied by an increase in ultimate strain following cooling. Following exposure to 600°C, the strength performance remained consistent with those at lower temperatures, whilst the strain response showed an increase ε_u and ε_f of 19-25% and 13-17% compared with the original values. Following exposure to higher temperatures, the loss in strength became more pronounced, as did the increase in ductility. After heating to 700°C, $f_{0.2p}$ and f_u reduced

by 10-17% and 3-5%, respectively, against the virgin values whereas, on the other hand, ε_u increased by 54-75% and ε_f rose by 40-58% in these same tests. Following heating to higher temperatures of 800°C and 900°C, $f_{0.2p}$ reduced by 23-30% and 49-51%, respectively, whereas f_u reduced by only 8-10% (800°C) and 19-20% (900°C). There were very significant changes in the strains ε_f the ultimate load and failure as ε_u and ε_f increased by 105-124% and 75-95%, respectively, after exposure to 800°C and 218-232% and 156-169% for the samples heated to 900°C. As with the data from grade 1.4301, this illustrates that the cold-rolling effect was regained in the samples that were heated to approximately 500-600°C, and then cooled, whereas it was permanently lost following exposure to higher levels of elevated temperature.

This phenomenon is further evidenced with a closer inspection of the total strain at failure ε_f, as this property was largely unchanged compared with the virgin sample following exposure to 500°C and subsequent cooling whilst the bars that were heated to higher temperatures had greater failure strains, albeit with a significant reduction in strength. As with grade 1.4301, there was little variation in the elastic modulus values with the minimum E across all tests being 180.6 GPa and the corresponding maximum values being 198.2 GPa, both of which are within 10% of the guideline value of 190 GPa in BS 6744 (2016).

The influence of cooling method on the stress-strain response of grade 1.4401 stainless steel rebars following exposure to either 500, 700°C or 900°C is illustrated in Fig. 4-6. Overall, as with grade 1.4301, there was a relatively small variation in the behaviour between samples that were cooled by different methods. In contrast to grade 1.4301, for all levels of temperature exposure, the grade 1.4401 bars that were air-cooled had the lowest level of ductility whilst the bars that were exposed to moderate-to-high temperatures and then cooled quickly by quenching in water, have slightly lower strengths than the other methods.

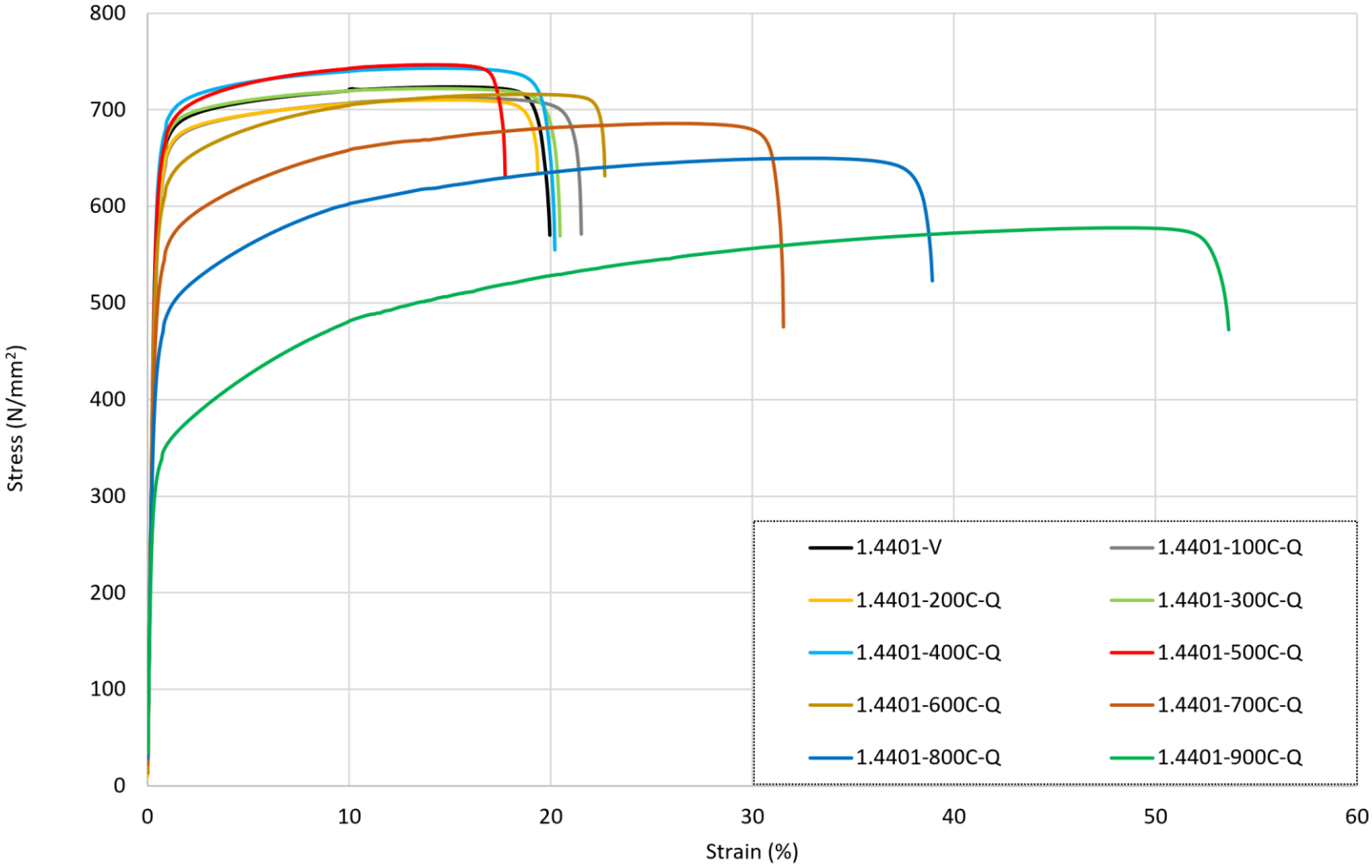
800
700
600
500
400
300
200
100
0
Stress (N/mm²)
0
10
20
30
40
50
60
Strain (%)
1.4401-V
1.4401-100C-Q
1.4401-200C-Q
1.4401-300C-Q
1.4401-400C-Q
1.4401-500C-Q
1.4401-600C-Q
1.4401-700C-Q
1.4401-800C-Q
1.4401-900C-Q

(a)

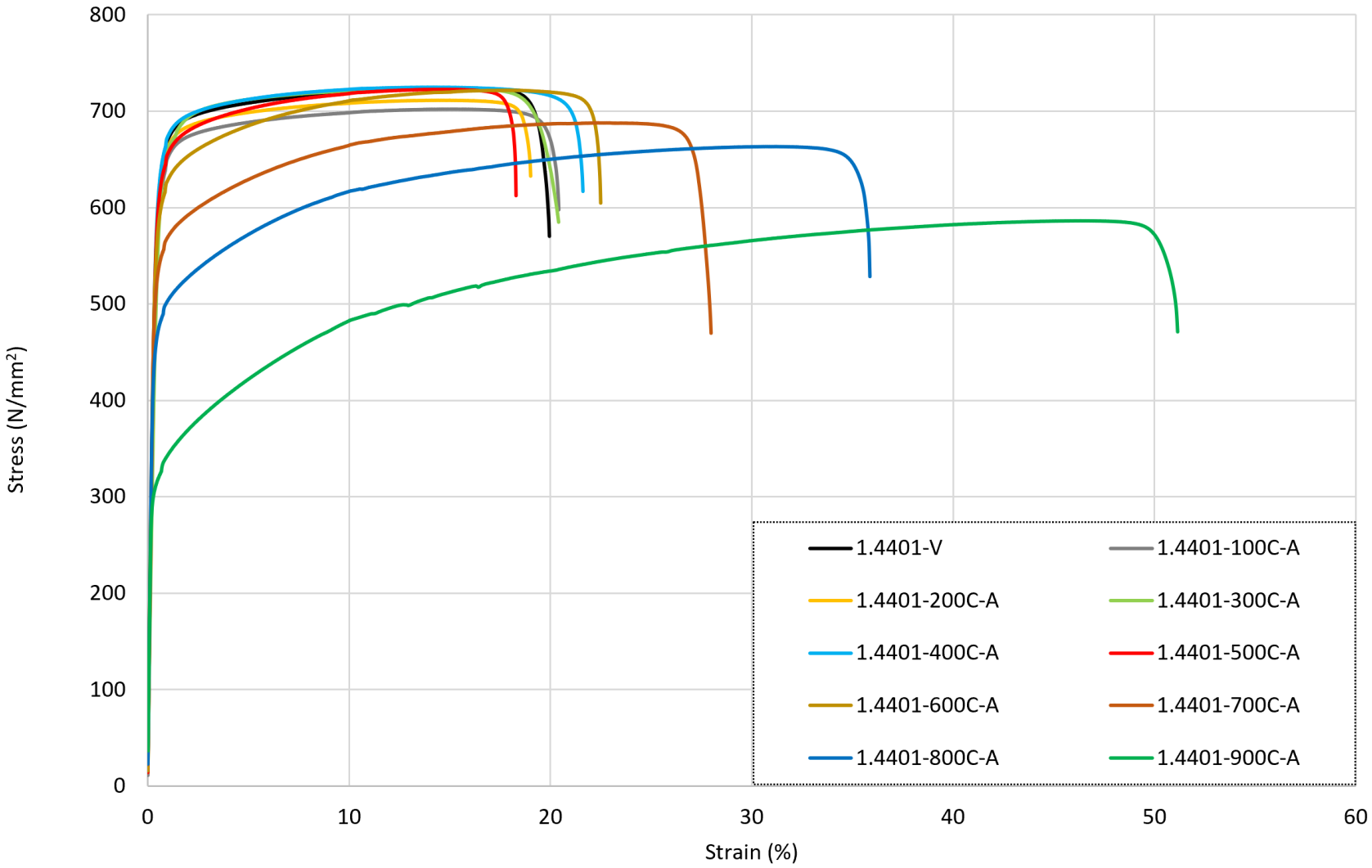
800
700
600
500
400
300
200
100
0
Stress (N/mm²)
0
10
20
30
40
50
60
Strain (%)
1.4401-V
1.4401-100C-A
1.4401-200C-A
1.4401-300C-A
1.4401-400C-A
1.4401-500C-A
1.4401-600C-A
1.4401-700C-A
1.4401-800C-A
1.4401-900C-A

(b)

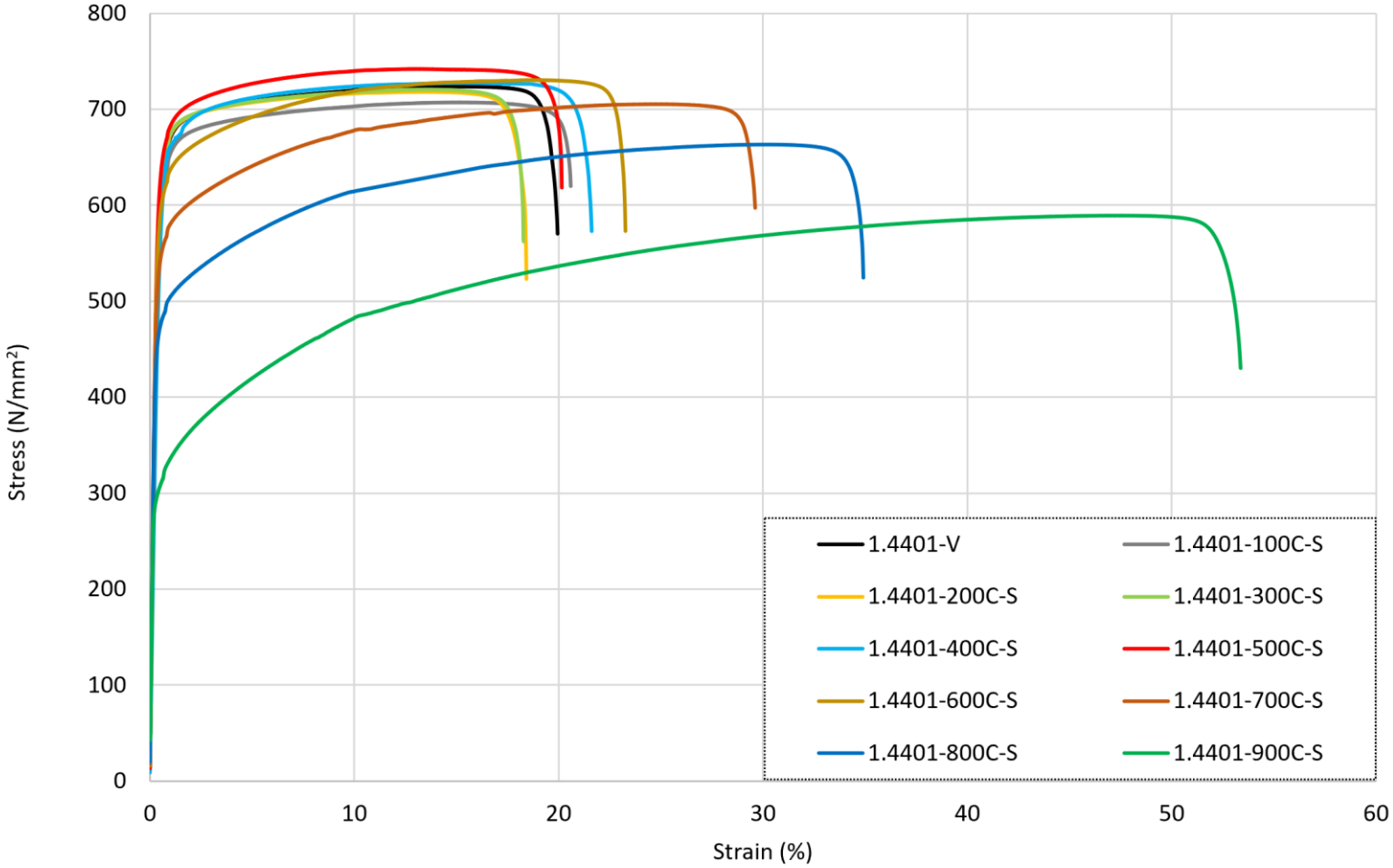

(c)

Figure 4-5: Stress-strain responses for grade 1.4401 stainless steel rebars following exposure to elevated temperature and then (a) quenched in water, (b) cooled naturally in air and (c) slow-cooled in the furnace.

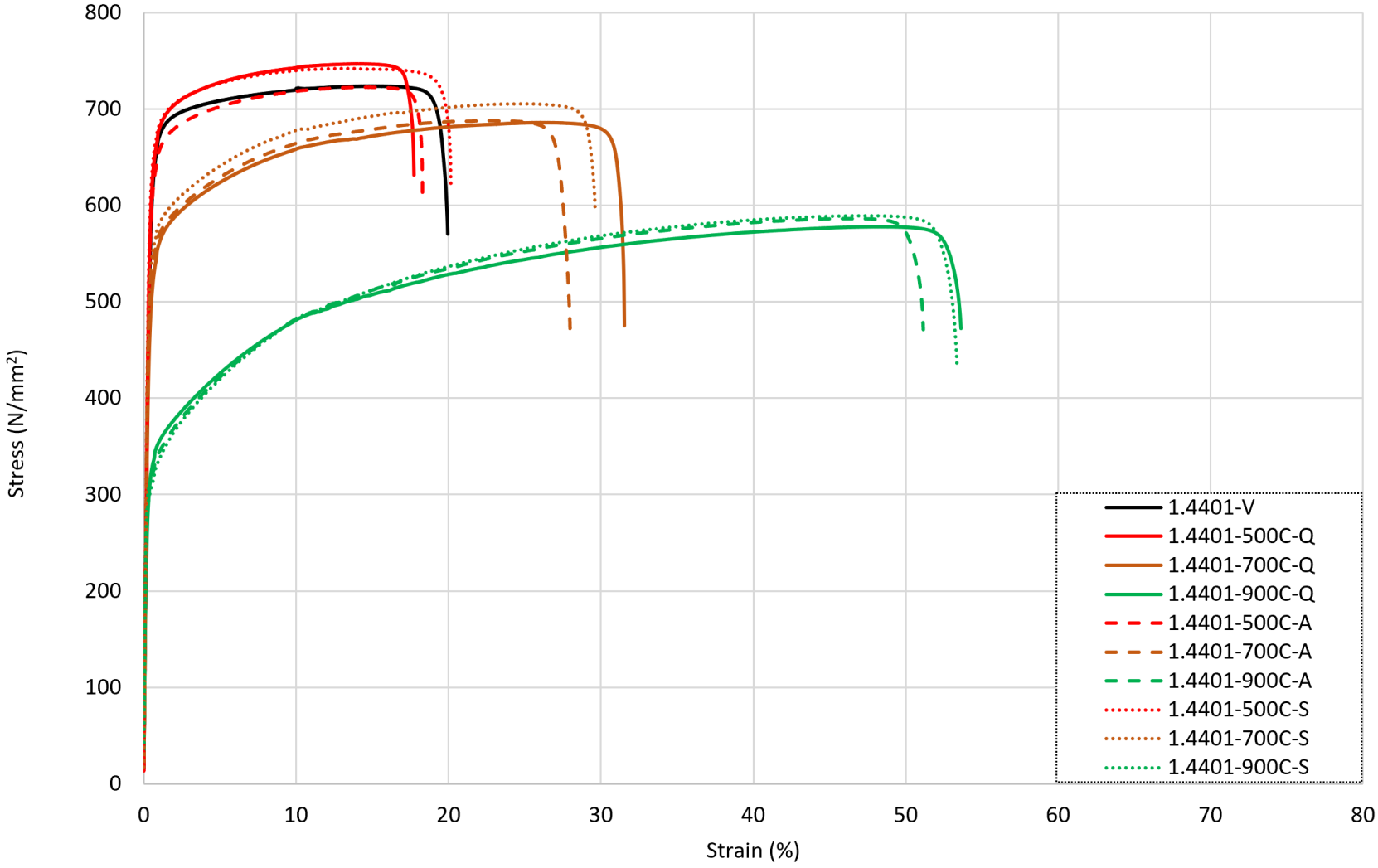

Figure 4-6: Stress-strain responses for grade 1.4401 stainless steel rebars following exposure to 500°C, 700°C and 900°C and various cooling.

4.4 Tensile Response of Austenitic Stainless Steel 1.4436

The full stress strain response from all grade 1.4436 samples, with a dimeter d of 8mm, are presented in Fig. 4-7 for (a) the bars quenched in water, (b) the air-cooled samples, and (c) the slow-cooled specimens. In addition, the data from the tests is given in table 4-4. It is noted that following exposure to low-to-moderate temperature conditions up to 500°C, there was a steady rise in the tensile strength of the samples. There was a relatively slow increase in $f_{0.2p}$ of between 1-5% per 100°C increment and totalling an increase of approximately 11% after heating to 500°C. The total strength, f_u, followed a similar trend and increased by around 5% following heating to 500°C, compared with the virgin sampled. In this same temperature range (samples that were heated up to 500°C), ε_u had a negligible change following heat exposure, regardless of the cooling method, whilst ε_f increased by around 19%. When comparing the numerical data presented in table 4-4 with the stress-strain responses given in Fig. 4-7, it is evident that this variation in strain is not owing to a change in shape of the response as this remained the same meaning that the material did not undergo any major transformations in grain or phase in this range. In Fig A.4-4, images of the fracture surface are presented, the zone is localised to the central 50mm zone within the extensometer.

Table 4-4: Post-fire properties of Stainless Steel Grade 1.4436 rebar. Labelled as the temperature of exposure followed by either -Q for quenched, -A for air-cooled and -S for slow-cooled.

Grade	1.4436					
	E (GPa)	$f_{0.2p}$ (N/mm^2)	f_u (N/mm^2)	ε_f (%)	ε_u (%)	n
Virgin	186.7	672.2	805.3	9.7	19.6	0.9
100°C-Q	181.7	678.0	794.4	9.9	19.9	0.9
200°C-Q	191.4	693.8	805.0	9.7	17.7	0.9
300°C-Q	185.9	720.8	822.6	9.7	19.9	0.9
400°C-Q	188.4	726.0	831.7	9.7	21.0	0.9
500°C-Q	186.3	728.0	842.3	9.7	17.7	0.9
600°C-Q	184.0	689.3	828.4	17.1	24.3	0.9
700°C-Q	192.6	601.0	778.2	19.7	24.5	1.0
800°C-Q	184.4	500.5	726.2	29.7	35.4	1.0
900°C-Q	196.0	261.7	617.6	56.0	61.8	1.3
100°C-A	180.2	664.4	790.9	9.7	19.6	1.0
200°C-A	184.3	682.0	795.9	9.7	19.5	0.9
300°C-A	193.5	717.2	815.9	9.7	18.1	0.9
400°C-A	182.0	731.1	825.8	9.8	17.2	0.9
500°C-A	185.8	745.4	846.0	9.9	15.8	0.9
600°C-A	189.2	710.2	831.1	15.5	21.8	0.9
700°C-A	181.9	620.8	781.5	22.0	28.0	1.0
800°C-A	190.0	529.9	728.3	29.6	35.2	1.0
900°C-A	190.5	262.5	614.9	55.7	61.7	1.3
100°C-S	192.3	664.7	789.2	9.7	19.6	0.9
200°C-S	187.2	684.5	791.6	9.7	18.1	0.9
300°C-S	182.1	723.2	813.5	9.7	16.8	0.9
400°C-S	184.8	727.2	821.8	9.6	18.4	0.9
500°C-S	189.2	735.4	841.5	9.6	21.6	0.9
600°C-S	184.9	687.5	816.4	16.8	22.3	0.9
700°C-S	181.6	622.7	777.7	21.6	27.5	1.0
800°C-S	189.5	522.9	725.9	30.0	35.6	1.1
900°C-S	188.8	265.1	621.0	59.4	67.2	1.3

After exposure to higher temperatures ranging from 600°C upwards, the overall shape of the residual stress-strain response changed as shown in Fig. 4-7, and became more nonlinear. Moreover, the tensile strength gradually declined. Following heating to 600°C, compared with the virgin sample, there was an increase in strength of between 2%-6% for $f_{0.2p}$ and 1%-3% for f_u whilst these values for the specimens heated to 700°C presented a loss of 7-11% for $f_{0.2p}$ and 3% for f_u. The strain response showed an increase in the ε_u and of 61-73% and 14-24%, respectively, for the samples heated to 600°C and 103-128% and 80-82%, respectively, for those heated to 700°C. After this, for the bars exposed to

higher temperatures, there was a significant reduction in the residual strength once the specimen had cooled, with a loss of 21-26% for $f_{0.2p}$ and 10% for f_u at 800°C and a loss of 61% for $f_{0.2p}$ and 23-24% for f_u at 900°C. There was an increase in ε_u of 206-210% for the bars heated to 800°C and 476-515% for those that were exposed to 900°C, compared with the virgin values, and corresponding increases in ε_f of 80-82% (800°C) and 215-343% (900°C). This resulted in greater roundedness of the overall response, as shown in Fig. 4-7. The modulus of elasticity E was observed to show little change as with the previous austenitic grades.

The influence of the three cooling methods for grade 1.4436 rebars that were exposed to temperatures of 500°C, 700°C and 900°C is presented in Fig. 4-8, together with the data for the virgin specimen. As for the other austenitic stainless steel grades discussed before, there were relatively minor differences in the residual response for grade 1.4436 for the different cooling methods. Samples heated to 500°C showed the greatest variance from the various cooling methods, with the total strain ε_f, showing a drop of 19% with the air-cooled sample and an increase of 10% with the slow-cooled sample.

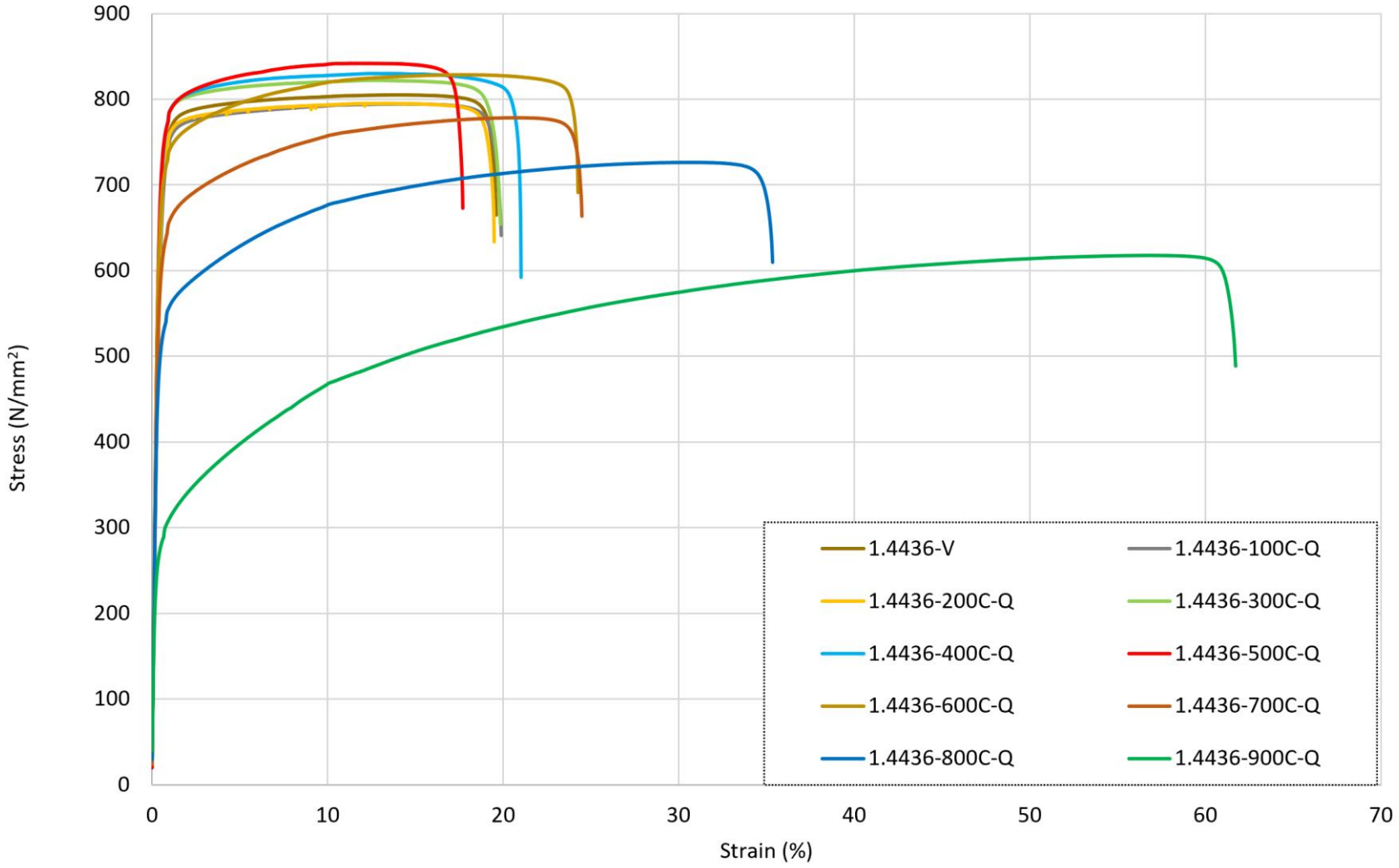
900
800
700
600
500
400
300
200
100
0
Stress (N/mm²)
0
10
20
30
40
50
60
70
Strain (%)
1.4436-V
1.4436-100C-Q
1.4436-200C-Q
1.4436-300C-Q
1.4436-400C-Q
1.4436-500C-Q
1.4436-600C-Q
1.4436-700C-Q
1.4436-800C-Q
1.4436-900C-Q

(a)

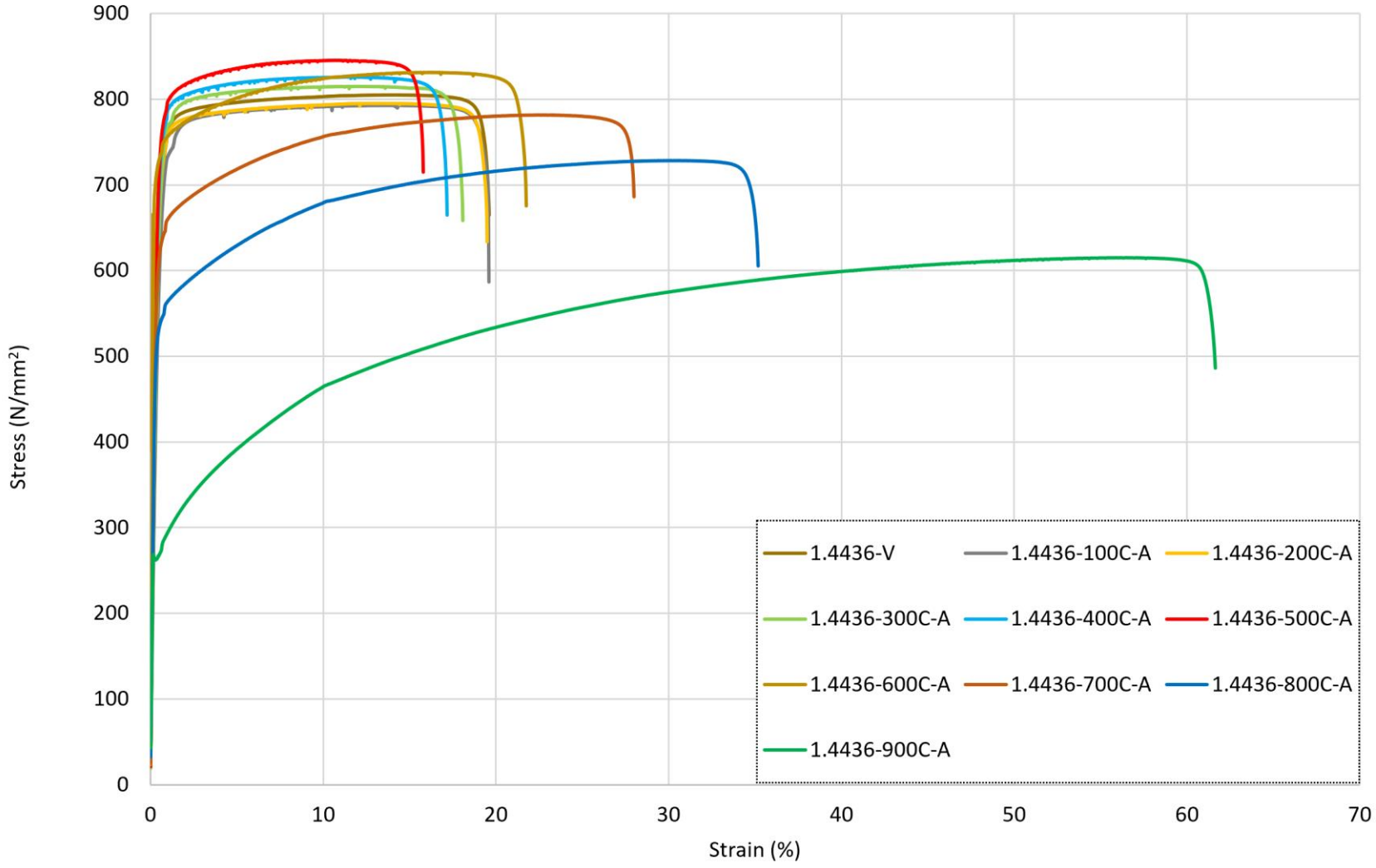
900
800
700
600
500
400
300
200
100
0
Stress (N/mm²)
0
10
20
30
40
50
60
70
Strain (%)
1.4436-V
1.4436-100C-A
1.4436-200C-A
1.4436-300C-A
1.4436-400C-A
1.4436-500C-A
1.4436-600C-A
1.4436-700C-A
1.4436-800C-A
1.4436-900C-A

(b)

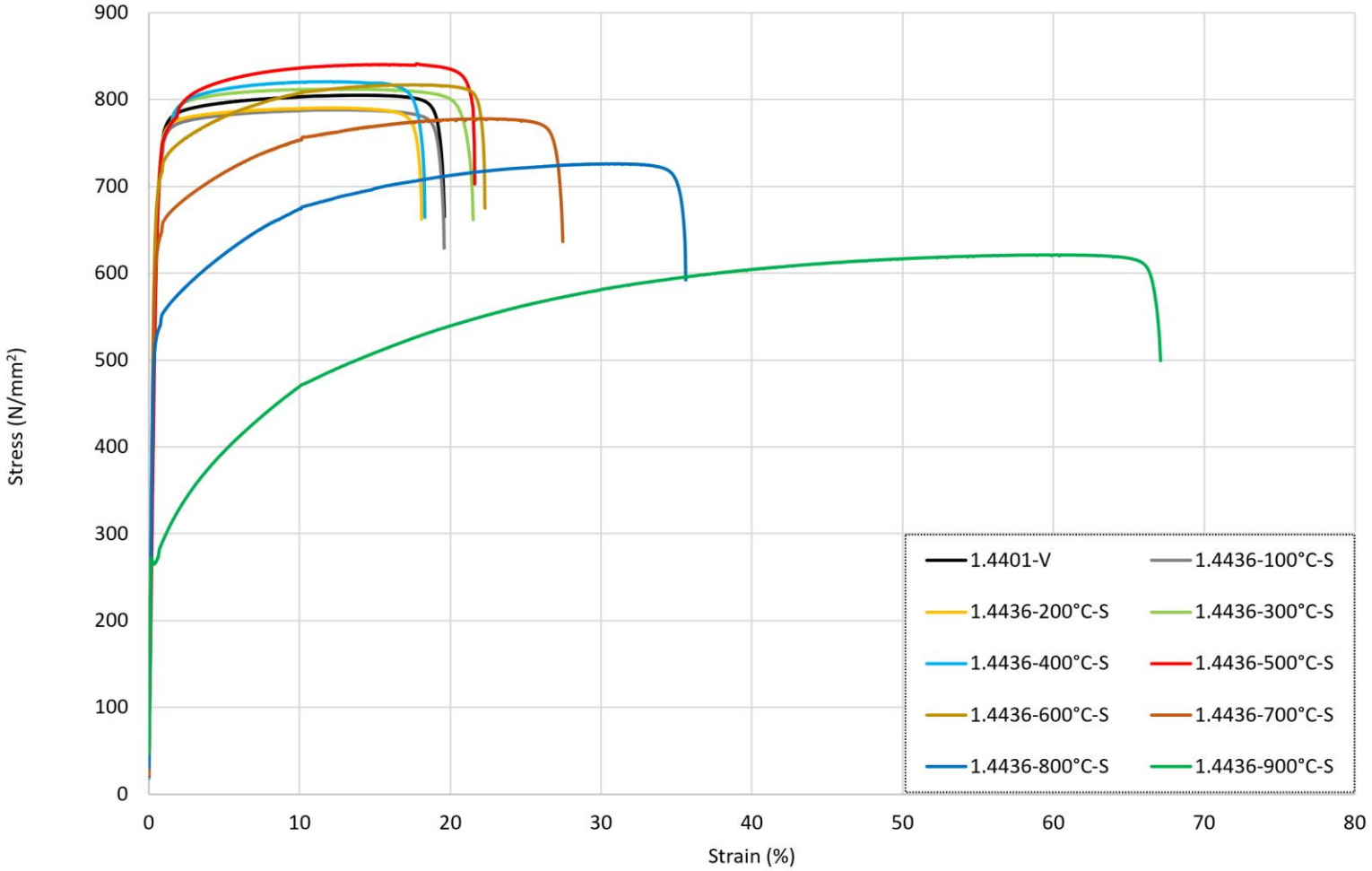

(c)

Figure 4-7: Stress-strain responses for grade 1.4436 stainless steel rebars following exposure to elevated temperature and then (a) quenched in water, (b) cooled naturally in air and (c) slow-cooled in the furnace.

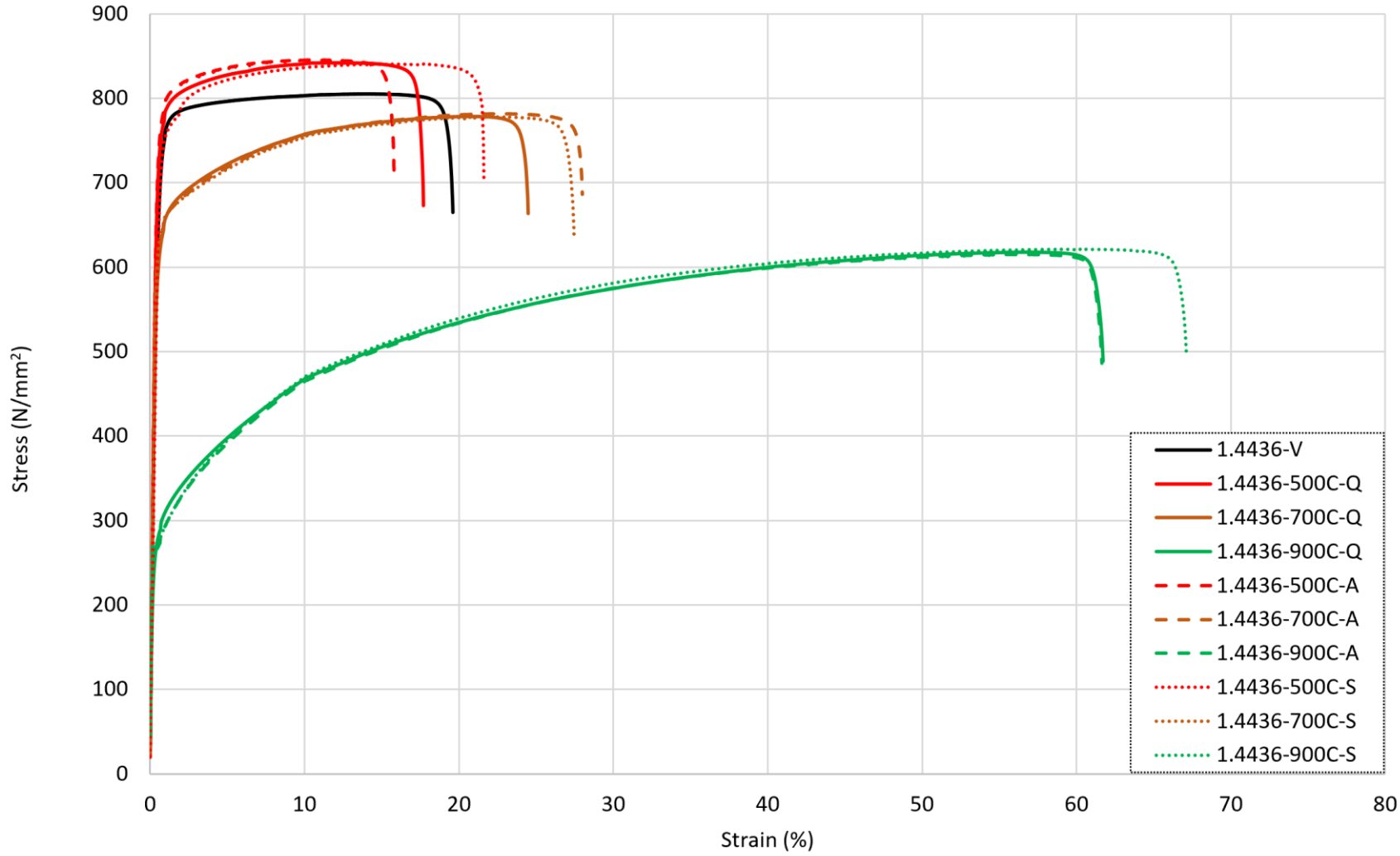

Figure 4-8: Stress-strain responses for grade 1.4401 stainless steel rebars following exposure to 500°C, 700°C and 900°C followed by cooling.

4.5 Results from the Metallurgical Investigation

In addition to the tensile tests previously described, a series of metallurgical tests were performed for grades 1.4301 and 1.4401 stainless steel rebar; grade 1.4436 was not included in the metallurgical testing as it is a subgrade of grade 1.4401 and did not display significantly different behaviour during the tensile testing or preliminary metallurgical investigations. The results in this section are given in terms of diffractograms, which present the intensity of the phase identification (intensity, which is a dimensionless measure) against the angle of detection (2theta). These are produced through X-ray diffraction for all samples which were heated to target temperatures between 100°C-900°C and then cooled using the three different methods described before (i.e., quenching in water, air-cooling and slow-cooling in the furnace). The position of both the austenite and martensite phase peaks are indicated in the diagrams, and are labelled with either a solid dot or empty circle for the austenite and martensite peaks, respectively. Notably, only 2theta between 40°-60° is presented as this the range of most significance for austenite/martensite microstructure transformation.

In addition to the X-ray diffraction study, a microscopic inspection of the grains was also conducted on the grade 1.4301 specimens that were exposed to a target temperature of 500°C and 900°C, and then cooled using one of the three cooling methods, and this is compared against similar data for a virgin sample.

4.5.1 Grade 1.4301

The diffractograms for the grade 1.4301 samples are shown in Fig. 4-9 for the bars that were (a) quenched in water, (b) air-cooled and (c) slow-cooled, respectively. Each diffractogram is compared against the unheated virgin sample. For the virgin sample, there was a small presence of martensite immediately after the austenite peak at 43.8° and this was a relatively minor phase, identified by the steady decline following the first peak, as opposed to the sharper and more uniform decline found at higher temperatures. It is noteworthy that martensite makes the material stronger and harder, compared with alloys without martensite. With reference to Fig. 4-9(a), this same pattern as demonstrated for the virgin sample was replicated for the sample that was exposed to 100°C before quenching in water as there was a small presence of martensite after the initial austenite phase between 43.5°-44°. For the rest of the quenched samples which were heated to 200°C and above, as well as all of the samples that were air-cooled or slow-cooled as shown in Fig. 4-9(b) and (c), there was no martensite phase visible in the diffractograms and there was a relatively smooth decline in terms of intensity visible from the first austenite peak.

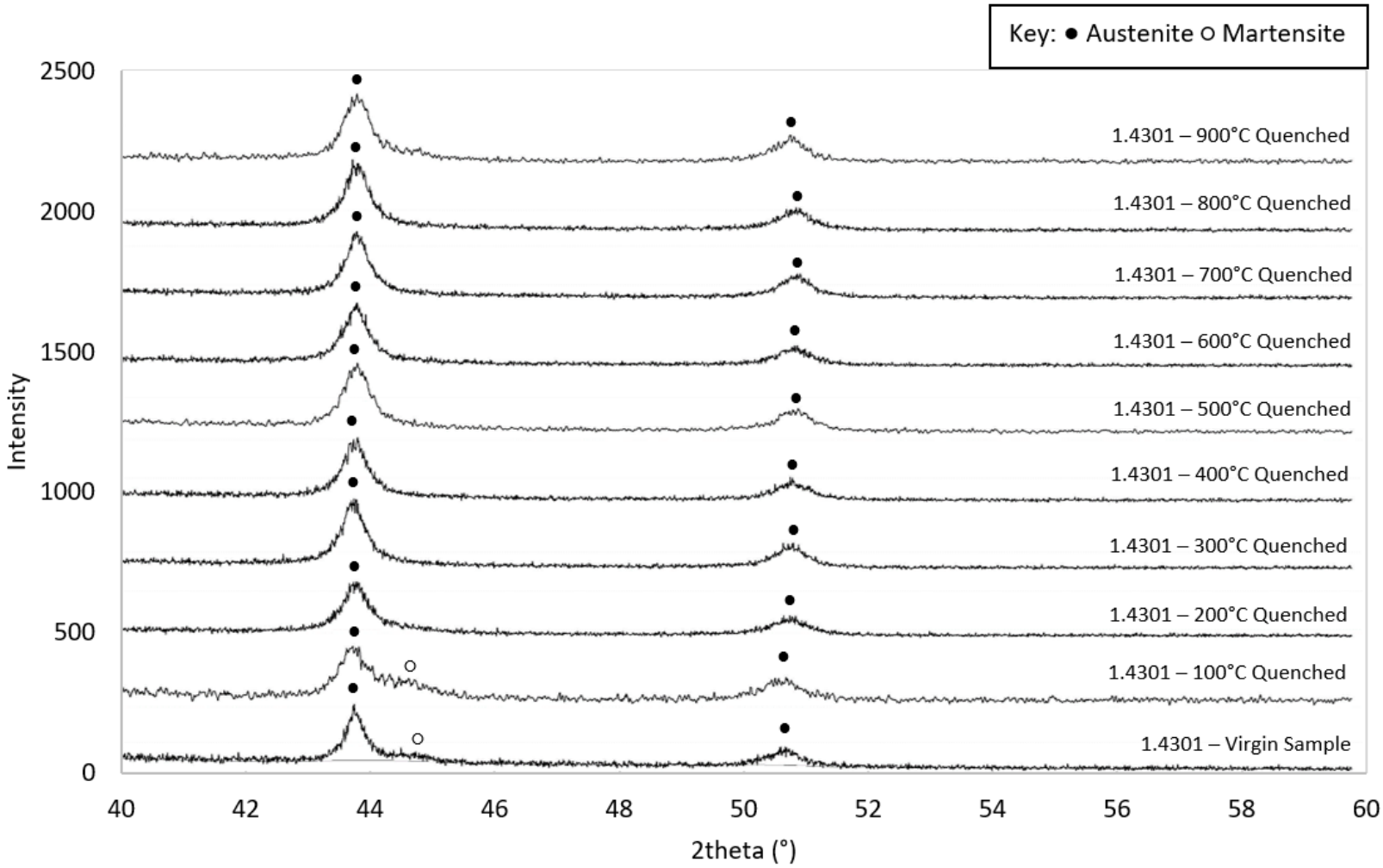
Key: ● Austenite ○ Martensite
1.4301 – 900°C Quenched
1.4301 – 800°C Quenched
1.4301 – 700°C Quenched
1.4301 – 600°C Quenched
1.4301 – 500°C Quenched
1.4301 – 400°C Quenched
1.4301 – 300°C Quenched
1.4301 – 200°C Quenched
1.4301 – 100°C Quenched
1.4301 – Virgin Sample
Intensity
2500
2000
1500
1000
500
0
40
42
44
46
48
50
52
54
56
58
60
2theta (°)

(a)

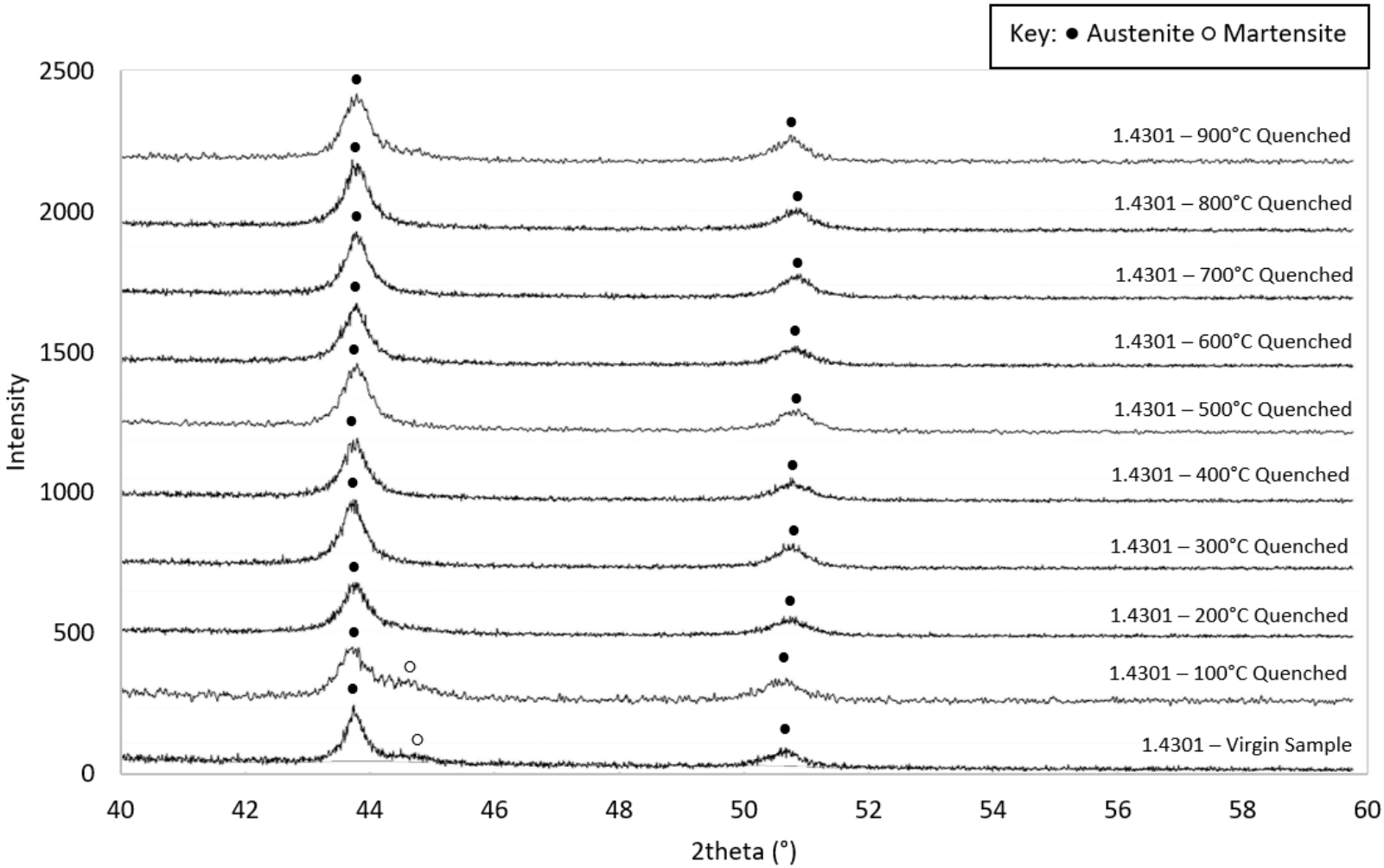
Key: ● Austenite ○ Martensite
1.4301 – 900°C Quenched
1.4301 – 800°C Quenched
1.4301 – 700°C Quenched
1.4301 – 600°C Quenched
1.4301 – 500°C Quenched
1.4301 – 400°C Quenched
1.4301 – 300°C Quenched
1.4301 – 200°C Quenched
1.4301 – 100°C Quenched
1.4301 – Virgin Sample
Intensity
2theta (°)
0
500
1000
1500
2000
2500
40
42
44
46
48
50
52
54
56
58
60

(b)

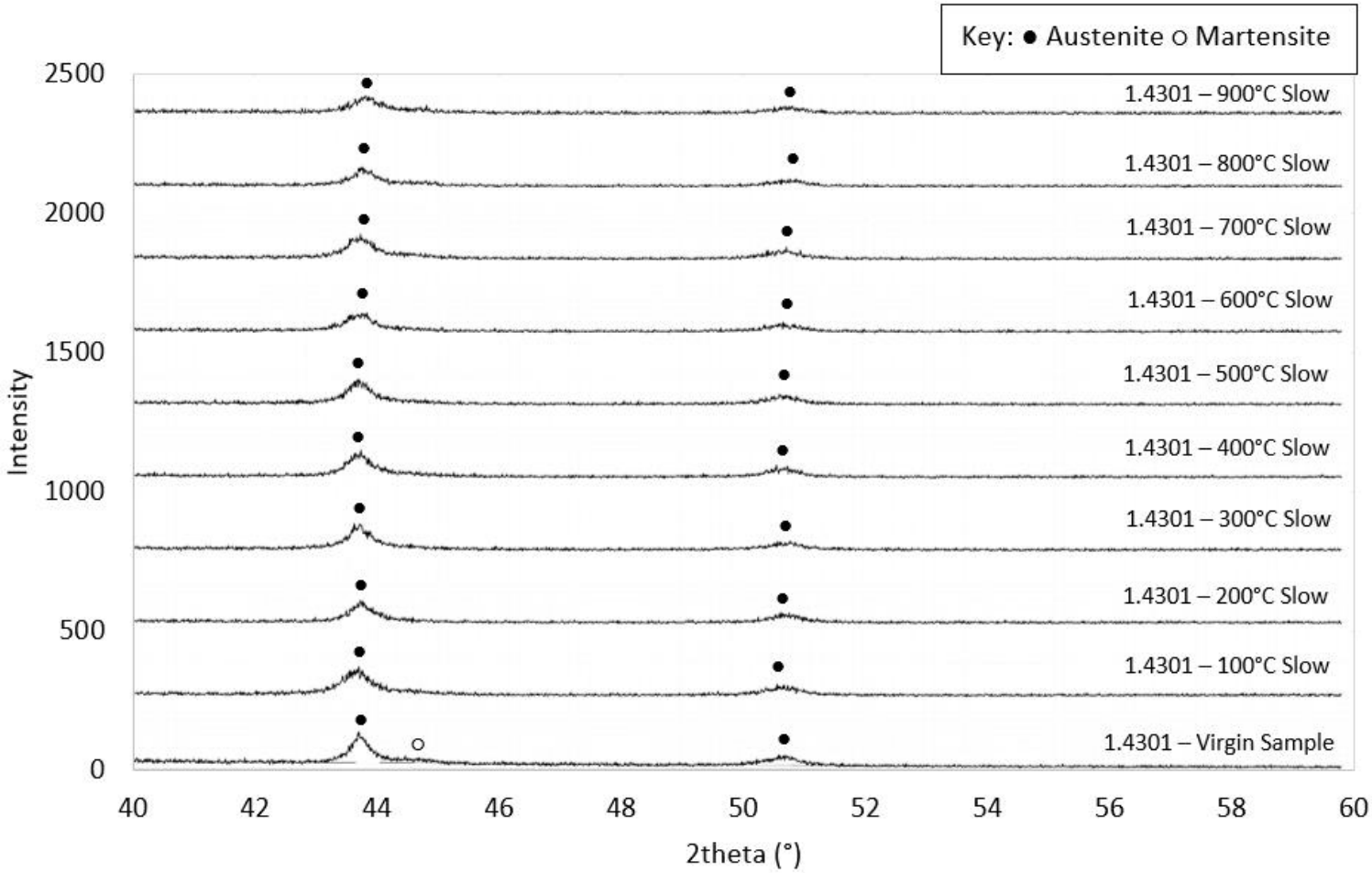

(c)

Figure 4-9: Data from the diffractograms for grade 1.4301 reinforcing bars that were heated to various temperatures as indicated and then cooled (a) quickly, by quenching in water, (b) naturally, in air, and (c) slowly, in the furnace.

For the grain inspection, the complete microscopic imagery for grade 1.4301 is presented in Fig. 4-10. From a visual inspection, the size, shape, and dispersion of the grain samples as well as a change in strengthening mechanisms are readily observed for (a) the virgin sample, (b-d) the samples heated to 500°C and then cooled and (e-f) those that were heated to 900°C before cooling. The virgin sample shown in Fig 4-10(a) has the strengthening mechanisms produced through cold-rolling labelled on this image, i.e., α´-martensite, ε-martensite, and twinning. It should be noted that the α´-martensite is identifiable by uniform needle like grains, ε-martensite can be identified through non-linear need like grains. The twinning feature is identifiable through the formation of new orientations not visible in the standard microstructure, whilst ghost-twinning is the residue of the twinning feature slowly reverting towards their original state. Following exposure to 500°C and subsequent cooling by all three cooling methods, the strengthening mechanisms become more defined, as shown in Fig. 4-10(b-d). This explains the 13-15% rise in $f_{0.2p}$ and 4-5% in f_u that was presented and discussed earlier in this paper for the specimens that were heated in this temperature range.

Theoretically, once the stainless steel is exposed to temperatures exceeding 727°C, the strengthened alloy begins to actively revert to γ-austenite through the formation of new γ-austenite grains within the grain boundaries of the α´-martensite grains, and, following exposure to 900°C, a complete transformation to γ-austenite is achieved, with some ghost twinning remaining visible. This is presented in Fig. 4-10(e-g) where, for the samples that were exposed to temperatures of 900°C before cooling (by any cooling method), the grains have reverted to an absolute γ-austenite alloy.

A comparison of the mean grain diameter of the samples exposed to 900°C, and subsequently cooled was also undertaken to understand the influence of grain size on the material. The quenched sample, as shown in Fig. 4-10(e), presents the largest mean grain diameter with a size of 42µm whilst the air-cooled sample, Fig. 4-10(f), presents a mean grain diameter of 36µm and the slow-cooled sample, Fig. 4-10(g) has the smallest grains with a mean grain diameter of 35µm. Despite a variance in grain size, no significant response in terms of the material strength was noted. On the other hand, in terms of strain, the ε_f values presented earlier in this paper for the grade 1.4301 rebar that was exposed to 900°C and then quenched showed the greatest increase of those examined in this study as it was 272% of the corresponding virgin sample value. The equivalent increase for the air-cooled and slow-cooled bars was 259% and 256%, respectively. This indicates that the larger the grain size, the greater the total strain at failure.

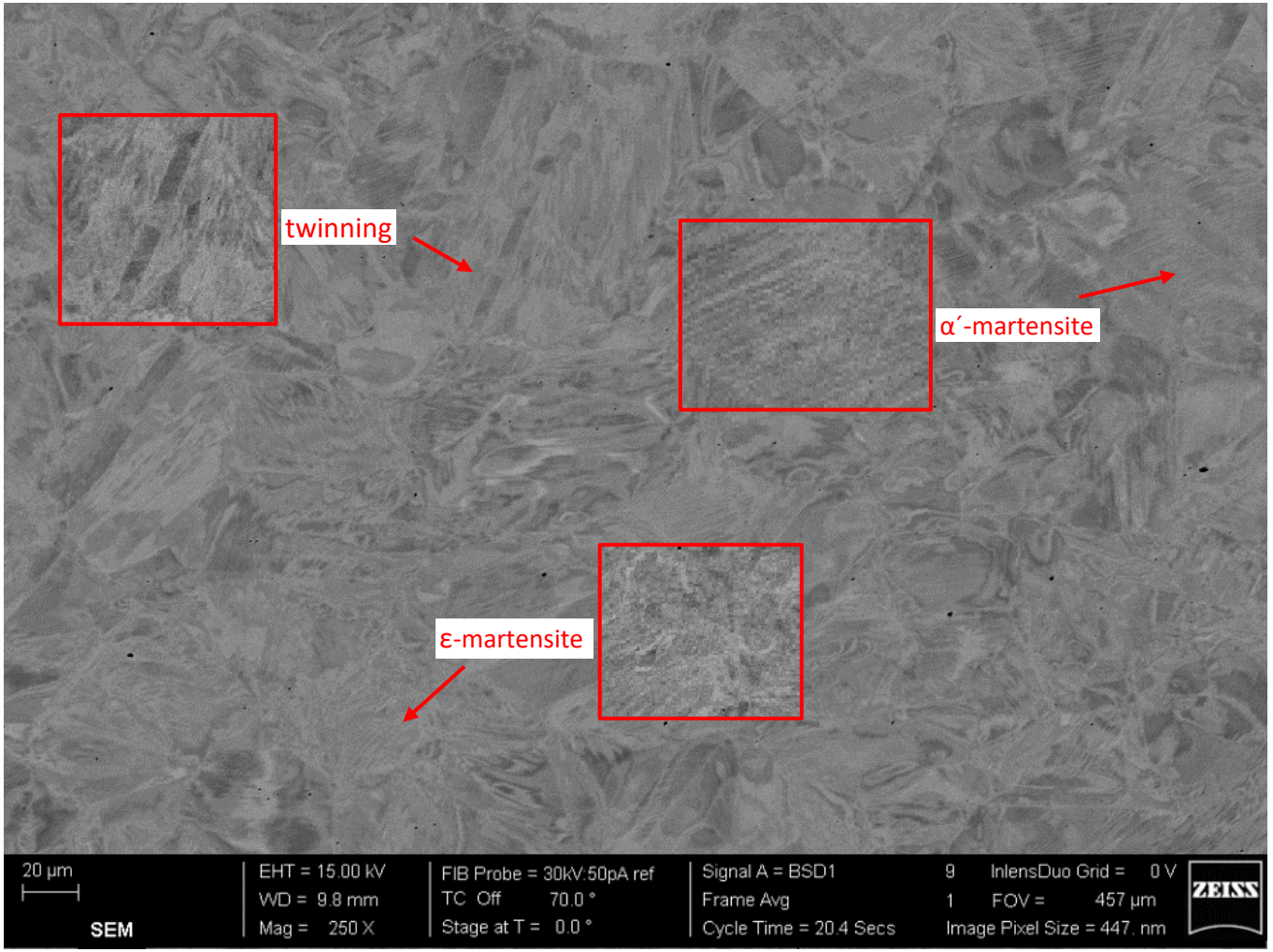
twinning
α´-martensite
ε-martensite
20 µm
SEM
EHT = 15.00 kV
WD = 9.8 mm
Mag = 250 X
FIB Probe = 30kV:50pA ref
TC Off 70.0 °
Stage at T = 0.0 °
Signal A = BSD1
Frame Avg
Cycle Time = 20.4 Secs
9 InlensDuo Grid = 0 V
1 FOV = 457 µm
Image Pixel Size = 447. nm
ZEISS

(a)

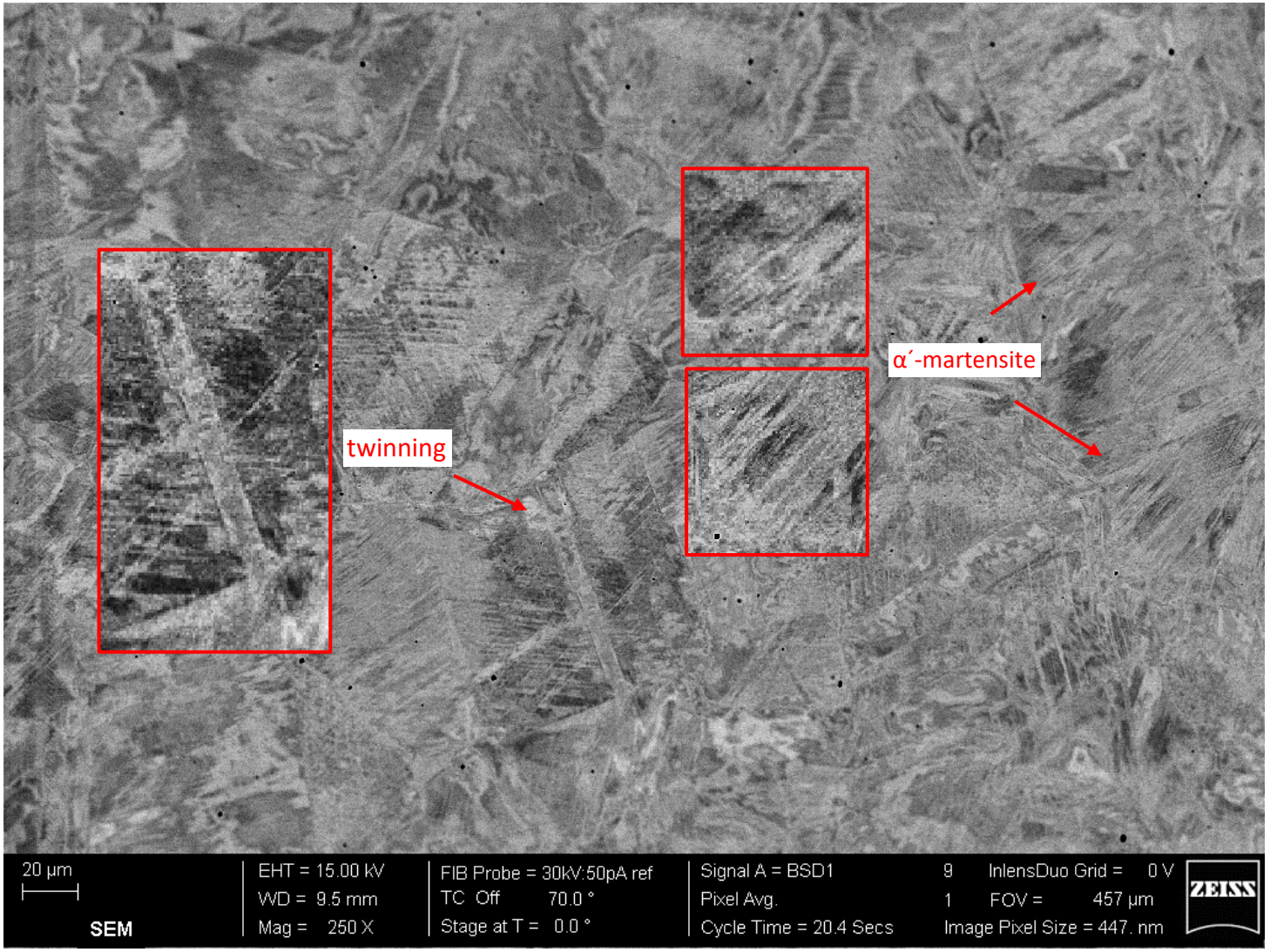
twinning
α´-martensite
20 µm
SEM
EHT = 15.00 kV
WD = 9.5 mm
Mag = 250 X
FIB Probe = 30kV:50pA ref
TC Off 70.0 °
Stage at T = 0.0 °
Signal A = BSD1
Pixel Avg.
Cycle Time = 20.4 Secs
9 InlensDuo Grid = 0 V
1 FOV = 457 µm
Image Pixel Size = 447. nm
ZEISS

(b)

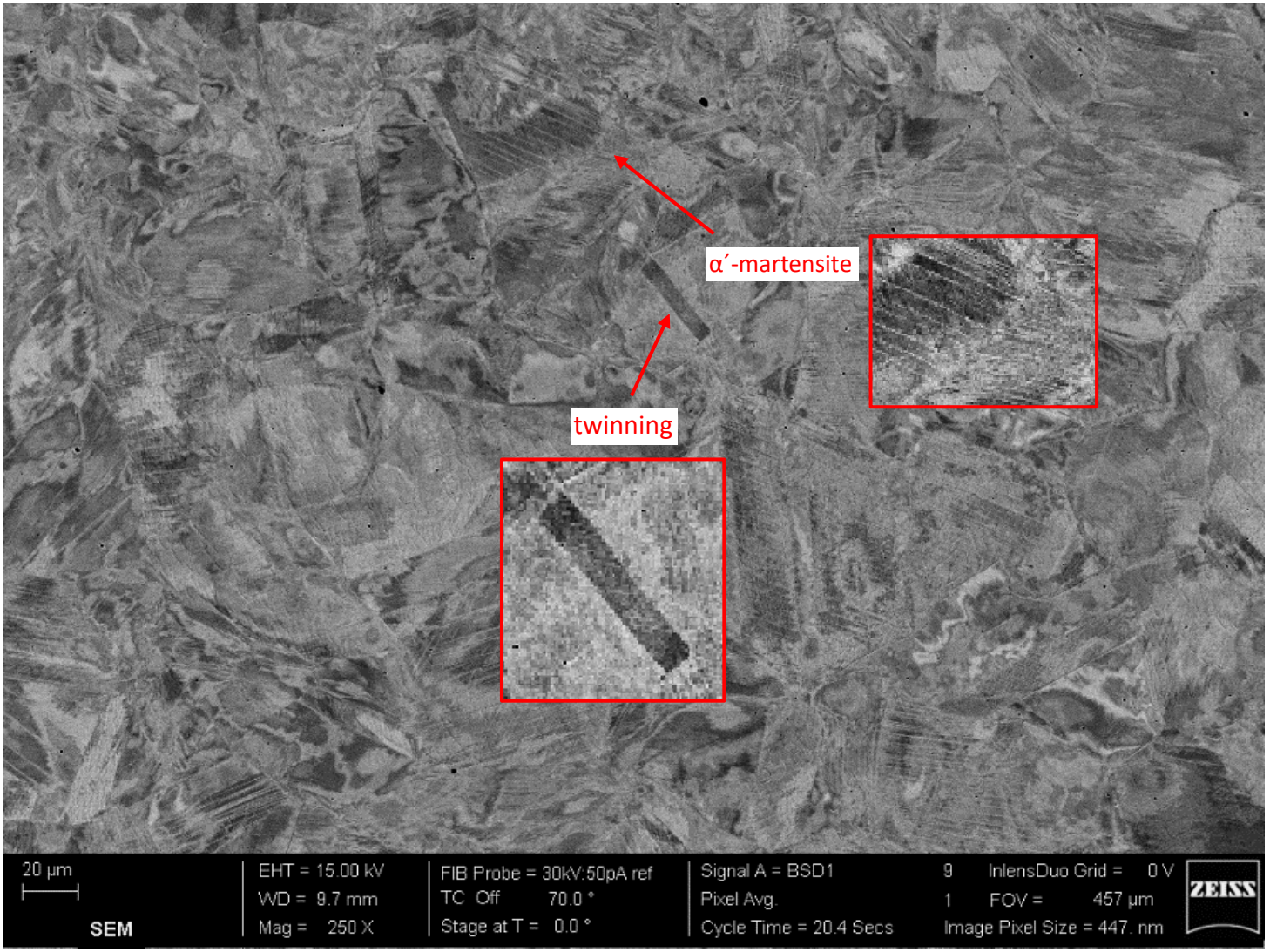
α´-martensite
twinning
20 µm
SEM
EHT = 15.00 kV
WD = 9.7 mm
Mag = 250 X
FIB Probe = 30kV:50pA ref
TC Off 70.0 °
Stage at T = 0.0 °
Signal A = BSD1
Pixel Avg.
Cycle Time = 20.4 Secs
9 InlensDuo Grid = 0 V
1 FOV = 457 µm
Image Pixel Size = 447. nm
ZEISS

(c)

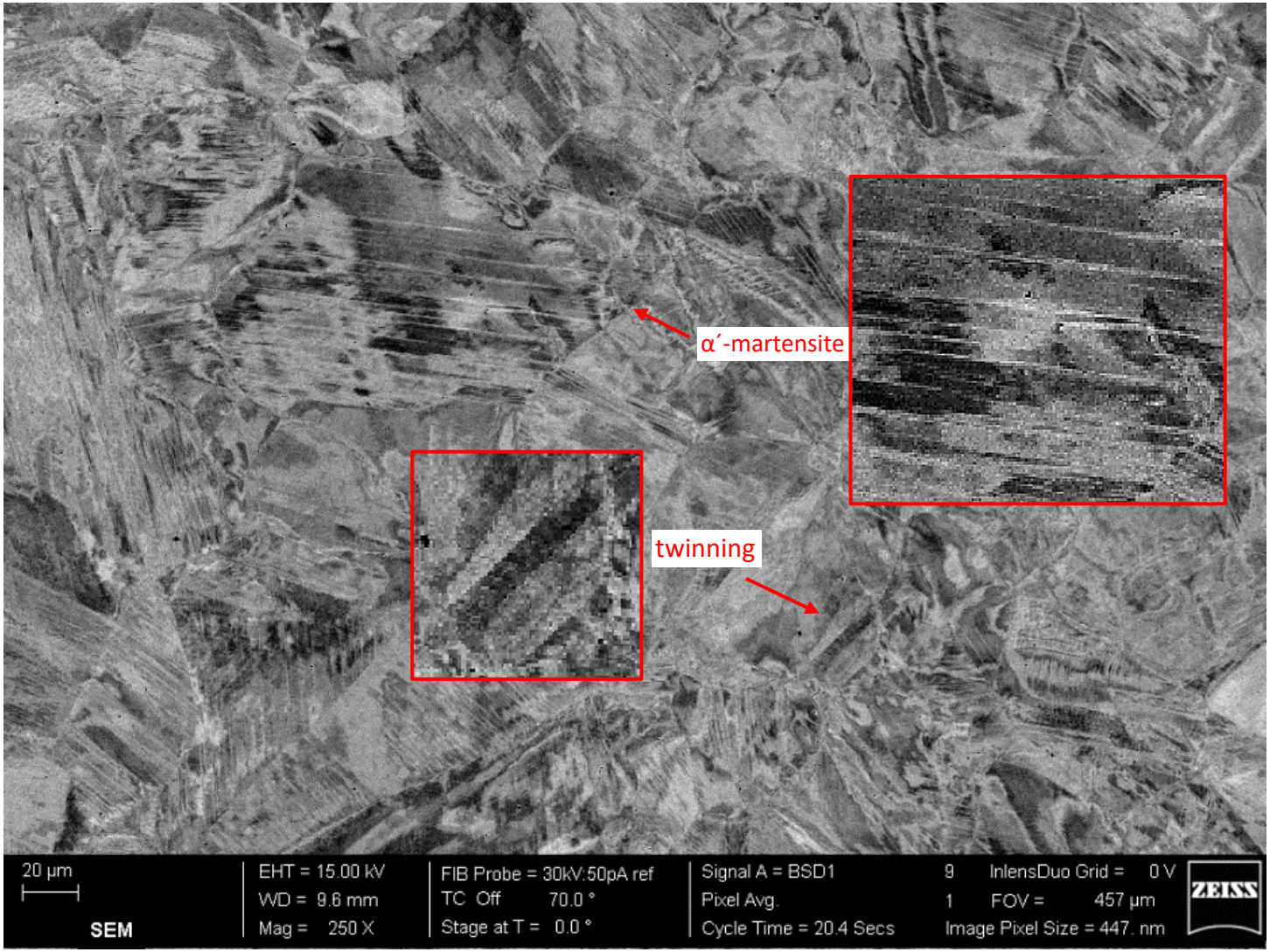
α´-martensite
twinning
20 µm
SEM
EHT = 15.00 kV
WD = 9.6 mm
Mag = 250 X
FIB Probe = 30kV:50pA ref
TC Off 70.0 °
Stage at T = 0.0 °
Signal A = BSD1
Pixel Avg.
Cycle Time = 20.4 Secs
9 InlensDuo Grid = 0 V
1 FOV = 457 µm
Image Pixel Size = 447. nm
ZEISS

(d)

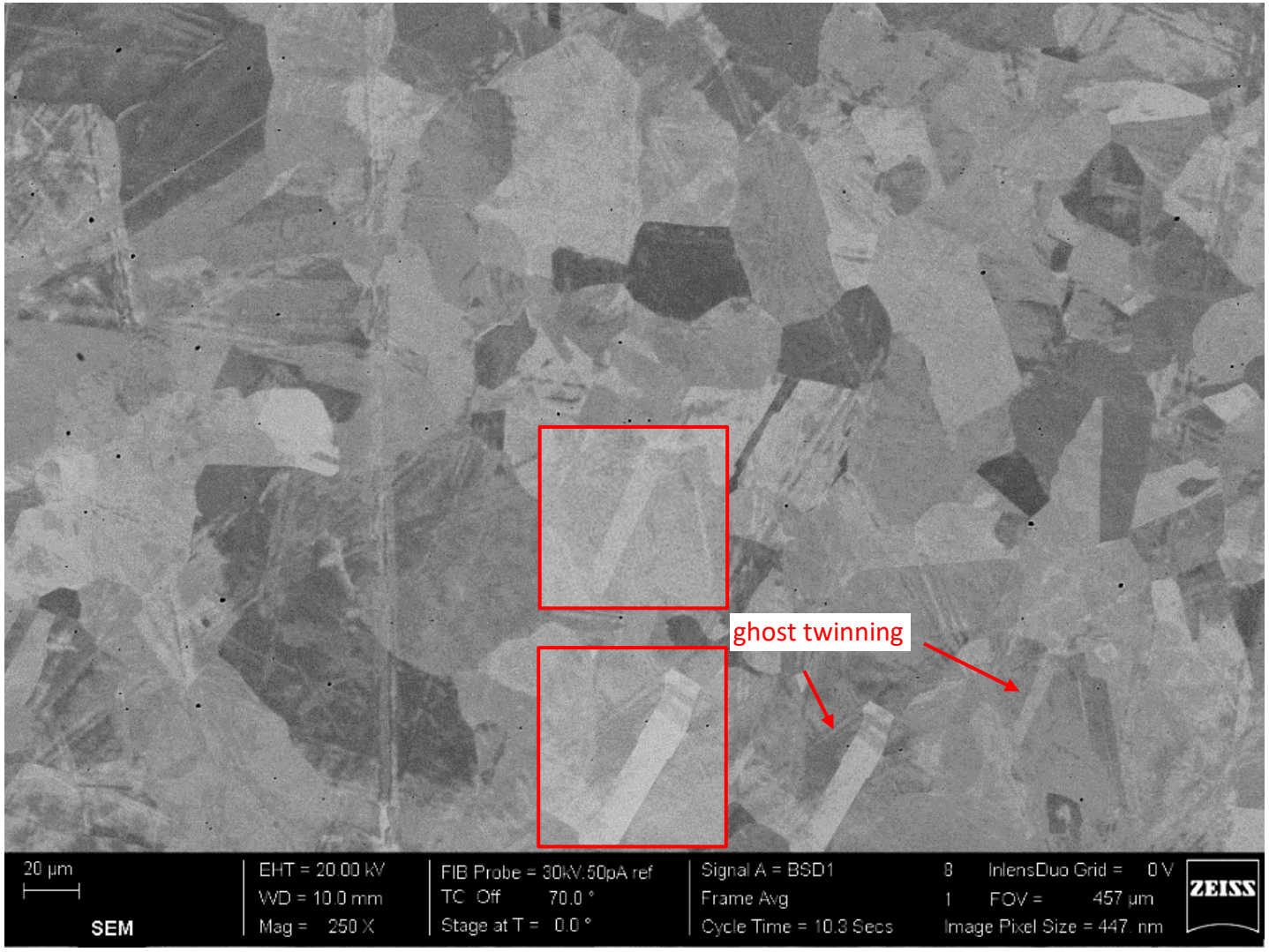
ghost twinning
20 µm
SEM
EHT = 20.00 kV
WD = 10.0 mm
Mag = 250 X
FIB Probe = 30kV:50pA ref
TC Off 70.0 °
Stage at T = 0.0 °
Signal A = BSD1
Frame Avg
Cycle Time = 10.3 Secs
8 InlensDuo Grid = 0 V
1 FOV = 457 µm
Image Pixel Size = 447. nm
ZEISS

(e)

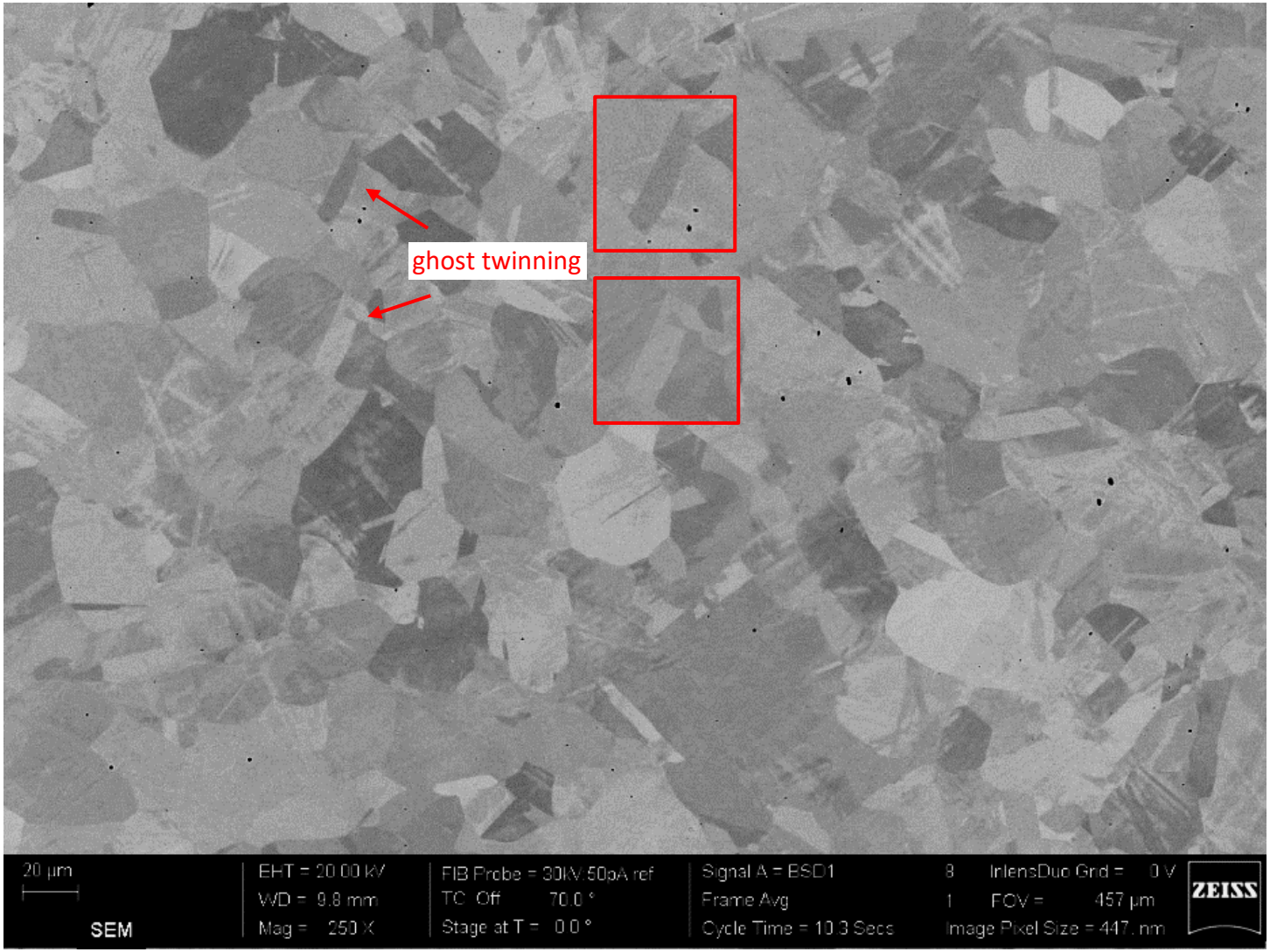
ghost twinning
20 µm
SEM
EHT = 20.00 kV
WD = 9.8 mm
Mag = 250 X
FIB Probe = 30kV 50pA ref
TC Off 70.0 °
Stage at T = 0.0 °
Signal A = BSD1
Frame Avg
Cycle Time = 10.3 Secs
InlensDuo Grid = 0 V
FOV = 457 µm
Image Pixel Size = 447. nm
ZEISS

(f)

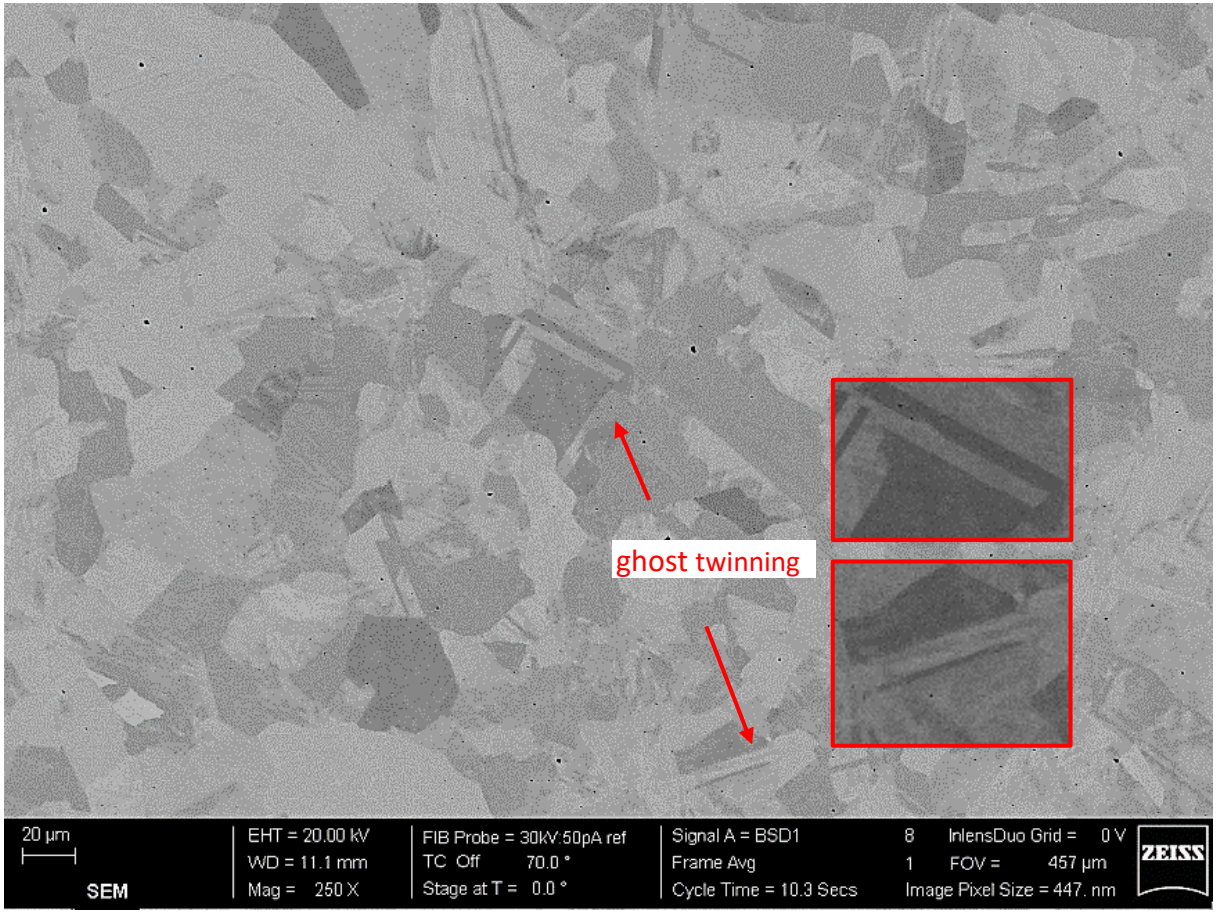

(g)

Figure 4-10: The grain imagery for grade 1.4301 reinforcing bars including (a) the virgin sample, (b) the bar exposed to 500°C and subsequently cooled by quenching in water, (c) the bar exposed to 500°C and subsequently cooled by air-cooling, (d) the bar exposed to 500°C and subsequently cooled by slow-cooling, (e) the bar exposed to 900°C and subsequently cooled by quenching in water, (f) the bar exposed to 900°C and subsequently cooled by air-cooling and (g) the bar exposed to 900°C and subsequently cooled by slow-cooling.

4.5.2 Grade 1.4401

The diffractograms for the grade 1.4401 samples are shown in Fig. 4-11 for the samples that were (a) quenched in water, (b) air-cooled, and (c) slow-cooled. Each diffractogram is compared with the virgin specimen which is found at the base of the diagrams. As was previously observed for grade 1.4301, the results for grade 1.4401 also show a small martensite presence visible between 44-45° for the virgin sample. For this grade, for all three cooling methods, only the austenite phase remains visible following any exposure to elevated temperature.

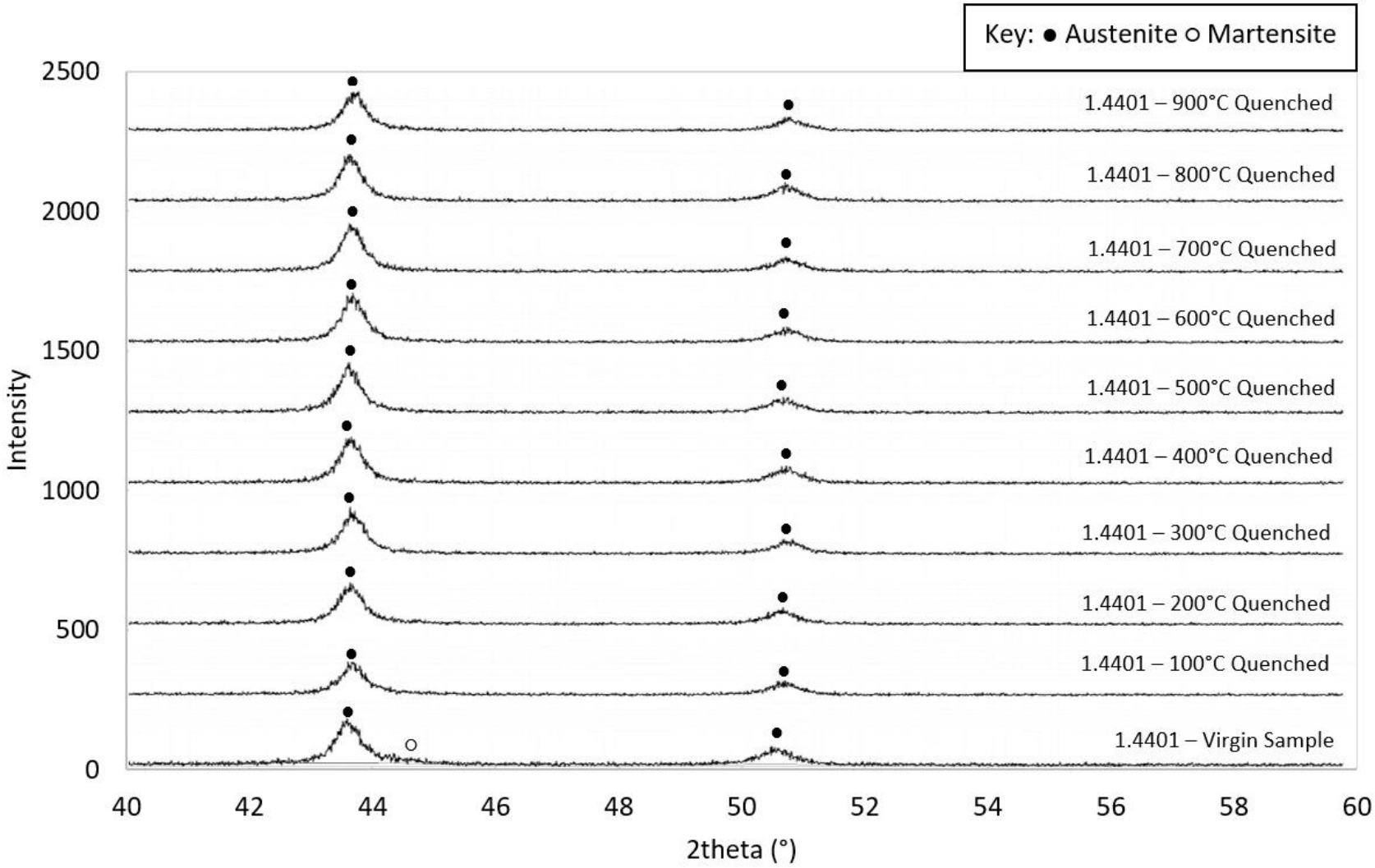
Key: ● Austenite ○ Martensite
1.4401 – 900°C Quenched
1.4401 – 800°C Quenched
1.4401 – 700°C Quenched
1.4401 – 600°C Quenched
1.4401 – 500°C Quenched
1.4401 – 400°C Quenched
1.4401 – 300°C Quenched
1.4401 – 200°C Quenched
1.4401 – 100°C Quenched
1.4401 – Virgin Sample
Intensity
2500
2000
1500
1000
500
0
40
42
44
46
48
50
52
54
56
58
60
2theta (°)

(a)

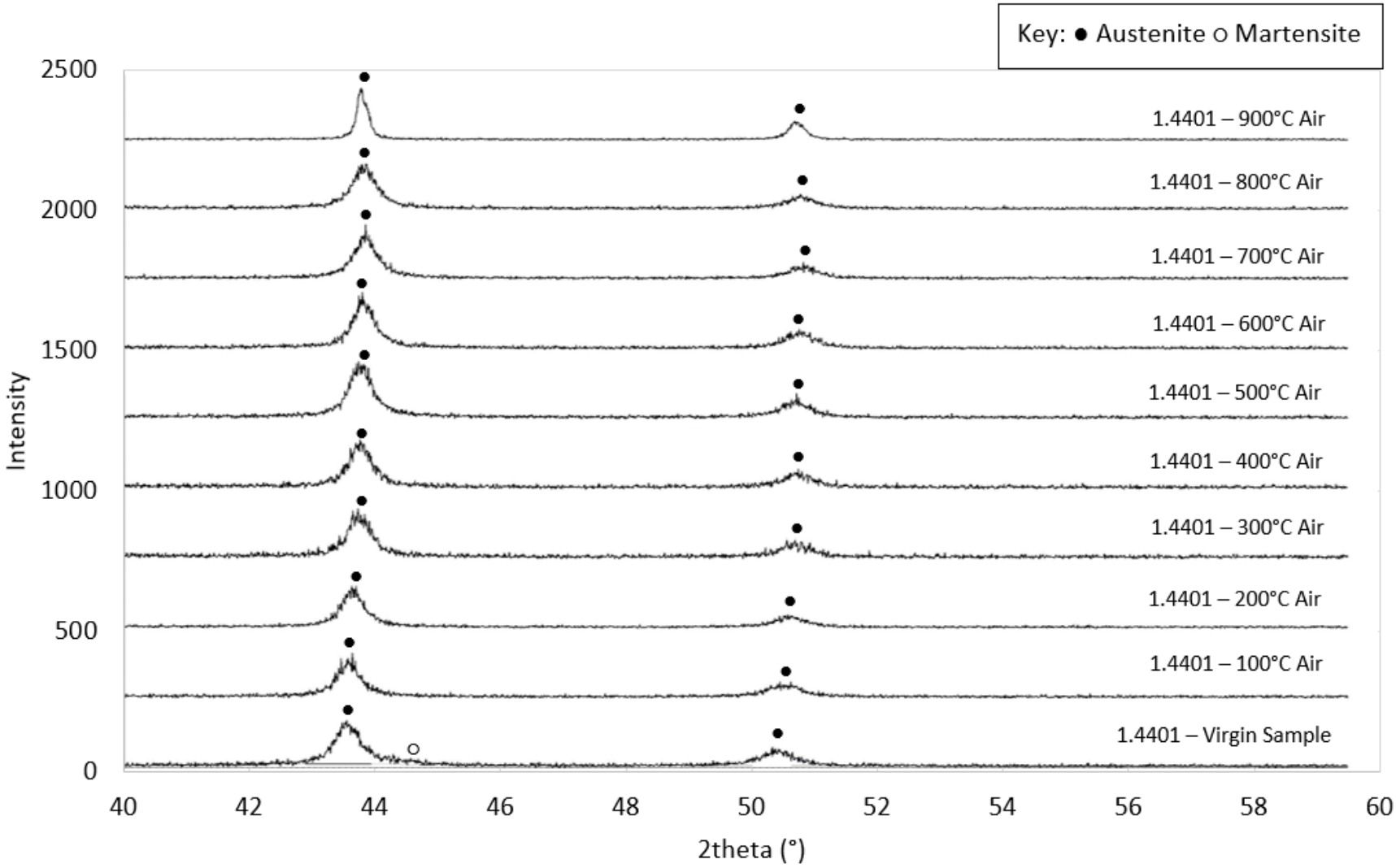
Key: ● Austenite ○ Martensite
1.4401 – 900°C Air
1.4401 – 800°C Air
1.4401 – 700°C Air
1.4401 – 600°C Air
1.4401 – 500°C Air
1.4401 – 400°C Air
1.4401 – 300°C Air
1.4401 – 200°C Air
1.4401 – 100°C Air
1.4401 – Virgin Sample
Intensity
2500
2000
1500
1000
500
0
40
42
44
46
48
50
52
54
56
58
60
2theta (°)

(b)

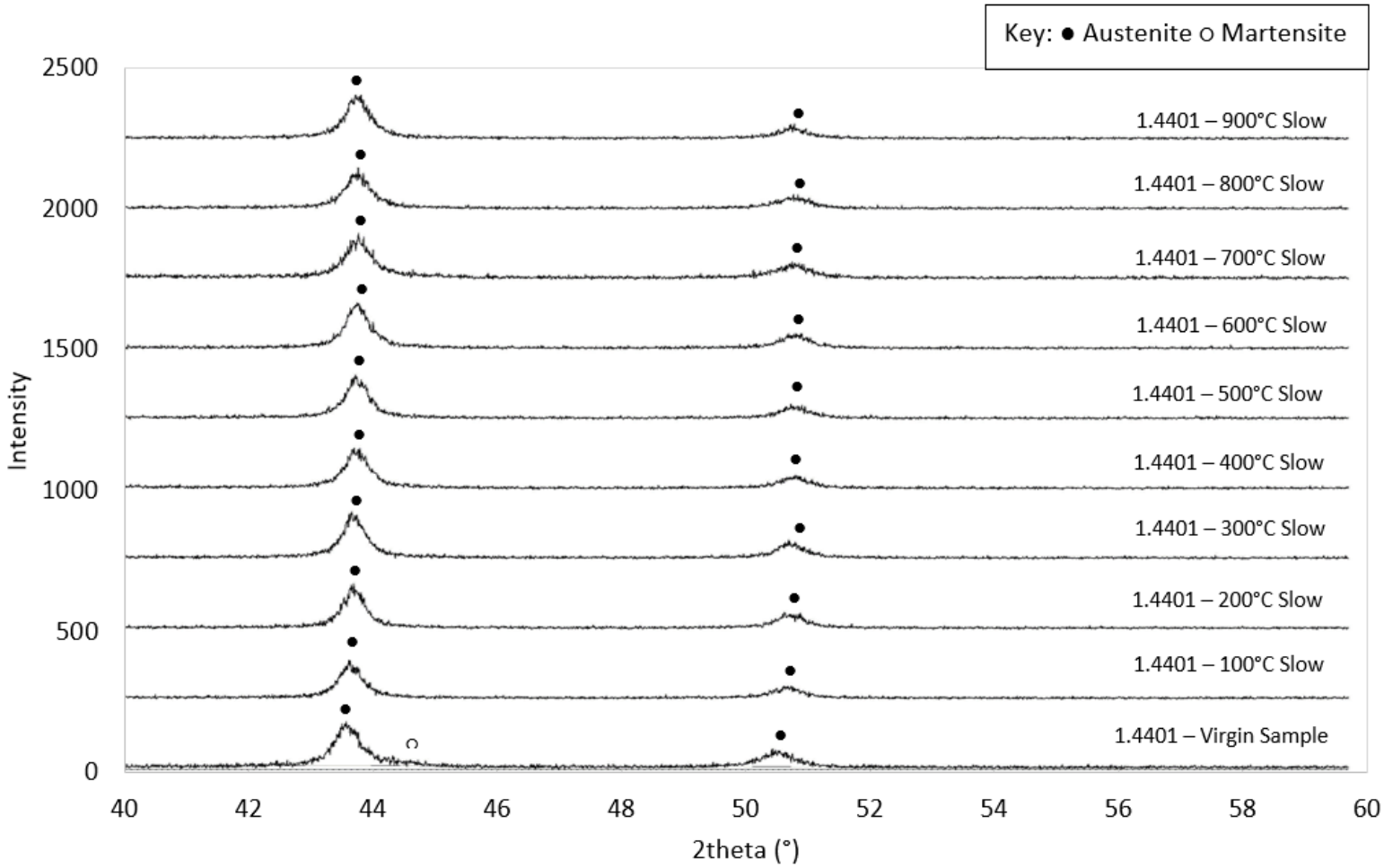

(c)

Figure 4-11: Data from the diffractograms for grade 1.4401 stainless steel reinforcing bars that were heated to various temperatures as indicated and then cooled (a) quickly, by quenching in water, (b) naturally, in air, and (c) slowly, in the furnace.

4.6 Concluding Remarks

This chapter presents the results obtained from the tensile testing of grades 1.4301, 1.4401 and 1436 austenitic stainless steel reinforcing bar and carbon steel B500B, as well as the XRD investigation into grades 1.4301 and 1.4401, and the subsequent microstructure imagery of grade 1.4301 rebar. In summary, all three grades of austenitic stainless steel rebar presented a similar response due to having a very similar microstructure. The method of cooling presented no significant change on the post-fire behaviour of the austenitic rebars. In each sample a unified trend of rising in strength until 500°C, then steadily declining in strength and increasing in ductility was noted.

Comparatively, the carbon steel rebar retained close to its original values with no significant changes observed when the samples were exposed to temperature of up to 500°C, then showed a gradual decrease in strength and increase in ductility after being exposed to higher temperatures, similar to the austenitic rebar. However, the method of cooling did influence the outcome for the quenched sample, through a sharp increase in strength and loss in ductility at 800-900°C.

Chapter 5 Residual Response of Duplex Stainless Steel Reinforcing Bar

This chapter presents the results from the tensile and metallurgical tests on two grades of duplex stainless steel reinforcement, namely grades 1.4362H and 1.4362C. These are hot-rolled and cold-rolled material grades, respectively. The results obtained and discussed herein demonstrate significantly different behaviour to those described in Chapter 4 for the austenitic stainless steel grades owing largely to the variation in metallurgy. Additionally, for the duplex stainless steel samples a lower bound temperature of 500°C was selected for the test programme as earlier studies on the austenitic stainless steels (presented in Chapter 4) showed that exposure to lower temperatures had a negligible effect on the residual properties. An upper bound temperature of 900°C was retained as this is considered a realistic limit on the temperature that rebar would be exposed to, during a fire.

5.1 Tensile Response of Duplex Grade 1.4362H

The grade 1.4362H were hot-rolled during their production. The results from the tensile tests are presented in tabular form in table 5-1, as well as the full stress-strain responses which are presented in Fig. 5-1 for (a) the samples quenched in water, (b) the air-cooled samples and (c) the slow-cooled samples. With reference to the sample names, as before, these indicate the temperature that the samples were heated to before cooling, as well as the cooling method, where Q, A and S indicate quenched in water, air-cooled and slow-cooled, respectively. Within Appendix B, Fig B.5-1 shows the fracture surface of the tested rebars, of the 300mm rebar the failure zone was localised to the central 50mm zone.

The first observation from these figures is that for all three cooling methods, there is a change in shape of the residual stress-strain response between the bars that were heated to 500°C and those that were

exposed to higher temperatures, before cooling. There is a distinct yield point visible for all of the bars that were heated to 500°C (and 600°C for the air-cooled specimens only), which was not present for the virgin samples, or those that were heated to higher temperatures. This yield point was followed by a sudden increase in strength. This is quite an unusual phenomenon for stainless steel material, and it is attributed to the nature of the duplex grain boundary. The separate austenite and ferrite grains undergo localised changes in relation to individual mechanical properties, causing a transformation in the grain boundary area (Dehghan-Manshadi et al., 2013).

Table 5-1: Post-fire properties of Duplex Stainless Steel Grade 1.4362H rebar. Labelled as the temperature of exposure followed by either -Q for quenched, -A for air-cooled and -S for slow-cooled.

	Hot-rolled 1.4362					
Specimen	E (GPa)	$f_{0.2p}$ (N/mm^2)	f_u (N/mm^2)	ε_f (%)	ε_u (%)	n
Virgin	204.9	615.7	803.0	16.0	21.7	0.9
500°C-Q	198.0	798.9	848.5	13.5	18.8	0.9
600°C-Q	197.0	688.8	803.4	15.6	20.9	0.9
700°C-Q	203.2	583.2	785.8	17.4	23.8	1.0
800°C-Q	211.6	531.1	774.2	18.4	24.2	1.0
900°C-Q	198.0	435.0	713.8	26.5	32.9	1.1
500°C-A	191.7	807.4	853.3	18.2	24.5	0.9
600°C-A	195.4	737.5	821.5	16.2	21.5	0.9
700°C-A	198.0	625.3	809.2	17.0	22.1	0.9
800°C-A	194.8	582.6	793.5	19.9	26.1	0.9
900°C-A	195.4	467.4	730.5	26.9	34.1	1.0
500°C-S	198.4	828.7	864.5	15.0	20.5	0.9
600°C-S	198.6	757.9	856.9	16.1	21.6	0.9
700°C-S	207.7	683.5	851.5	17.7	23.7	0.9
800°C-S	199.0	644.8	821.8	18.4	23.8	0.9
900°C-S	201.2	505.4	762.7	24.2	29.9	1.0

In addition, for the bars that were exposed to 500°C, all three cooling methods responded with a significant increase in $f_{0.2p}$, from 615.7 N/mm^2 for the virgin sample (i.e. room temperature, before exposure to elevated temperature) to 798.9 N/mm^2 for the quenched, 807.4 N/mm^2 for the air-cooled and 828.7 N/mm^2 for the slow-cooled specimens. This represents an increase in the residual 0.2% proof strength of between 30-35% following exposure to 500°C and then subsequent cooling. The increase was greatest for the slowest cooled specimens as the slow-cooled specimens allow for greater setting and definition of the grain, leading to a more stable microstructure following fire exposure. Moreover, it is noteworthy that 500°C is the annealing point for this material (Mondal et al., 2020), and therefore changes in properties are to be expected. The residual value for the total

strength f_u also increased following exposure to 500°C and cooling, although not to the same extent as $f_{0.2p}$. The increase in the residual f_u value was between 6-8%, with the slowest cooled specimens again showing the greatest increase of the three cooling rates examined. This disproportionate change in the residual values of $f_{0.2p}$ and f_u results in the specimens cooled by all three cooling methods failing the $f_u/f_{0.2p}$ stress ratio requirement as outlined in BS 6744 (2016) and Annex C of Eurocode 2 Part 1-1 (2004). This stipulates that in order to meet ductility Class B, $f_u/f_{0.2p}$ should be equal to at least 1.08. In this thesis, the stress ratio for the post-fire properties of the quenched samples has a value of 1.062, the air-cooled sample is 1.056 and the slow-cooled sample is 1.043.

The strain response shows a similar level of reduction for the residual values of both the ultimate strain ε_u and the total strain at failure ε_f, although there was significant variation in the level of reduction depending on the cooling rate. The samples that were quenched in water, and therefore cooled the quickest, had a residual value for ε_f which is 13% less than the corresponding virgin specimen. On the other hand, the air-cooled bars showed an increase in residual ε_f of 13% and the slow-cooled samples had a reduction in ε_f compared with the corresponding virgin sample of 6%. It is noteworthy that the specimens that were cooled the quickest and the slowest of the three scenarios both exhibited a reduction in ε_f compared to their corresponding virgin values, whereas the specimens that were heated at an intermediary rate had an increase in residual ε_f. This is most likely owing to the metallurgical changes that take place. As previously discussed, the grain boundary between the austenitic and ferritic grains is very unstable and can lead to unpredictable results for strains.

After exposure to 600°C there was a lower increase in the residual value of $f_{0.2p}$ compared to f_u allowing for the required stress ratio of at least 1.08 to be achieved across all three cooling methods. A trend is established for the residual strength, with the quenched samples showing the lowest increase of the three cooling rates examined at 12% for $f_{0.2p}$ and just over 1% for the f_u. The air-cooled samples had an intermediary increase of 20% for $f_{0.2p}$ and 2% for f_u. The slow cooled samples had the greatest rise relative to the virgin sample of 23% for $f_{0.2p}$ and 7% for f_u. The strain response demonstrated minimal change across all three cooling methods, remaining at just over 1% for both ε_u and ε_f for the air-cooled and slow-cooled methods, whereas the quenched had a 2% reduction in ε_f and 4% at ε_u.

After exposure at 700°C and subsequent cooling, the variations in the strength response between the cooling methods becomes more noticeable. Compared with the corresponding virgin samples, for the quenched samples, there was a reduction in residual $f_{0.2p}$ and f_u of 5% and 2%, respectively. For the air-cooled rebars, there was an increase in residual strength compared to the virgin values of 2% for $f_{0.2p}$ and 1% for f_u. The slow-cooled rebars showed the greatest residual increases of 11% for $f_{0.2p}$ and 6% for f_u. For the strain response there was a minor increase across all three cooling methods, but

with no notable pattern between the different cooling regimes. Overall, ε_u increased by between 6-11% compared with the virgin values following heating to 700°C and subsequent cooling, whilst the corresponding range for ε_f was between 2-10%.

A consistent trend in these observations is also shown for the bars that were exposed to temperatures of 800°C and then cooled. For those that were cooled quickly, by quenching in water, the specimens showed a large decrease of 14% in the residual value of $f_{0.2p}$ compared with the corresponding virgin values. There was also a reduction in residual $f_{0.2p}$ of 5% for the air-cooled samples compared with the virgin values. Conversely, for the slowest-cooled specimens, there was an increase in residual $f_{0.2p}$ of 5% compared with the virgin samples. The tensile strength f_u followed the same trend but the cooling rate had a negligible influence on the post-fire values. There was a reduction of 4% compared with the virgin f_u value for the quenched samples, a decrease of 1% for the air-cooled bars and an increase of 2% for the slow-cooled specimens. On the other hand, the strain response had an increase of 15-24% for ε_u and 10-20% for ε_f, compared with the corresponding virgin values, with no clear pattern for the different cooling rates.

After exposure to this highest temperature examined in this programme, 900°C, the previously-discussed trends of a reduction of residual strength and an increase in ductility for all three cooling methods are more significant. The loss of strength across the various cooling methods was most prominent for the quenched samples, whilst the slow-cooled rebars retained the greatest proportion of their original strength. A reduction of 18-29% was found in the $f_{0.2p}$ whereas the f_u reduced by between 5-11%. Additionally, apart from the slow-cooled samples, which retained $f_{0.2p}$ values of 505.4 N/mm^2, the air-cooled and quenched samples failed to meet the technical $f_{0.2p}$ requirement of 480 N/mm^2 set out in BS6744 (2016).

A closer inspection of the variations in behaviour between the three different cooling methods is presented in Fig. 5-2; in this image, the data for hot-rolled grade 1.4362H rebars is presented, for illustration. For all temperature levels, the slow-cooled bars have the highest levels of strength retention overall, followed by the air-cooled bars and then the samples that were quenched. The level of strength loss for the quenched was greatest for those bars that were exposed to relatively higher temperatures. The opposite trend is observed for the air-cooled samples, as those samples that were heated to relatively low levels of elevated temperature experienced a greater relative loss in strength than those that were heated to higher temperatures. This is similar for the slow-cooled samples, which experienced greater changes in the residual strength properties following exposure to relatively low levels of elevated temperature prior to cooling. For the slow cooled samples, at the lower temperature

range the most increase was noted against the virgin samples, and for the high temperature range the least loss was noted.

It is more challenging to draw conclusions about the residual ductility and strain behaviour compared with the strength response, as the differences between the three cooling methods were less significant. All of the samples examined in this programme achieved the required strain requirements of at least 5% ε_u and 14% ε_f following exposure to elevated temperature and then cooling, at any rate.

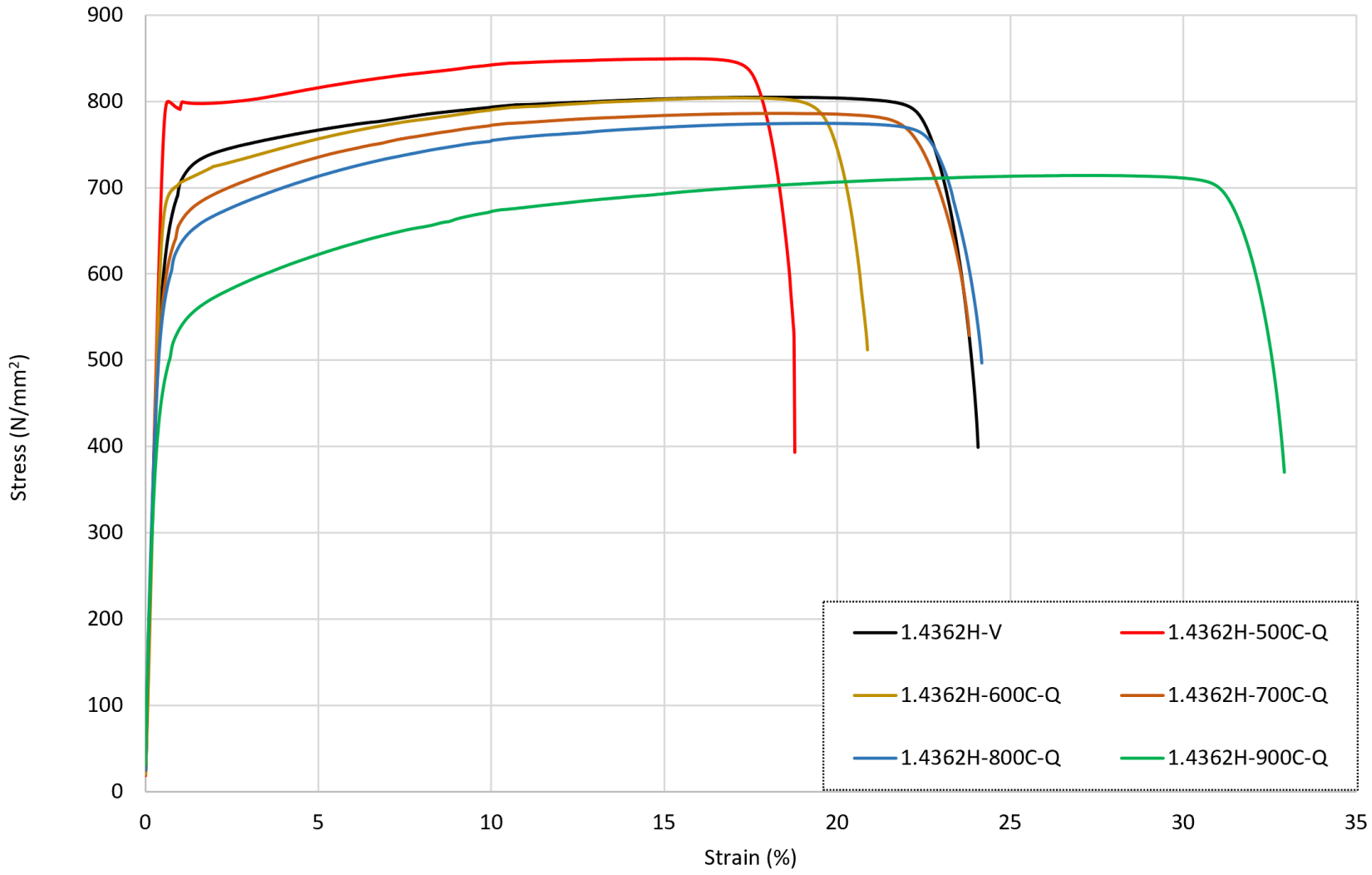
900
800
700
600
500
400
300
200
100
0
Stress (N/mm²)
0
5
10
15
20
25
30
35
Strain (%)
1.4362H-V
1.4362H-500C-Q
1.4362H-600C-Q
1.4362H-700C-Q
1.4362H-800C-Q
1.4362H-900C-Q

(a)

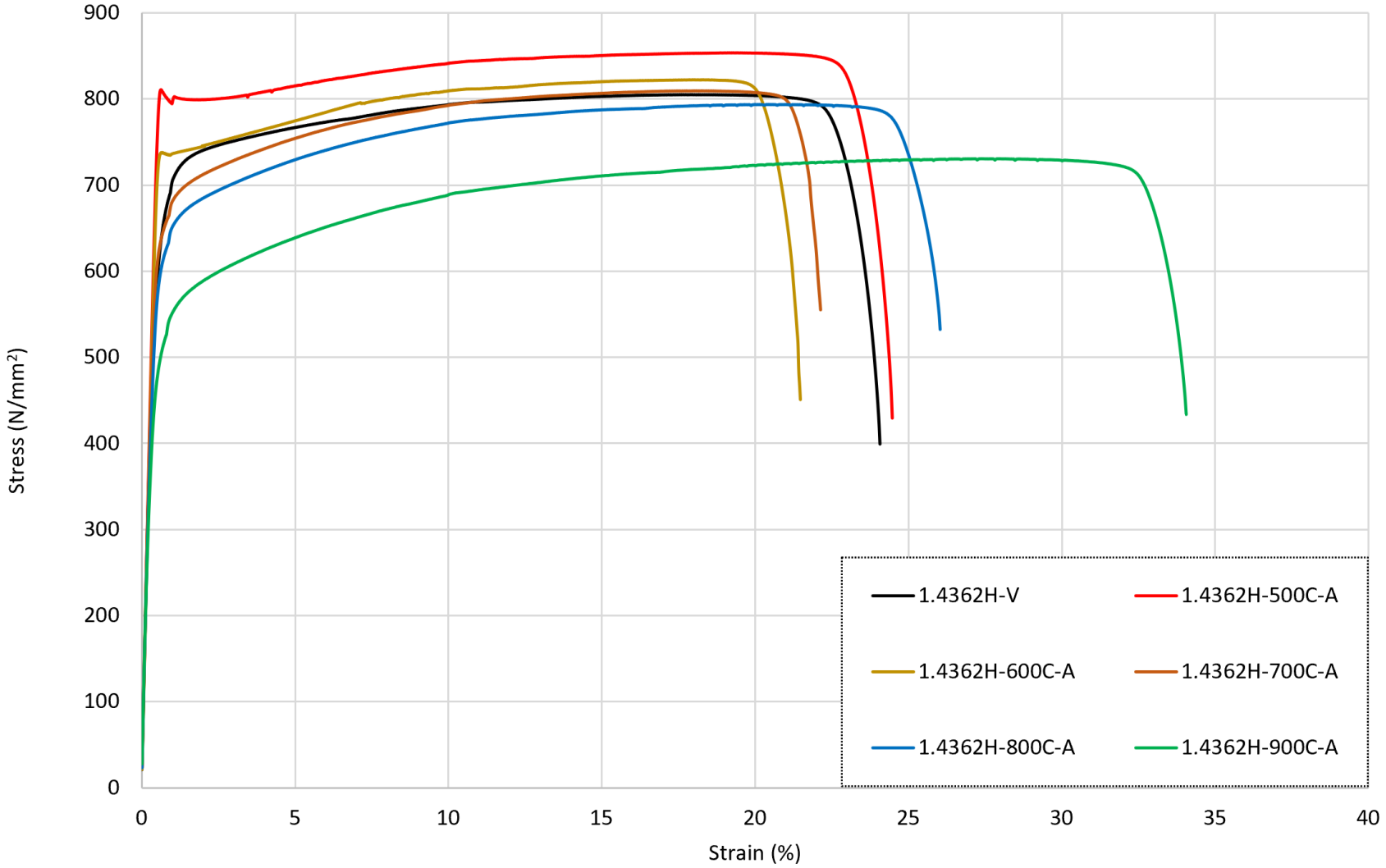
900
800
700
600
500
400
300
200
100
0
Stress (N/mm²)
0
5
10
15
20
25
30
35
40
Strain (%)
1.4362H-V
1.4362H-500C-A
1.4362H-600C-A
1.4362H-700C-A
1.4362H-800C-A
1.4362H-900C-A

(b)

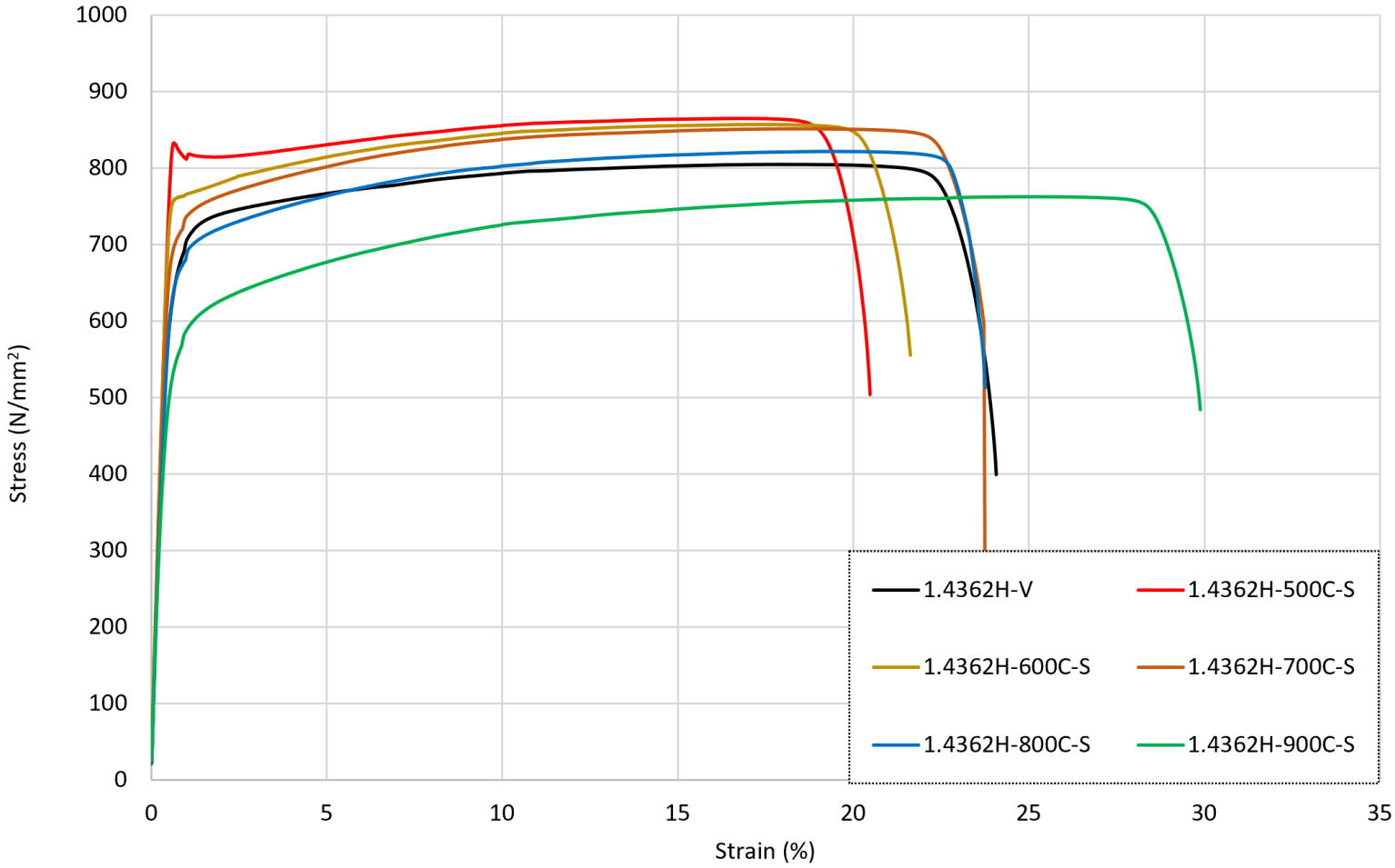

(c)

Figure 5-1: Stress-strain response for grade 1.4362H hot-rolled duplex stainless steel rebars following exposure to various degrees of elevated temperature and then cooled by (a) quenching in water, (b) naturally, in air and (c) slowly, in the furnace

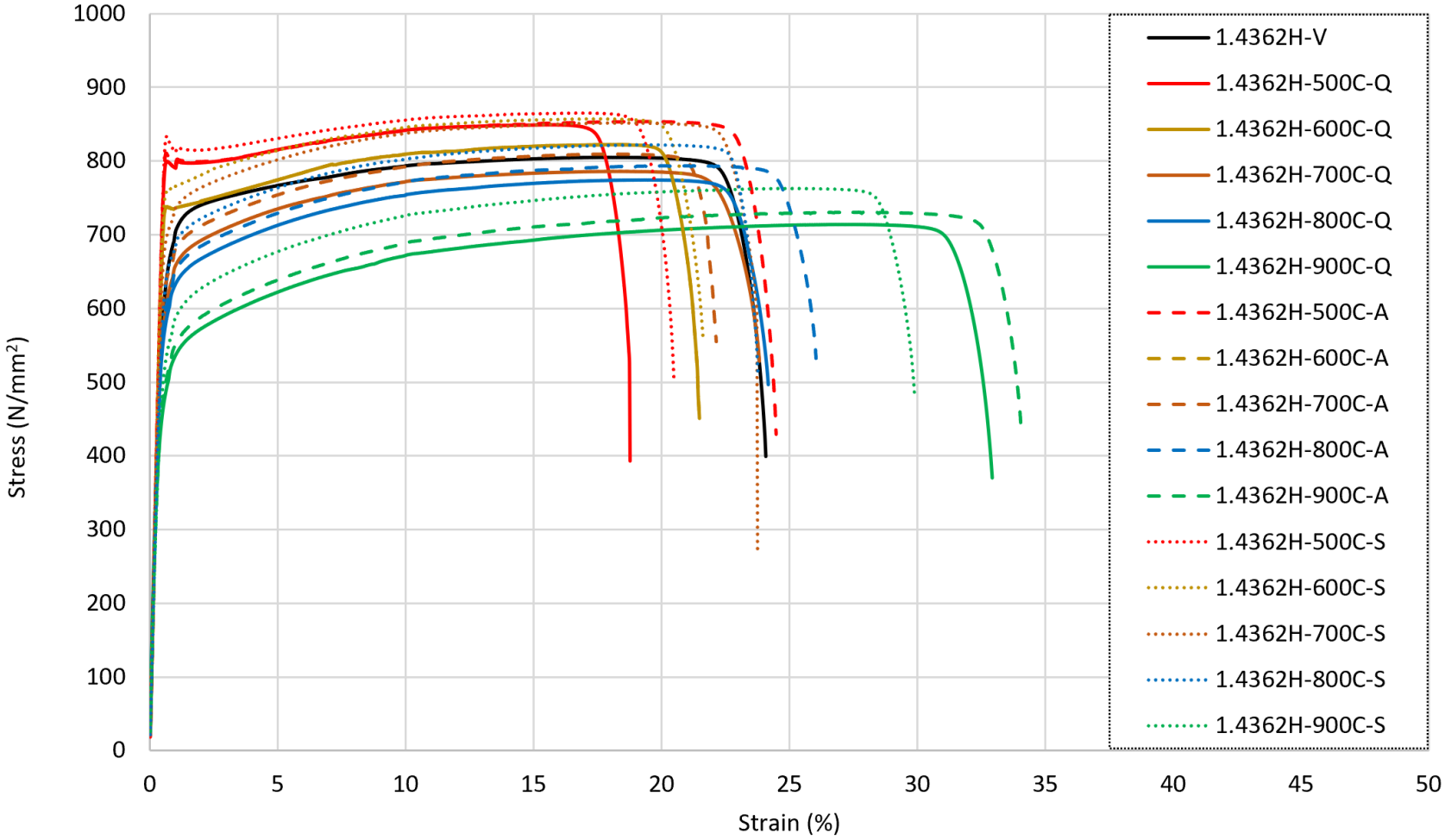

Figure 5-2: Stress-strain response for grade 1.4362H hot-rolled duplex stainless steel rebars following heating to various temperature before subsequent cooling

5.2 Cold-Rolled Grade 1.4362C Reinforcing Bar

This section presents and analyses the data from the tensile tests on cold-rolled grade 1.4362C duplex stainless steel reinforcing bar, making comparisons with the equivalent hot-rolled rebars where appropriate. The fracture surface is presented in Fig B.5-2, notably due to material limitations, 150mm samples where tested. The extensometer length remained the central 50mm, with the failure consistently taking place within this region. The numerical data is given in table 5-2 and Fig. 5-3 presents the stress-strain responses for all of the cold-rolled specimens following exposure to elevated temperatures between 500-900°C and subsequent cooling through either (a) quenching, (b) air-cooling or (c) slow-cooling. Before assessing the residual values post-heating, it is noteworthy to observe the significant differences between the virgin sample values for the hot-rolled and cold-rolled rebars. The $f_{0.2p}$ and f_u values were 615.7 N/mm^2 and 803.0 N/mm^2, respectively, for the hot-rolled bars and 836.8 N/mm^2 and 941.5 N/mm^2, respectively, for the cold-rolled rebars in the same grade. Even more notable is the differences in strain values; ε_u was 16% for the hot-rolled rebars and just 1.5% for the cold-rolled bars.

Table 5-2: Post-fire properties of Duplex Stainless Steel Grade 1.4362C rebar. Labelled as the temperature of exposure followed by either -Q for quenched, -A for air-cooled and -S for slow-cooled.

	Cold-rolled 1.4362					
Specimen	E (GPa)	$f_{0.2p}$ (N/mm^2)	f_u (N/mm^2)	ε_f (%)	ε_u (%)	n
Virgin	200.9	836.8	941.5	19.3	19.7	0.9
500°C-Q	202.3	924.2	976.6	21.6	22.1	0.8
600°C-Q	198.1	848.2	945.8	18.4	18.9	0.8
700°C-Q	199.6	735.5	886.9	22.5	22.8	0.8
800°C-Q	199.4	529.5	792.9	59.0	59.3	1.0
900°C-Q	202.5	429.5	708.0	59.1	59.4	1.1
500°C-A	198.7	938.5	1003.3	19.1	19.5	0.9
600°C-A	197.9	913.4	981.2	19.2	19.6	0.8
700°C-A	197.9	785.4	915.0	18.9	19.4	0.8
800°C-A	202.9	605.6	798.6	39.4	39.8	1.0
900°C-A	198.0	443.9	731.0	55.1	55.4	1.1
500°C-S	204.1	976.1	1006.2	23.3	23.8	0.8
600°C-S	207.1	950.2	1004.1	18.9	19.4	0.8
700°C-S	191.6	849.0	947.9	19.1	19.7	0.7
800°C-S	206.9	636.4	816.1	56.3	56.7	0.9
900°C-S	207.2	485.5	760.4	56.7	57.1	0.9

For the post-fire samples, following exposure to either 500°C or 600°C, all of the samples exhibited an increase in strength, both $f_{0.2p}$ and f_u, compared with the unheated virgin samples, regardless of the cooling method. This pattern reversed for the bars that were heated to higher temperatures before cooling, as they lost strength. Considering first the specimens that were heated to 500°C, the bars that were quenched in water had the lowest increase in $f_{0.2p}$, rising to 924.2 N/mm^2, followed by the air-cooled samples which increased to 938.5 N/mm^2 and then the slow-cooled samples which had the greatest increase in residual 0.2% proof strength, changing to 976.1 N/mm^2; these values equate to increases of between 10-17% compared with the virgin values. On the other hand, f_u showed an increase of between 4-7% compared with the virgin values. The residual $f_{0.2p}$ and f_u strength values following exposure to 500°C result in these bars failing to meet the stress ratio criteria of $f_u/f_{0.2p}$ being at least equal to 1.08. The quenched samples had a stress ratio of 1.057, the air-cooled sample was 1.069 and the slow-cooled sample was 1.031.

From the stress-strain responses presented in Fig. 5-3, the changes in residual strains following exposure to 500°C and then cooling are quite different to those observed for the hot-rolled bars. For the cold-rolled bars, ε_u changed from 1.5% for the virgin sample to 6.1%, 4.8% and 3.7% for the quenched, air-cooled and slow-cooled samples, respectively. This is because some, and differing, levels of the cold-working in the material was permanently lost following heating. The differences in ε_f following heating and cooling were much more similar to those observed for the hot-rolled bars. This property ε_u changed from 19.7% for the virgin sample to 22.1%, 19.5% and 23.8% for the quenched, air-cooled and slow-cooled samples, respectively.

For the samples exposed to temperatures of 600°C and then subsequently cooled, the response is very similar to that of the 500°C sample set. For $f_{0.2p}$, the quenched samples presented the least variation relative to the virgin specimens, with an increase of 1% from 836.8 N/mm^2 to 848.2 N/mm^2 for $f_{0.2p}$, whereas the air-cooled sample presented a rise of 9% to 913.4 N/mm^2, and the slow-cooled samples rose by 14% to 950.2 N/mm^2. On the other hand, the f_u values also increased by 1%, 4% and 7%, for the quenched, air-cooled and slow-cooled samples, respectively. As the quenched samples reflect the least change from the virgin values, these meet the stress ratio requirement of 1.08 with a ratio of 1.115, whilst the air-cooled and slow-cooled bars fail to meet this requirement with ratios of 1.074 and 1.058, respectively. For the strain response, a more consistent increase between the three cooling methods was observed, with ε_u rising by between 321%-413% overall and ε_f presenting a loss of between 1-4% against the virgin sample. It is clear that for the cold-rolled duplex stainless steel samples, there are quite different behaviours between the ultimate and failure strains. In cold-rolled rebars, the ultimate strain occurs sooner in the overall stress-strain curve as the material gains more ductility in the elastic region following heating and cooling, as the grains relax. The ferrite grains are

more prone to change within this temperature range compared with the austenite grains, and tend to lose any cold-rolling properties. The microstructural features induced through the cold-rolling process begin to dissipate in the ferrite grains following heating, and the stress strain curves begins to change shape to match a more idealized stainless steel curve, whereas the cold-rolled properties induced into the austenite show little to no difference.

Following exposure to 700°C and subsequent cooling, the residual $f_{0.2p}$ values were quite dependent on the cooling method. The samples that were cooled quickly by quenching lost some strength, decreasing by 12% to 735.5 N/mm^2 compared with 836.8 N/mm^2 for the virgin samples. Similarly, the air-cooled samples also lost strength recording a residual value for $f_{0.2p}$ of 785.4 N/mm^2 (a reduction of 4%). On the other hand, the slow-cooled samples did not change to a great extent and in fact increased by 1% to 849 N/mm^2. In this temperature range, the austinite grains gradually begin to dissipate the cold-worked strength but as the change is very minor, they require rapid cooling to stabilise this change; therefore, a relatively slower cooling rate results in more of the cold-worked strength being recovered. The ultimate strength, f_u, followed a similar trend with the quenched and air-cooled samples decreasing in value by 6% and 3% compared with the virgin sample, respectively, whilst the slow-cooled samples increased by 1%. All of the samples examined met the stress ratio requirement $f_u/f_{0.2p}$ being at least equal to 1.08. For the strain response, similar to the samples exposed to 600°C, no distinctive pattern is visible across the three cooling methods. The residual ultimate strain value ε_u increased by 383%-413% against the virgin samples whilst for the failure strain ε_f, the quenched sample had a significant 16% rise, whereas both the air-cooled and slow-cooled samples changed by less than 1%.

After exposure to 800°C followed by the various cooling methods, the pattern in the stress response remains consistent for both the $f_{0.2p}$ and f_u to those discussed before. The quenched sample lost a significant amount of its strength, with the $f_{0.2p}$ and f_u dropping by 37% and 16% to 529.5 N/mm^2 and 792.9 N/mm^2, respectively. The air-cooled samples exhibited lower strength losses of 28% and 15% for $f_{0.2p}$ and f_u, respectively, whilst $f_{0.2p}$ and f_u for the slow-cooled samples decreased the least, reducing by 24% and 13% to 636.4 N/mm^2 and 816.1 N/mm^2, respectively. All of the samples examined met the stress ratio requirement of $f_u/f_{0.2p} \geq 1.08$. For the strain behaviour, the samples exposed to temperatures of 800°C presented the greatest increases against the virgin sample values whilst also presenting a different shape for the overall stress-strain response. The ultimate strain ε_u increased by 2363% from 1.5% to 48.8% for the quenched sample, 2428% from 1.5% to 49.7% for the air-cooled samples and 2168% from 1.5% to 45.9% for the slow-cooled samples. The residual failure strain values ε_f also increased from their corresponding virgin-state values, with increases of 201%, 199% and 188%, respectively, for the quenched, air-cooled and slow-cooled specimens, resulting in a more elongated

stress-strain curve. The large disparity between the increase in ε_u relative to ε_f is because of the active dissipation of the cold-worked strength as described before, however a complete dissipation is not achieved, thus resulting in a reduction (or sag) in the stress-strain curve, as seen for all three cooling methods in Fig 5-3. Essentially, these bars yielded before 10% strain was reached, and then strain hardened until around 50% strain before necking occurred. It is noteworthy that this observation was not evident for the bars that were heated to 900°C, as discussed later.

After exposure to the highest temperature included in this thesis, 900°C, followed by cooling, the residual $f_{0.2p}$ and f_u values decreased by 49% and 25% for the quenched samples compared to the virgin values, 47% and 22%, respectively, for the air-cooled samples, and 42% and 19% for the slow-cooled rebars. Although all three samples met the stress requirement of $f_u/f_{0.2p} \geq 1.08$, only the slow-cooled sample met the minimum $f_{0.2p}$ requirement of 480 N/mm^2 in accordance with BS 6744 (2016). For the ductility, all of the specimens cooled by any of the three methods exhibited an increase in ε_u and ε_f, and the stress-strain curve also indicated that most of the cold-working in the material was lost during heating and not recovered. As before, the changes in ε_u were most significant as the quenched ultimate strain increased by ε_u 1652%, the air-cooled specimens rose by 1374% and the slow-cooled bars grew by 1234%. The equivalent residual improvements to ε_f were 202%, 181% and 190% of the corresponding virgin values for the quenched, air-cooled and slow-cooled samples, respectively.

In order to specifically compare the influence of cooling rate, Fig. 5-4 presents all of the stress-strain data from tests on cold-rolled grade 1.4362C duplex stainless steel, heated to a range of values and then cooled by one of the three cooling rates examined. The change in shape that occurred for samples that were heated to 500-700°C and then cooled compared with those that were heated to 800-900°C, is consistent for all cooling rates. It is clear that the cold-working effect that was introduced to the bars during production, was permanently lost at a temperature between 700-800°C. Another observation is that the overall residual strength of the quenched samples was consistently lowest of those tested, followed by the air-cooled specimens whilst the slow-cooled bars regained the greatest proportion of their original strength. In terms of ductility, there is no significant pattern across all three cooling methods and temperature exposure levels. For bars that were exposed to 500-700°C, there was no significant change to the maximum strains recorded, whereas following heating to higher temperatures, as previously discussed, the maximum strains increased significantly, owing to the loss of the cold-working effect. For all bars that were exposed to 600°C and above, the minimum specified requirement of ε_u being at least 5% was consistently achieved (BS 6744, 2016).

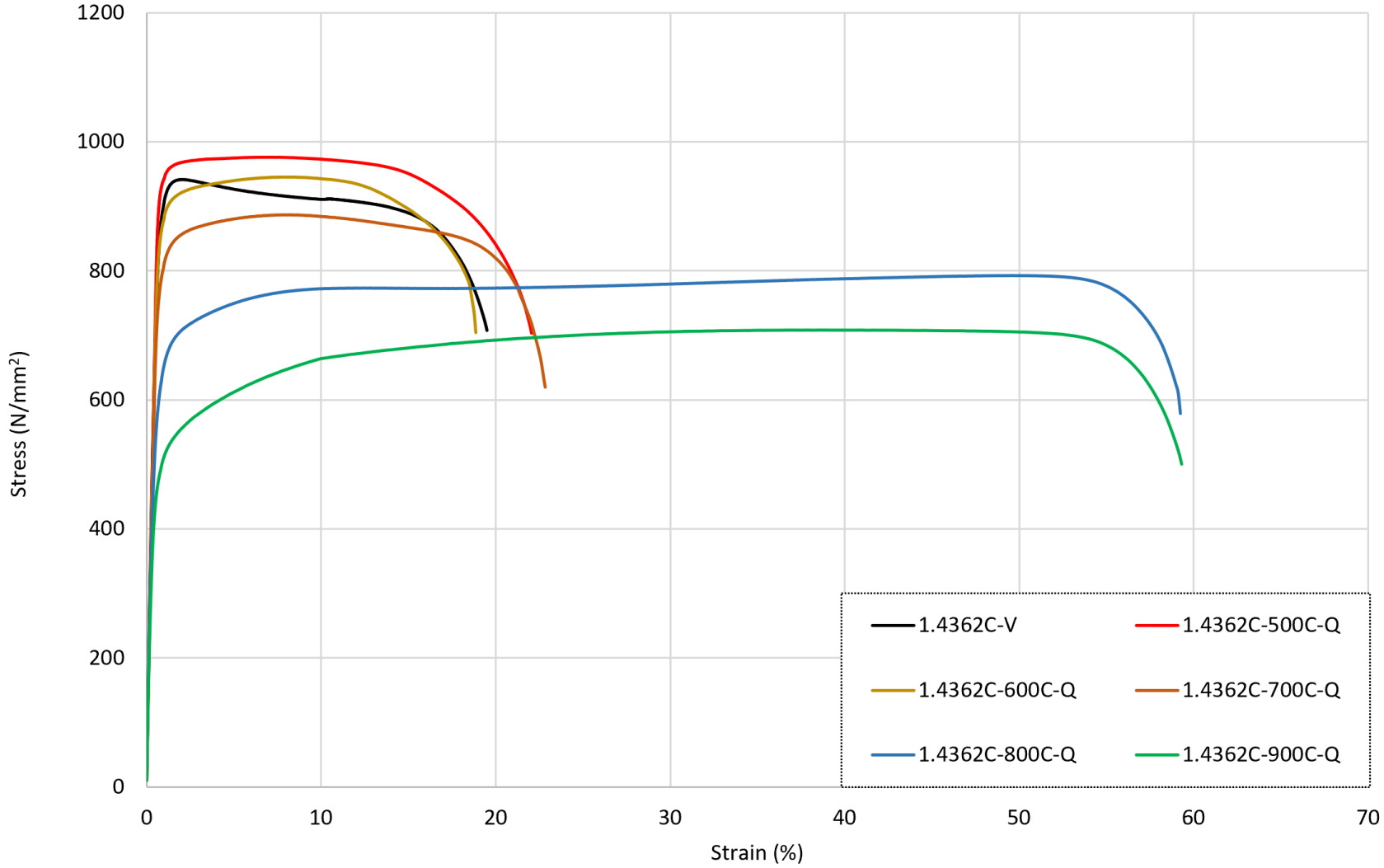
1200
1000
800
600
400
200
0
Stress (N/mm²)
0
10
20
30
40
50
60
70
Strain (%)
1.4362C-V
1.4362C-500C-Q
1.4362C-600C-Q
1.4362C-700C-Q
1.4362C-800C-Q
1.4362C-900C-Q

(a)

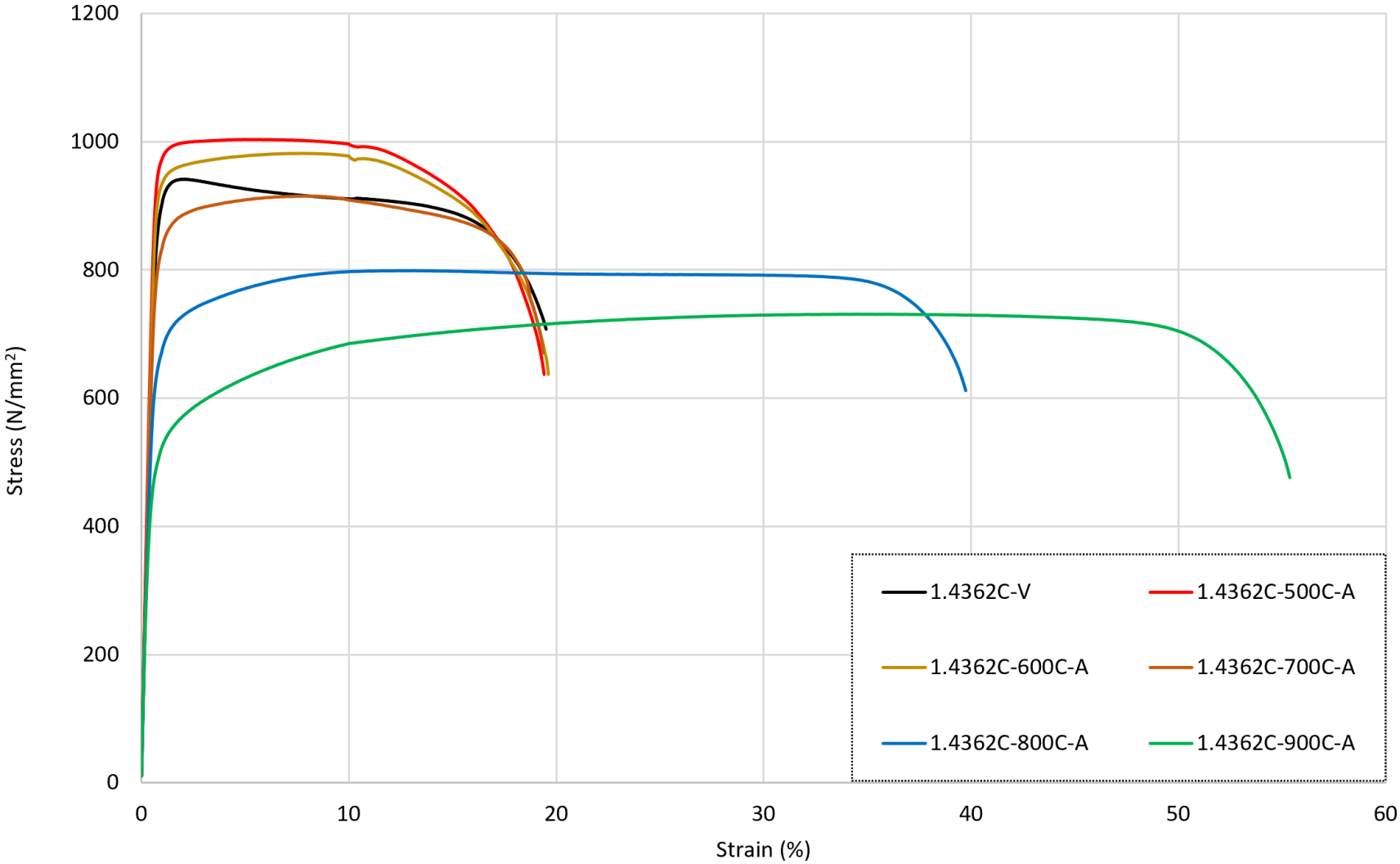
1200
1000
800
600
400
200
0
Stress (N/mm²)
0
10
20
30
40
50
60
Strain (%)
1.4362C-V
1.4362C-500C-A
1.4362C-600C-A
1.4362C-700C-A
1.4362C-800C-A
1.4362C-900C-A

(b)

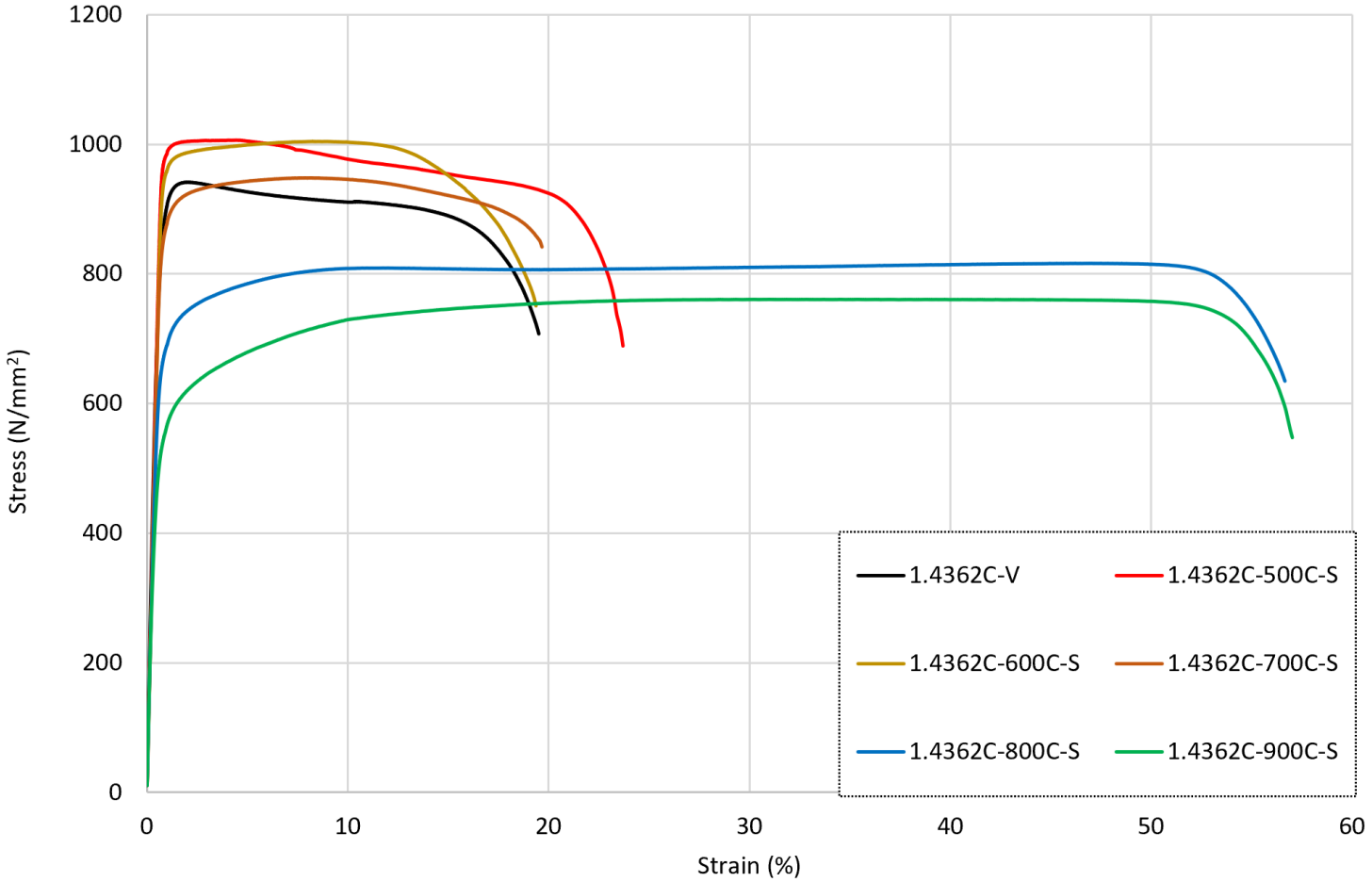

(c)

Figure 5-3: Stress-strain response for grade 1.4362C cold-rolled duplex stainless steel rebars following exposure to various degrees of elevated temperature and then cooled by (a) quenching in water, (b) naturally, in air and (c) slowly, in the furnace

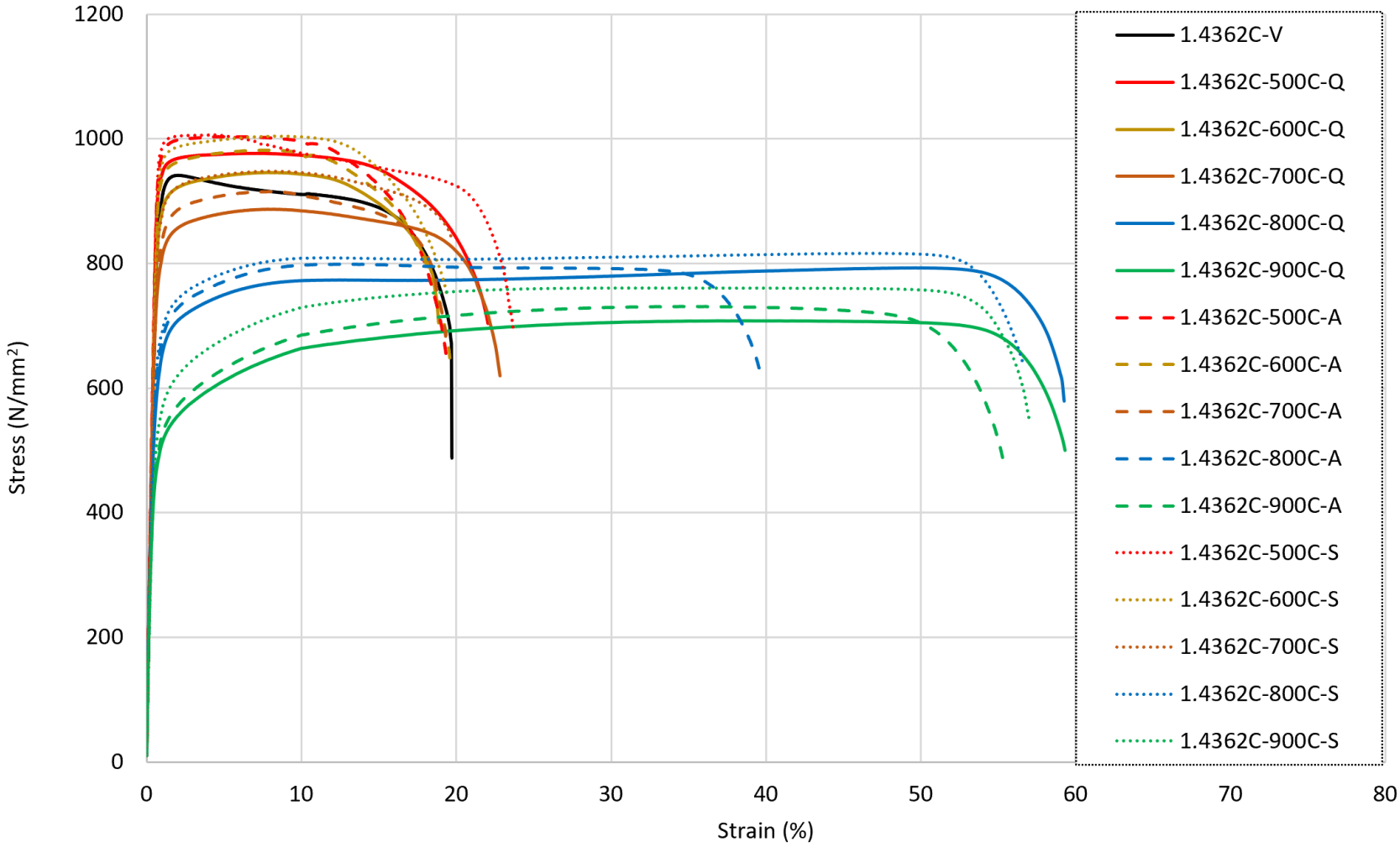

Figure 5-4: Stress-strain response for grade 1.4362C cold-rolled duplex stainless steel rebars following heating to various temperature before subsequent cooling

5.3 Results from the Metallurgical Investigation

One of the key aims of this work was to study not only the tensile characteristics of duplex stainless steel reinforcement following fire exposure but also the key metallurgical phenomena that occur, in order to develop a full understanding of the behaviour. As with all duplex stainless steel alloys, prominent austenite and ferrite grains are present. In this work, material characterization was carried out to determine if there is a change between the balance in the austenite and ferrite grains following elevated temperature exposure and to understand the consequent change in microstructure. This was done using two methods (i) an initial inspection was conducted through X-ray diffraction (XRD), for phase identification and monitoring of phase changes, and (ii) through microscopic imagery to obtain a visual inspection of the size, shape and dispersion of the grains.

5.3.1 XRD Examination

The diffractograms obtained from the XRD investigation are given in Figs. 5-5 and 5-6, and indicate the presence of the phase (intensity) against the angle of discovery (2theta). Fig. 5-5 presents the data for hot-rolled grade 1.4362H reinforcing bars that were heated to various temperatures as indicated and then cooled either (a) by quenching in water, (b) naturally, in air, or (c) slowly, in the furnace at a controlled rate of 1°C/min. Fig. 5-6 presents the corresponding images for the cold-rolled rebars. The position of both the austenite (solid dot) and ferrite (empty dot) peaks are labelled in the images along the x-axis. Notably, for 2theta, only between 40°-90° is presented as this is the range prone to significant change.

There is no significant change of phase visible for specimens that were cooled at different rates. The diffractograms for both the hot- and cold-rolled samples remain almost identical, with phase peaks at the same location. Through further analysis using the DIFFRAC.EVA phase identification software (Bruker, 2021), the ratio of austenite to ferrite was found to be 1:3, or 25% austenite and 75% ferrite, on average, for both the virgin cold-rolled and hot-rolled samples. The 1:3 ratio was quite consistent for the cold-rolled samples, with the exception of the air-cooled samples at 700°C, which presented an increase to 35% austenite and 65% ferrite retention, which can also be observed in Fig. 5-6(b). For the hot-rolled samples, the austenite-ferrite ratio was significantly less stable, with the samples that were heated to 500°C and 800-900°C before being quenched or slow-cooled presenting a change of austenite between 35-40% and a retention of ferrite between 60-65%; all of the air-cooled samples remained stable. Austenite is more stable than ferrite at higher temperatures, for the quenched and slow-cooled samples, the conditions for the ferrite nucleation are not met, resulting in a decline in the ferrite content and a rise in the austenite grains.

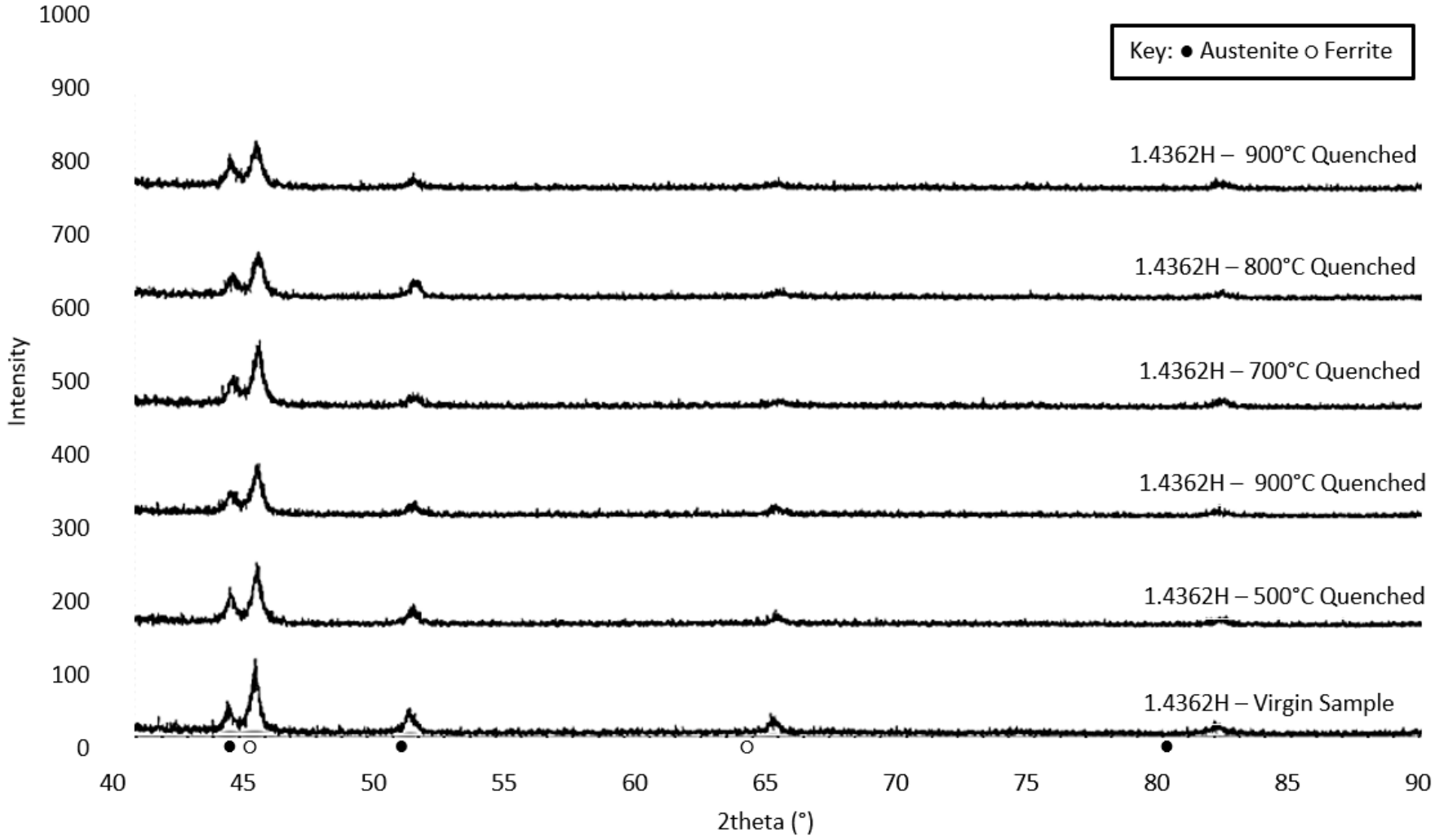
Key: ● Austenite ○ Ferrite
1.4362H – 900°C Quenched
1.4362H – 800°C Quenched
1.4362H – 700°C Quenched
1.4362H – 900°C Quenched
1.4362H – 500°C Quenched
1.4362H – Virgin Sample
Intensity
2theta (°)
1000
900
800
700
600
500
400
300
200
100
0
40
45
50
55
60
65
70
75
80
85
90

(a)

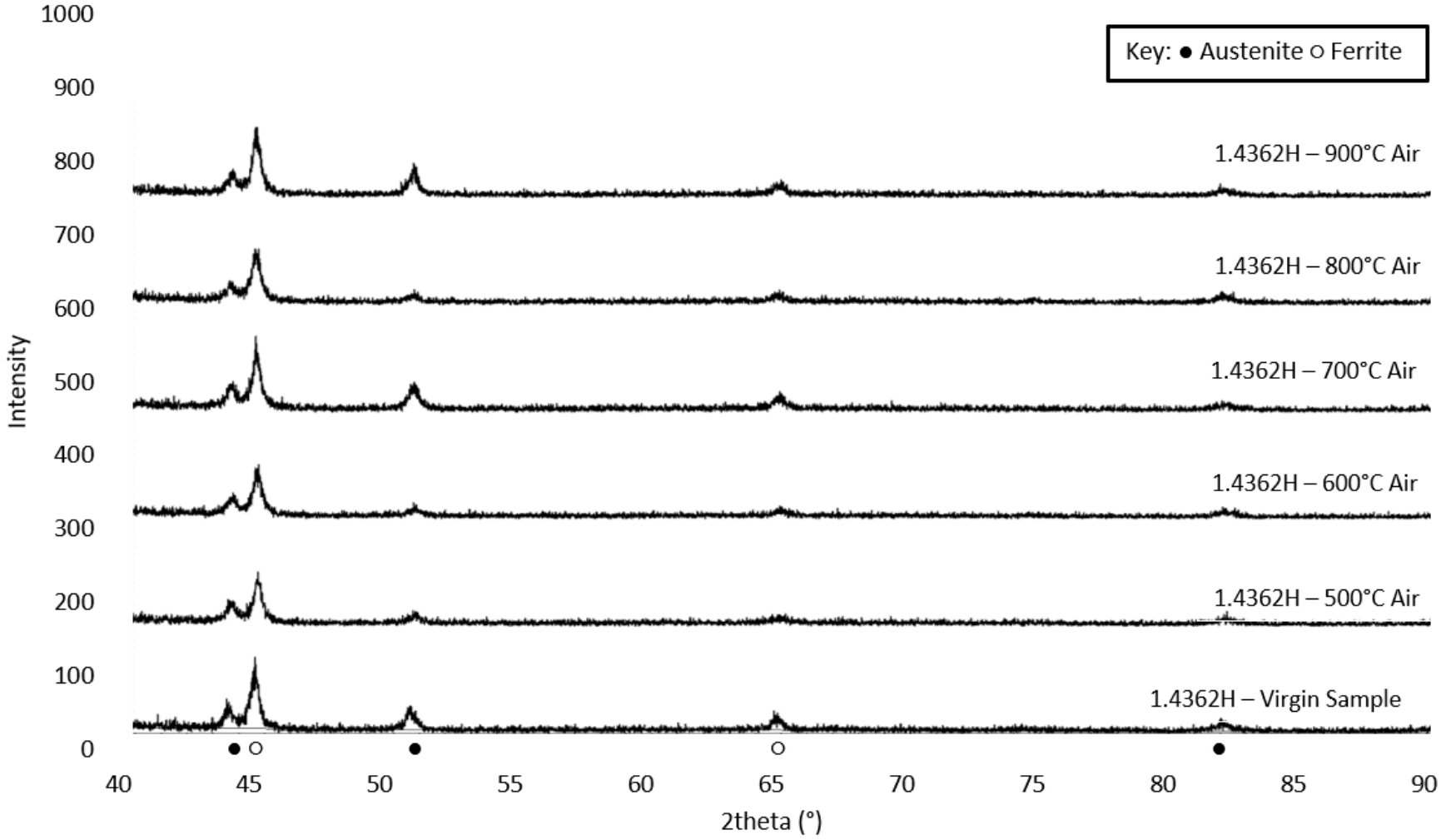
Key: ● Austenite ○ Ferrite
1.4362H – 900°C Air
1.4362H – 800°C Air
1.4362H – 700°C Air
1.4362H – 600°C Air
1.4362H – 500°C Air
1.4362H – Virgin Sample
Intensity
2theta (°)
1000
900
800
700
600
500
400
300
200
100
0
40
45
50
55
60
65
70
75
80
85
90

(b)

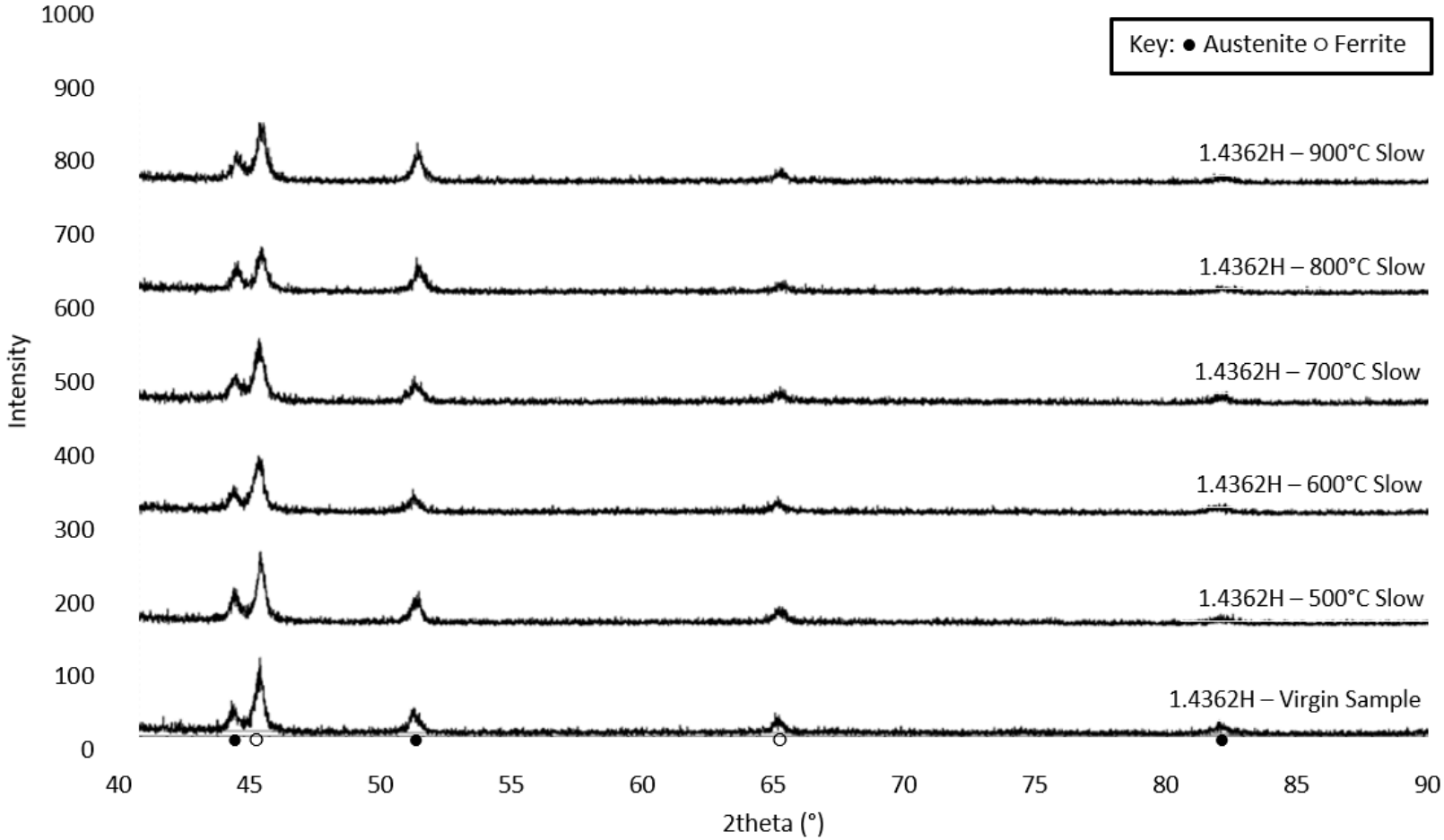

(c)

Figure 5-5: Diffractograms for grade 1.4362H hot-rolled reinforcing bar that were heated to various temperatures as indicated and then cooled (a) quickly, by quenching in water, (b) naturally, in air, and (c) slowly, in the furnace.

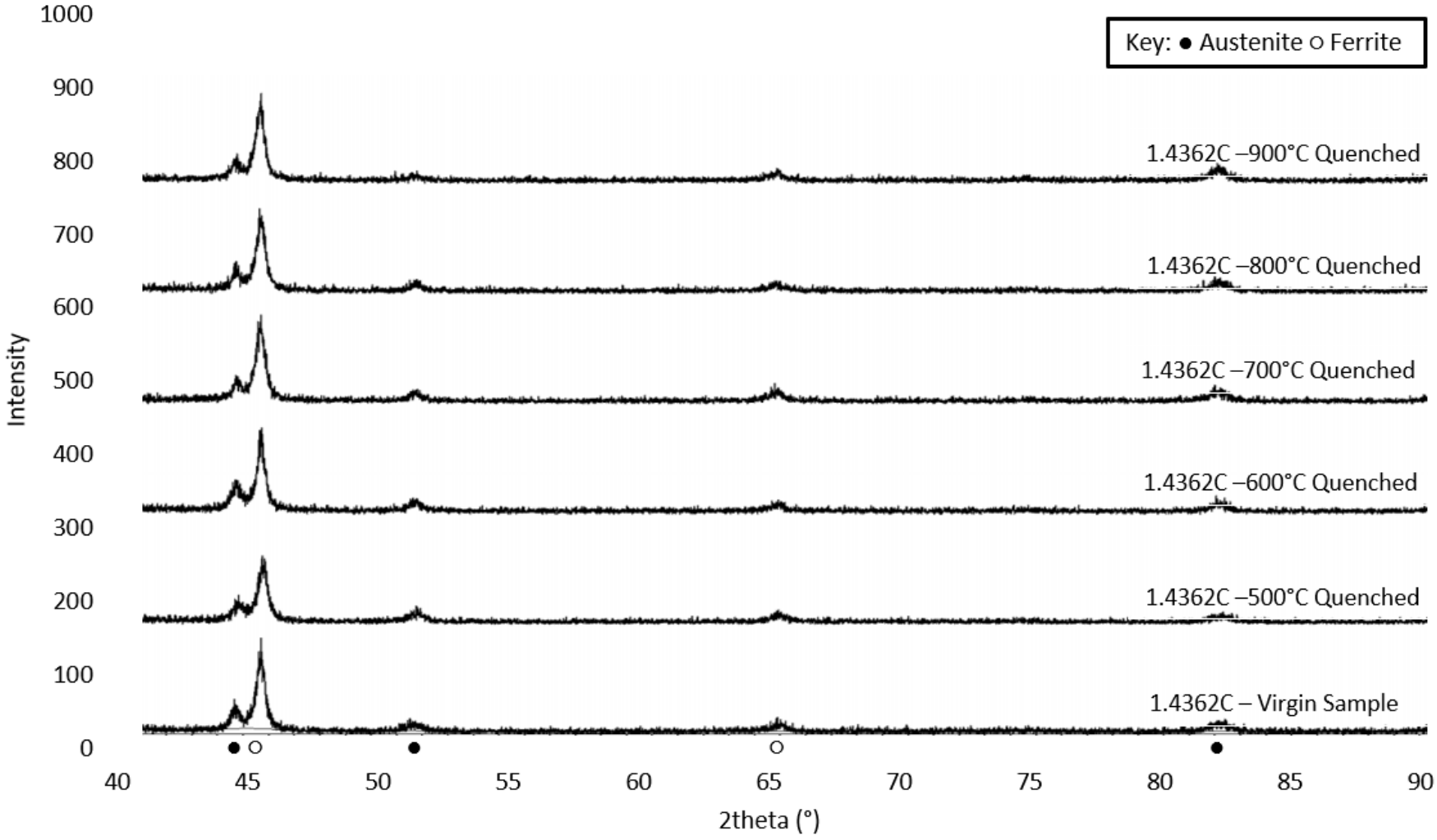
Key: ● Austenite ○ Ferrite
1.4362C –900°C Quenched
1.4362C –800°C Quenched
1.4362C –700°C Quenched
1.4362C –600°C Quenched
1.4362C –500°C Quenched
1.4362C – Virgin Sample
Intensity
2theta (°)
0
100
200
300
400
500
600
700
800
900
1000
40
45
50
55
60
65
70
75
80
85
90

(a)

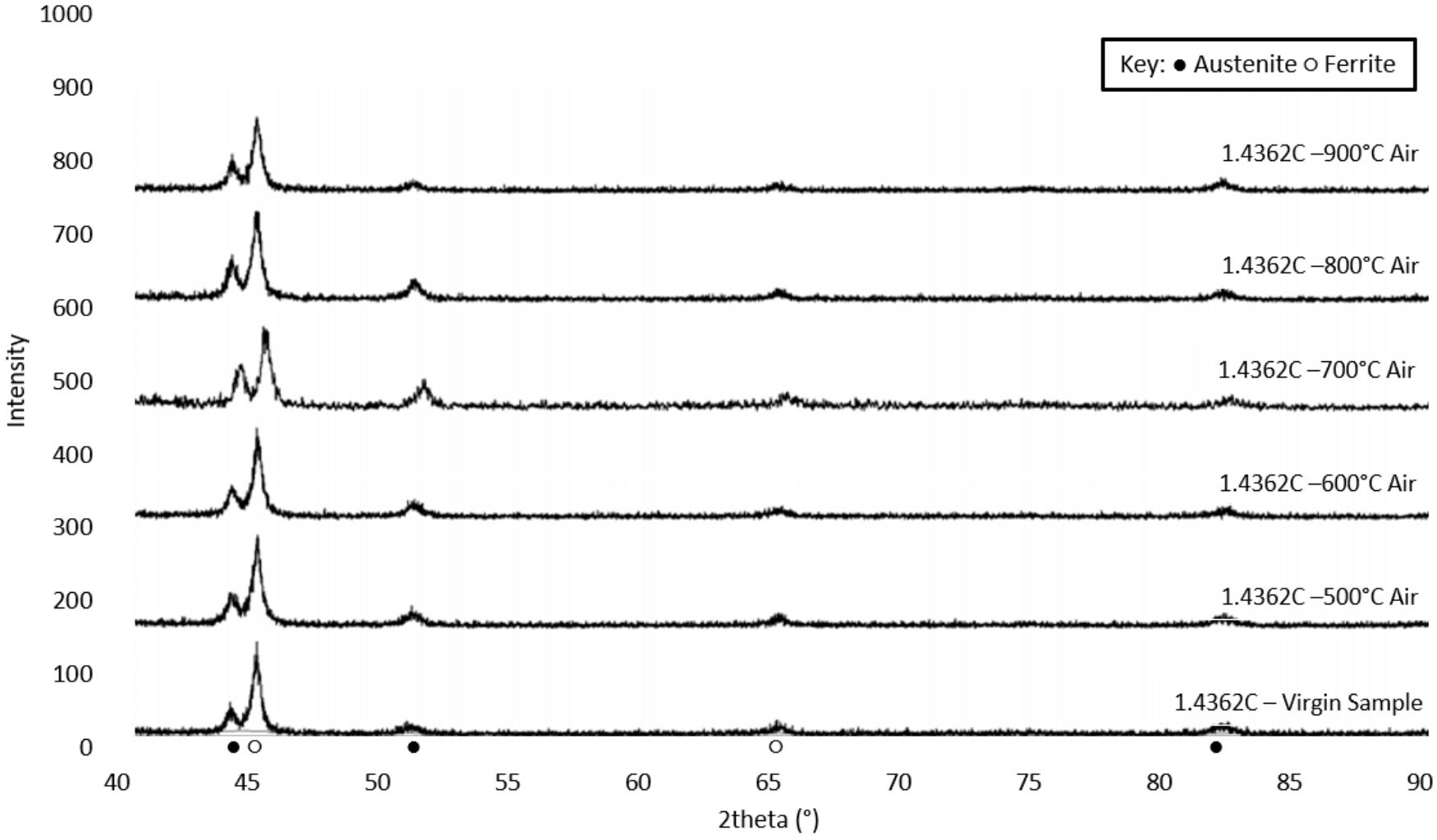
Key: ● Austenite ○ Ferrite
1.4362C –900°C Air
1.4362C –800°C Air
1.4362C –700°C Air
1.4362C –600°C Air
1.4362C –500°C Air
1.4362C – Virgin Sample
Intensity
2theta (°)
0
100
200
300
400
500
600
700
800
900
1000
40
45
50
55
60
65
70
75
80
85
90

(b)

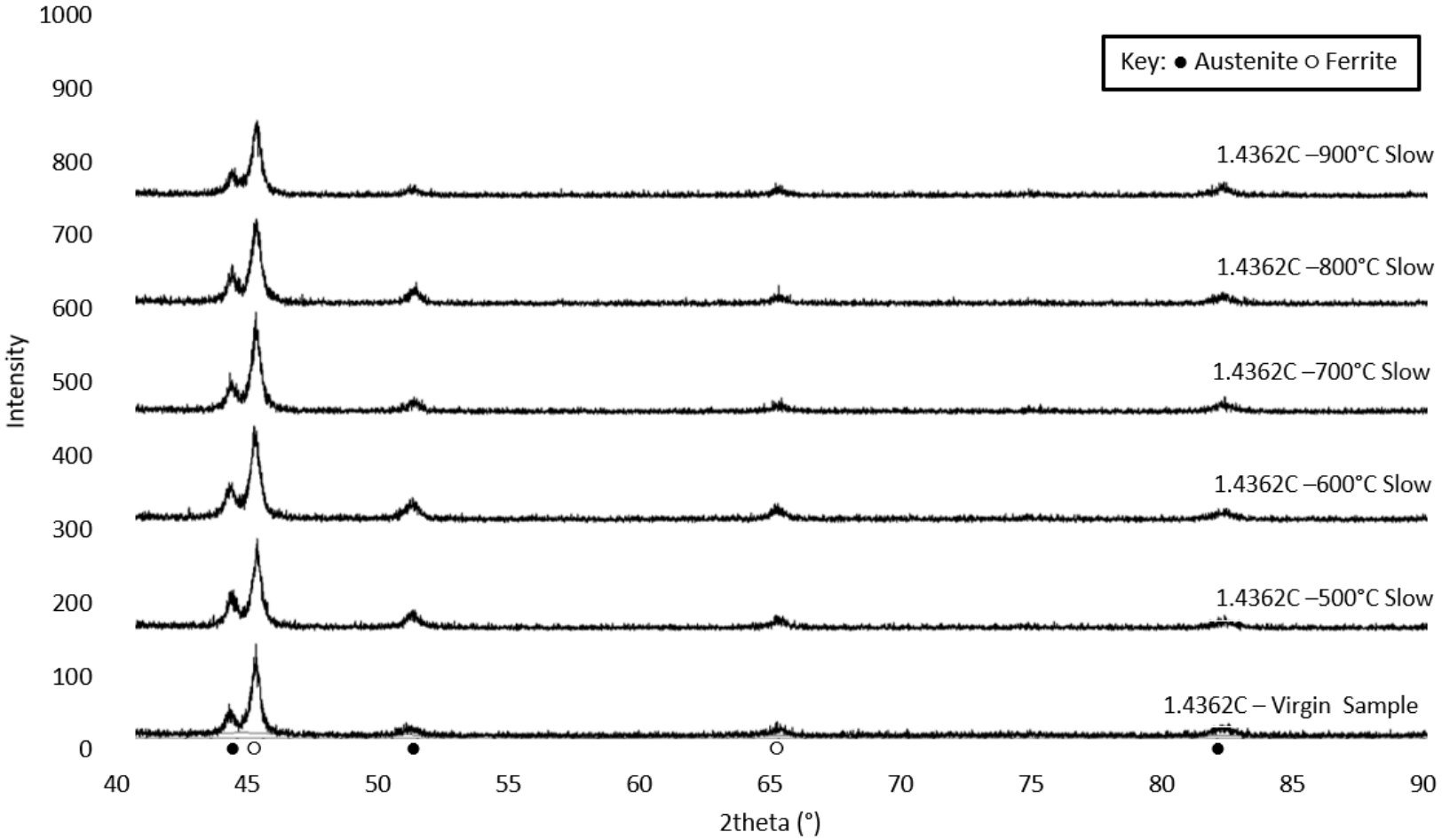

(c)

Figure 5-6: Diffractograms for grade 1.4362C cold-rolled reinforcing bar that were heated to the various temperatures as indicated and then cooled (a) quickly, by quenching in water, (b) naturally, in air, and (c) slowly, in the furnace.

5.3.2 Microscopic Investigation

Microscopic imagery enables a visual inspection of the size, shape and dispersion of the grains in a metallic material. To study the change in grains for grade 1.4363 duplex stainless steel reinforcement, the complete imagery is presented in Fig. 5-7, for (a) the hot-rolled rebars in their virgin (i.e. unheated) state, (b) the equivalent images for the cold-rolled virgin materials, (c) the cold-rolled rebars exposed to 700°C and subsequently quenched in water to cool rapidly, (d) the cold-rolled bars exposed to 700°C and subsequently air-cooled, (e) the cold-rolled reinforcing bar exposed to 700°C and subsequently slow-cooled, and (f) the cold-rolled rebars exposed to 700°C and subsequently slow-cooled, magnified to enable a closer inspection. The bars that were heated to 700°C are selected here for illustrative purposes and because this was the lowest level of temperature exposure at which the bars retained comparable tensile properties to their virgin values, in the tensile testing. It should be noted that at this stage, due to the duplex nature of the alloy, both austenite and ferrite are present, and these are identified as δ-ferrite which are darker grains in the images and γ-austenite which are the lighter grains.

For the virgin hot-rolled sample as shown in Fig. 5-7(a), several small grain clusters can be found, and these smaller grains are formed from larger recrystalising during the hot-rolling process. The small grains act as the primary strengthening mechanism for hot-rolled reinforcing bars. This is explained by the Hall-Petch relationship which indicates that the smaller the grain size, the higher the material strength (Hansen, 2004). For the cold-rolled virgin sample as shown in Fig. 5-7(b), the primary strengthening mechanism is the formation of α'-martensite in the γ-austenite grains during the cold-rolling process as a response to the stresses induced by the manufacturing process pushing the material to recrystallise. Deformation in the δ-ferrite grains are minimal as the γ-austenite is more ductile and prone to change, and thus the plastic deformation defaults to the γ-austenite grains. The presence of α'-martensite can be identified through visual grain deformation, as highlighted in Fig. 5-7(b).

Following exposure to 700°C and subsequent cooling, all three cooling methods as shown in Fig. 5-7(c-e) present more visible γ-austenite and α'-martensite grains. After exposure to 700°C and subsequent cooling there is good retention of the tensile properties (i.e. $f_{0.2p}$, f_u, ε_u and ε_f) due to the samples not being exposed to the active recrystallisation temperature of 727°C, after this point, the α'-martensite grains would see active reversion to γ-austenite, resulting in an increase in ductility paired with a loss of strength. For the slow-cooled sample, almost identical tensile strength (f_u and $f_{0.2p}$) values are retained but, upon close inspection of Fig. 5-7(f), it is clear that the δ-ferrite grain boundary has undergone change. The grain boundary has a development of nitride precipitation phase present;

chromium alloys such as stainless steels are prone to the formation of the σ phase once they are exposed to temperatures in excess of 550°C (Alinejad and Abbasi, 2021) and then cooled slowly. This is important because the σ-phase compromises the corrosion resistance of the alloy.

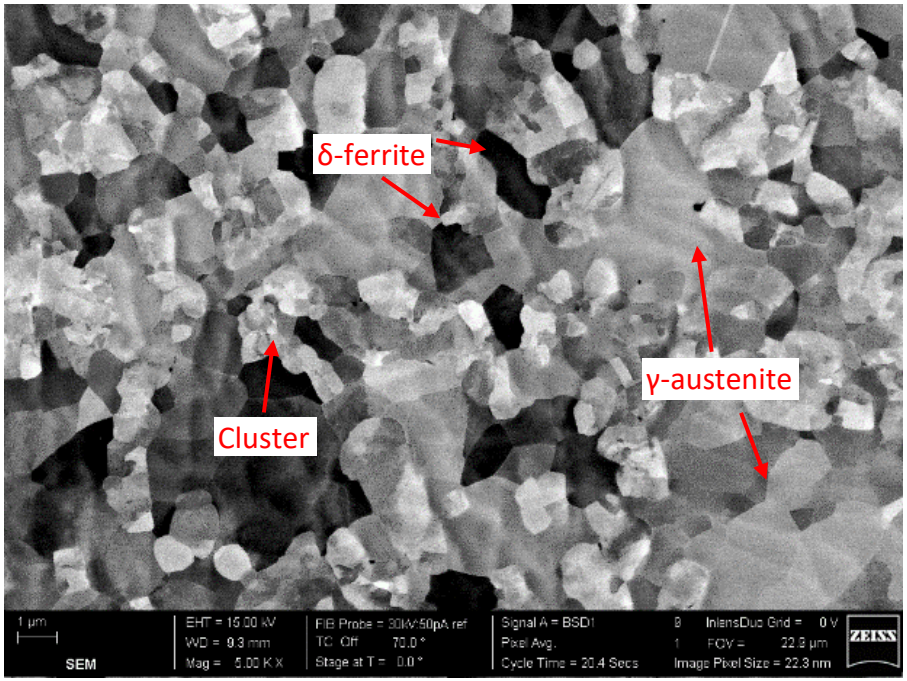
δ-ferrite
γ-austenite
Cluster
1 µm
SEM
EHT = 15.00 kV
WD = 9.3 mm
Mag = 5.00 K X
FIB Probe = 30kV:50pA ref
TC Off 70.0 °
Stage at T = 0.0 °
Signal A = BSD1
Pixel Avg.
Cycle Time = 20.4 Secs
InlensDuo Grid = 0 V
FOV = 22.8 µm
Image Pixel Size = 22.3 nm
ZEISS

(a)

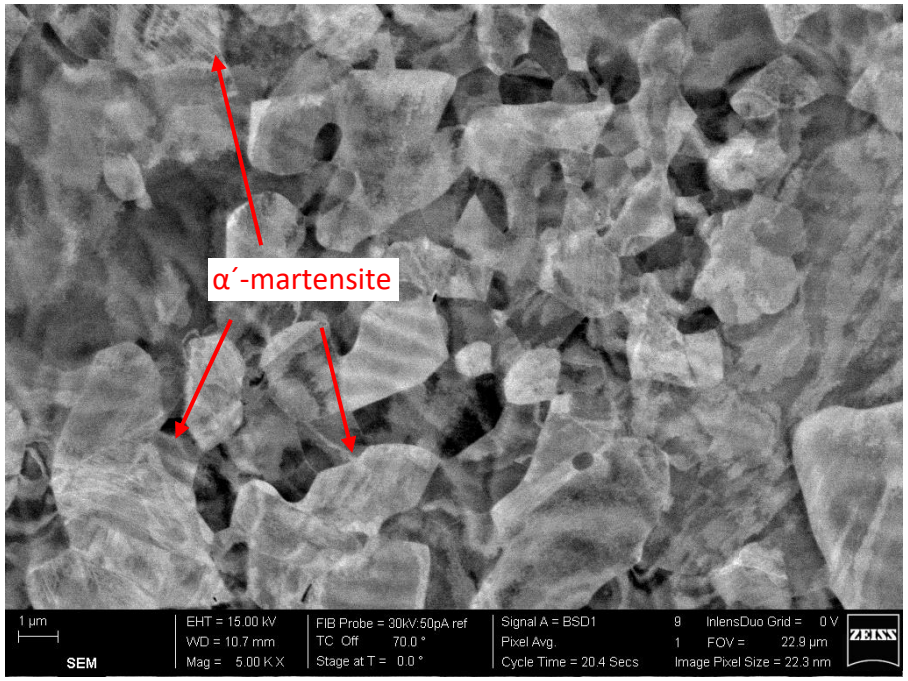
α´-martensite
1 µm
SEM
EHT = 15.00 kV
WD = 10.7 mm
Mag = 5.00 K X
FIB Probe = 30kV:50pA ref
TC Off 70.0 °
Stage at T = 0.0 °
Signal A = BSD1
Pixel Avg.
Cycle Time = 20.4 Secs
InlensDuo Grid = 0 V
FOV = 22.9 µm
Image Pixel Size = 22.3 nm
ZEISS

(b)

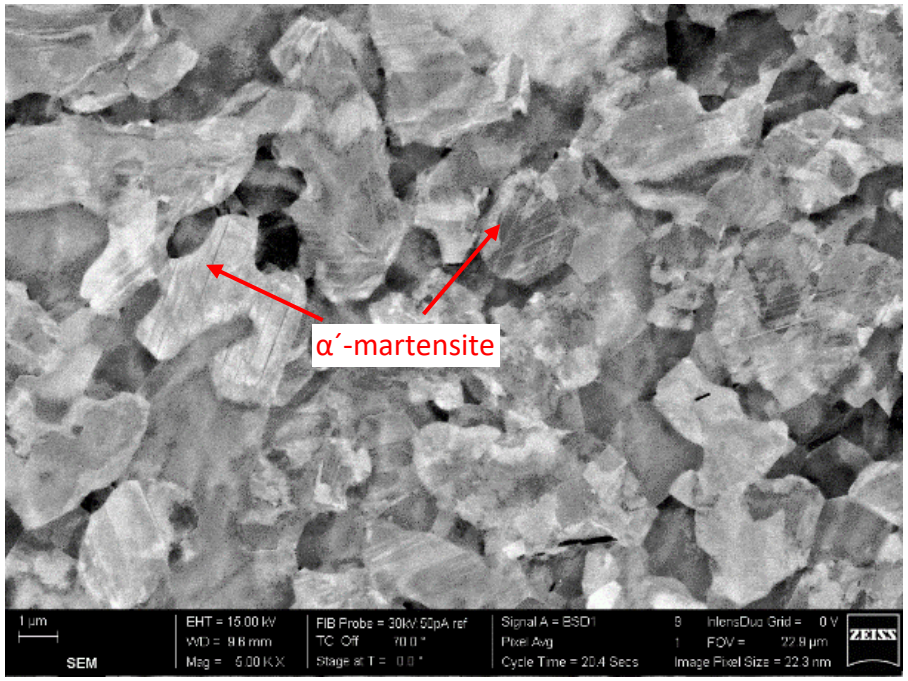
α´-martensite
1 µm
SEM
EHT = 15.00 kV
WD = 9.8 mm
Mag = 5.00 K X
FIB Probe = 30kV:50pA ref
TC Off 70.0 °
Stage at T = 0.0 °
Signal A = BSD1
Pixel Avg
Cycle Time = 20.4 Secs
InlensDuo Grid = 0 V
FOV = 22.8 µm
Image Pixel Size = 22.3 nm
ZEISS

(c)

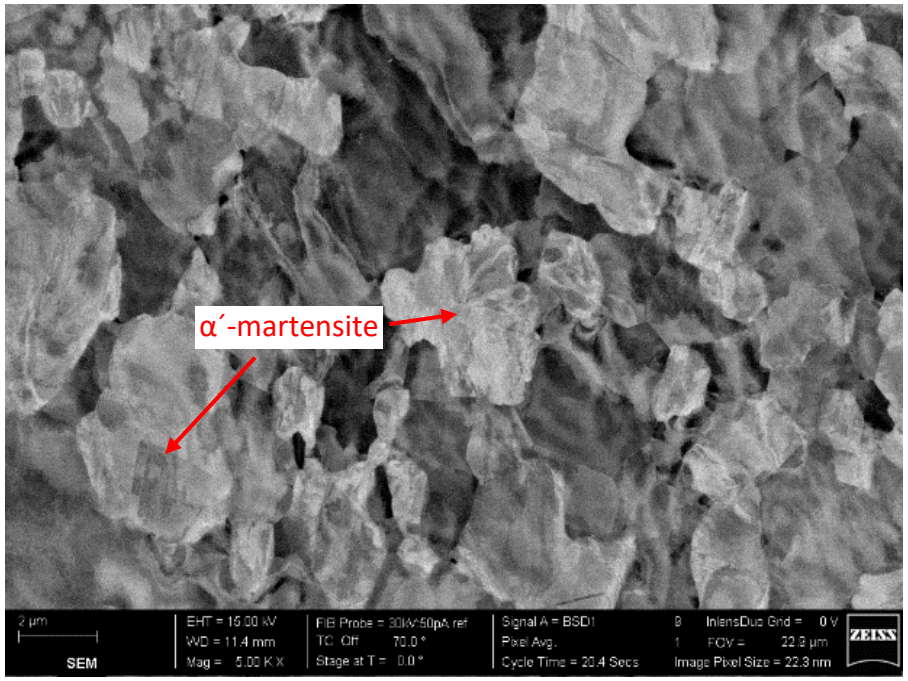
α´-martensite
2 µm
SEM
EHT = 15.00 kV
WD = 11.4 mm
Mag = 5.00 K X
FIB Probe = 30kV:50pA ref
TC Off 70.0 °
Stage at T = 0.0 °
Signal A = BSD1
Pixel Avg
Cycle Time = 20.4 Secs
InlensDuo Grid = 0 V
FOV = 22.8 µm
Image Pixel Size = 22.3 nm
ZEISS

(d)

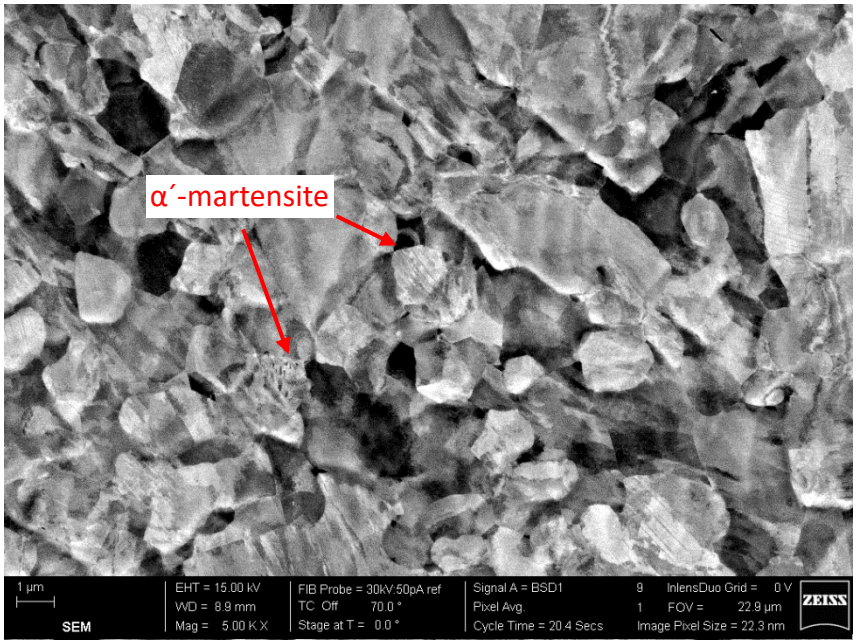

(e)

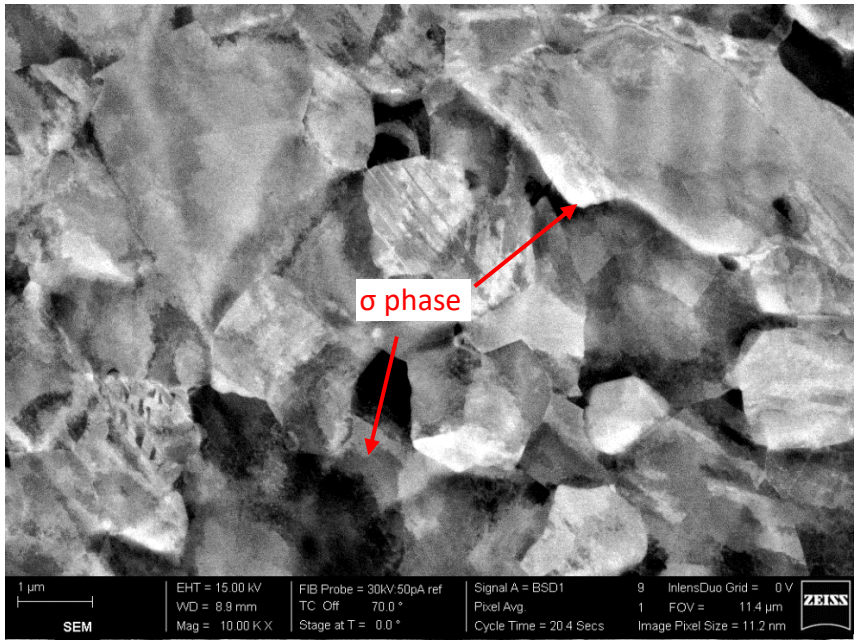

(f)

Figure 5-7: The grain imagery for grade 1.4362 reinforcing bar including (a) the hot-rolled virgin sample, (b) the cold-rolled virgin sample, (c) the cold-rolled bar exposed to 700°C and subsequently quenched, (d) the cold-rolled bar exposed to 700°C and subsequently air-cooled, (e) the bar exposed to 700°C and subsequently slow-cooled, the bar exposed to 700°C and subsequently slow-cooled further magnified.

5.4 Concluding Remarks

This chapter highlights the results obtained from the tensile testing of hot-rolled and cold-rolled grade 1.4362 duplex stainless steel reinforcing bar, and subsequent material investigation. In summary, both sample sets produced a very different set of results due to very different initial microstructural compositions. In comparison to the austenitic rebars, the method of cooling was a significant influence on the post-fire behaviour and led to a more varied set of results.

There was a double yield phenomenon identified in the hot-rolled 1.4362 rebar and although outside the scope of the current work, it is clear that this requires a more focused investigation in the future. The reason for the exclusion of this detailed study within the current study is that it requires the microstructural changes to be monitored at elevated temperatures, and this currently not possible with the facilities available at Brunel University London.

Chapter 6 Discussion on The Residual Properties of Stainless Steel Rebar Following a Fire

This chapter aims to provide a more detailed analysis of the results presented in earlier chapters, focussing the properties which are important for practicing engineers, and discuss the residual tensile properties of the stainless steel reinforcing bar following a fire and subsequent cooling. This discussion is presented in three sections; first the behaviour of austenitic stainless steel is discussed and compared against broader data found in literature, followed by a similar discussion for duplex stainless steel rebar and this is followed by a section to explaining the structural design implications of this work which concludes with the presentation of new recommended reduction factors. The reduction factors are designed to be of use to engineers wishing to study the structural integrity of stainless steel reinforced structure or element following a fire scenario.

6.1 Austenitic Stainless Steel Reinforcing Bar

For austenitic stainless steel reinforced concrete structures to remain viable for reuse following a fire, the residual tensile values of the reinforcement bars need to meet the requirements as given in Part 7 of BS 4449 (2016). Which is described as having a minimum $f_{0.2p}$ of at least 480n/mm^2, a ε_u of at least 5% and a $f_{0.2p}/f_u$ ratio of at least 1.08.

All three cooling methods studied in this investigation provide no significant variation in the results based on the cooling rate. The tensile behaviour for the three studied austenitic grades (i.e. grades 1.4301, 1.4401 and 1.4436) can be broken down into three different stages based on the level of temperature exposure, and these are discussed hereafter.

Following relatively low levels of temperature exposure of up to 500°C, all three materials showed no significant loss in the proof stress $f_{0.2p}$ or ultimate tensile stress f_u but may experience some reduction in the failure strain ε_f compared with the unheated virgin sample. This is because following exposure to temperatures of up to 500°C, new γ-austenite grains are not formed in the alloy due to not meeting the active recrystilisation temperature range, whilst any strengthening and brittleness is the result of the ε-martensite completing the transformation to α´-martensite. For grades 1.4401 and 1.4436, the addition of molybdenum in the alloy makes these materials slightly more resistant to change following exposure to temperatures of up to 500°C, and there are insignificant changes to the microstructure. This is further supported by the measured tensile properties (i.e. $f_{0.2p}$, f_u, ε_f and ε_u) which remain within 10% of their corresponding virgin sample values, whilst the grade 1.4301 samples have a significant increase in strength and a reduction of ductility. Following heating and cooling in the range of 100°C-500°C, all samples met the all the tensile requirements as set out in Part 7 of BS 4449.

When exposed to moderate temperatures of 600-700°C, regardless of the cooling rate, all of the samples showed an increase in strength compared with the virgin samples, although this was less than for the samples that were heated to 500°C before cooling. They also had notable changes in the strain behaviour. For example, following exposure to 600°C and subsequent cooling, grades 1.4301 and 1.4436 had a disproportionately high increase in ε_u relative to ε_f. For 1.4301, the increase in ε_u was 56-67% whilst ε_f increased by between 3 and 10% compared with the virgin sample. The grade 1.4436 samples had an increase of 61-72% for ε_u and an increase of 11-24% for ε_f compared with the corresponding virgin values. Grade 1.4401 presented more comparable increases in ε_u and ε_f, equal to 19-25% and 13-17% respectively. The reason for this higher increase in ε_u for different grades is largely owing to the level of cold-rolling which was done to the rebars during production. In the test programme, the rebars began to lose their mechanically-induced cold-rolled properties following exposure to higher levels of elevated temperature, thus resulting in a more curved stress-strain response appearing, at this stage the graph presents the material to be more ductile and prone to yielding. This same pattern of behaviour was also observed for the samples that were heated to 700°C. Overall, the grade 1.4301 rebars retained more of their tensile properties compared with the molybdenum-containing grades 1.4401 and 1.4436. Following heating and subsequent cooling in the range of 600°C-700°C, all three grades met the tensile property requirements as set out in part of BS 4449.

For the samples exposed to 800°C, all of the grades showed different levels of reduction in the strength accompanied by a greater increase in ductility. This is because the stainless steels had begun to actively undergo recrystallisation but failed to do so completely due to a shortage in either temperature or time of exposure. On the other hand, for the samples heated to 900°C, the

requirements for active recrystallisation were achieved, resulting in a complete γ-austenite dominant microstructure, at this stage the strength and ductility of the rebar should be reverted to a stage similar to before cold-rolling. Following high temperature exposure 800°C and 900°C, the samples no longer consistently met the minimum $f_{0.2p}$ value of 480N/mm^2.

With reference to the influence of cooling method, and therefore cooling rate, on the retention of strength and ductility for austenitic stainless steel reinforcement, as previously stated, this parameter does not appear to have a major influence on the tensile response. This observation is clear from the results of the tensile tests and was also verified from the material characterisation and microscopic imagery, as identical results were observed for the three cooling methods. The understanding is that, within this study, the method of cooling bares no influence on the tensile or metallurgical response. A further confirmation of this is the images of the post-testing specimens presented in Appendix A, showing to be near-identical regardless of cooling method.

Regarding the modulus of elasticity *E*, it is noteworthy that there was very little change observed for any of the specimens examined within chapter 4 and 5 of this thesis. This is to be expected as for all stainless steels (and carbon steel), regardless of the heat treatment or level of mechanical work, the modulus of elasticity should remain near to that of its parent element, i.e. iron, at 200 GPa (Beddos and Parr, 1999). The slight variation in elastic modulus values presented herein can be understood as being attributed to the testing process and laboratory limitations, as also described by other researchers (e.g. Chen et al., 2016; Lord and Morell., 2010).

When comparing the results of the rebar tested to broader data presented in the literature, reduction factors taken from work done by Molkens, et al., (2020) and Gao, et al., (2018) can be compared, as both sets are quenched following heating. Data taken from Molkens, et al., (2020) presents 4 data points at 20°C, 250°C, 500°C and 750°C for coupons cut from a grade 1.4301 cold-rolled sheet. Whilst the data taken from Gao, et al., (2018) shows the residual performance of grade 1.4301 coupons cut from a hot-rolled sheet, at a temperature range of 20°C and 200°C-1100°C rising in increments of 100°C.

The comparative findings are shown in Fig. 6-1 and 6-2. Within Fig. 6-1, the proof stress is shown. In comparison to the collected data within this thesis, the data taken from Molkens, et al., (2020) shows a very small rise followed by a steady decline. Data taken from Gao, et al., (2018) shows an immediate decline following any sort of heating. Both samples show a dip in strength after 500°C, with the Gao, et al., (2018) data, showing an additionally harsher decline after 800°C. In Fig 6-2, the tensile stress is shown. Both sets of data compared show minimal change of under 2% throughout testing. Only at 1100°C does coupon show a somewhat major loss in strength.

Comparing the coupon data to the rebar data within this thesis, it is observable that the rebars tested do not follow the same trend. Within the proof stress, there is a much sharper rise and loss in strength, whilst in all sets 500°C remains a crucial turning point. For the tensile stress, there is no crucial turning point for the coupons, the retain uniformity until 1100°C, whilst the rebar show a somewhat increase in strength until 600°C followed by a sharp decline. Therefor it is concluded that the rebar findings are unique and cannot be compared to coupons.

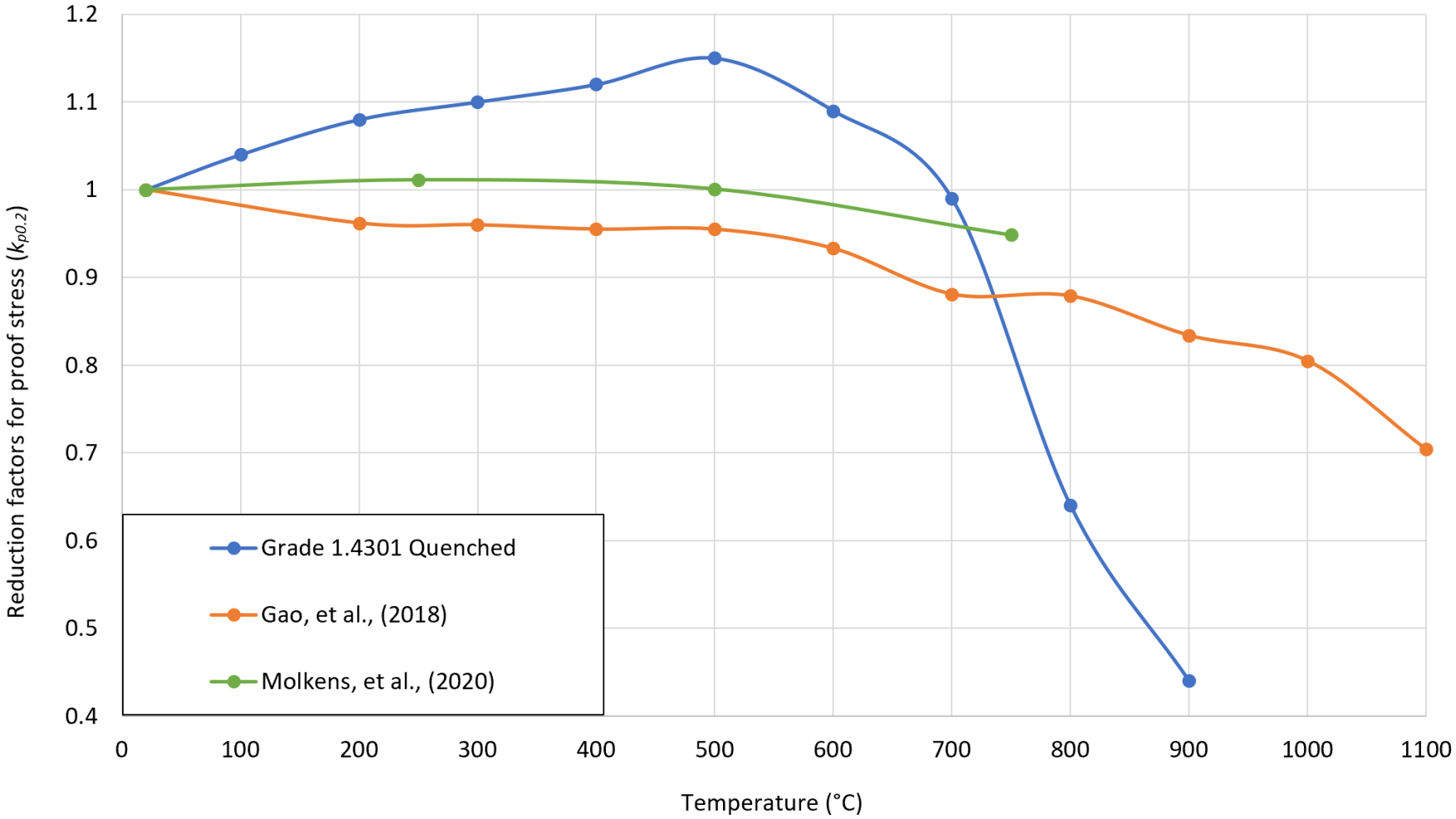

Figure 6-1: Comparative response of the proof stress of grade 1.4301 following heating and subsequent quenching.

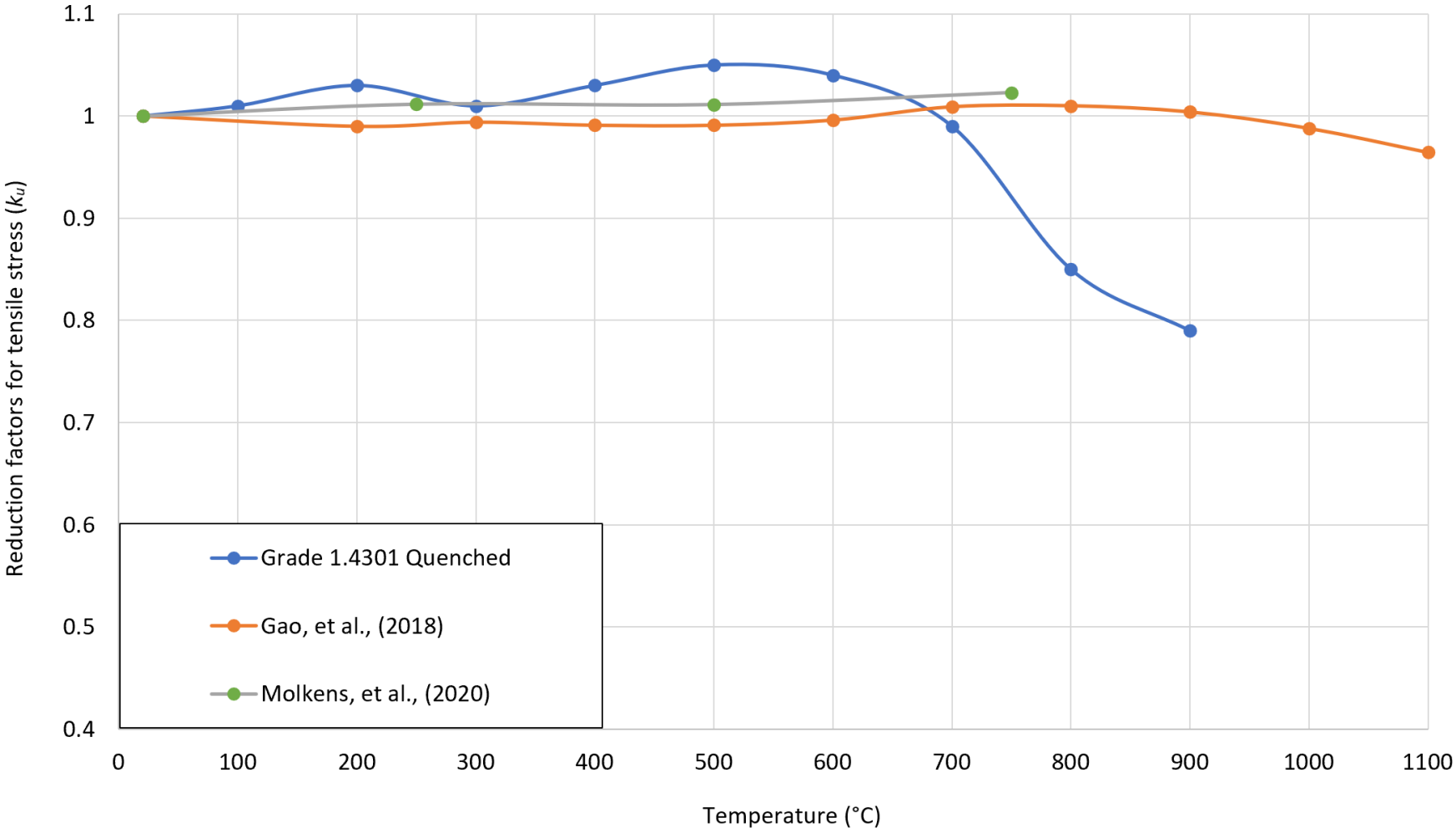

Figure 6-2: Comparative response of the tensile stress of grade 1.4301 following heating and subsequent quenching.

6.2 Duplex Stainless Steel Reinforcing Bar

For the detailed investigation of the residual tensile properties of duplex stainless steel reinforcing bars (1.4362H and 1.4362C) after exposure to elevated temperature before subsequent cooling, a number of key observations are made. First, regardless of the level of temperature exposure, for the samples cooled quickly through quenching in water, both of the measured strength parameters ($f_{0.2p}$ and f_u) exhibited the least gain in residual properties of the three cooling methods when heated to 500-700°C and the greatest loss following higher temperature exposures. On the other hand, the slow-cooled samples demonstrated the greatest increase in residual strength compared with the corresponding virgin values following exposure to 500-700°C and the lowest loss of strength following exposure to higher temperatures.

The variance in performance following the different cooling methods is due to changes in the internal stresses, particularly in the ferrite grains. During the gradual heating process, which was the same for all specimens, the residual stresses present in the alloy were slowly released. When the alloy was cooled quickly through quenching in water following elevated temperature exposure, new stresses formed due the sudden temperature reduction, and these were retained in the material as residual stresses due to rapid recrystallisation. The presence of residual stresses resulted in poorer performance retention in terms of the post-fire tensile properties compared with the air-cooled and slow-cooled specimens (for all levels of temperature examined). When the specimens were air-cooled, the alloy cooled at an intermediate rate and, for the samples that were heated to a temperature less than the recrystallization temperature of 727°C, a tempering effect was then produced upon cooling which allowed for the residual stresses to be partially relaxed. This resulted in post-fire properties which were better than the quenched samples but less good compared with the slow-cooled rebars, for all levels of temperature exposure examined. For the bars that were slow-cooled, the phenomenon was similar to an annealing process, with the slowest cooling rate allowing for the gradual growth of new grains and the development of less residual stresses, thus resulting in the highest overall post-fire tensile property values compared with their quenched and air-cooled counterparts for each examined temperature level.

For the different levels of temperature exposure examined, the results varied greatly between the hot-rolled and cold-rolled samples. For the hot-rolled rebars exposed to temperatures of 500°C and 600°C and subsequently cooled, well-defined yield points were observed in the residual stress-strain curves. These well-defined yield points were the product of an unstable austenitic-ferritic grain boundary. The cold-rolled samples tested under the same conditions presented a more rounded

yielding behaviour, typical of stainless steel, with the exception of the cold-rolled sample exposed to 500°C and slow-cooled, which retained more of the original cold-worked properties.

For the samples that were exposed to temperatures of 700°C and 800°C, the hot-rolled duplex stainless steel rebars had good overall retention of their tensile properties compared with the original values, generally retaining within 15% of the original strength and 25% of the original strain values. For the cold-rolled bars exposed to 700°C, all three cooling methods resulted in a good retention of the original tensile values. However, as discussed, the slow-cooled sample presented an additional undesirable transformation of the σ phase within the grain boundaries. The σ-phase consists of chromium rich zones, which deprive the surrounding area of chromium, effectively compromising the resistance of the alloy towards pitting corrosion in the depleted zones. Once the cold-rolled specimens were exposed to temperatures of 800°C and subsequently cooled, regardless of cooling method, the alloy had begun to actively lose the strength induced through cold-rolling. For all samples exposed to temperatures of 900°C and subsequently cooled, a significant loss of strength and increase in strain was recorded, an indication of the grain reverting to γ-austenite. At this stage, most of the strength induced through the heating and cooling process, regardless of the production method, was lost.

When examining results obtained for the modulus of elasticity *E*, the same interpretation as the austenitic rebar is presented. Regardless of machining or heat treatment, at an ambient temperature the modulus of elasticity remains similar to the parent element of the alloy, Iron. Any minor discrepancy observed can be attributed the testing procedure and laboratory conditions.

The collected duplex data can be analysed against broader data available in coupon form collected by Tao et al., (2018) and Huang & Young (2018). Within both sets of literature, all coupons (1.4162, 1.4362 and 1.4462) are cut from sheet material and tested at temperatures ranging from 200°C-1000°C.

The comparative results for both the yield and tensile stress are presented in Fig. 6-3 and 6.4. The comparative average data for 1.4362H and 1.4362C is presented later herein in table 6-4. Within Fig 6-3, examining from 500°C onwards, grade 1.4362H shows a far greater rise than the comparative literature, whilst 1.4362C shows a similar rise if proof stress. However, in both the 1.4362H and 1.4362C sets there is a far greater loss in strength when compared to the coupon data extrapolated from the literature. Notably the coupons retained a proof stress value closer to their virgin samples, this trend is also seen in the tensile stress in Fig. 6-4. In the tensile stress, both rebars peaked at 500°C and continuously declined, whilst all three coupons showed a further increase in strength at the 700°C and 800°C mark. This behaviour was not unique to the coupons. Again, as with the austenitic data collected, although similarities can be interpreted, the data collected from the rebar is unique.

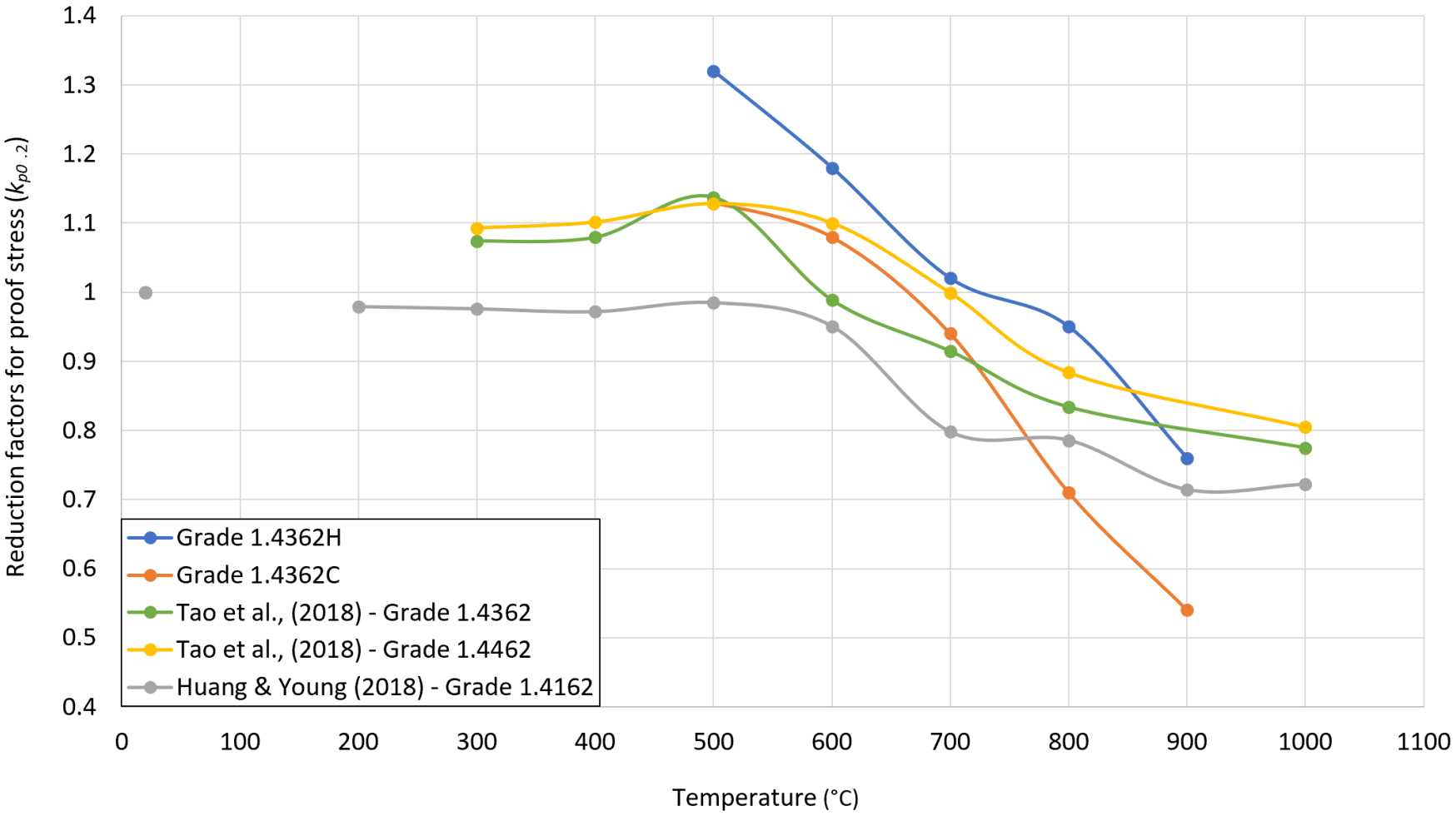

Figure 6-3: Comparative response of the proof stress of duplex stainless steel following heating and subsequent cooling.

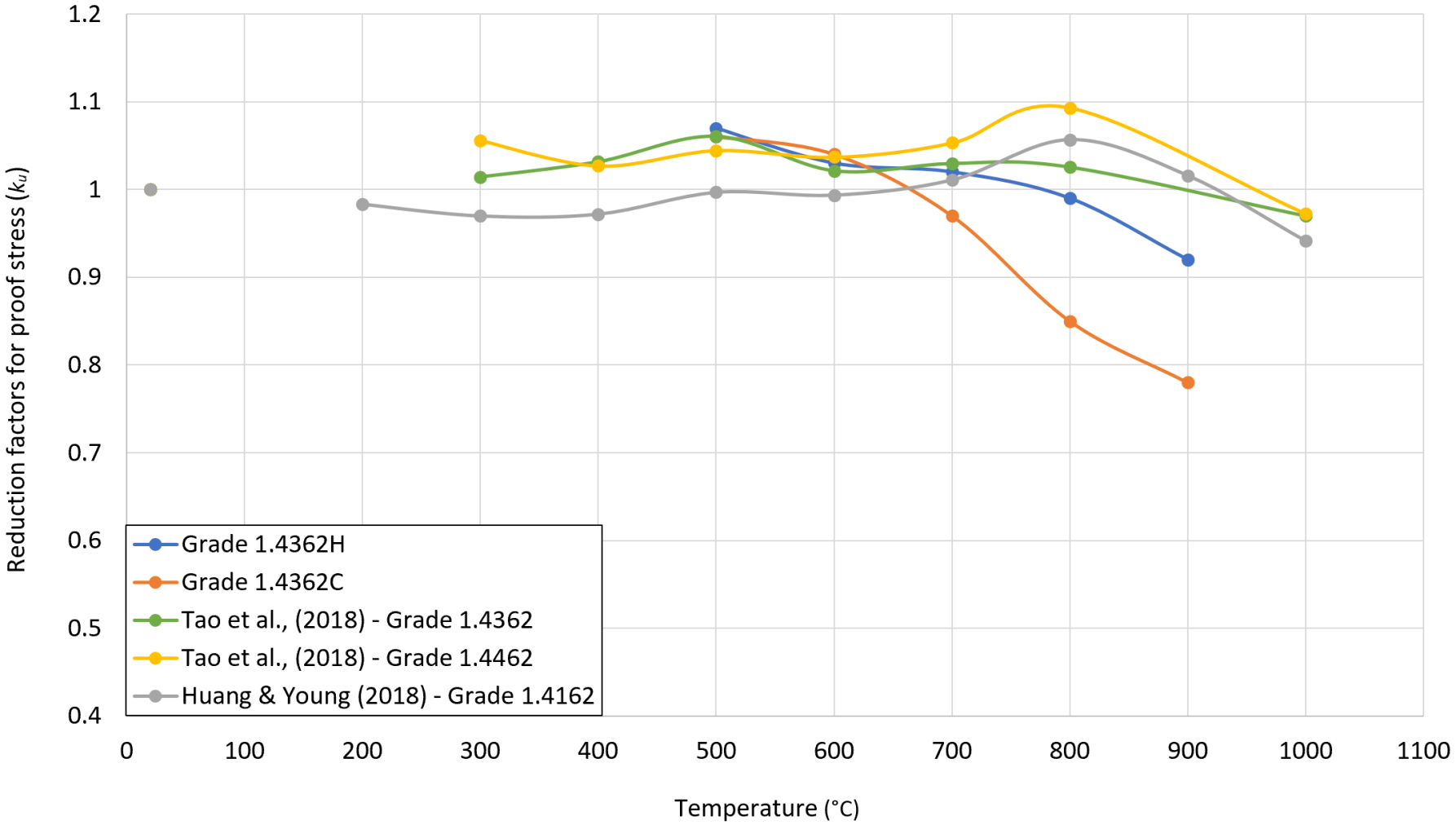

Figure 6-4: Comparative response of the tensile stress of duplex stainless steel following heating and subsequent cooling.

6.3 Proposed Reduction Factors for RC Structures

Based on the findings of this thesis, a series of residual strength retention factors for the stainless steel reinforcing bar are recommended. For the austenitic grade's retention factors are recommended from 100-900°C, whilst for the duplex grade's retention factors are recommended from 500-900°C. The proposed retention factors are given as $k_{p0.2}$ and k_u which represent the ratio of the 0.2% proof strength and ultimate strength of a given material at elevated temperature, respectively, to the corresponding original values at 20°C. The values presented in tables 6-1 to 6-3 present the actual retention factors, with table 6-1 for the quenched, table 6-2 for the air-cooled and table 6-3 for the slow-cooled data. Some of the values presented in the tables are greater than unity as these property values increased following temperature exposure. In practice, it might not be possible for an engineer to know the cooling rate that occurred. Therefore, table 6-4 presents a single set of recommended retention factors which can be applied for any cooling rate safely, based on the findings of the experiments presented herein. These may not be as efficient as employing for the individual cooling methods, but can be more widely applied when the cooling method is unknown.

Comparative graphs for the austenitic grades and duplex grades are also presented in Fig. C.6-1 and C.6-2, respectfully. Within the appendix, In Fig. C.6-1, the austenitics show a slight variance in the $k_{p0.2}$ but are almost identical in the k_u. Whereas in Fig. C.6-2, within the appendix, for both the hot-rolled and cold-rolled duplex grade 1.4362 reduction factors present a large difference between the two sets for both the $k_{p0.2}$ and k_u response.

Table 6-1: Actual retention factors for stainless steel reinforcing bar following heating and subsequent quenching in water.

Grade	1.4301		1.4401		1.4436		1.4362H		1.4362C	
	$k_{p0.2}$	k_u	$k_{p0.2}$	k_u	$k_{p0.2}$	k_u	$k_{p0.2}$	k_u	$k_{p0.2}$	k_u
Virgin	1.00	1.00	1.00	1.00	1.00	1.00	1.00	1.00	1.00	1.00
100°C	1.04	1.01	0.96	0.98	1.01	0.99	-	-	-	-
200°C	1.08	1.03	0.96	0.99	1.03	1.00	-	-	-	-
300°C	1.10	1.01	1.01	1.00	1.07	1.02	-	-	-	-
400°C	1.12	1.03	1.06	1.03	1.08	1.03	-	-	-	-
500°C	1.15	1.05	1.03	1.03	1.08	1.05	1.30	1.06	1.10	1.04
600°C	1.09	1.04	0.94	0.99	1.03	1.03	1.12	1.00	1.01	1.00
700°C	0.99	0.99	0.83	0.95	0.89	0.97	0.95	0.98	0.88	0.94
800°C	0.64	0.85	0.70	0.90	0.74	0.90	0.86	0.96	0.63	0.84
900°C	0.44	0.79	0.51	0.80	0.39	0.77	0.71	0.89	0.51	0.75

Table 6-2: Actual retention factors for stainless steel reinforcing bar following heating and subsequent air-cooling.

Grade	1.4301		1.4401		1.4436		1.4362H		1.4362C	
	$k_{p0.2}$	k_u	$k_{p0.2}$	k_u	$k_{p0.2}$	k_u	$k_{p0.2}$	k_u	$k_{p0.2}$	k_u
Virgin	1.00	1.00	1.00	1.00	1.00	1.00	1.00	1.00	1.00	1.00
100°C	1.02	1.01	0.97	0.97	0.99	0.98	-	-	-	-
200°C	1.03	1.00	0.97	0.98	1.01	0.99	-	-	-	-
300°C	1.11	1.03	1.02	1.00	1.07	1.01	-	-	-	-
400°C	1.15	1.04	1.03	1.00	1.09	1.03	-	-	-	-
500°C	1.13	1.04	1.00	1.00	1.11	1.05	1.31	1.06	1.12	1.07
600°C	1.11	1.03	0.96	1.00	1.06	1.03	1.20	1.02	1.09	1.04
700°C	1.03	1.00	0.87	0.95	0.92	0.97	1.02	1.01	0.94	0.97
800°C	0.75	0.88	0.77	0.92	0.79	0.90	0.95	0.99	0.72	0.85
900°C	0.47	0.77	0.51	0.81	0.39	0.76	0.76	0.91	0.53	0.78

Table 6-3: Actual retention factors for stainless steel reinforcing bar following heating and subsequent slow-cooling.

Grade	1.4301		1.4401		1.4436		1.4362H		1.4362C	
	$k_{p0.2}$	k_u	$k_{p0.2}$	k_u	$k_{p0.2}$	k_u	$k_{p0.2}$	k_u	$k_{p0.2}$	k_u
Virgin	1.00	1.00	1.00	1.00	1.00	1.00	1.00	1.00	1.00	1.00
100°C	1.00	0.99	1.06	0.98	0.99	0.98	-	-	-	-
200°C	1.07	1.01	1.02	0.99	1.02	0.98	-	-	-	-
300°C	1.11	1.02	1.01	1.00	1.08	1.01	-	-	-	-
400°C	1.12	1.03	1.05	1.01	1.08	1.02	-	-	-	-
500°C	1.15	1.05	1.04	1.03	1.09	1.04	1.35	1.08	1.17	1.07
600°C	1.09	1.02	0.98	1.01	1.02	1.01	1.23	1.07	1.14	1.07
700°C	1.04	1.01	0.90	0.97	0.93	0.97	1.11	1.06	1.01	1.01
800°C	0.67	0.86	0.77	0.92	0.78	0.90	1.05	1.02	0.76	0.87
900°C	0.46	0.77	0.49	0.81	0.39	0.77	0.82	0.95	0.58	0.81

Table 6-4: Recommended retention factors for stainless steel reinforcing bar regardless of cooling method.

Grade	1.4301		1.4401		1.4436		1.4362H		1.4362C	
	$k_{p0.2}$	k_u	$k_{p0.2}$	k_u	$k_{p0.2}$	k_u	$k_{p0.2}$	k_u	$k_{p0.2}$	k_u
Virgin	1.00	1.00	1.00	1.00	1.00	1.00	1.00	1.00	1.00	1.00
100°C	1.02	1.00	1.00	0.98	1.00	0.98	-	-	-	-
200°C	1.06	1.01	0.98	0.99	1.02	0.99	-	-	-	-
300°C	1.11	1.02	1.02	1.00	1.07	1.01	-	-	-	-
400°C	1.13	1.03	1.04	1.01	1.08	1.03	-	-	-	-
500°C	1.14	1.05	1.03	1.02	1.10	1.05	1.32	1.07	1.13	1.06
600°C	1.10	1.03	0.96	1.00	1.03	1.02	1.18	1.03	1.08	1.04
700°C	1.02	1.00	0.87	0.96	0.91	0.97	1.02	1.02	0.94	0.97
800°C	0.69	0.86	0.75	0.91	0.77	0.90	0.95	0.99	0.71	0.85
900°C	0.46	0.78	0.50	0.81	0.39	0.77	0.76	0.92	0.54	0.78

6.4. Structural Design Guidance and Implications

Following on from the recommended reduction factors presented, this section presents the key design guidance and implications from the elevated temperature testing section of this thesis. Currently, stainless steel rebar design guidance is very limited. As covered in section 2.4.2, Eurocode 2 is the most widespread deign guidance for RC fire design, however, this does not include any guidance for stainless steel rebar and is limited to carbon steel. Individual design manuals specified for stainless steel rebar such as 'Guidance on the use of stainless steel reinforcement' by the Concrete Society (1998) and the 'Guide for the use of stainless steel reinforcement in concrete structures' by the Norwegian Building Research Institute (2006) provide no guidance on the post-fire behaviour of stainless steel reinforcement. Therefor the residual factors presented are the only set available and should be applied the guidance mentioned herein.

When designing a structure with stainless steel rebar, due to the costs associated with stainless steel, applications are often limited to structures prone to corrosion; these are often set in marine or industrial/polluted environments such as bridges and piers. It is important to recall that stainless steel rebar is not immune to corrosion, and simply more resistant towards it compared with traditional carbon steel. For engineers designing structures with stainless steel rebar, it should be noted that the combination of a heavy marine environment and a fire scenario will increase the likelihood of concrete cover failing through spalling, leaving the rebar exposed to the fire conditions.

Regardless of the whether the concrete cover fails, care should be taken to select a suitable rebar grade with a stable microstructure. When designers consider the comparative microstructural performance of carbon steel rebar to stainless steel rebar, the overall post-fire performance of the austenitic grades is more dependable and better overall. The microstructure is stable, allowing for consistent performance regardless of cooling method. For carbon steel rebar, the chance of a brittle failure is possible under a quenched scenario and in a marine environment, the environmental influence can even lead to brittle failure without direct quenching of the rebar (Ba et al., 2019). For duplex 1.4362 rebar the microstructure is to some extent volatile, although there is no brittle failure scenario, there is less consistency in the failure patterns unlike the austenitic rebar and the additional risk of an σ-phase can compromise the corrosion resistance of the alloy.

The direct implications for design are the recommendations for residual tensile properties for stainless steel rebar following exposure to fire. These residual factors can be used as a guideline for the assessment of the post-fire tensile properties of stainless steel rebar in a non-destructive manor. The passive implication of this study includes the overall addition of novel information in the tensile and metallurgical performance of stainless steel rebar, currently largely undocumented and thus useful

for future researchers wishing to further study or improve on the subject. In addition, the excellent performance of austenitic stainless steels within this study evidences the possibility of more innovative uses of stainless steel rebar scenarios away from marine settings and towards high-risk fire settings.

Going forward, designers should have overall more confidence in stainless steel rebar when exposed to fire scenarios and following exposure to a fire scenario, especially if using the austenitic grades due to their stable microstructure. When evaluating the reusability of the rebar, it is important to consider it as a case-by-case scenario, the environment of exposure can possibly influence the outcome. Overall, as long as the concrete cover is not exposed, the rebar embedded within will be satisfactory for reuse regardless of grade. If exposed through macroscopic cracking, or complete exposure due to concrete spalling, the stable microstructure of austenitic rebars will prevail as long as the active recrystallisation temperature is not achieved for a prolonged period; moreover, the method of cooling bears no influence on the residual behaviour. For duplex 1.4362 rebar on the other hand, the formation of a σ-phase can compromise the corrosion resistance of the alloy following exposure to elevated temperature but, apart from this, the cold-worked samples will perform similarly to austenitic rebars. This is due to the strengthening mechanism being primarily active in the austenite phase of the duplex alloy.

6.5 Concluding Remarks

This chapter discusses the complete residual tensile test results presented earlier in Chapters 4 and 5, and uses this information to propose a set of reduction factors for use by engineers when studying stainless steel rebar following a fire scenario. Following this, a set of design guidance is given for successful use of these reduction factors. For the austenitic stainless steel rebar data, the various cooling rates examined resulted in little difference between the data collected, whilst the corresponding data obtain for duplex stainless steel reinforcement presented more of a varied response. This is a strong indicator of the microstructure stability, with the austenitic stainless steel rebars being less likely to undergo change compared with the duplex stainless steel grades. This is further supported by the metallurgical investigation, where the austenitic stainless steel data is very uniform in comparison with the corresponding duplex data.

From the reduction factors presented in Fig. C.6-1 and C.6-2, the three austenitic stainless steel grades examined herein demonstrated a very similar trend to each other. To further simplify the proposed reduction factors, a single set of ‘austenitic’ stainless steel reinforcement reduction factors could be proposed, as presented in table 6-5. Notably, austenitic stainless steel rebar is often very limited in terms of grades used (1.4301, 1.4401 and their subgrades) and commonly restricted to cold-rolled

material for cost-efficiency in manufacturing. If using a single set of reduction factors for austenitics, then 'super-austenitic' rebars would not be included as each grade would require its own specialist study.

Within the duplex stainless steels, although grade 1.4362 is currently the most popular grade for rebar, a single set of reduction factors is not advised as the metallurgical properties can vary greatly from grade to grade within the duplex family. Even with grade 1.4362, both the hot-rolled and cold-rolled data set presented a strong variation in the data collected.

Table 6-5: A single set of recommended retention factors for austenitic stainless steel reinforcing bar.

Grade	Austenitic	
	$k_{p0.2}$	k_u
20	1	1
100	1.01	0.99
200	1.02	1.00
300	1.07	1.01
400	1.08	1.02
500	1.09	1.04
600	1.03	1.02
700	0.93	0.98
800	0.74	0.89
900	0.45	0.79

Chapter 7 Elevated Temperature Response

This chapter presents the results from a series of elevated temperature tests on stainless steel reinforcing bar, conducted to determine the changes in tensile properties during exposure to different levels of fire. The tests were conducted under isothermal test conditions, and on two grades of stainless steel rebar, namely austenitic grade 1.4301 and duplex grade 1.4362. Only one of the austenitic grades examined previously in the post-fire studies was included in these experiments due to the results obtained from the post-fire testing in Chapters 4 and 6, which showed very little difference in results across the austenitic data. This was owing to their similar microstructures, and this is expected to be the same for the elevated temperature tests. These tests are important in order to provide further context and evidence on the post-fire properties previously discussed.

This chapter is broken down into 2 parts, first is the presentation of results and observations from the testing regime, and second is the proposal of reduction factors and comparison with existing values, as recommended by Gardner et al., (2016). The methodology, and test plan for the elevated temperature tests is presented in Section 3.3.3 of this thesis.

7.1 Test Results

7.1.1 Grade 1.4301

Table 7-1 presents the changes in key properties including the 0.2% proof strength ($f_{0.2p,\theta}$), ultimate strength ($f_{u,\theta}$) and total strain at failure at failure ($\varepsilon_{f,\theta}$) following exposure to various levels of elevated temperature between 100 and 800°C. The corresponding stress-strain curves are presented in Fig. 7-1. It is observed that when the rebars are exposed to temperatures of 100°C, there is a significant loss in $\varepsilon_{f,\theta}$, total strain at failure, which decreased by 37% against the virgin value ε_f. $\varepsilon_{f,\theta}$ further declines by

65% against ε_f at 200°C and 69% at 300°C. Following this, between the temperature range of 300-700°C, the loss in $\varepsilon_{f,\theta}$ decreases with the incremental increase of the temperature, with recorded losses of 62%, 52%, 39% and 11% respectively. Then, at 800°C, there is a gain of 49% in $\varepsilon_{f,\theta}$ relative to ε_f from the virgin sample. This increase in ductility is due to the austenitic rebar reaching the active recrystallization condition of at least 737°C and maintaining the temperature long enough to begin forming new and more ductile austenite grains.

For the strength response the data is presented for two property values namely $f_{0.2p,\theta}$, the 0.2% proof stress at temperature θ, and $f_{u,\theta}$, the ultimate tensile stress at θ. Both values show a consistent decline as the temperature rises, but in varying proportions, compared with $f_{0.2p}$. At 100°C, no loss is recorded for $f_{0.2p,\theta}$, whereas f_u presents a loss of 10% against $f_{0.2p}$ for the virgin unheated sample. At 200°C, $f_{0.2p,\theta}$ presents a loss of 18% against $f_{0.2p}$, whilst $f_{u,\theta}$ loses 17% of its original value, resulting in a very rounded stress-strain response, as seen in Fig. 7-1. Following exposure to 300°C, 400°C and 500°C, $f_{0.2p,\theta}$ exhibits losses of between 22-27% relative to $f_{0.2p}$ from the virgin sample, and losses of between 20-27% for $f_{u,\theta}$ when compared to f_u for the virgin sample. When exposed to a higher temperature range of 600-800°C the samples present more significant losses in strength for each temperature increment. At 600°C, a loss of 40% for $f_{0.2p,\theta}$ and 42% for $f_{u,\theta}$ is recorded against the corresponding values from the virgin samples. At 700°C, the strength losses increase to 55% for $f_{0.2,p,\theta}$ and 56% for $f_{u,\theta}$ compared with $f_{0.2p}$ and f_u. At 800°C, the corresponding losses are even greater at 78% for both $f_{0.2p,\theta}$ and $f_{u,\theta}$ against the virgin sample.

Table 7-1: Isothermal response of Grade 1.4301.

	1.4301			
	$f_{0.2p,\theta}$ (N/mm^2)	$f_{u,\theta}$ (N/mm^2)	$\varepsilon_{f,\theta}$ (%)	n
Virgin	695.4	885.9	21.2	1.0
100°C	698.3	797.2	13.3	1.0
200°C	572.2	732.2	7.4	1.0
300°C	507.2	712.7	6.7	1.1
400°C	516.4	692.0	8.1	1.0
500°C	539.3	649.4	10.2	1.1
600°C	418.3	513.7	12.9	1.1
700°C	310.6	391.5	18.9	1.0
800°C	155.6	194.1	31.7	1.2

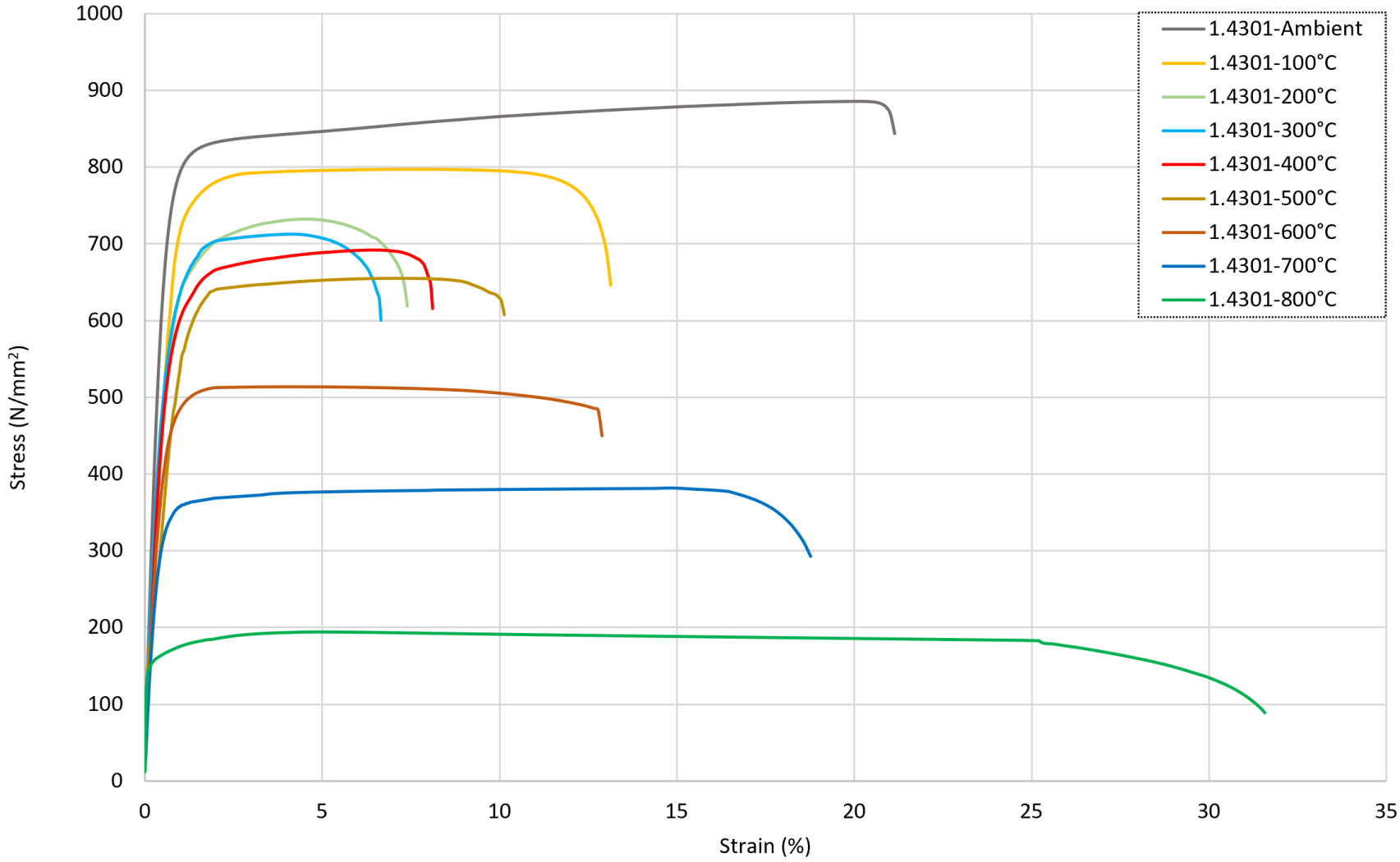

Figure 7-1: Stress-strain responses for austenitic Grade 1.4301 stainless steel rebars under isothermal loading conditions.

7.1.2 Grade 1.4362

Table 7-2 presents the change in key properties including the 0.2% proof strength ($f_{0.2p,\theta}$), ultimate strength ($f_{u,\theta}$) and total strain at failure ($\varepsilon_{f,\theta}$) following exposure to various levels of elevated temperature θ between 100 and 800°C for grade 1.4362 stainless steel rebars. The corresponding stress-strain curves are presented in Fig. 7-2. It is observed that when the rebars are exposed to temperatures of 100-400°C, $\varepsilon_{f,\theta}$ presented a consistent reduction of between 55-57% compared with ε_f from the virgin sample. On the other hand, for the bars that were heated to between 500 and 700°C, $\varepsilon_{f,\theta}$ presented a slightly less significant reduction of around 45-50% compared with ε_f. During exposure to 800°C, there was a significant change to the $\varepsilon_{f,\theta}$ values achieved which were much more similar to those observed for the virgin values, with a reduction of just 9% against ε_f . This increase in ductility between the sample heated at 700°C and 800°C is due to the active recrystallisation of the austenite phase within the duplex alloy, in the same manner as the austenitic rebar.

In terms of the strength parameters, at 100°C there is a 19% and 9% reduction in $f_{0.2p,\theta}$ and $f_{u,\theta}$ compared with the $f_{0.2p}$ and f_u values from the virgin sample, respectively. Between the range of 200-400°C, a consistent loss of 26-27% for $f_{0.2p,\theta}$ and 16-20% for $f_{u,\theta}$ is recorded against $f_{0.2p}$ and f_u. During exposure to higher temperatures of 500°C and 600°C, a loss of 37% is recorded for $f_{0.2p,\theta}$, however for $f_{u,\theta}$ a loss of 22% is presented at 500°C and 41% at 600°C. During heating to 700°C, it is notable that there is a rapid decline in the strength of the material, corresponding to reductions of 65% and 58% for $f_{0.2p,\theta}$ and $f_{u,\theta}$, respectively, compared with $f_{0.2p}$ and f_u from the unheated samples. At 800°C, there is an even greater reduction of 82% and 78% for $f_{0.2p,\theta}$ and $f_{u,\theta}$, respectively, compared with $f_{0.2p}$ and f_u and it is clear that following exposure to this high level of elevated temperature, the material has lost the vast majority of its strength. It is interesting to compare this to the ductility which, as noted before, was quite similar to the virgin values during heating to 800°C. Clearly, the metallurgical phenomena and changes that are occurring in the rebars during this high level of temperature exposure are significant.

Table 7-2: Isothermal response of Grade 1.4362.

	1.4362			
	$f_{0.2p,\theta}$ (N/mm^2)	$f_{u,\theta}$ (N/mm^2)	$\varepsilon_{f,\theta}$ (%)	n
Virgin	836.8	941.5	19.7	0.9
100°C	674.2	854.5	8.9	1.0
200°C	607.3	787.0	8.3	1.0
300°C	615.6	782.5	8.6	1.0
400°C	606.8	751.5	8.4	1.1
500°C	523.1	734.4	10	1.2
600°C	528.3	553.5	9.8	1.2
700°C	289.1	395.9	10.8	1.3
800°C	148.2	211.4	18.0	1.6

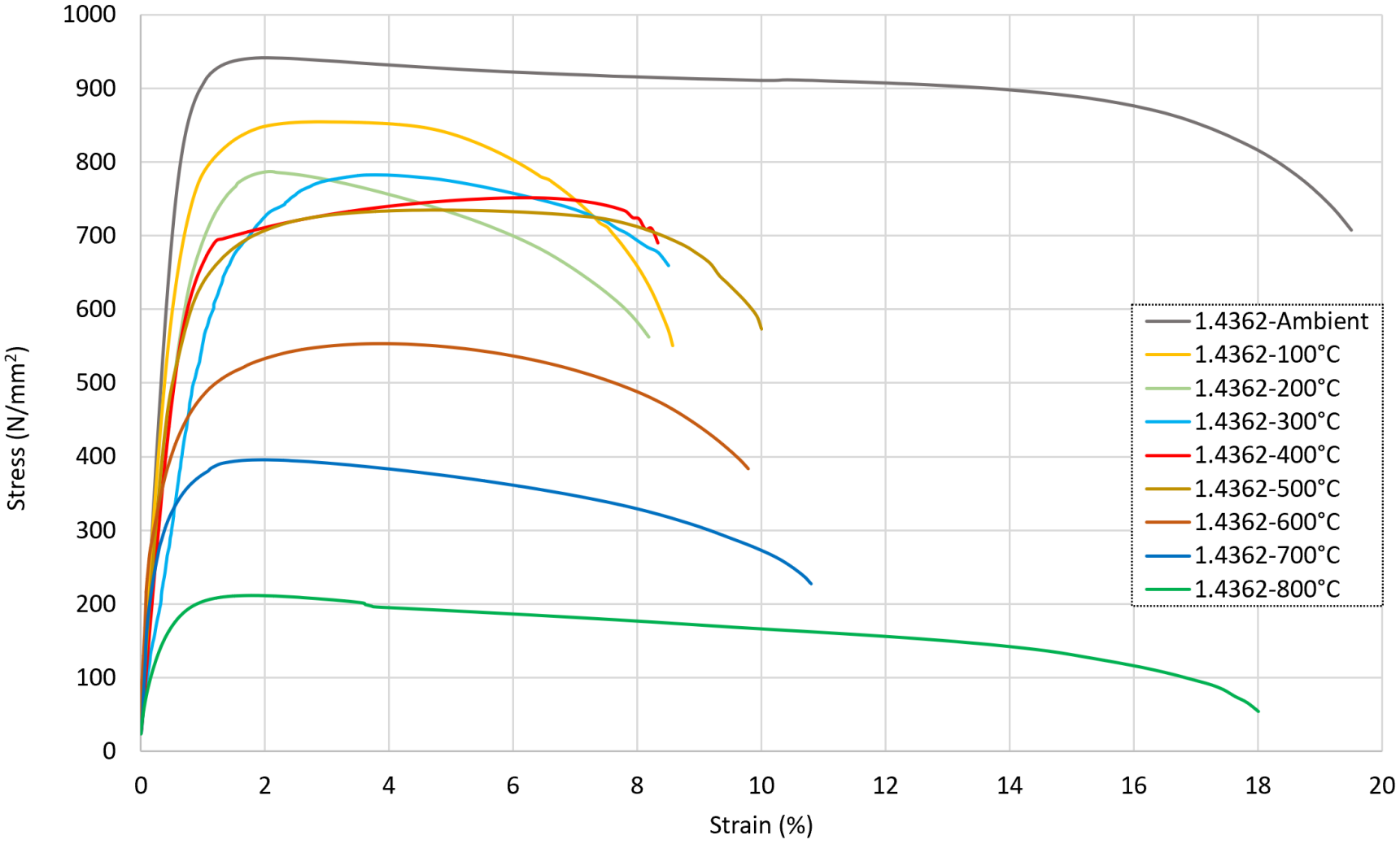

Figure 7-2: Stress-strain responses of duplex Grade 1.4362 stainless steel rebars under isothermal loading conditions.

7.2 Discussion

The results obtained from the practical testing presented in table 7-1 and 7-2 are compared against the corresponding reduction factors proposed by Gardner et al., (2016) including the reduction factors for the 0.2% proof stress ($k_{0.2p}$), ultimate tensile stress (k_u) and total strain for failure (ε_{fk}), which are given in table 7-3. To facilitate this comparison, these reduction factors are employed to determine the resulting 0.2% proof strength ($f_{0.2p,\theta,calc}$), ultimate strength ($f_{u,\theta,calc}$) and total strain at failure ($\varepsilon_{f,\theta,calc}$) at various levels of elevated temperature. The results for $f_{0.2p,\theta}$, $f_{u,\theta}$ and $\varepsilon_{f,\theta}$ and the calculated variant are summarised in Fig. 7-3 for grade 1.4301 austenitic stainless steel rebars and in Fig. 7-4 for the grade 1.4362 duplex stainless steel bars.

Fig. 7-3(a) presents the 0.2% proof stress ($f_{0.2p,\theta}$) for austenitic grade 1.4301. Between the temperature ranges of 100-700°C, the $f_{0.2p,\theta}$ consistently retains 13-32% more of their original strength compared with $f_{0.2p,\theta,calc}$, with 500°C having the greatest difference at 32%. It is interesting to note in Fig. 7-3(a) that there is a minor increase in the $f_{0.2p,\theta}$ value at 400°C and 500°C compared with 300°C; the reason for this is due to the fundamental change in curvature for the stress-strain graph. As discussed earlier in Section 4.5.1, within grade 1.4301, the strengthening mechanisms produced during cold-rolling phase become more defined at temperatures of 400°C and 500°C. On the other hand, for the $f_{0.2p,\theta}$ at 800°C, the specimen retains 25% less strength than $f_{0.2p,\theta,calc}$ for the same temperature.

In Fig. 7-3(b) both the tested and calculated ultimate tensile stress ($f_{u,\theta}$) show more similarity towards each other compared with the 0.2% proof strength data. In the temperature range of 100-500°C, the $f_{u,\theta}$ consistently retains up to 10% more ultimate strength compared with $f_{u,\theta,calc}$, whilst at 600°C and 700°C both $f_{u,\theta}$ specimens perform within 2% of the $f_{u,\theta,calc}$ values. At 800°C the $f_{u,\theta}$ achieved is 18% lower than $f_{u,\theta,calc}$, which is in line with the 0.2% proof strength observations. With reference to Fig. 7-3(c), it is observed that for the rebars exposed up to temperatures of up to 500°C, $\varepsilon_{f,\theta}$ is similar to $\varepsilon_{f,\theta,calc}$. For the rebars exposed to temperatures above 500°C, the tested specimens consistently show a higher value for $\varepsilon_{f,\theta}$ compared with $\varepsilon_{f,\theta,calc}$, and closer to the original values. This increase in ductility is due to the active dissipation of the cold-rolled strengthening mechanism, and introduction of new austenite grains.

Fig 7-4(b) presents the duplex grade 1.4362, with Fig. 7-4(a) presenting the 0.2% proof stress ($f_{0.2p,\theta}$). It is clear that overall, the values obtained in the current study are quite similar to those determined by Gardner et al., (2016). When exposed to temperatures of 100°C and 200°C, the $f_{0.2p,\theta}$ perform within 3% of $f_{0.2p,\theta,calc}$. Comparatively at 300-800°C, the $f_{0.2p,\theta}$ showed consistent rise from $f_{0.2p,\theta,calc}$, starting at 7% at 300°C and consistently increasing until the $f_{0.2p,\theta}$ is 61% higher than $f_{0.2p,\theta calc}$ at 800°C. In Fig. 7-

4(b) the ultimate tensile stress ($f_{u,\theta}$) shows a similarity to the 0.2% proof strength when exposed to temperatures of 100°C and 200°C, with the $f_{u,\theta}$ performing within 3% of the $f_{u,\theta,calc}$. From 300-800°C the $f_{u,\theta}$ consistently achieved 5-25% higher results than $f_{u,\theta,calc}$. In Fig. 7-4(c) the total strain at failure ($\varepsilon_{f,\theta}$) are presented, and it is observed that the $\varepsilon_{f,\theta}$ trends and values are quite different from the $\varepsilon_{f,\theta,calc}$ values. From 100°C-600°C, the $\varepsilon_{f,\theta}$ consistently underperformed against the $\varepsilon_{f,\theta,calc}$ by between 97-138%. At 700°C, the difference decreases to 45%, whilst at 800°C the $\varepsilon_{f,\theta}$ overperformed by 35% against $\varepsilon_{f,\theta,calc}$.

Table 7-3: Reduction factors taken from Gardner et al., (2016) and applied to the tested virgin samples to calculate the comparative results.

	Grade 1.4301			Grade 1.4362		
Temperature (°C)	$k_{0.2p}$	k_u	ε_{fk}	$k_{0.2p}$	k_u	ε_{fk}
20	1	1	1	1	1	1
100	0.8	0.86	0.56	0.83	0.94	1
200	0.67	0.77	0.42	0.75	0.87	1
300	0.62	0.74	0.42	0.69	0.79	1
400	0.58	0.74	0.42	0.58	0.7	1
500	0.53	0.68	0.42	0.43	0.59	1
600	0.48	0.59	0.33	0.27	0.47	1
700	0.39	0.43	0.25	0.14	0.33	0.8
800	0.28	0.26	0.15	0.07	0.2	0.6

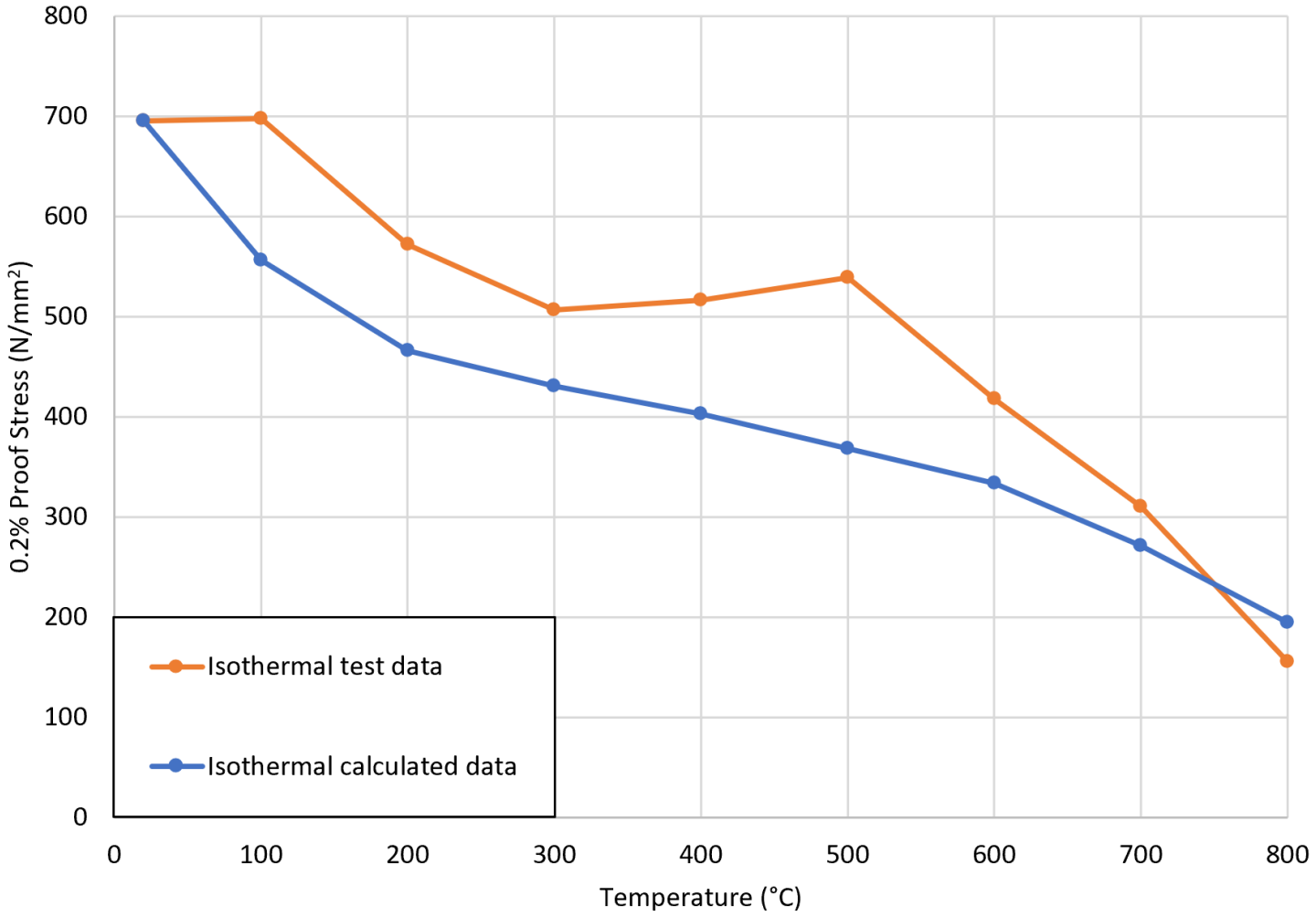
800
700
600
500
400
300
200
100
0
0.2% Proof Stress (N/mm²)
0
100
200
300
400
500
600
700
800
Temperature (°C)
Isothermal test data
Isothermal calculated data

(a)

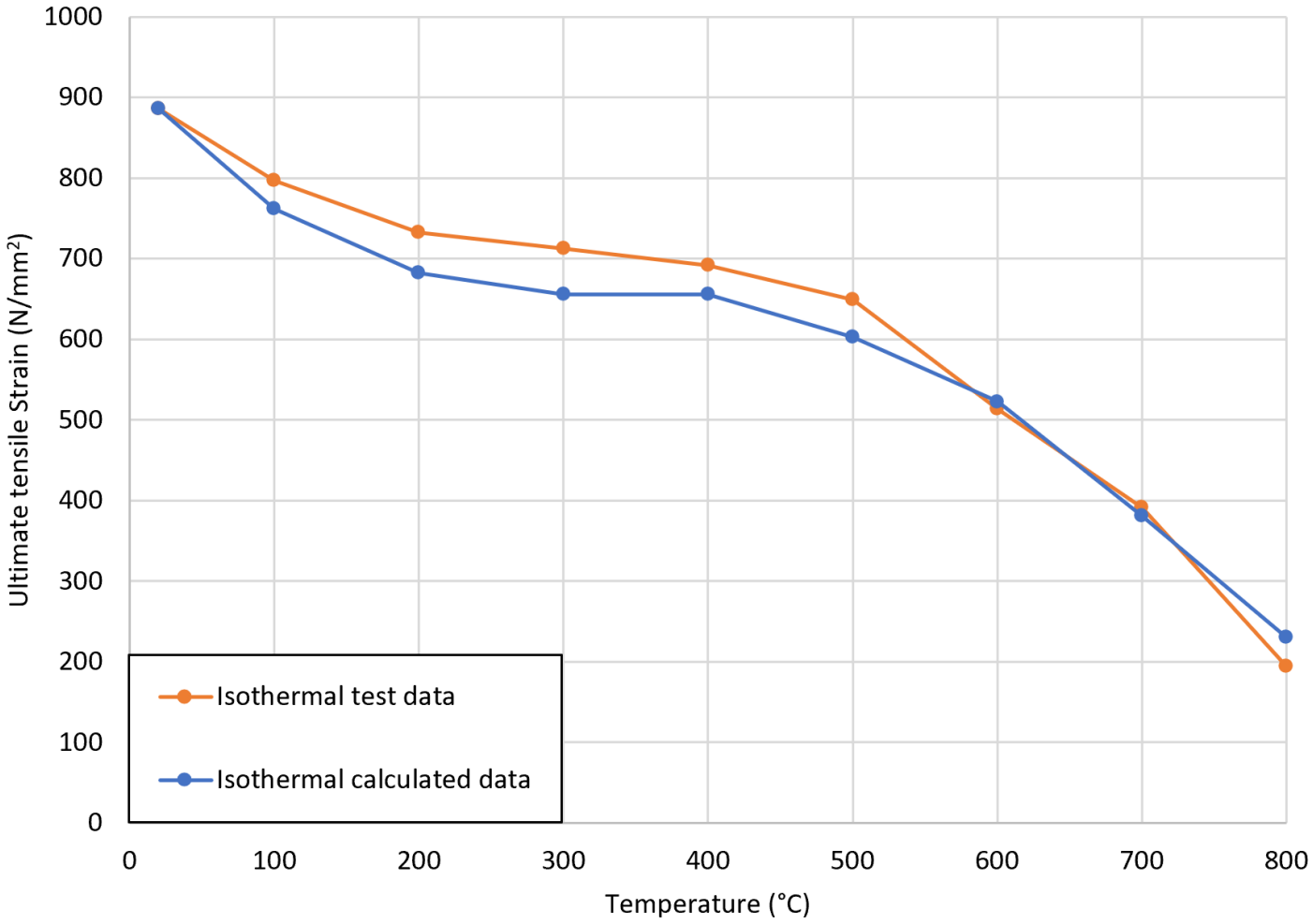
1000
900
800
700
600
500
400
300
200
100
0
Ultimate tensile Strain (N/mm²)
0
100
200
300
400
500
600
700
800
Temperature (°C)
Isothermal test data
Isothermal calculated data

(b)

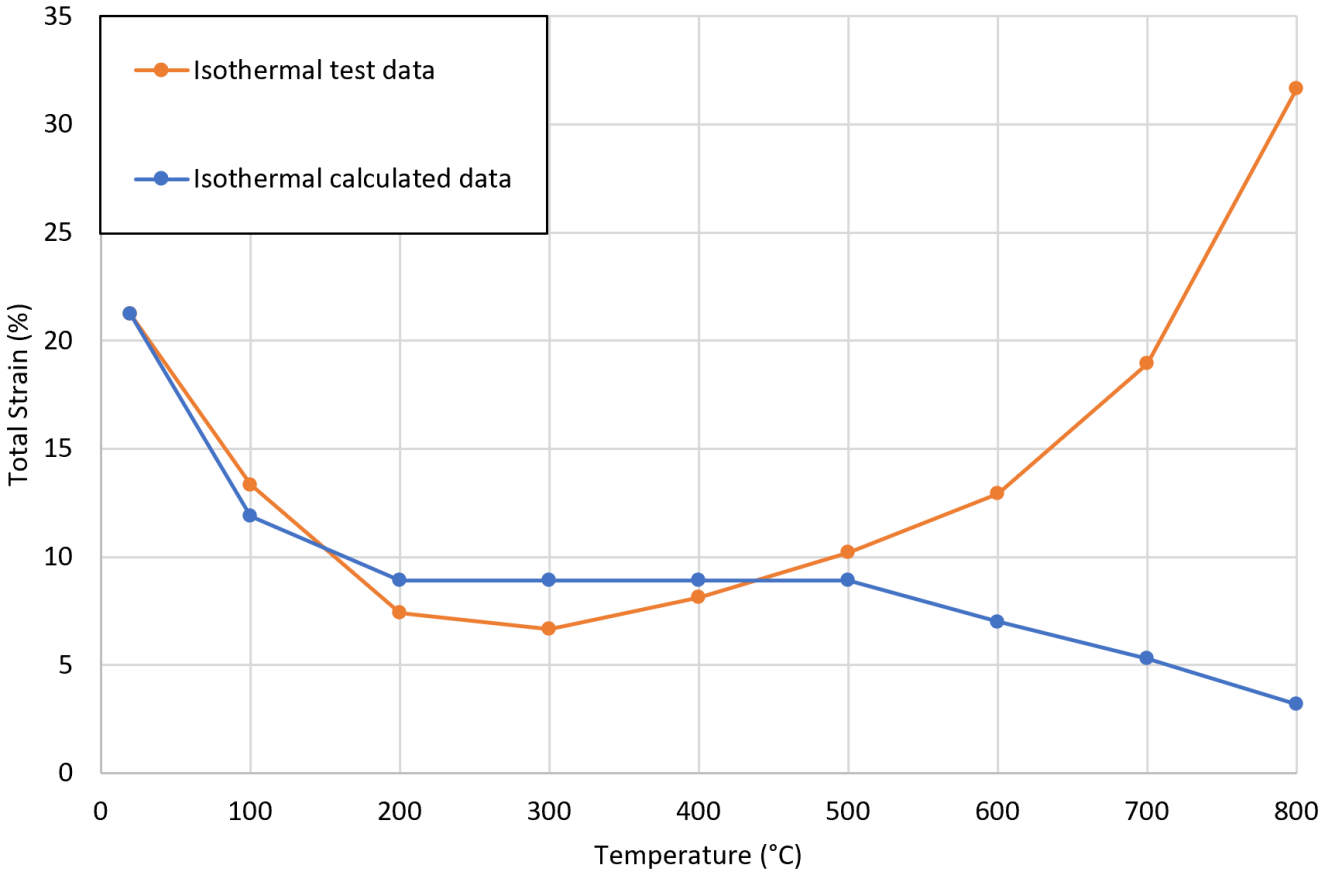

(c)

Figure 7-3: Austenitic Grade 1.4301 tests results in comparison to Gardner et al. (2016) reduction factors, (a) 0.2% proof stress, (b) ultimate tensile stress and (c) total strain at failure.

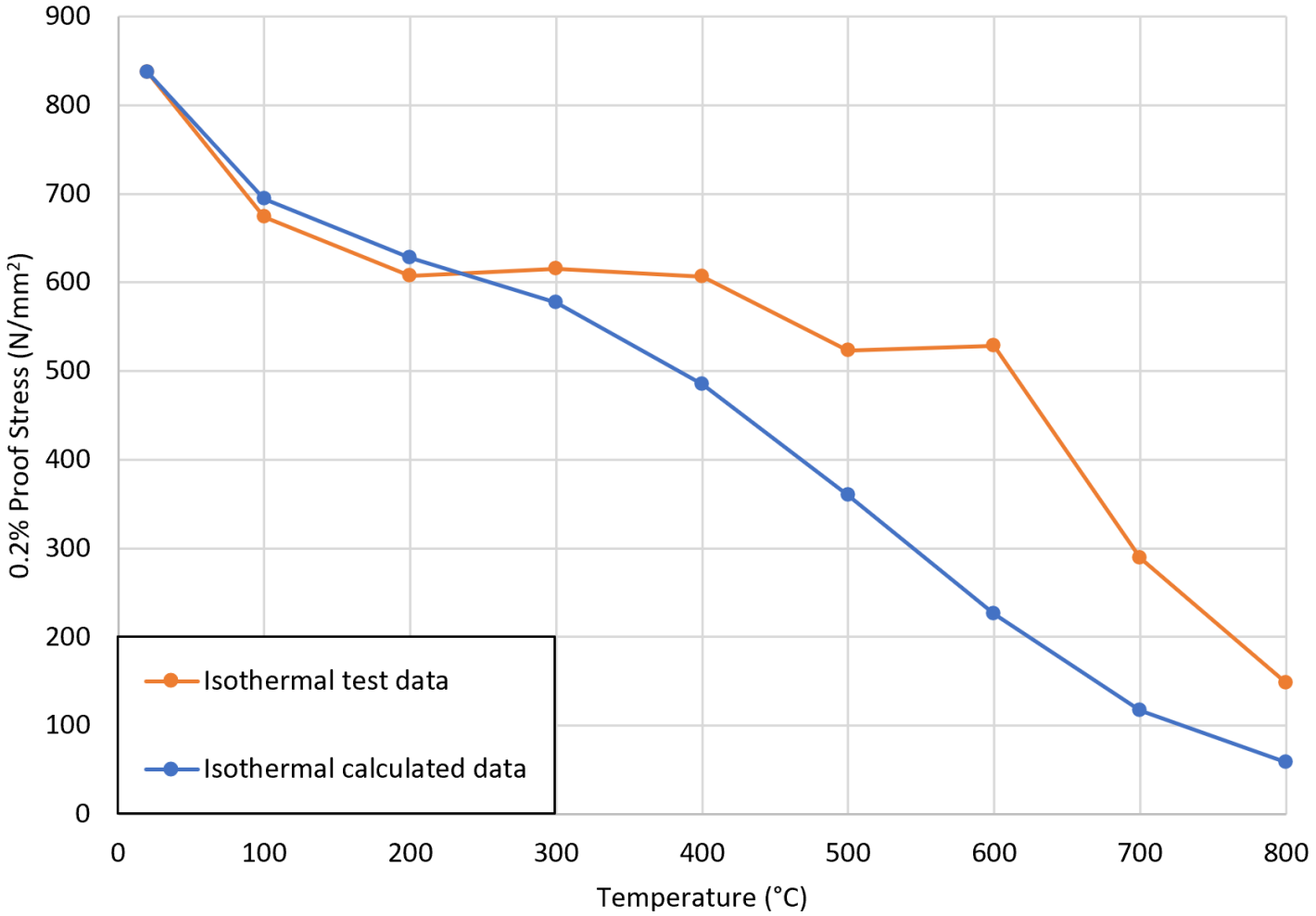
900
800
700
600
500
400
300
200
100
0
0.2% Proof Stress (N/mm²)
0
100
200
300
400
500
600
700
800
Temperature (°C)
Isothermal test data
Isothermal calculated data

(a)

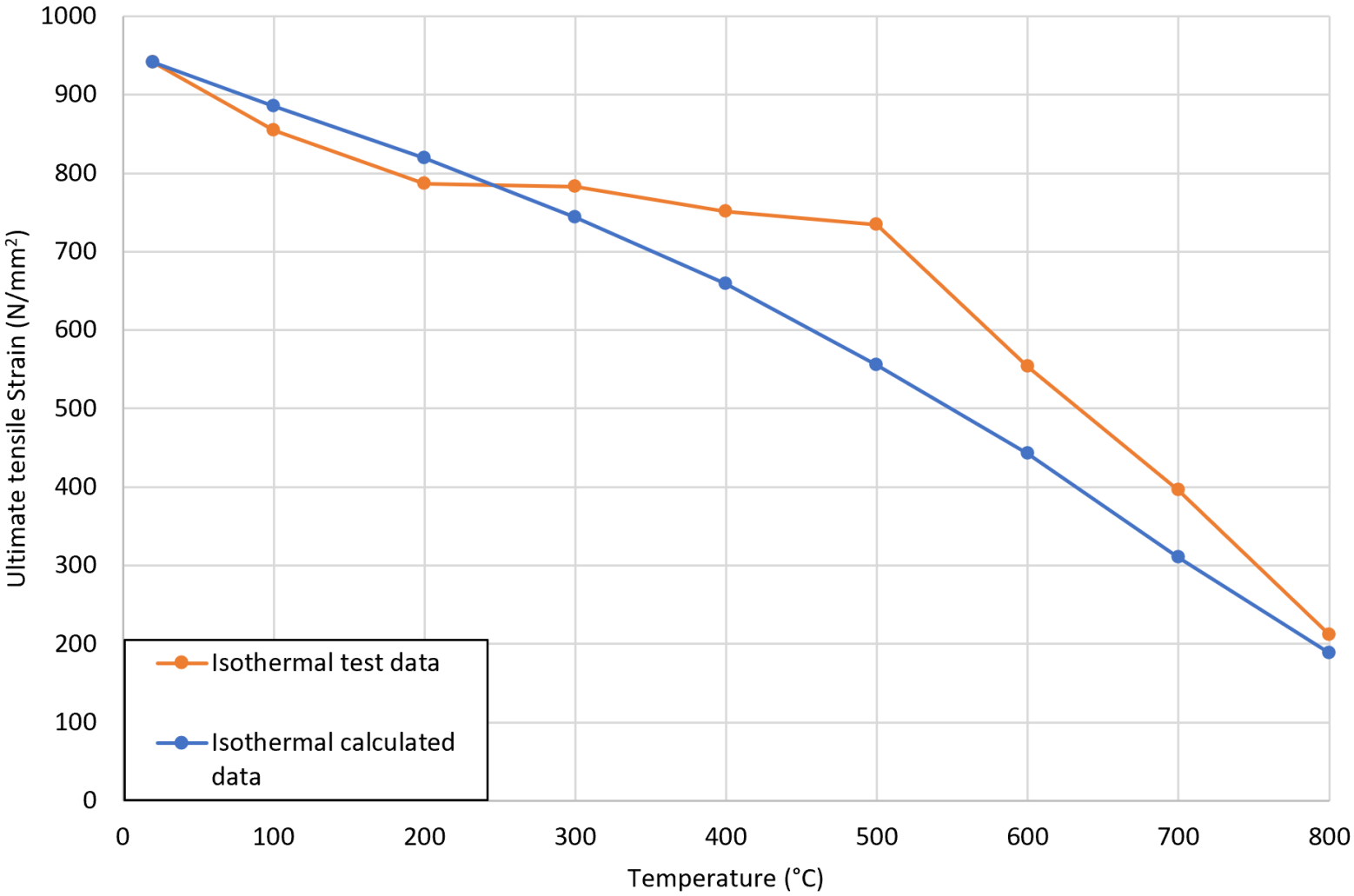
1000
900
800
700
600
500
400
300
200
100
0
Ultimate tensile Strain (N/mm²)
0
100
200
300
400
500
600
700
800
Temperature (°C)
Isothermal test data
Isothermal calculated data

(b)

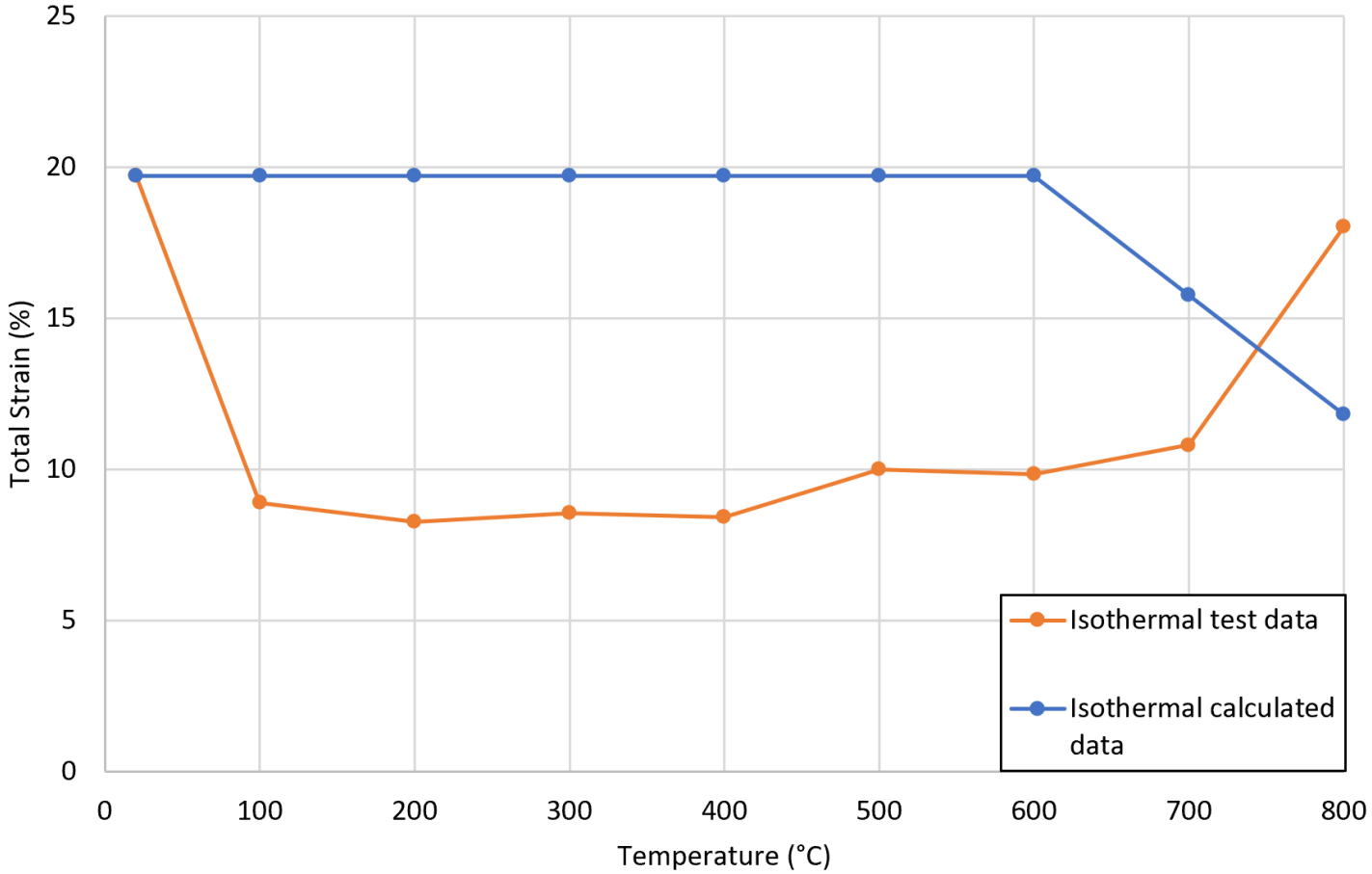

(c)

Figure 7-4: Duplex Grade 1.4362 tests results in comparison to Gardner et al. (2016) reduction factors, (a) 0.2% proof stress, (b) ultimate tensile stress and (c) total strain at failure.

To assess the reliability of the reinforcing bars tested, a reliability analysis was carried out in line with ASCE specifications (ASCE, 2002), the criteria for this test is for cold-formed stainless steel structural components at ambient temperatures, and not reinforcing bar at elevated temperatures. As such, an Initial target reliability index (β) of 2.5 was adopted to accurately reflect the change in material (Huang & Young, 2017). Using this, the resistance factor (φ) of is calculated using formula 7-1. The results obtained from the reliability index are presented in table 7-4.

$$\varphi = 1.5(M_m F_m P_m) * \exp\left(-\beta\sqrt{V^2{}_M + V^2{}_F + C_p V^2{}_P + V^2{}_Q}\right) \quad (7\text{-}1)$$

The statistical parameters are defined in the ASCE specification as $\mathrm{M_m} = 1.10$, $\mathrm{F_m} = 1.00$, $\mathrm{V_m} = 0.10$, $\mathrm{V_F} = 0.05$, $\mathrm{V_Q} = 0.21$. Whilst the variable parameters $\mathrm{P_m}$ and $\mathrm{V_P}$ are derived from the test data as mean value of tested-to-predicted load ratios and coefficient of variation of tested-to-predicted load ratios. A correction factor of $\mathrm{C_p}$ is calculated through formula 7-2. With *n* being the total number of tests.

$$C_p = (n-1)/(n-3) \quad (7\text{-}2)$$

Table 7-4: Reliability analysis for grades 1.4301 and 1.4362 at elevated temperature.

	1.4301				
	E	$f_{0.2p,\theta}$	$f_{u,\theta}$	$\varepsilon_{f,\theta}$	**n**
COV	0.14	0.34	0.33	0.53	0.06
Resistance factor (ϕ)	0.67	0.37	0.38	0.25	0.62
Reliability index (β)	2.5	2.5	2.5	2.5	2.5
	1.4362				
COV	0.14	0.39	0.33	0.31	0.16
Resistance factor (ϕ)	0.64	0.29	0.37	0.34	0.93
Reliability index (β)	2.5	2.5	2.5	2.5	2.5

7.3 Concluding Remarks

This chapter presents the results and discussion from the elevated temperature test programme including in this thesis. At first, the results from the practical testing phase are presented in section 7.1, and these are then discussed against existing reduction factors by Gardner et al. (2016) in section 7.2.

Comparatively within the two grades tested, the austenitic rebar presents a more consistent pattern across the practical test data compared with the duplex rebar. For the 0.2% proof strength ($f_{0.2p,\theta}$) and ultimate strength ($f_{u,\theta}$), there is excellent consistency between the results of the current programme and the reduction factors proposed by Gardner et al. (2016). Overall, the rebars follow a consistent

trend of declining in strength as the temperature rises. For the strain comparison, the $\varepsilon_{f,\theta}$ and $\varepsilon_{f,\theta,calc}$ present significantly different results within both types of rebar, and this inconsistency is attributed to the degree of cold-rolling during the manufacturing phase of the rebar.

From the data collected, the reduction factors proposed for Gardner et al. (2016) show that the stress retention factors are accurate, whilst for the strain, especially for the duplex, require further investigation.

Chapter 8 Conclusions and Suggestions for Future Research

In this chapter, the key research findings and principal conclusions reached in this thesis are presented. This is followed by recommendations for future research, building on the work presented in this thesis.

8.1 Conclusions

This thesis presents a detailed analysis on the behaviour of stainless steel reinforcement during exposure to a fire scenario and following exposure to fire scenario, followed by a range of cooling regimes. A total of 162 unique tensile data sets and 73 metallurgical data sets are presented. The testing regime covered the most common found types of stainless steel rebar, grades 1.4301, 1.4401, 1.4436 and two variations of grade 1.4362. For post-fire temperature testing, there was a strong absence of information in the available literature prior to this work, and therefore it was difficult for engineers to make informed decisions on the structural integrity of stainless steel reinforced concrete structures following a fire. The levels of temperature exposure examined were selected to give the full range of possible behaviours and with consideration to what would provide the most informative response. The cooling methods were designed to replicate possible real life scenarios that the rebar may come under, including cooling naturally in air (air-cooling), cooling quickly through water (rapid-cooling), replicating the fire service, and an intermediary cooling rate or cooling slowly in the oven (slow-cooling) to replicate the rebar cooling within a concrete cover.

When considering the overall post-fire response of the austenitic grade rebars, all three grades inspected presented a very uniform response of showing an initial increase in strength, of up to 15% for the $f_{0.2p}$, until 500°C alongside a slight reduction in ductility. This was then followed by a gradual decrease in strength and increase in ductility as the mechanically induced strength was lost and the

pure austenite phase was formed, this resulted in a characteristic change in the shape of the stress-strain curve. The carbon steel B500B rebar presented uniform response for the air-cooled, slow-cooled and quenched rebar up to 700°C, whilst after quenching in water past the critical recrystallisation temperature of 727°C caused the formation of a brittle microstructure. The cooling rate was not shown to have a significant influence on the retention of the tensile properties in the austenitic rebars. Following exposure to the lower and moderate examined temperature range, in all circumstances the austenitic rebar remained useable and retained all of its strength and whilst retaining its original ductility in the lower temperature range. Up until the 700°C range, all austenitic rebar samples met the tensile properties as set out by Part 7 of BS 4449. When an austenitic rebar has been exposed to temperatures of 800°C and 900°C, it should be noted that it is not fit for use. At this stage, it was found that the austenitic rebar had undergone active recrystallisation and has formed a γ-austenite dominate microstructure without the necessary strengthening mechanisms.

When examining the two duplex grade rebar, the importance of knowing the method of manufacturing becomes apparent. Within this study, both hot-rolled and cold-rolled rebars were tested under post-elevated temperature conditions. Both hot-rolled and cold-rolled duplex were influenced by the method of cooling, due to, unlike the austenitic rebars, the duplex rebars having a far more unstable microstructure, and thus being more prone to change under the same influence. The prone microstructure was especially noticeable in the hot-rolled rebar, which presented a second yield-like phenomena in the stress-strain data when exposed to temperatures of 500°C and 600°C. Within the cold-rolled sample, the corrosion resistance may be compromised due to the formation of a σ-phase in the grain boundary, this can be seen in the microscopic imagery at 700°C. When comparing to the tensile properties as set out by part 7 of BS 4449, all tested cold-rolled and hot-rolled samples met the strength requirements until 800°C, regardless of cooling method. However similar to the austenitic rebar, a more ductile response was noted following exposure to higher temperatures and subsequent cooling. When comparing both methods of production against each other the hot-rolled rebars presented greater changes overall in the residual material behaviour following a fire scenario.

For the isothermal testing at elevated temperatures, the two tested grades where 1.4301 and 1.4362, both in cold-rolled formed. Both grades performed complexly different to each other; with the common factor being the strength of both rebars gradually declining as the temperature rose. The austenitic rebar retained enough strength to be mechanically viable until 500°C whilst the duplex retained enough strength until 600°C, with both exhibiting a constant loss in strain. After prolonged exposure to adequate recrystallization conditions, at 800°C neither rebar retained any of the strength from the strengthening mechanisms when cold-rolling. When comparing the test data obtained with

work done on concrete exposure by Raouffard and Nishiyama (2016) and the EN 1991-1-2 (2002) fire curve, conclusively as long as the concrete cover is not exposed, the stainless steel rebar should not rise above 500°C and should retain enough strength to be safe for use. Once the cover has been exposed at higher temperatures, the rebar would lose the cold-rolled strength and not be considered safe under elevated temperature conditions.

Overall, when comparing the collected stainless steel data in both post- fire and elevated temperature scenarios to the currently available guidance for carbon steel rebar, the stainless steel rebar far outperforms the current guidelines. As stated by Gardner et al., (2016), there is a need for more efficient design guidance for stainless steel rebar, the novel information presented herein aims to contribute towards that.

8.3 Recommendations for Further Research

Previously there was a complete absence of literature on the residual performance of stainless steel reinforcing bar following a fire, whilst limited work was available on the elevated temperature performance of stainless steel rebar. The observations and conclusions drawn in this thesis present a variety of important issues that could benefit from additional work, these are highlighted as follows.

This thesis focused on the tensile properties of stainless steel rebar under static load conditions, further research could include an analysis if the material hardness and fracture toughness, as well as a study into the properties under cyclic loading.

For austenitic stainless steel reinforcing bar, an important factor in strength retention lies in the initial cold-rolling strength. Often stainless steel rebar has no definite yield strength range, with austenitics ranging from 600 MPa to 900 MPa, meaning overengineered bars are often used. With more transparency in the manufacturing method and a larger variety of rebar; data could be obtained to help austenitic cold-rolled rebar manufacturing obtain greater efficiency on a constant basis.

Furthermore, the microstructure for austenitic rebar is very stable throughout the whole manufacturing method. Further research could be undertaken in the development of AI assisted data determination on the actual strength retention on a case-by-case scenario.

Within the duplex reinforcing bar, this study covers grade 1.4362. Additional studies can be undertaken with the same programme model on other duplex grades as, unlike austenitics, there is a huge variance in the elemental composition of the various duplex grades such as 1.4462 and 1.4162.

Grade 1.4362 rebar has a more unstable microstructure than the austenitics when exposed to elevated temperatures in both tested scenarios. Additional microstructural investigations, such as neutron diffraction at elevated temperatures, on determining the austenite-ferrite relationship in the alloy could benefit in the stabilisation of the alloy.

For the elevated temperature testing, the programme within this thesis was limited two of the most popular grades within each rebar type; grade 1.4301 for austenitics and 1.4362 for duplex. The testing programme could benefit from an increased variety in test specimens, especially multiple samples from different manufacturers for the same grade to determine the best possible trends. In addition, elevated temperature testing for the metallurgical investigation is also possible with specialist equipment, this could help in determining the cause of the double yield phenomena found in hot rolled duplex grade 1.4362 rebar.

When researching stainless steel rebar in and following fire scenarios, it is important to remember that these rebars are designed for heavy marine settings and thus spending their lifecycle under the effects of heavy weathering. As stainless steel rebar is not immune to corrosion, it is simply more resistant towards it; practical testing on weathered rebar may yield different results and should be a discussion of investigation.

References

Ala-Outinen, T., (1996). Fire resistance of austenitic stainless steels Polarit 725 (EN 1.4301) and Polarit 761 (EN 1.4571), *VTT Building Technology*.

ASCE – American Society of Civil Engineers (2002) Specifications for the Design of Cold-Formed Stainless Steel Structural Members SEI/ASCE 8-02. *ASCE Library.*

Alinejad, H. and Abbasi, M., (2021). Effects of precipitated phases on the magnetic properties of 2304 duplex stainless steel*. Journal of Magnetism and Magnetic Materials*, Volume 537.

Arup, (2020). Samuel De Champlain Bridge Corridor. *[Online] Available at: https://www.arup.com/projects/samuel-de-champlain-bridge* [Accessed 04 12 2021].

Ba, G., Miao, J., Zhang, W. and Liu, J., (2019). Influence of reinforcement corrosion on fire performance of reinforced concrete beams. *Construction and Building Materials*, Volume 213, pp. 738-747.

Beddos, J. and Parr, J. G., (1999). Introduction to Stainless Steel. 3rd ed. *ASM International*.

Bertolini, L. and Gastaldi, M., (2011). Corrosion resistance of low-nickel duplex stainless steel rebars. *Materials and Corrosion,* 62(2), pp. 120-129.

Bhadeshia, H. and Honeycombe, R., (2017). Steels: *Microstructure and Properties*. 4th ed.

Bruker, (2021). The Swiss Army Knife of the X-ray Diffractionist. *[Online] Available at: https://www.bruker.com/en/products-and-solutions/diffractometers-and-scattering-systems/x-ray-diffractometers/diffrac-suite-software/diffrac-eva.htm*l [Accessed 07 10 2021].

BS 4449+A3, (2016). Steel for the reinforcement of concrete, Weldable reinforcing steel, Bar, coil and decoiled product specifications. *British Standard Institute (BSI).*

BS 6744, (2016). Stainless steel bars. Reinforcement of concrete. Requirements and test methods. *British Standards Institute (BSI).*

BS EN 10088-3, (2014) Technical delivery conditions for semi-finshed products, bars, rods, wire sections and bright products of corrosion resisting steels for general purpose. *British Standards Institute (BSI).*

Cardoso, J. L., Pacheco, M. S., Araujo, A. and Riberio, J., (2018). Stainless Steel Rebar for Marine Environment: Study of Galvanic Corrosion with Carbon Steel Rebars Used in the Same Concrete Structure. *Corrosion Conference and Expo*.

Chadwick, G.A., (1972). *Metallography of Phase Transformations*.

Chang, Y. F., Chen, Y. H., Sheu, M. S. & Yao, G. C., 2006. Residual stress-strain relationship for concrete after exposure to high tempretatures. *Cement and Concrete Research,* Issue 38, pp. 1995-2005.

Chen, Y. H., Chang, Y. F., Yao, C. Y. and Sheu, M. S., (2009). Experimental research on post-fire behaviour of reinforced concrete columns. *Fire Safety Journal*, Issue 44, pp. 741-748.

Chen, Z., Gandhi, U., Lee, J. and Wagoner, R. H., (2016). Variation and consistency of Young's modulus in steel. *Journal of Materials Processing Technology*, Volume 227, pp. 227-243.

Concrete Society, 1998. Guidance on the use of stainless steel reinforcement, *The Concrete Society* .

Dehghan-Manshadi, A., Barnett, M. R. and Hodgson, P. D., (2013). Microstructure evolution during hot deformation of duplex stainless steel. *Materials Science and Technology,* 23(12), pp. 1478-1484.

EN 1991-1-2, (2002). Eurocode 1: Actions on structures - Part 1-2: General actions - Actions on structures exposed to fire. *European Committee for Standardization (CEN).*

EN 1992-1-1, (2004). Eurocode 2: Design of concrete structures - Part 1-1: General rules and rules for buildings. *European Committee for Standardization (CEN).*

EN 1993-1-2, (2005). Eurocode 3: Design of steel structures - Part 1-2: General rules - Structural fire design. *European Committee for Standardization (CEN).*

Felicetti, R., Gambarova, P. G. and Meda, A., (2009). Residual Behaviour of steel rebars and R/C sections after a fire. *Construction and Building Materials,* Issue 23, pp. 3546-3555.

Gao, X.; Zhang, X.; Liu, H.; Chen, Z.; Li, H., (2018). Residual mechanical properties of stainless steels S30408 and S31608 after fire exposure. *Construction and Building Materials,* Issue 165, pp. 82-92.

Gardner, L., Bu, Y., Francis, P., Baddoo, N. R., Cashell, K. A., McCann, F., (2016). Elevated tempreture material properties of stainless steel reinforcing bar. *Construction and Building Materials,* Volume 114, pp. 997-997.

Gardner, L., Insausti, A., Ng, K. and Ashraf, M., (2010). Elevated temperature material properties of stainless steel alloys. *Journal of Constructional Steel Research*, Volume 66, pp. 634-647.

Garlock, M., Paya-Zaforteza, I., Kodur, V. R. and Gu, L., (2012). Fire Hazard in Bridges: Review, Assessment and Repair Strategies. *Engineering Structures*, Volume 35.

Gedge, G., (2003). Rationale for using Stainless Steel Reinforcement in the UK Construction Industry.

Government of Canada, (2021). Pont Samuel-De Champlain - Foire aux questions. *[Online] Available at: https://www.infrastructure.gc.ca/nbsl-npsl/faq-fra.html#q1* [Accessed 16 11 2021].

Hansen, N., (2004). Hall–Petch relation and boundary strengthening. *Scripta Materialia*, 51(8), pp. 801-806.

Huang, Y. and Young, B., (2014). The art of coupon testing. *Journal of Constructional Steel Research*, Volume 96, pp. 159-175.

Huang, Y. & Young, B., (2017). Post-fire Behaviour of Ferritic Stainless Steel Material. *Construction and Building Materials,* , 157, pp. 654-667.

Huang, Y. & Young, B., (2018). Mechanical Properties of lean duplex stainless steel at post-fire condition. *Thin-Walled Structures,* Volume 130, pp. 564-576.

International Stainless Steel Forum, (2020). The Stainless Steel Family, *International Stainless Steel Forum (ISSF).*

Lord, J. D. and Morrell, R. M., (2010). Elastic modulus measurement - obtaining reliable data from the tensile test. *Metrologia*, Issue 47, pp. S41-S49.

Malaska, M.; Cashell, K.; Alanen, M.; Mela, K.; Afshan, S., (2019). Experimental behaviour of stianless steel cellilar beam in fire*. Nordic Steel Construction Conference*.

Molkens, T.; Cashell, K.; Malaska, M.; Alanen, M.; Rossi, B., (2020). Post-fire behaviour of structural stainless steel. *Eurosteel.*

Molkens, T., Colie, R. V. and Gernay, T., (2017). Assessment of damage and residual load bearing capacity of a concrete slab after fire: Applied reliability-based methodology. *Engineering Structures,* Issue 150, pp. 969-985.

Mondal, R. et al., (2020). Solution Annealing of Super Duplex Stainless Steel: Correlating Corrosion Performance with Grain Size and Phase-Specific Chemistry. *Metallurgical and Materials Transactions*, pp. 2480-2494.

Nickel Institute, (2013). Progresso Pier built with nickel-containing stainless steel, *Nickle Institute.*

Norwegian Building Research Institute, 2006. Guide for the use of stainless steel reinforcement in concrete structures*, Noric Innovation Centre*.

Pramanik, B. A. and Kumar, A., (2015). Stainless Steel: Microstructure, *Mechanical Properties and Methods of Application*..

Raouffard, M. M. and Nishiyama, M., (2016). Residual Load Bearing Capacity of Reinforced Concrete Frames after Fire. *Journal of Advanced Concrete Technology*, 14(10), pp. 625-633.

Rodrigues, D. G., Maria, G. G. B., Viana, B. A. L. and Santos, D. B., (2019). Effect of low cold-rolling strain on microstructure, texture, phase transformation, and mechanical properties of 2304

lean duplex stainless steel, *Materials Characterization.*

Special Metals Corporation, (1998). Inconel. *Special Metals Corporation (SPC*).

Sun, S. C., Mu, J. W., Jiang, Z. H., Ji, C. T., Lian, J. S., Jiang, Q., (2014). Effect of cold rolling on tensile properties and microstructure of high nitrogen alloyed austenitic steel. *Materials Science and Technology*, 2(30), pp. 1446-151.

Tao, Z., Wang, X., Hassan, K., Song, T., Xie, L., (2018). Behaviour of three types of stainless steel after exposure to elevated temperatures. *Journal of Constructional Steel Research*, Volume 152, pp. 296-311.

The Steel Construction Institute, (2017). Design Manual for Structural Stainless Steel 4th Edition*, Steel Construction Institute (SCI)*.

Twilt, L., (1988). Strength and Deformation Properties of Steel at Elevated Temperatures: Some Practical Implications. *Fire Safety Journal*, Volume 13, pp. 9-15.

William, H., G., P. R., Marino, F. P. and al, e., (2009). Corrosion Resistant Alloys for Reinforced Concrete, *US Department of Highways*.

World Stainless Fourm, (2016). River Delta Crossing - ISSF Stainless Steel in Infrastructure, *worldstainless.org.*

Yuli, D., Weicheng, F., Qingan, W. and Y, B., (1996). Study on Residual Load-Bearing Capacity and Reliability Index of Reinforced Concrete Slab Post-Fire.

Zeng, D., Lo, K., Cheang, K. and Lai, J., (2012). Remaining Strengths and Pitting Resistance of AISI 316 After a Fire Attack: Implications for Use as Concrete Rebars*. ASM International*, Issue 22, pp. 1481-1489.

Appendix

Appendix A

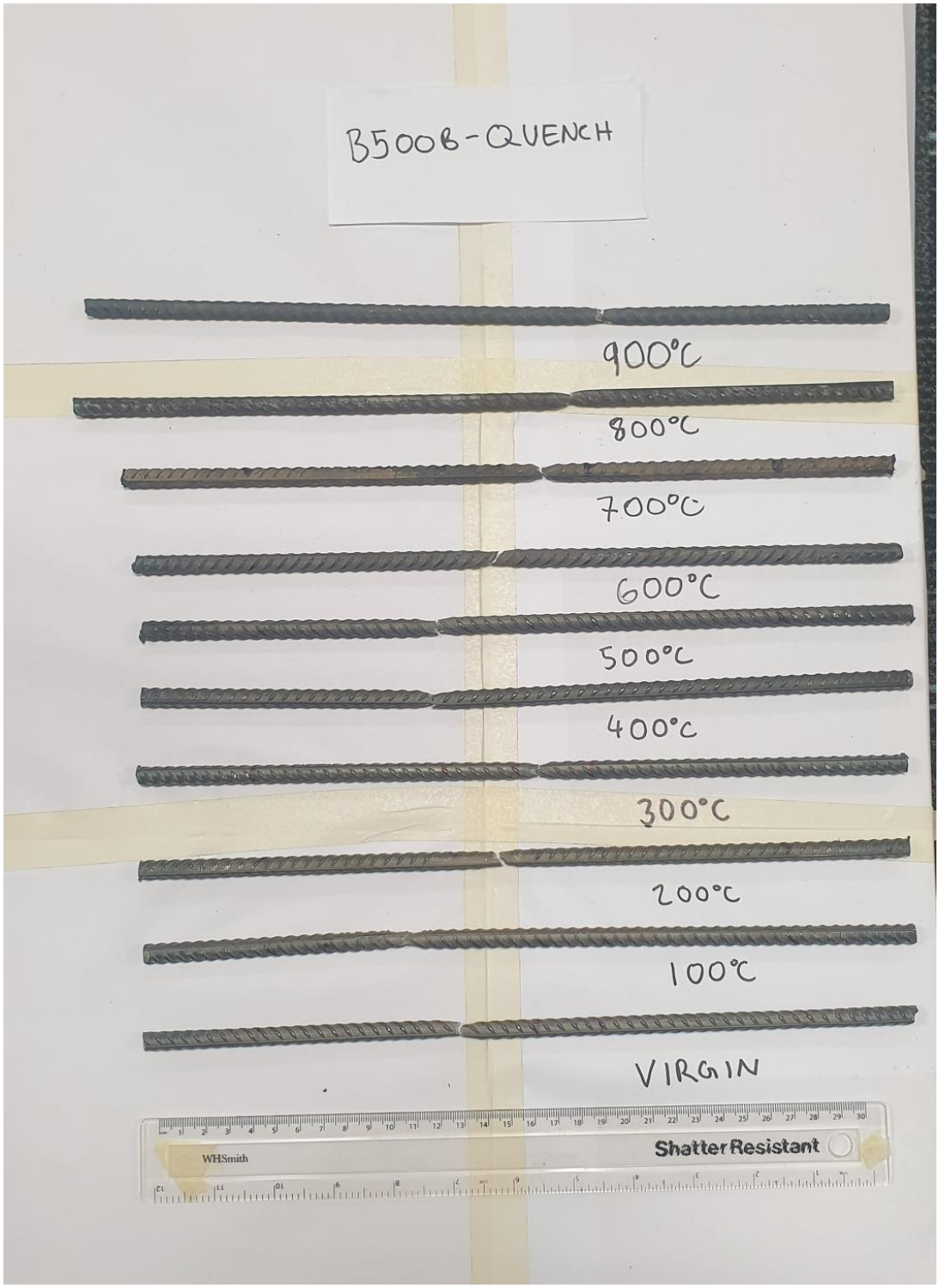

(a)

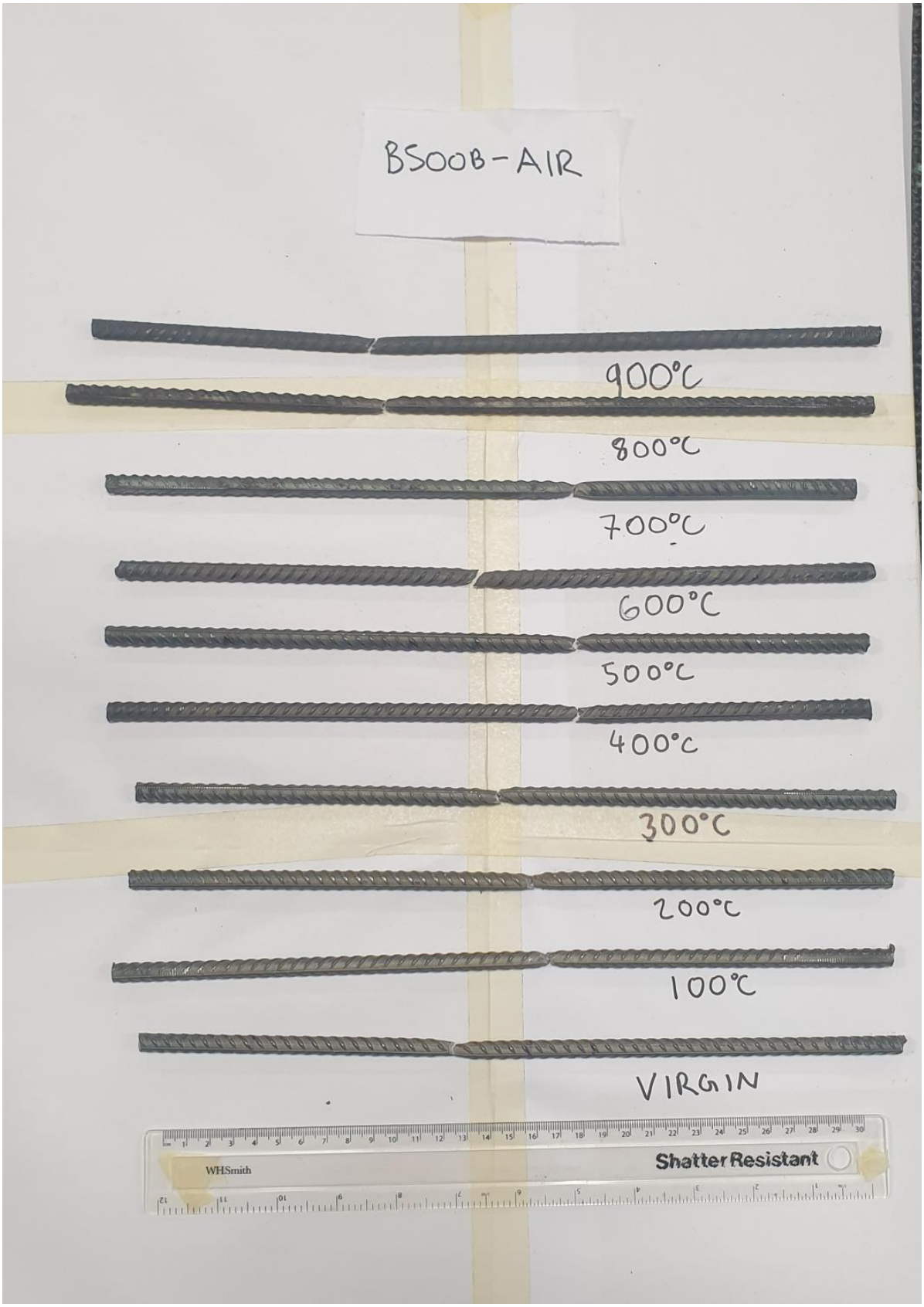
BS00B-AIR
900°C
800°C
700°C
600°C
500°C
400°C
300°C
200°C
100°C
VIRGIN
WHSmith
Shatter Resistant

(b)

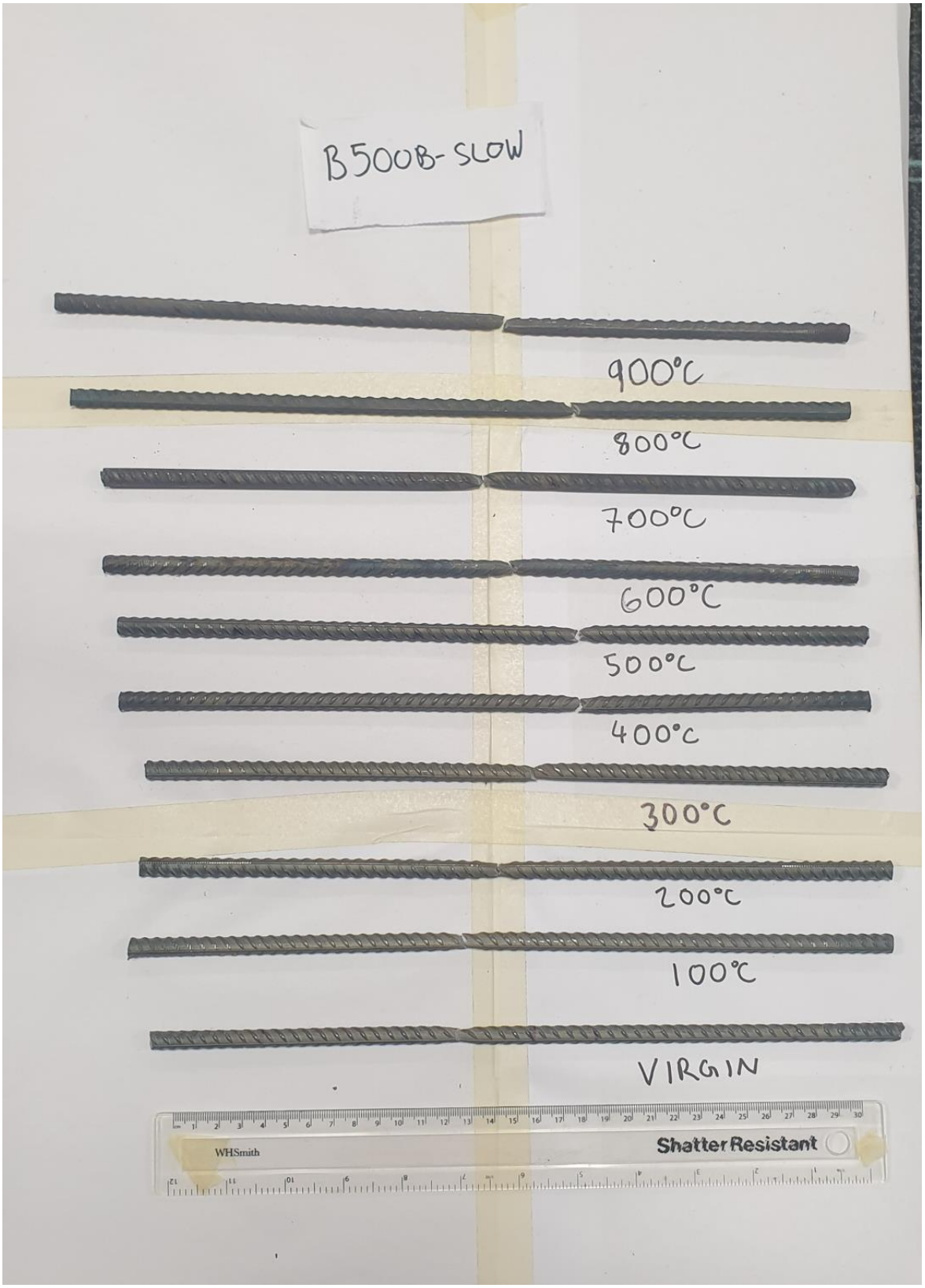

(c)

Figure A.4-1: The fracture location of carbon steel B500B rebar, with (a) as quenched, (b) air-cooled and (c) slow cooled samples.

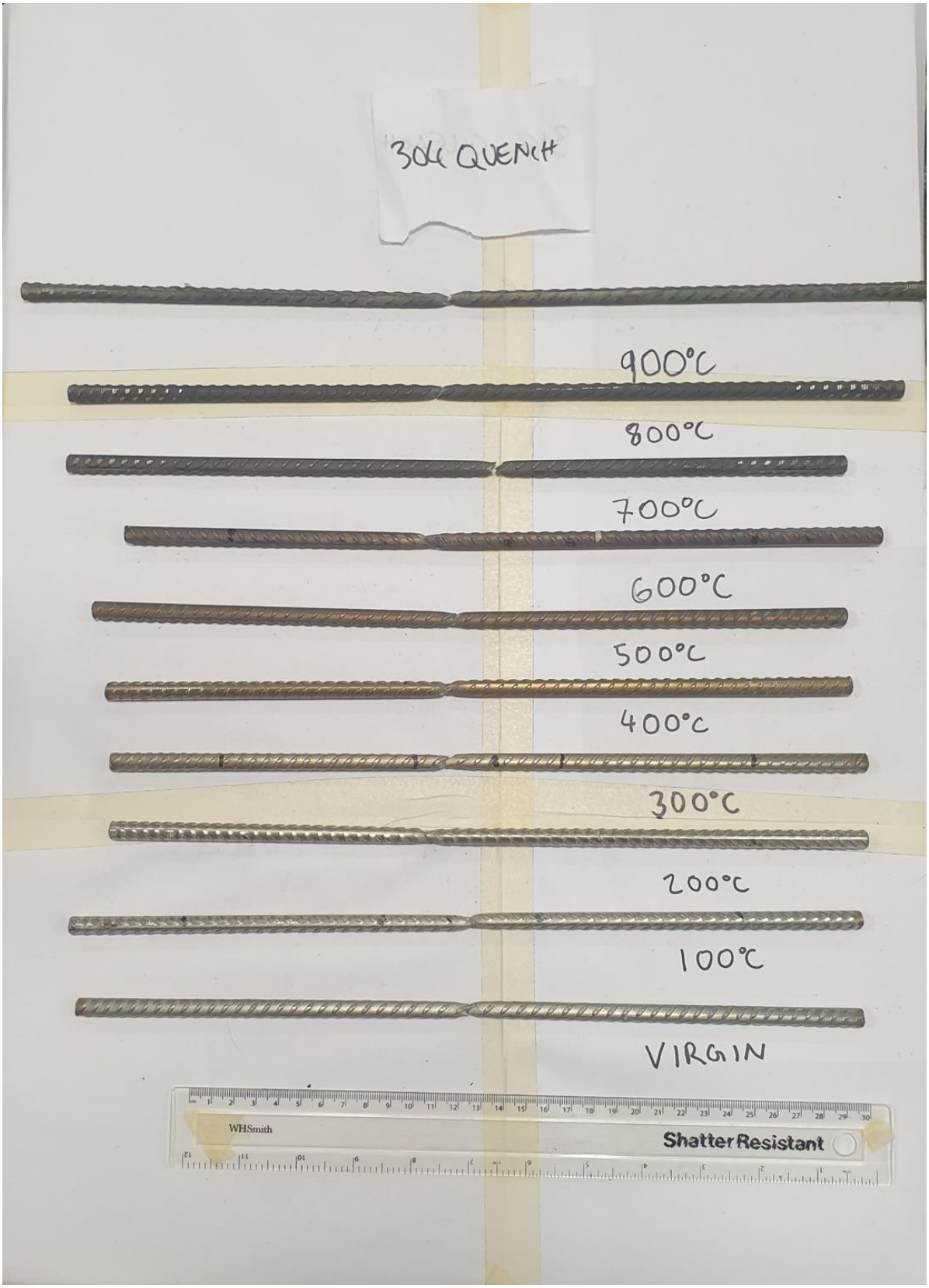
30C QUENCH
900°C
800°C
700°C
600°C
500°C
400°C
300°C
200°C
100°C
VIRGIN
WHSmith
Shatter Resistant

(a)

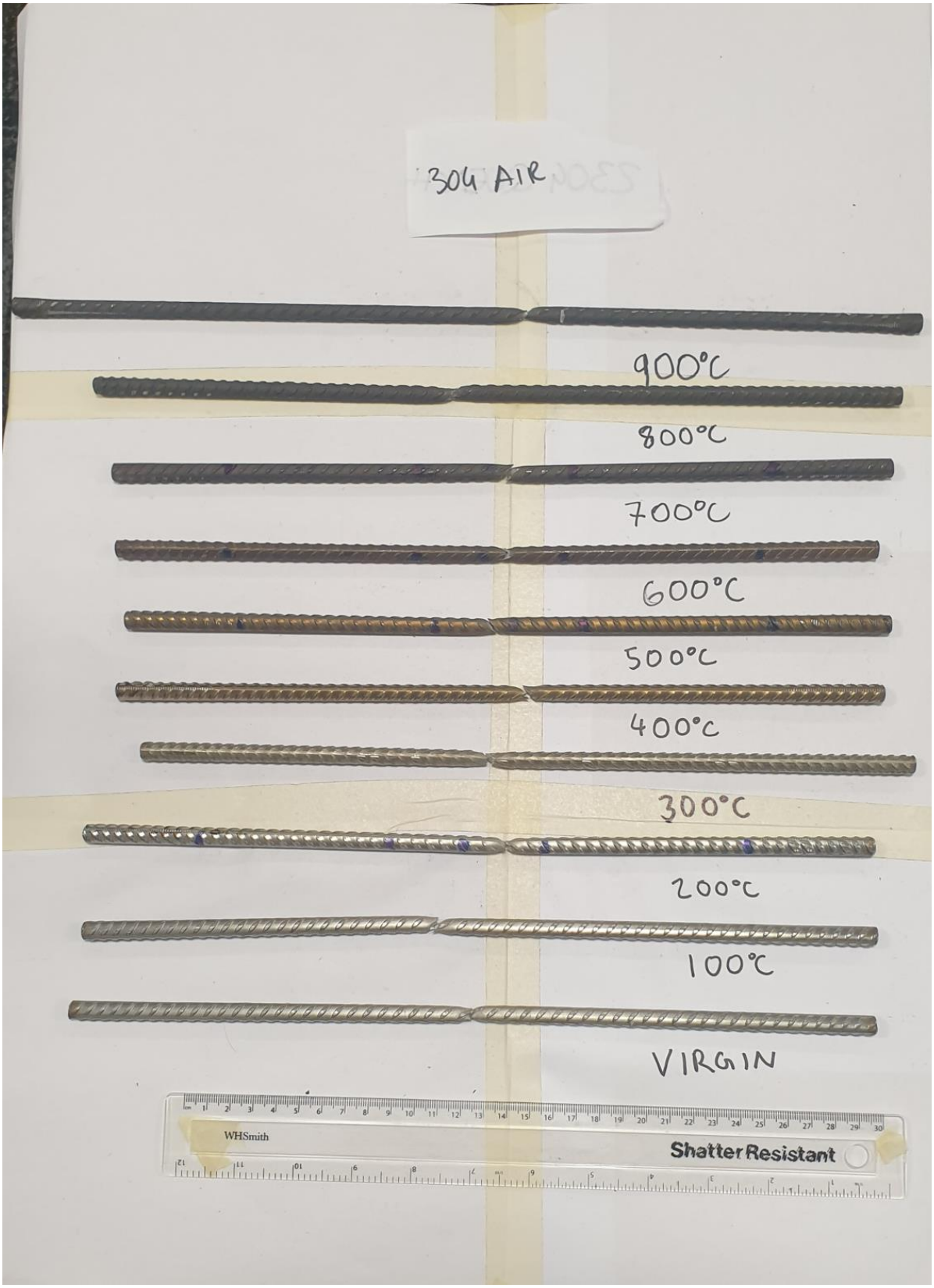
304 AIR
900°C
800°C
700°C
600°C
500°C
400°C
300°C
200°C
100°C
VIRGIN
WHSmith
Shatter Resistant

(b)

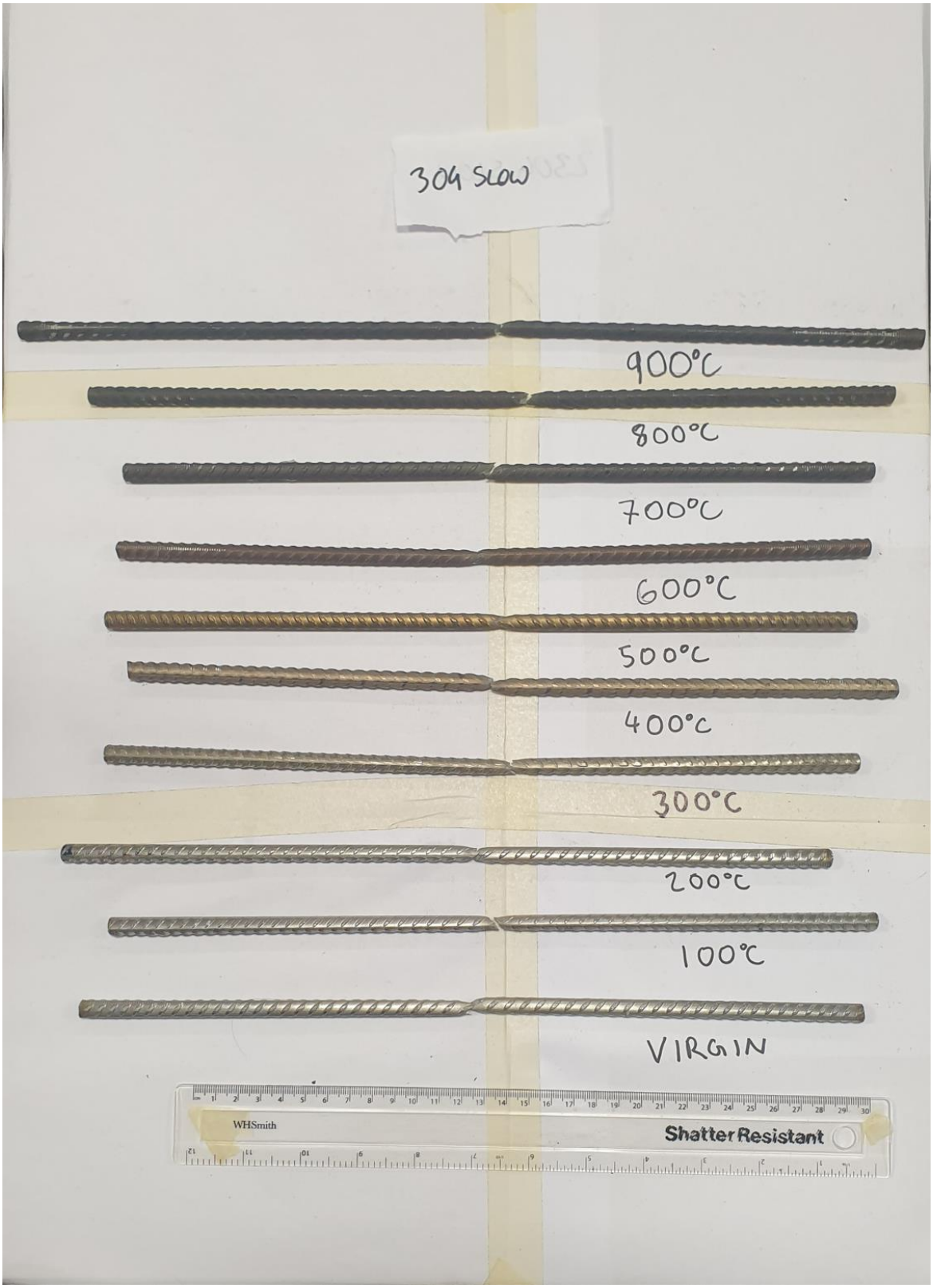

(c)

Figure A.4-2: The fracture location of austenitic stainless steel grade 1.4301, with (a) as quenched, (b) air-cooled and (c) slow cooled samples.


316 QUENCH
900°C
800°C
700°C
600°C
500°C
400°C
300°C
200°C
100°C
VIRGIN
WHSmith
Shatter Resistant

(a)


316 AIR
900°C
800°C
700°C
600°C
500°C
400°C
300°C
200°C
100°C
VIRGIN
WHSmith
Shatter Resistant

(b)

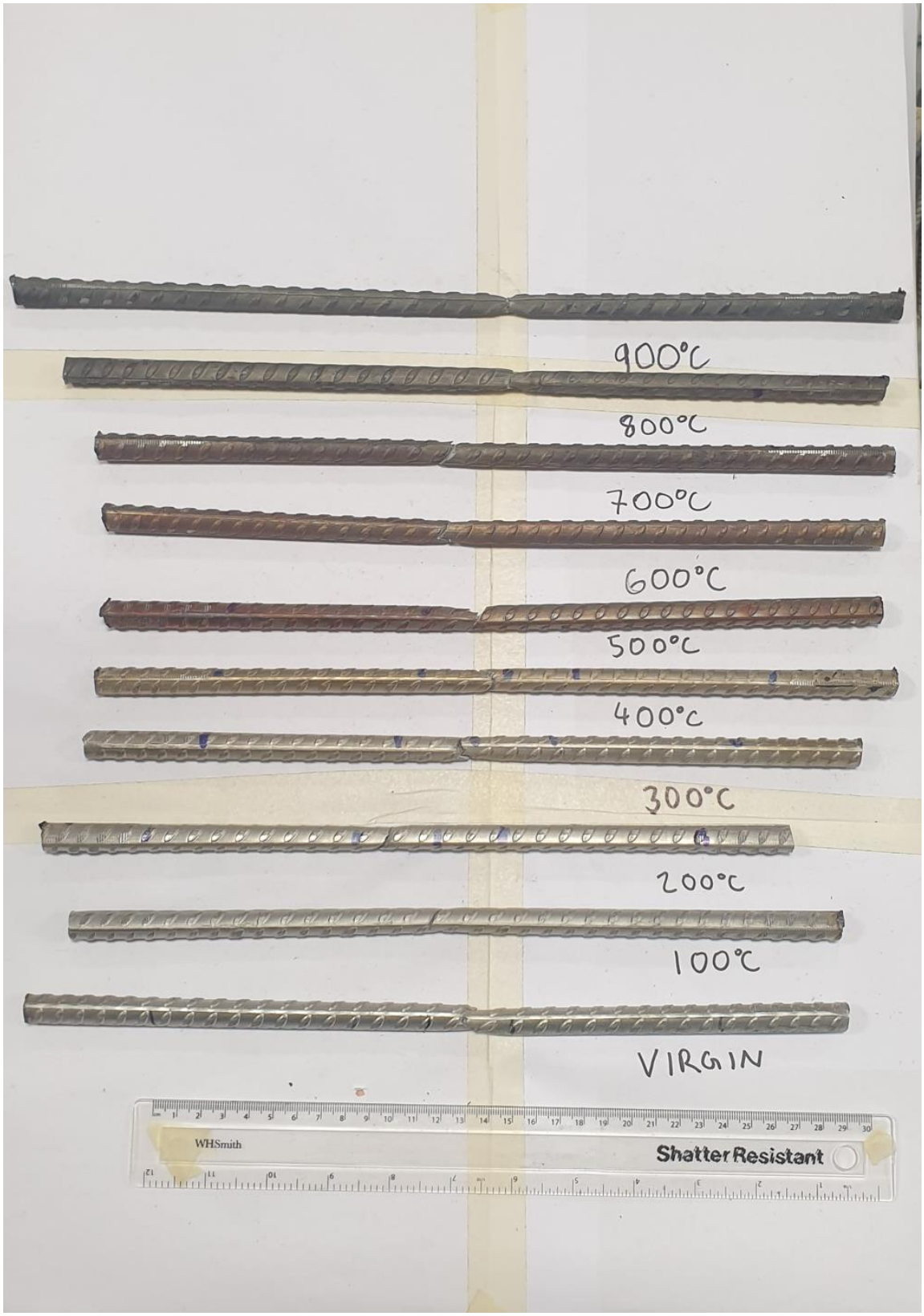

(c)

Figure A.4-3: The fracture location of austenitic stainless steel grade 1.4401, with (a) as quenched, (b) air-cooled and (c) slow cooled samples.

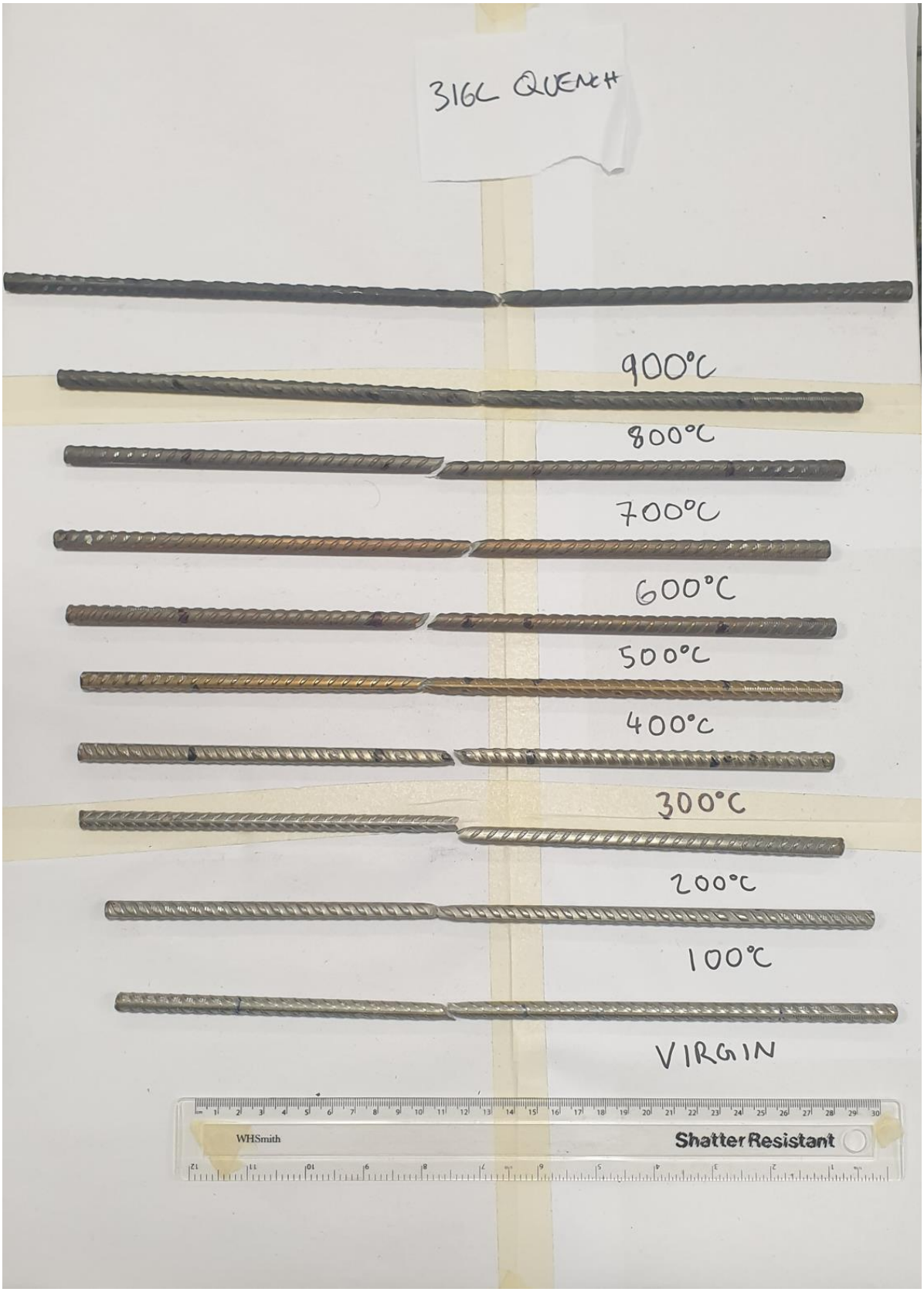
316L QUENCH
900°C
800°C
700°C
600°C
500°C
400°C
300°C
200°C
100°C
VIRGIN
WHSmith
Shatter Resistant

(a)

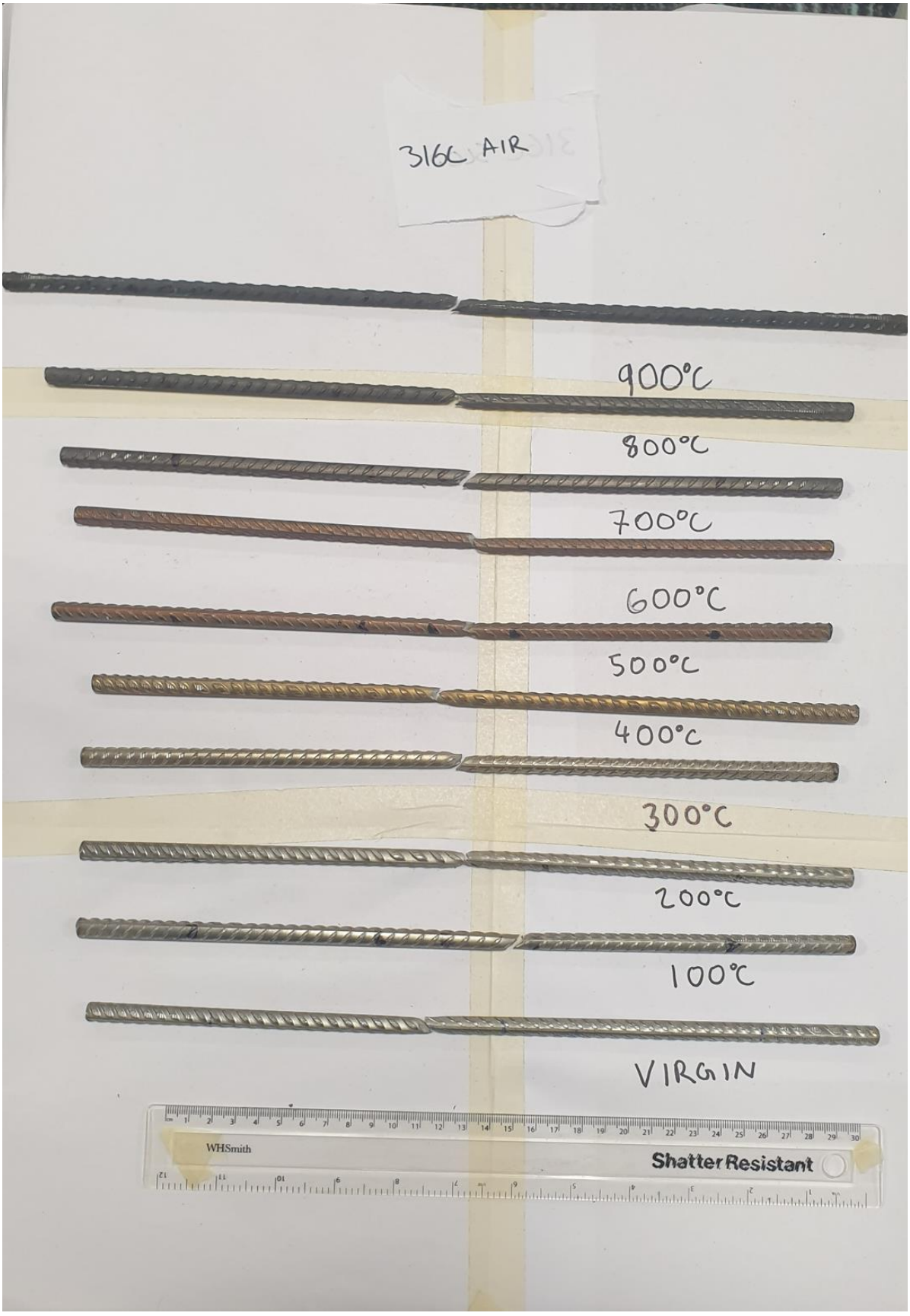
316L AIR
900°C
800°C
700°C
600°C
500°C
400°C
300°C
200°C
100°C
VIRGIN
WHSmith
Shatter Resistant

(b)

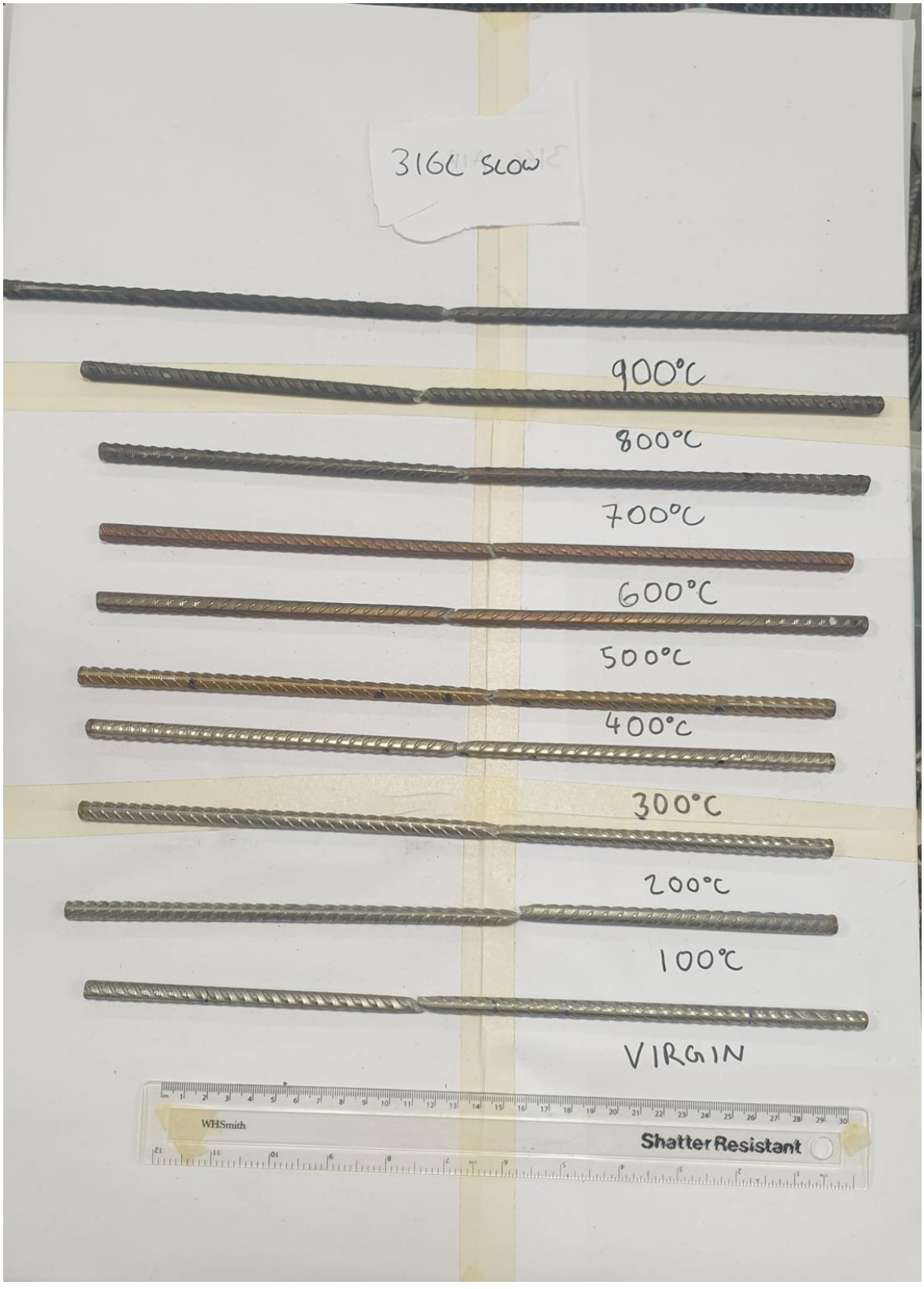

(c)

Figure A.4-4: The fracture location of austenitic stainless steel grade 1.4436, with (a) as quenched, (b) air-cooled and (c) slow cooled samples.

Appendix B

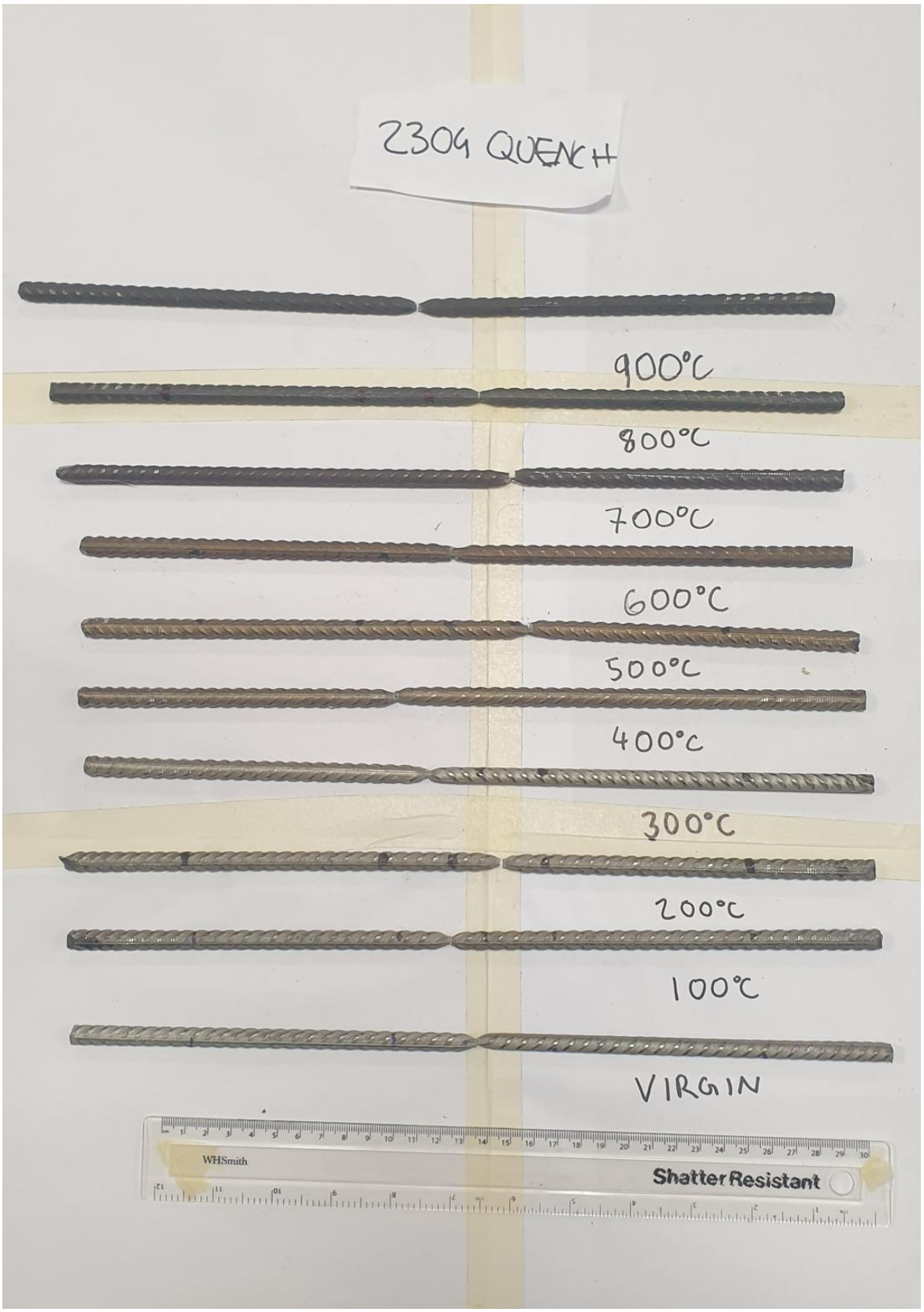
2304 QUENCH
900°C
800°C
700°C
600°C
500°C
400°C
300°C
200°C
100°C
VIRGIN
WHSmith
Shatter Resistant

(a)

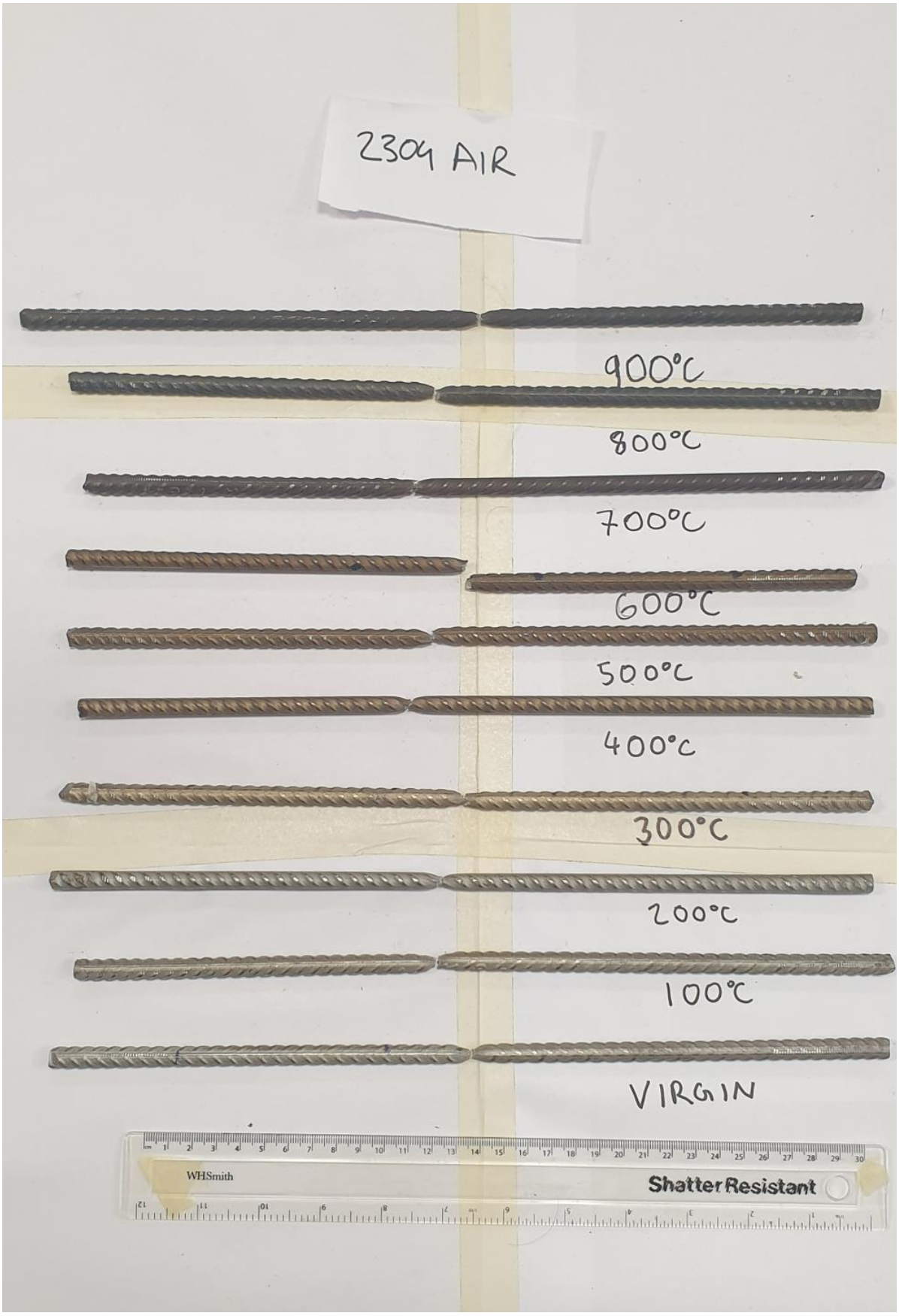
230Y AIR
900°C
800°C
700°C
600°C
500°C
400°C
300°C
200°C
100°C
VIRGIN
WHSmith
Shatter Resistant

(b)

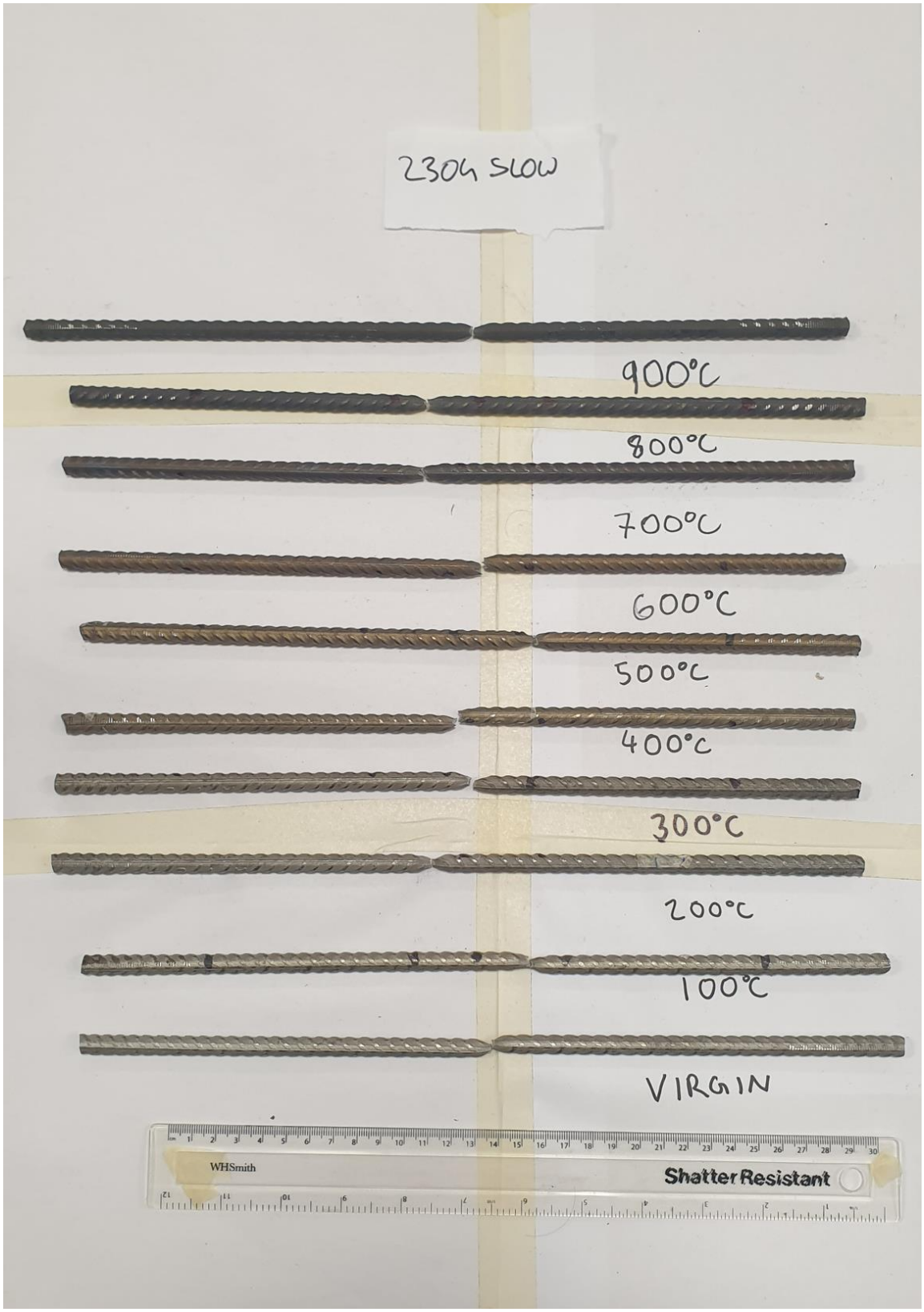

(c)

Figure B.5-1: The fracture location of hot-rolled duplex steel 1.4362 rebar, with (a) as quenched, (b) air-cooled and (c) slow cooled samples.

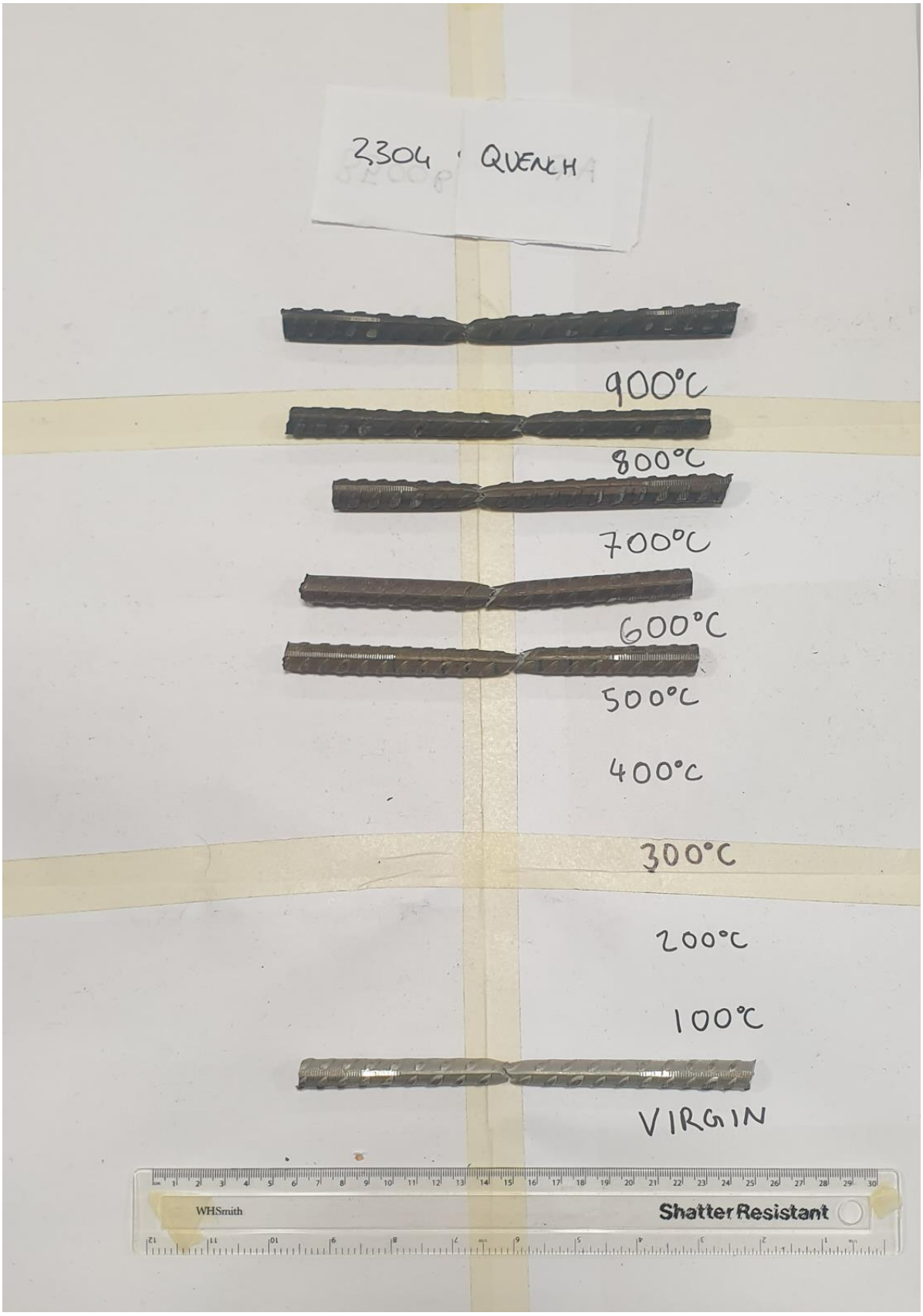
2304 : QUENCH
900°C
800°C
700°C
600°C
500°C
400°C
300°C
200°C
100°C
VIRGIN
WHSmith
Shatter Resistant

(a)

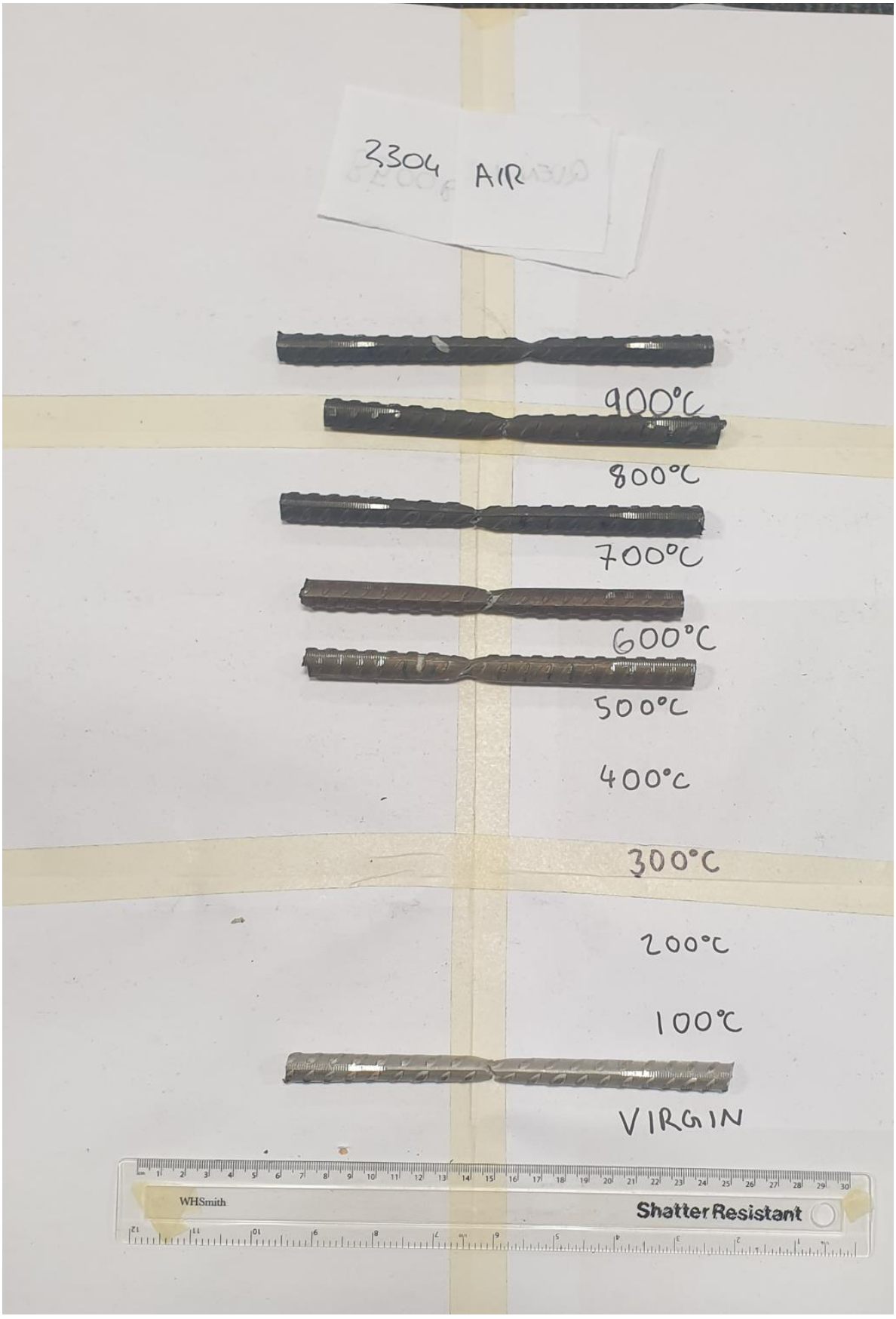
3304 AIR
900°C
800°C
700°C
600°C
500°C
400°C
300°C
200°C
100°C
VIRGIN
WHSmith
Shatter Resistant

(b)

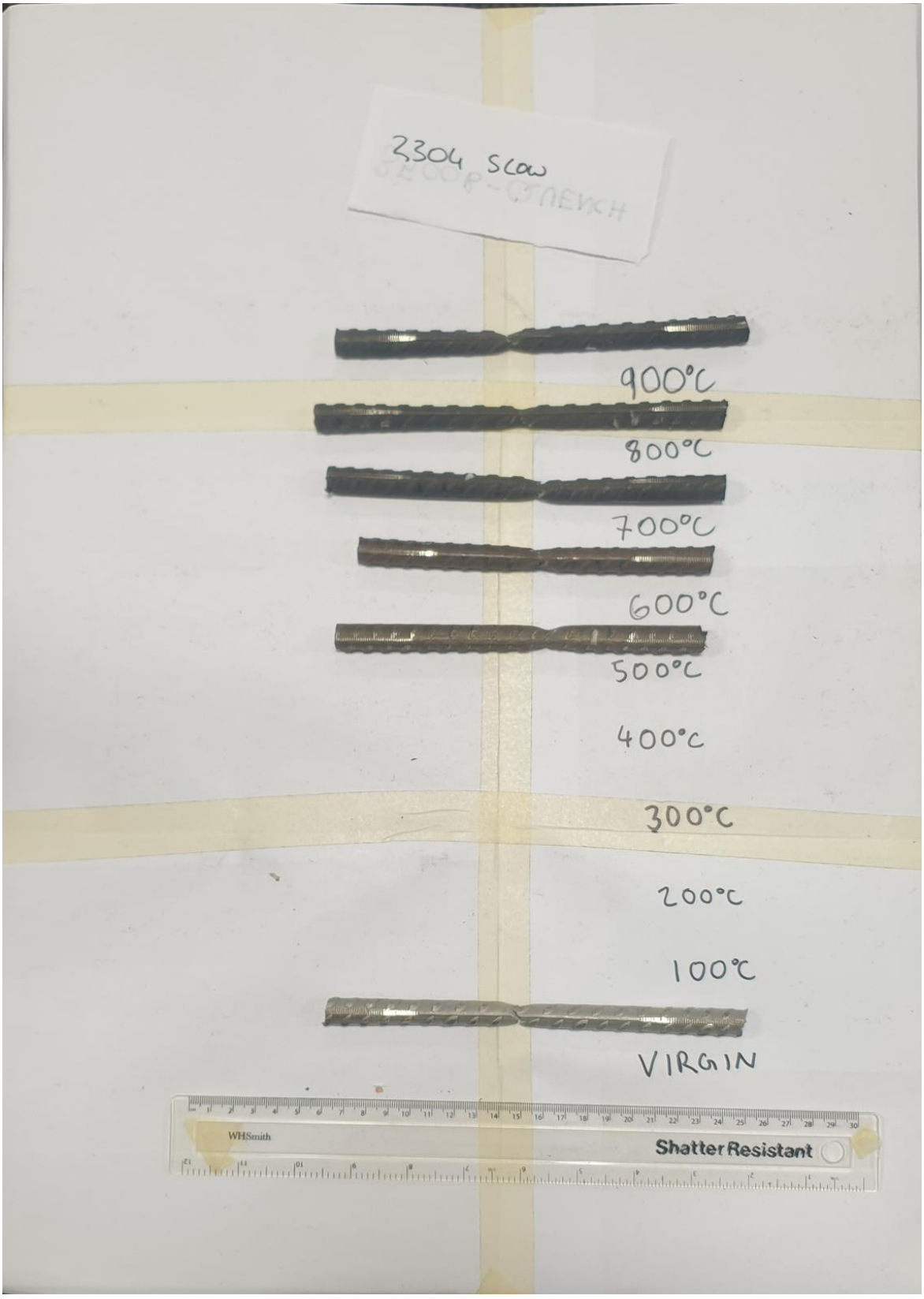

(c)

Figure B.5-2: The fracture location of cold-rolled steel grade 1.4362, with (a) as quenched, (b) air-cooled and (c) slow cooled samples.

Appendix C

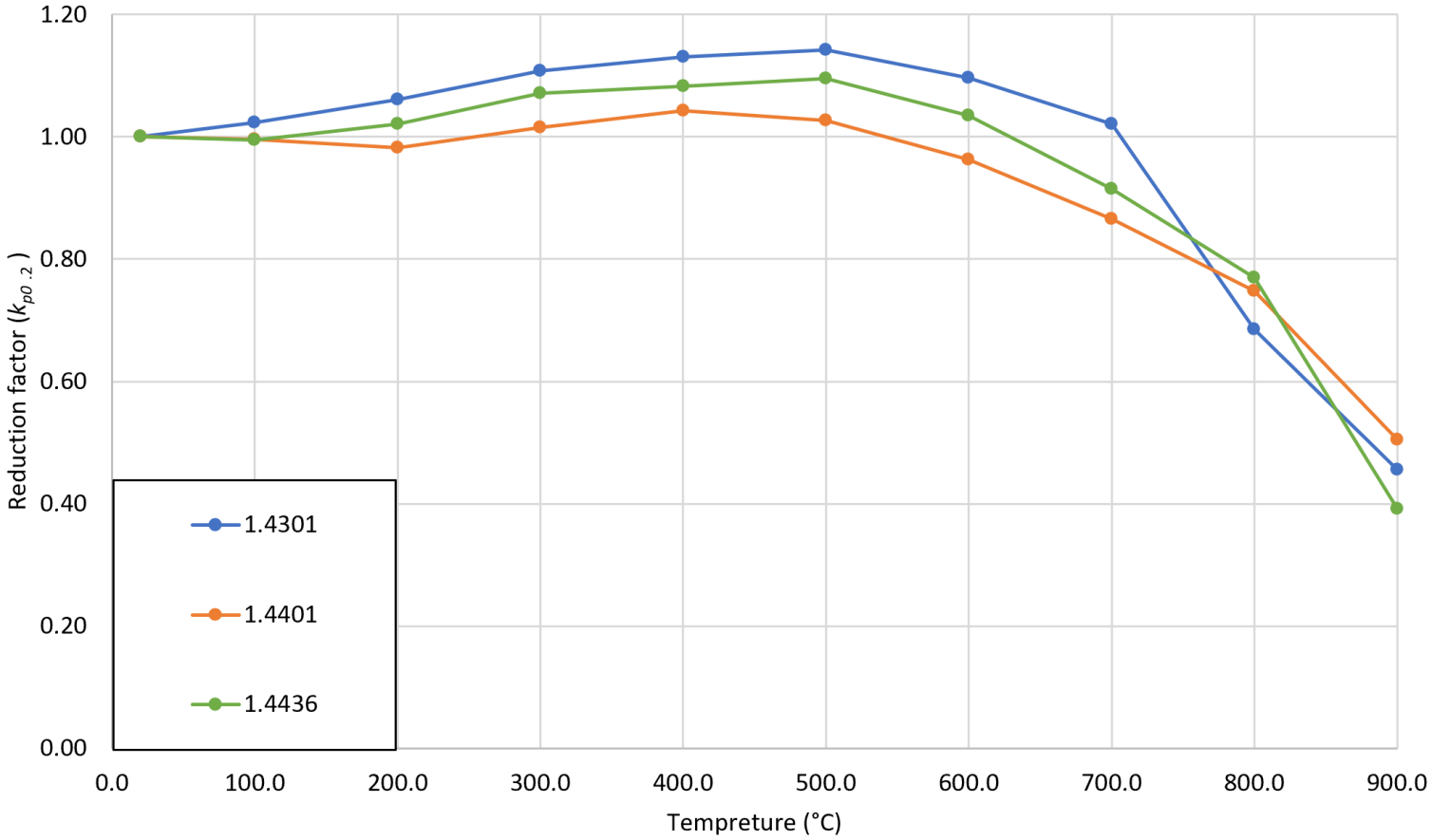
1.20
1.00
0.80
0.60
0.40
0.20
0.00
Reduction factor ($k_{p0.2}$)
0.0
100.0
200.0
300.0
400.0
500.0
600.0
700.0
800.0
900.0
Tempreture (°C)
1.4301
1.4401
1.4436

(a)

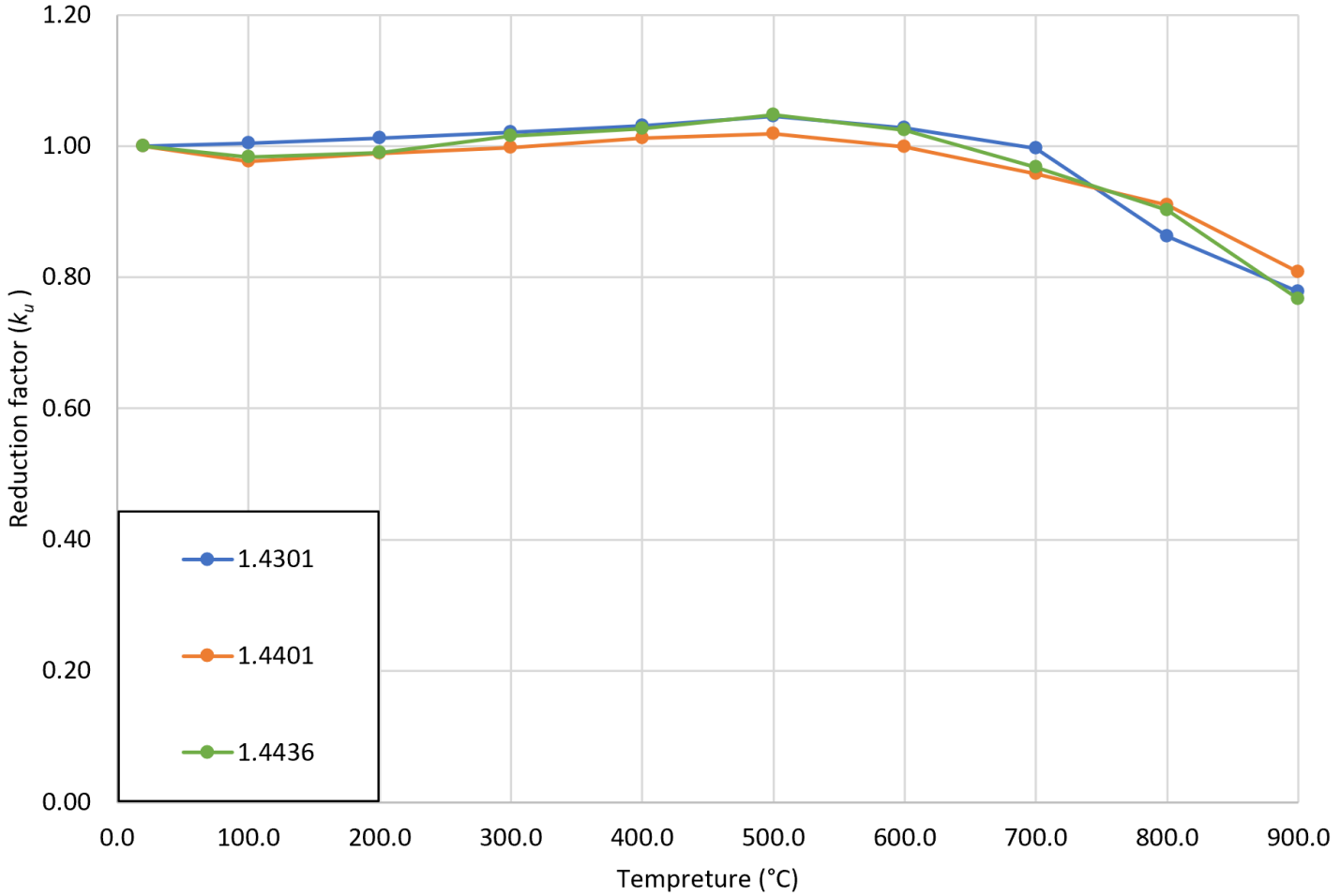

(b)

Figure C.6-3: Comparative recommended reduction factors for austenitic stainless steel reinforcing bars.

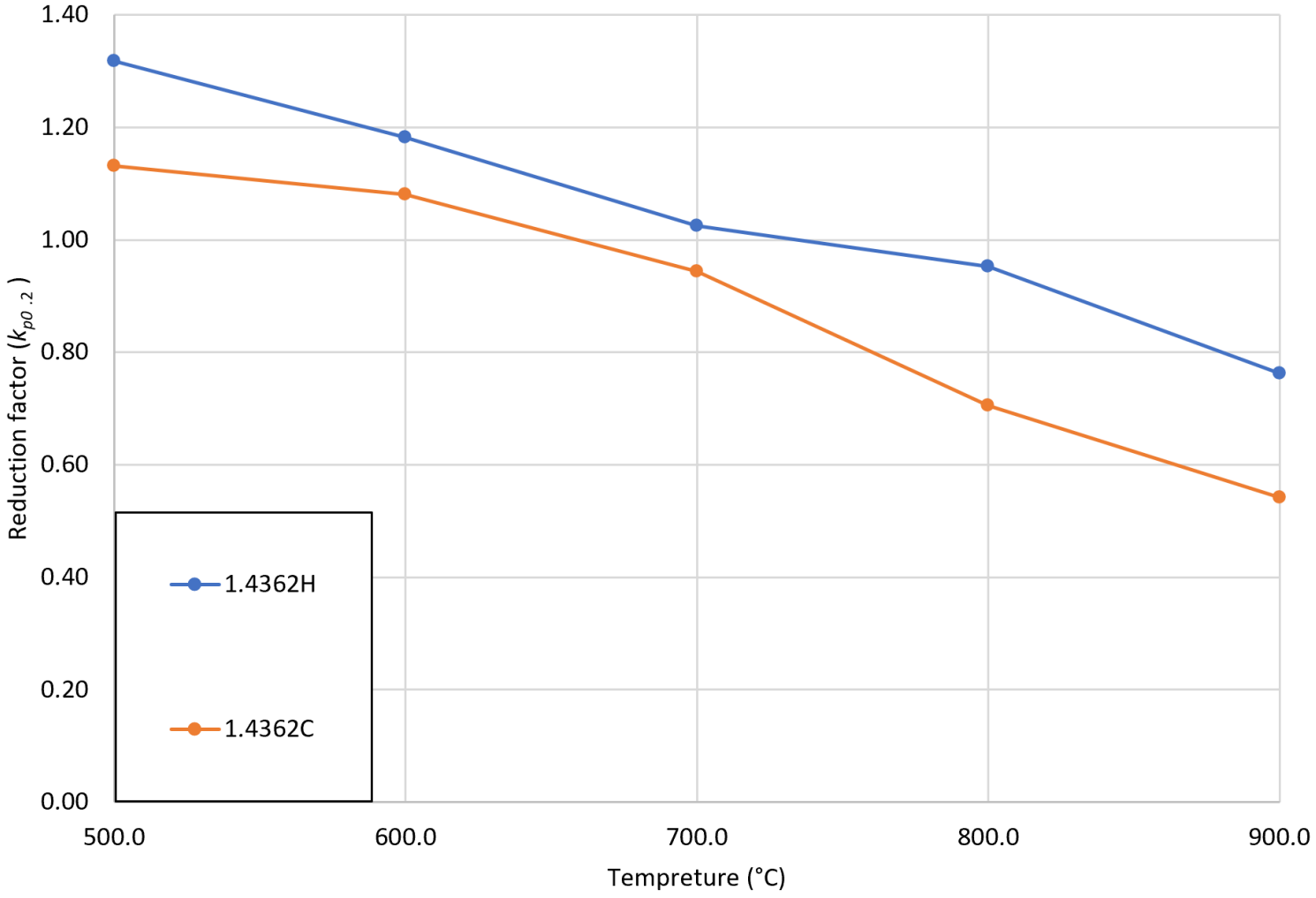
1.40
1.20
1.00
0.80
0.60
0.40
0.20
0.00
Reduction factor ($k_{p0.2}$)
1.4362H
1.4362C
500.0
600.0
700.0
800.0
900.0
Tempreture (°C)

(a)

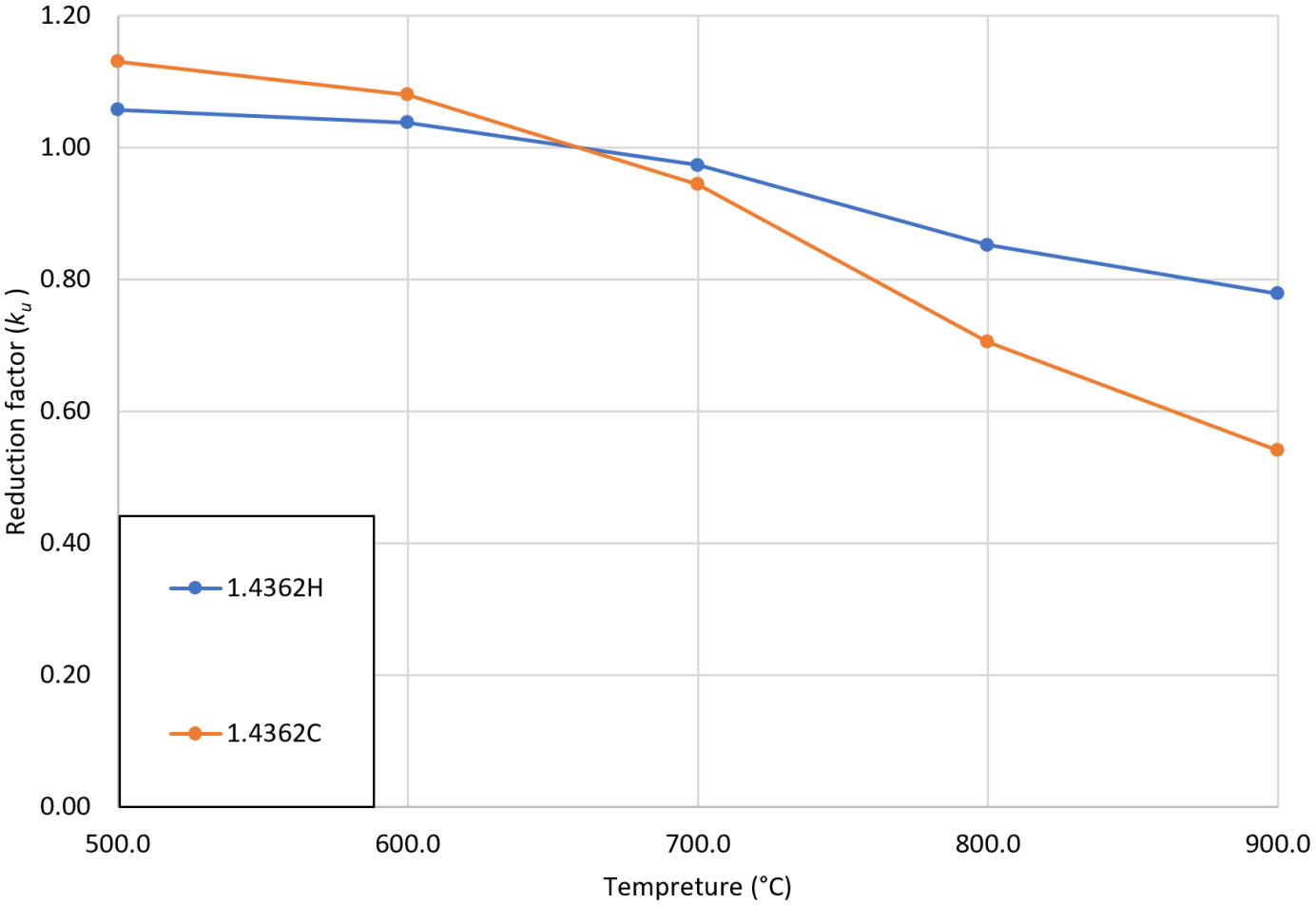

(b)

Figure C.6-4: Comparative recommended reduction factors for duplex stainless steel reinforcing bars.

This page is intentionally left blank.